DOE/ER/54345--306

UC-426

UNIVERSITY OF WISCONSIN, MADISON, WISCONSIN

PLASMA PHYSICS

RECEIVED
OCT 19 1998
OSTI

CONTROLLING FLUCTUATIONS AND TRANSPORT IN THE REVERSED FIELD PINCH WITH EDGE CURRENT DRIVE AND PLASMA BIASING

Darren J.G. Craig

DOE/ER/54345-306

September 1998

MASTER

DISTRIBUTION OF THIS DOCUMENT IS UNLIMITED

NOTICE

This report was prepared as an account of work sponsored by an agency of the United States Government. Neither the United States nor any agency thereof, nor any of their employees, makes any warranty, expressed or implied, or assumes any legal liability or responsibility for any third party's use or the results of such use of any information, apparatus, product or process disclosed in this report, or represents that its use by such third party would not infringe privately owned rights.

Printed in the United States of America
Available from
National Technical Information Service
U.S. Department of Commerce
5285 Port Royal Road
Springfield, VA 22161

NTIS Price codes
Printed copy: A09
Microfiche copy: A01

DISCLAIMER

This report was prepared as an account of work sponsored by an agency of the United States Government. Neither the United States Government nor any agency thereof, nor any of their employees, make any warranty, express or implied, or assumes any legal liability or responsibility for the accuracy, completeness, or usefulness of any information, apparatus, product, or process disclosed, or represents that its use would not infringe privately owned rights. Reference herein to any specific commercial product, process, or service by trade name, trademark, manufacturer, or otherwise does not necessarily constitute or imply its endorsement, recommendation, or favoring by the United States Government or any agency thereof. The views and opinions of authors expressed herein do not necessarily state or reflect those of the United States Government or any agency thereof.

DISCLAIMER

Portions of this document may be illegible in electronic image products. Images are produced from the best available original document.

CONTROLLING FLUCTUATIONS AND TRANSPORT IN THE REVERSED FIELD PINCH WITH EDGE CURRENT DRIVE AND PLASMA BIASING

by

Darren J. G. Craig

A dissertation submitted in partial fulfillment

of the requirements for the degree of

Doctor of Philosophy

(Physics)

at the

University of Wisconsin - Madison

1998

CONTROLLING FLUCTUATIONS AND TRANSPORT IN THE REVERSED FIELD PINCH WITH EDGE CURRENT DRIVE AND PLASMA BIASING

Darren J. G. Craig

Under the supervision of Professor Stewart C. Prager and Dr. Gennady Fiksel

At the University of Wisconsin - Madison

ABSTRACT

Two techniques are employed in the Madison Symmetric Torus (MST) to test and control different aspects of fluctuation induced transport in the Reversed Field Pinch (RFP). Auxiliary edge currents are driven along the magnetic field to modify magnetic fluctuations, and the particle and energy transport associated with them. In addition, strong edge flows are produced by plasma biasing. Their effect on electrostatic fluctuations and the associated particle losses is studied. Both techniques are accomplished using miniature insertable plasma sources that are biased negatively to inject electrons. This type of emissive electrode is shown to reliably produce intense, directional current without significant contamination by impurities.

The two most important conclusions derived from these studies are that the collective modes resonant at the reversal surface play a role in global plasma confinement, and that these modes can be controlled by modifying the parallel current profile outside of the reversal surface. This confirms predictions based on magnetohydrodynamic (MHD) simulations that auxiliary current drive in the sense to flatten the parallel current profile can be successful in controlling magnetic fluctuations in the RFP. However, these studies expand the group of

magnetic modes believed to cause transport in MST and suggest that current profile control efforts need to address both the core resonant magnetic modes and those resonant at the reversal surface. The core resonant modes are not significantly altered in these experiments; however, the distribution and/or amplitude of the injected current is probably not optimal for affecting these modes.

Plasma biasing generates strong edge flows with shear and particle confinement likely improves in these discharges. These experiments resemble biased H modes in other magnetic configurations in many ways. The similarities are likely due to the common role of electrostatic fluctuations in edge transport.

Acknowledgements

I would first like to thank my advisor, Stewart Prager, for his ability to see directly to the heart of the matter and bring it out in the research. His direction throughout this thesis work has been invaluable. I especially appreciate the tremendous effort he makes to yield his attention to his students amidst the fury of defending fusion research in this country and abroad.

My thanks also go out to my committee members -- Professors Jim Callen, Ray Fonck, Cary Forest, and Paul Terry. I would like to thank Jim Callen and Cary Forest in particular for their careful reading of this thesis.

To my friend and mentor, Gennady Fiksel, Спасибо большое! Were it not for a certain fellowship proposal which you submitted, I would probably never have come to Wisconsin and worked on what I thought for sure were weapons. I cannot possibly overstate the contribution you have made to my education and to this thesis work. May you never run out of envelopes for those *ex nihilo* derivations!

Many thanks also to John Sarff who could always understand what I was talking about regardless of how clearly I said it and whose many ideas and suggestions led to some of the key results in this thesis. Thanks also to Daniel Den Hartog for teaching me much about spectroscopy and optics. I look forward to learning even more. Thanks to Abdulgader Almagri for showing me how to make Rogowski probes that really work and to Don Holly who taught me the golden rule of optics which I will never forget. Thanks also to Matt Stoneking, Chris Hegna, and Carl Sovinec for illuminating many aspects of plasma physics on my behalf and to the many professors and fellow students who challenged me to learn some amazing things about physics and the world around me while in graduate school.

I would also like to acknowledge our very capable staff of engineers and technicians including Tom Lovell for his many contributions to the gun project, Mark Thomas for his

design and construction of the gun power supplies and support systems, Roch Kendrick for his countless ideas in the midst of crisis and for his development of a more durable Rogowski shroud, Steve Oliva for his design of the gun valve drivers and the many hours of work spent on designing and constructing the gun gas handling system, John Laufenberg for his unending dedication to making things work, and Mikhail Reyfman for constructing and repairing many of the electrical components used in this work.

My thanks also to my fellow plasma graduate students of the past and present -- Derek Baver, Ted Biewer, Brett Chapman, Jim Chapman, Ching-shih Chiang, Neal Crocker, Vineet Dhyani, Eduardo Fernandez, Paul Fontana, Alex Hansen, Nick Lanier, Cavendish McKay, Kevin Mirus, Uday Shah, and Dmitry Sinitsyn -- who have made my graduate school experience truly memorable and who all, at some point or another, have made individual contributions to the research presented in this thesis. A special thanks to Jay Anderson for his help in constructing and testing many of the plasma guns.

I would also like to acknowledge Kay Shatrawka, Larry Smith, Paul Wilhite, Dale Schutte, and the many undergraduates who have made innumerable contributions to this project and the MST program in general.

To my parents and brothers, thank-you for your constant support and encouragement throughout the many years of education and for helping me to see the many opportunities.

I sincerely appreciate the constant love and support of my truly great wife, Karen. Thanks for spurring me on when my energies were draining and for listening to all of the often long-winded explanations of how the guns and the plasma are doing this or that. I look forward to life after grad school with you.

"Now to Him who is able to do immeasurably more than all we ask or imagine, according to His power that is at work in us, to Him be glory ... for ever and ever!"

Ephesians 3:20

(Funding for this program was made possible by a grant from the U.S.D.O.E.)

TABLE OF CONTENTS

Abstract i

Acknowledgements iii

Table of Contents v

1. Introduction 1

1.1 Transport and Fluctuations in the RFP 1

1.1.1 Overview 1

1.1.2 Transport Reduction by Current Profile Control 3

1.1.3 Transport Reduction by Plasma Biasing 6

1.2 Motivation for Electrostatic Current Injection 7

1.2.1 Results of MHD Simulations 7

1.2.2 Results of Inductive Current Profile Control in MST 9

1.2.3 Electrostatic Current Injection Concept 10

1.3 Overview and Outline 13

2. Biased Plasma Guns as Current Sources 18

2.1 Source Configuration and Hardware 18

2.1.1 Source Configuration 18

2.1.2 Puff Valve 21

2.1.3 Power Supplies 24

2.1.4 Test Stand Configuration 26

2.2 The Internal Discharge 30

2.2.1 General Features 33

2.2.2 Measurements of Plasma Production 36

2.2.3 Spectroscopic Measurements 42

2.3 Plasma Guns as Current Sources 47

2.4 Summary 53

3. Electrostatic Current Injection and Biasing in MST 56

3.1 MST Diagnostics 56

3.1.1 Interferometer Measurements 58

3.1.2 Thomson Scattering Measurements 59

3.1.3 Hydrogen Radiation Measurements 59

3.1.4 Impurity Ion Flow Measurements 60

3.1.5 Magnetic Fluctuation Measurements 64

3.1.6 Langmuir Probe Measurements 66

3.1.7 Rogowski Probe Measurements 69

3.2 Current Injection in a Closed Field Line System 70

3.2.1 Overview 70

3.2.2 Plasma Biasing 73

3.2.3 Dependence of Bias Circuit Impedance on Plasma and Gun Parameters 75

3.3 Distribution of Injected Currents in MST 81

3.3.1 Edge Magnetic Equilibrium Measurements 82

3.3.2 Measurements of Injected Current from Plasma Guns 88

3.3.3 Cylindrical Equilibrium Modeling of MST Discharges with Current Injection 103

3.4 Summary 106

4. Results of Fluctuation and Transport Control Experiments 109

4.1 Overview and Methods 109

4.1.1 Overview of Results 109

4.1.2 Distinguishing Between Multiple Causes and Effects 111

4.2 The Effect of Current Profile Control on Fluctuations and Confinement 113

4.2.1 Behavior of Magnetic Fluctuations with Electrostatic Current Drive 114

4.2.2 Changes in Particle Confinement Due to Electrostatic Current Drive 125

4.2.3 Changes in Energy Confinement Due to Electrostatic Current Drive 131

4.3 The Effect of Plasma Biasing on Fluctuations and Confinement 135

4.3.1 Flows in Biased Discharges 136

4.3.2 Changes in Electrostatic Fluctuations Due to Plasma Biasing 143

4.3.3 Changes in Particle Confinement Due to Plasma Biasing 149

4.3.4 Magnetic Fluctuations and Energy Confinement in Biased Discharges 157

4.4 The Impact of Injector Insertion on Confinement 158

4.5 Summary 164

5. Summary and Discussion 169

5.1 Main Results and Implications 169

5.2 Possible Extensions of This Work 171

1. INTRODUCTION

Reversed Field Pinch (RFP) research is driven by two broad goals. The first is to develop a magnetic configuration in which hot plasmas can be confined for producing controlled fusion reactions and ultimately attractive electric power. The second is to understand the principles at work in hot magnetized plasmas purely for the sake of enriching our physics knowledge. In this thesis, electron currents will be injected from a set of unique electrodes and used to modify both the current profile and the potential profile in the edge of a large RFP plasma. The response of fluctuations in the magnetic field, density, and electric potential will be examined as well as changes in the global confinement properties. This work contributes toward both of the research goals mentioned above. Current profile control and plasma biasing can increase confinement, leading to a more attractive fusion concept, while at the same time it should provide a knob for controlling fluctuations and testing our understanding of the role they play in confined plasmas.

In the following sections I review the current understanding of transport in the RFP and present motivation for accomplishing edge current drive and plasma biasing with an electrostatic injection scheme I also give an overview and outline of the remainder of this dissertation.

1.1 Transport and Fluctuations in the RFP

1.1.1 Overview

The RFP concept has been studied for many years. (For a review of RFP physics see references [1,2,3,4].) It is now well understood that the transport of particles and energy out of the plasma is, as in other magnetic configurations, orders of magnitude greater than what one would get by simply considering the motion of magnetized particles that occasionally

collide with one another. The difference is ascribed to the presence of turbulence which is effective in enhancing mixing in all fluids, including plasmas.

Recent work in the Madison Symmetric Torus (MST) device [5] has focused on directly measuring the particle and energy fluxes due to different components of the turbulence in order to identify which underlying processes are most important. The measurements [6,7] have confirmed a long held suspicion that fluctuations in the magnetic field are primarily responsible for the global confinement properties in the RFP. Magnetic fluctuations in the RFP are large (~ 1%) in comparison to devices like the tokamak, perhaps because the confining magnetic field is about an order of magnitude lower than in those devices. The lower magnetic field is good from a reactor design standpoint, but the strong magnetic fluctuations that arise must be controlled if the concept is to have good enough plasma confinement to produce efficient fusion energy.

Particle and energy fluxes due to fluctuations always arise due to a correlated product of two or more fluctuating quantities. If all quantities are represented by $A = A_0 + A_1$, where A_0 is the mean value and A_1 is the fluctuating part, then the radial flux of particles due to density fluctuations, for example, is given by $\Gamma = \langle n_1 v_{r1} \rangle$ where n is the density, v_r is the radial flow velocity, and $\langle\ \rangle$ denotes an average over a fluctuation period. This simply says that if the density and velocity fluctuations are well correlated and if density is high where the fluctuating flows are outward but low where flows are inward, then there is a net flux of particles outward. The amplitude of the flux is related to the amplitude of the fluctuations, the degree of coherence, and the phase relation between the two fluctuating quantities.

Fluctuation-induced transport can be minimized in several ways. Reduction can occur by reducing the amplitude of either fluctuating quantity, reducing the coherence between the fluctuations, or changing the phase relationship between them. A given mode amplitude is determined by a balance between the rate of energy transfer into and out of the mode. Energy can flow into the mode from the equilibrium (e.g., if the mode is linearly

unstable) or by nonlinear transfer of energy from other modes. Energy can flow out of a mode into the equilibrium (e.g., through quasilinear processes), into other modes by nonlinear coupling, or into the thermal energy of the fluid through dissipation. The universal solution to reducing turbulent fluxes is to remove the free energy source that drives the fluctuations. However, in some cases the transport can be reduced by changing one of the other ingredients.

1.1.2 Transport Reduction by Current Profile Control

The RFP configuration is a toroidal magnetic configuration that can be distinguished by the radial profile of the "safety factor"

$$q \equiv \frac{1}{2\pi} \int_0^{2\pi} \left(\frac{d\phi}{d\theta} \right) d\theta \tag{1.1}$$

where ϕ is the toroidal angle, θ is the poloidal angle, and the derivative and integrals are done following a magnetic field line. The safety factor is a measure of how far one moves toroidally in making one complete poloidal transit along a magnetic field line. Figure 1.1 shows a typical RFP q profile computed with a cylindrical equilibrium model with MST-like parameters. The two distinguishing characteristics are that $q < 1$ everywhere in the plasma and that there is a zero crossing near the edge, beyond which the toroidal field is in the opposite direction to that in the center.

Along this q profile there are an infinite number of rational surfaces at which perturbations may be resonant. A resonant perturbation is one described by

$$B_{mn}(r,\theta,\phi,t) = B_{mn}(r) e^{i(m\theta + n\phi - \omega t)} \tag{1.2}$$

where $q = m/n$ somewhere in the plasma; or more generally, it is a perturbation for which the component of the wavevector parallel to the magnetic field is zero. Figure 1.1 also shows the location of the resonant surfaces for several magnetic modes that are present in the MST device.

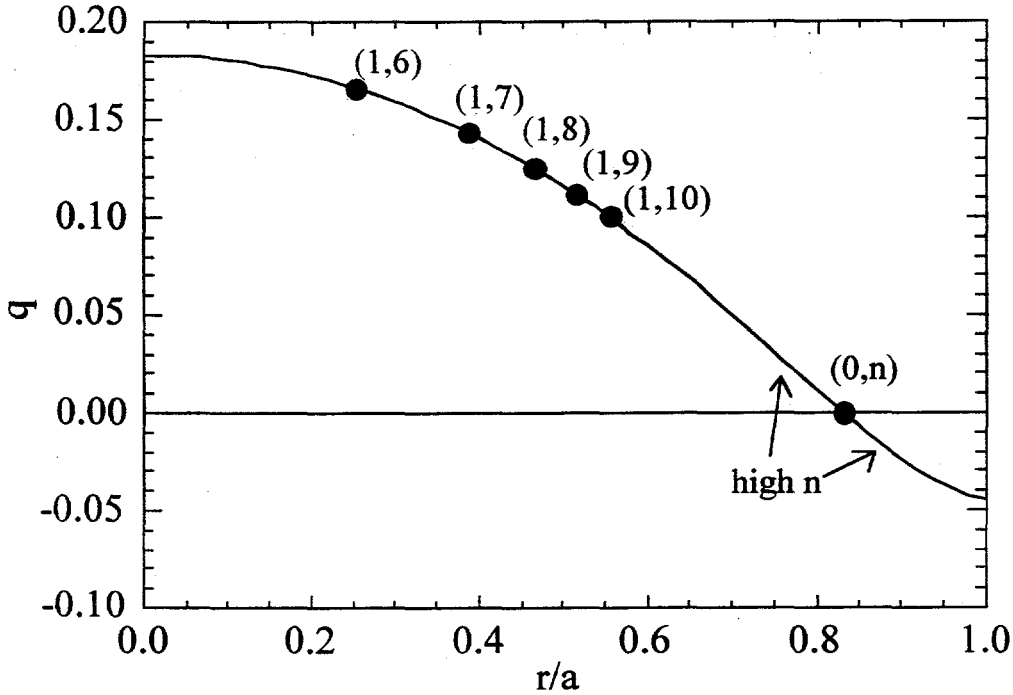

Figure 1.1. A typical RFP safety factor profile is shown along with the positions of several mode-resonant surfaces.

In the core, modes with (m,n) = (1,6), (1,7), ... will be resonant and strong kink-tearing instabilities are observed with these mode numbers in MST [8,9]. Several MHD simulations have predicted [10,11] that these modes should be unstable due to radial gradients in the component of current density along the magnetic field. Indeed, these modes are unstable in MST and compose a large fraction of the total power residing in magnetic fluctuations. These "core" modes are actually global instabilities (i.e., $B_{mn}(r)$ is very broad) and although most sensitive to the current gradient near the resonant surface, they can be affected by the entire current profile.

The parallel current profile naturally peaks in the RFP due to the combined effect of a parallel applied electric field that peaks on axis and a hollow resistivity profile. The modes

act to relax the current gradient by opposing the applied electric field in the core and driving current along the magnetic field in the edge. This process is called the RFP dynamo and converts poloidal flux generated by toroidal currents in the core into toroidal flux generated by poloidal currents in the edge [12,13,14].

Although these modes help to sustain the magnetic configuration, they cause the magnetic field in the core of the discharge to become stochastic. In fact, the measured electron particle and heat fluxes [6,7] are well described by considering the thermal motion of particles in a stochastic magnetic field [15] subject to ambipolar constraints [16]. In this case, the transport can be modeled as diffusive with a coefficient

$$\chi \approx L_c v_{th} \left| \frac{B_1}{B_0} \right|^2 \tag{1.3}$$

where L_c is the correlation length (determined by the number of modes present, degree of overlap, etc.), v_{th} is a characteristic velocity along the field, and B_1 and B_0 are the magnitudes of the fluctuating and equilibrium magnetic fields, respectively.

If the diffusive picture is correct, than the only acceptable way to reduce the transport caused by these fluctuations is to reduce B_1. This can be done either by changing the linear drive for the instabilities (i.e., flattening the parallel current profile) or by changing the saturated amplitudes through quasilinear or nonlinear mechanisms. The most straightforward technique is to modify the current profile by adding parallel current at radii greater than the mode resonant surfaces.

The core modes are not the only magnetic fluctuations present in MST. There are also modes with (m,n) = (0,1), (0,2), ... resonant at the reversal surface and these modes can have amplitudes comparable to or greater than the core modes in some situations. In Chapter 4, experimental evidence for the contribution of these modes to particle and energy transport will be presented. The previous measurements [6,7] of magnetic-fluctuation-induced transport did not identify the m=0 modes as significant, but this is probably because in normal

discharges they are usually stationary in the lab frame. Hence, they cannot be distinguished from the equilibrium unless large spatial arrays of probes are used. It appears that any attempt to improve RFP plasma confinement through current drive should address these modes as well as the core modes.

For completeness, it should be mentioned that on either side of the reversal surface there are exists a multitude of closely spaced, localized modes with high toroidal mode numbers. These modes are locally resonant and do not appear to play a direct role in particle and energy transport. They do, however, participate in the nonlinear coupling processes that link all modes together and hence are a part of the overall RFP picture.

These ideas suggest that an interesting, experiment would be to drive currents in the edge in the sense to flatten or steepen the parallel current profile and monitor the response of the magnetic fluctuations. One predicts that if the core and m = 0 modes are decreased, then confinement should increase. Conversely, if the core and m = 0 modes are driven, confinement should decrease. If one can reduce the magnetic fluctuations enough, the core magnetic field will no longer be stochastic and transport should be reduced significantly.

1.1.3 Transport Reduction by Plasma Biasing

It has been well established that a gradient in the radial electric field can reduce the anomalous transport produced by electric field fluctuations in magnetically confined plasmas [17,18,19]. Such effects, associated with the shear in E×B flows, occur in numerous configurations including tokamaks [20], stellarators [21], and magnetic mirrors [22]. In most cases, the turbulence and transport are believed to be dominated by small-scale electrostatic fluctuations, which are thereby amenable to reduction by shear flow. The electric field gradient and improved confinement (known as H mode) can occur spontaneously under certain conditions [20] or can be induced with various edge perturbations including the insertion of biased electrodes into the plasma edge [23,24].

Although confinement in the RFP is dominated by magnetic fluctuations, electrostatic fluctuations do play a role in edge particle transport [25]. They do not, however, appear to be a significant source of energy transport at any radius. The magnetic fluctuations that account for most particle and energy losses are unlikely to be affected by flow shear away from their resonant surfaces. It is thus possible that the generation of flow shear in the edge may reduce particle transport without affecting energy transport to any significant degree.

This motivates another experiment in which the plasma is biased to produce edge flows. If shear in the flow develops, then transport by electrostatic fluctuations may be decreased and particle confinement improved. One does not expect, however, that magnetic fluctuations or energy confinement would be substantially different with biasing. Also, all improvements in particle confinement should be limited to the edge and hence steep edge density gradients should be observed.

1.2 Motivation for Electrostatic Current Injection

There are two reasons, in addition to those given above, for driving edge currents with electrostatic sources. The first is that MHD simulations show that magnetic fluctuations can be significantly reduced and confinement significantly improved by driving auxiliary currents in the edge of the RFP. The second is that inductive current drive experiments in MST have demonstrated [26,27] that core magnetic fluctuations can be reduced and that confinement can be improved by modifying the current profile. These experiments, however, are intrinsically transient and require large changes in the magnetic equilibrium.

1.2.1 Results of MHD Simulations

Several simulation codes have been used to examine the details of tearing mode stability, nonlinear coupling, the dynamo, and many other features of normal RFP discharges.

One of these, a 3-D, nonlinear, resistive MHD code called DEBS [28], has also recently been used to estimate what impact auxiliary current drive might have on magnetic fluctuations and transport. One important result of this work was to show that with appropriate choice of auxiliary current drive, the core modes, which normally make the magnetic field stochastic throughout most of the plasma, could be reduced and good flux surfaces formed. A detailed summary of these studies is given in reference [11]; a few of the highlights will be presented here.

Generic edge current drive was modeled by including an ad hoc electron force (electric field) in the parallel component of Ohm's law. The auxiliary electric field was given a Gaussian radial distribution and the location, width, and amplitude of the distribution were varied to determine what parameters worked best for reducing mode amplitudes. In general, modes could be affected whenever the auxiliary current was placed outside the resonant surfaces. The closer to the wall the current injection radius was, the greater the number of modes which could be stabilized but the larger the current needed to stabilize all targeted modes. The width of the distribution did not matter too much for stability, but wider distributions generally broadened the range of other parameters for which mode amplitudes were reduced.

When auxiliary current was placed inside a mode's resonant surface, the mode was made more unstable. For example, the $m = 0$ modes in the simulations were linearly stable without current drive and were sustained at finite amplitude by nonlinear power flow from core modes. When current drive was placed inside the $q = 0$ radius the core modes were reduced and the nonlinear power flow was reduced, but the current gradient at the reversal surface was increased and the $m = 0$ modes became linearly unstable. Thus, the simulations suggest that both the modes in the core and those at the reversal surface need to be considered in tailoring the current profile for best results.

These parameter scans were performed with a toroidally and poloidally symmetric auxiliary current. This approximation is not exactly valid in the electrostatic current drive experiments discussed in this thesis. To test the effect of injection geometry, the current was introduced in the simulations using various sets of segmented "electrodes." As expected, symmetric configurations were better for stability and discrete systems tended to drive modes unstable with mode numbers corresponding to the spatial structure of the injection. As a practical matter, however, it was noted that symmetric systems are very inefficient since the current that is injected travels only a short distance and there is a great deal of magnetic flux which intercepts the electrodes. The best scheme when these considerations were taken into account was a distributed array with a large number of injectors. In this scheme, current from each injector can make many poloidal transits and hence the current driven by the circuit is multiplied in the plasma. Also, if the number of injectors is large, the modes that are driven directly by the injection are further out in radius so a greater fraction of the plasma can be made stable.

These results are very exciting but one should remember that although the code is complex, it is not complete. There are many aspects of RFP physics that are not included (e.g., flow effects, non-Maxwellian velocity distributions, field errors, etc.) and it is always possible that some of these effects are important as well. The actual situation could be better or worse. It is also worth noting that due to computational constraints, the Lundquist number used in the simulations was about two orders of magnitude below that in MST experiments.

1.2.2 Results of Inductive Current Profile Control in MST

One of the simplest ways to drive a large amount of current in a symmetric fashion is to change the toroidal magnetic flux rapidly and allow the induced electric field to drive poloidal currents in the edge. To add to the background current, toroidal flux must be

removed. To drive current against the background, toroidal flux should be added. Experiments in which toroidal flux is removed have been done in MST [26,27] with substantial success. The scheme is called Pulsed Poloidal Current Drive (PPCD) and in the best cases, core magnetic fluctuations can be reduced by about a factor of two and energy confinement is increased by a factor of 4-5.

Although these are quite impressive results, and they go a long way toward demonstrating that current profile control works as expected, the process is inherently transient. Toroidal magnetic flux cannot be removed indefinitely. Also, the currents that are driven penetrate into the plasma on a time scale of about 10 ms; hence the current drive is not steady in space or time. Because the penetration time depends on the resistivity, the experiment is sensitive to plasma conditions.

Another inconvenience in these experiments is that the magnetic equilibrium is necessarily drastically affected. Typically, about half of the total toroidal magnetic flux is removed by injecting large amounts of negative flux at the edge. As a result, the magnitude of q at the edge can sometimes be comparable to that in the core (although the sign is opposite).

The PPCD experiments show that current profile control can be beneficial. However, any improvements are inherently transient and changes in the current profile are accompanied by severe modifications to the magnetic equilibrium. Hence, the current profile is not the only significant difference in discharges with current drive. To fully explore the impact of auxiliary edge current drive in the RFP, a scheme with more flexibility is needed.

1.2.3 Electrostatic Current Injection Concept

Electrostatic current injection refers to the process of driving current along the magnetic field by applying an electrostatic voltage between electrodes that intercept field

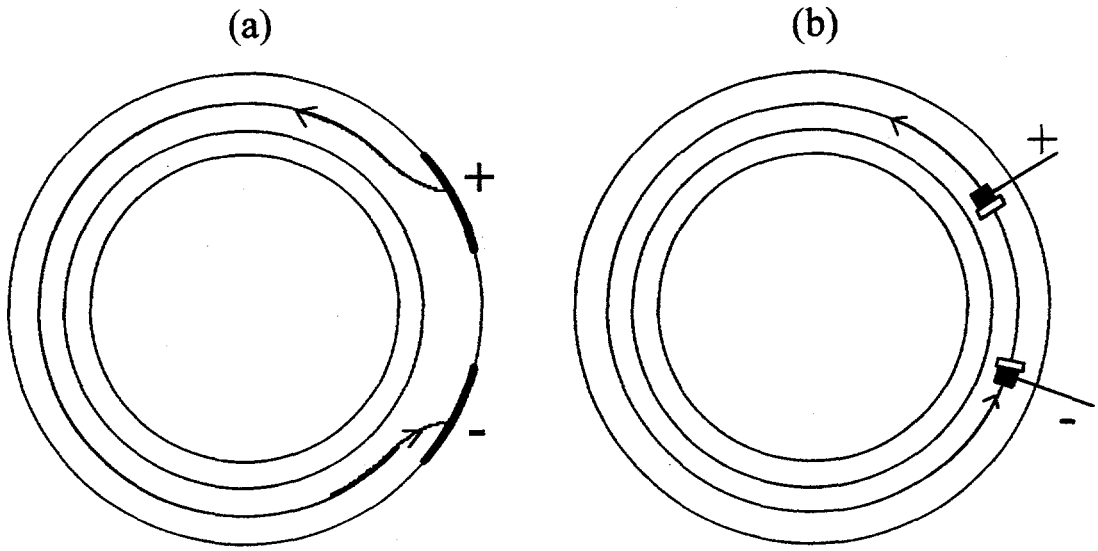

Figure 1.2. Schematic diagrams are shown for electrostatic current drive in a divertor geometry (a), and a closed field line geometry with insertable electrodes (b).

lines. One way this can be done is in a divertor configuration (see Figure 1.2a) where a portion of the edge magnetic flux is distorted to intersect with biased plates on the vessel wall. It can also be accomplished by inserting electrodes into a closed field line system and applying a potential between them as shown in Figure 1.2b. If a single electrode is inserted in the plasma and a potential is applied between this electrode and the vessel wall, current can be driven across magnetic field lines between the electrode and the wall. If, in addition, the electrode is constructed so that current can be emitted in one direction only, magnetic field aligned current can be injected and the circuit completed by cross-field currents to the wall. This is the scheme that will be used in this work and a schematic diagram is shown in Figure 1.3. Electrons are injected along field lines and an electron current equal to the injected current is simultaneously driven across magnetic field lines to the wall.

When using this type of current injection, it is particularly important to design the electrode carefully. It is fairly simple to bias an insertable electrode and drive current across

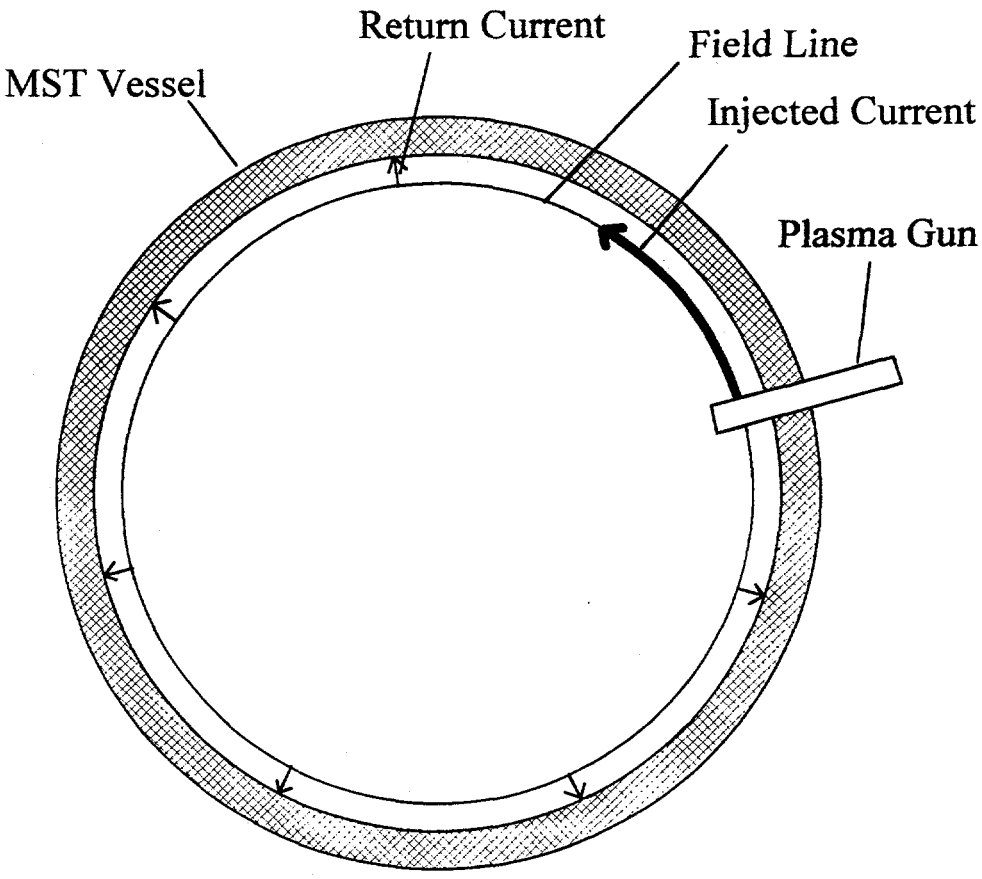

Figure 1.3. A schematic diagram of electrostatic current drive in MST is shown. For a detailed drawing of the plasma gun, see Figure 2.1.

magnetic field lines to the wall. It is much more difficult, however, to drive directional current along the magnetic field with such an electrode. The electrode used in this work is composed of a miniature insertable plasma source that is biased to inject electrons [29]; its characteristics are discussed in detail in Chapter 2.

Electrostatic current injection has several advantages as a scheme for driving edge currents. Although the injectors used in MST are pulsed for 10 ms, there is in principle no reason why such a system cannot be used to drive current steady state. There is no intrinsic modification of the magnetic equilibrium as in PPCD experiments; hence electrostatic current

drive experiments can more clearly show the effect of changing only the current profile. Depending on the design of the electrodes, the current that is driven can be placed at different radii throughout the edge and, as mentioned in Section 1.2.1, the system can be made very efficient if many discrete sources are used together.

The main disadvantage of all electrostatic current drive systems is that magnetic field lines are required to intercept material surfaces at some point. This means that there will be enhanced losses due to particles streaming along the field to the electrodes. Also, any currents naturally driven in the edge will be cut off by the electrodes. Hence, the injected current must first replace the lost currents before any auxiliary currents can be driven. In some circumstances there is also a practical limitation connected with the ability of electrode materials to withstand plasma heat fluxes. This may limit the depth to which electrodes can be inserted in a closed field line system and in MST limits the experiments to low plasma currents.

One important advantage of using the particular setup shown in Figure 1.3 is that both edge current drive and plasma biasing can be accomplished with the same system. Since the electrical conductivity is very low perpendicular to magnetic field lines, the injected current first charges up the plasma until a strong electric field is established that can drive the return currents back to the wall. Hence, parallel current drive and plasma biasing can be explored simultaneously. There is some complication in determining which observations are due to current drive and which are due to plasma biasing but the effects are easily sorted out by comparing and contrasting several different types of shots as discussed in Chapter 4.

1.3 Overview and Outline

The remainder of this thesis is divided into 4 chapters. In Chapter 2, the character of biased plasma guns as current sources are discussed. Since this is a novel approach to

current drive and biasing in a magnetic confinement device, some space will be allocated to describe both the internal arc discharge of the source and the way in which the source is used to inject current. Many experiments were performed with the source on a separate test stand to determine its operational limits, impurity characteristics, and performance as an emissive electrode. The results of these tests will be presented in Chapter 2.

In Chapter 3, the process of electrostatic current injection and biasing in MST will be discussed. There are several key differences between current extraction in the test stand and current drive in MST. One of the most important is that in MST current is driven both along and across magnetic field lines. The cross-field current drive facilitates plasma biasing but also increases the effective impedance of the injection circuit. The amount of the increase depends on both the edge plasma parameters and the specific geometry of the injection system in a way that is roughly consistent with simple notions of radial conductivity.

For purposes of modifying the magnetic fluctuations through current profile control, it is important to know where the injected current goes after leaving the gun and what the combined distribution of currents from many injectors looks like in MST. An empirical toroidal model for describing edge magnetic field line trajectories is presented in this chapter. It is used in conjunction with probe measurements of actual injected currents to place limits on the extent to which current stays attached to the field line on which it was injected. The results are used to forecast the distribution of current driven with 16 injectors. Results of cylindrical equilibrium modeling of current injection discharges will also be presented.

In Chapter 4, the results of experiments designed to control fluctuations and transport using the plasma guns are presented. Several different types of shots are compared and contrasted to isolate the effects of injector presence, plasma biasing, and directional current drive. The impact of each on fluctuations and confinement is described. Edge current drive is shown to have a substantial effect on the $m = 0$ modes resonant at the reversal surface. These modes increase when current is driven against the background current and decrease

when injected current adds to the background. The core resonant modes are not reduced in a time-averaged sense in these experiments although the sawtooth oscillations in which they participate are affected. Both particle and energy confinement respond to the changes in m = 0 mode amplitudes which strongly suggests that these modes are an important factor in determining global confinement in MST.

Plasma biasing is shown to bring about strong edge E×B flows as expected and a considerable increase in the number of stored particles despite no significant change in the hydrogen part of the source term. The contribution of impurities to the particle source term is discussed and estimates suggest that it is probably not enough to account for all of the observed increase in stored particles. Hence, particle confinement likely improves with biasing and an observed steeper edge density gradient supports this conclusion. Although electrostatic fluctuations are modified by plasma biasing, magnetic fluctuations are not strongly affected and the energy confinement does not improve. These results are all consistent with the picture that electrostatic fluctuations contribute to particle transport in the edge and are amenable to the effects of sheared E×B flows. They are also consistent with the idea that energy confinement is determined by magnetic fluctuations which do not respond to the flow structures created in these experiments.

The changes in confinement due to insertion of the injectors are also discussed. It is shown that the loop voltage and magnetic fluctuations increase when injectors are inserted. The perturbation in the loop voltage is sensitive to the plasma density and to the degree of reversal in a way that again points to the significant role of the m = 0 modes in the global power balance.

In Chapter 5 the results are summarized and suggestions for future work are made.

References

[1] Sergio Ortolani and Dalton D. Schnack, *Magnetohydrodynamics of Plasma Relaxation*, World Scientific Publishing Co., Singapore (1993).

[2] H.A.B. Bodin, A.A. Newton, Nucl. Fusion **20**, 1255 (1980).

[3] H.A.B. Bodin, Nucl. Fusion **30**, 1717 (1990).

[4] S. Ortolani, Plasma Phys. Controlled Fusion **31**, 1665 (1989).

[5] R.N. Dexter *et al.*, Fusion Technol. **19**, 131 (1991).

[6] G. Fiksel, S.C. Prager, W. Shen, and M. Stoneking, Phys. Rev. Lett. **72**, 1028 (1994).

[7] M.R. Stoneking *et al.*, Phys. Rev. Lett. **73**, 549 (1994).

[8] H.P. Furth, J. Killeen, and M.N. Rosenbluth, Phys. Fluids **6**, 459 (1963).

[9] S. Assadi, S.C. Prager, and K.L. Sidikman, Phys. Rev. Lett. **69**, 281 (1992).

[10] E.J. Caramana, R.A. Nebel, and D.D. Schnack, Phys. Fluids **26**, 1305 (1983).

[11] C.R. Sovinec, Ph.D. thesis, University of Wisconsin - Madison (1995).

[12] E.J. Caramana and D.A. Baker, Nucl. Fusion **24**, 423 (1984).

[13] H.R. Strauss, Phys. Fluids **28**, 2786 (1985).

[14] H. Ji, A.F. Almagri, S.C. Prager, and J.S. Sarff, Phys. Rev. Lett. **73**, 668 (1994).

[15] A.B. Rechester and M.N. Rosenbluth, Phys. Rev. Lett. **40**, 38 (1978).

[16] P.W. Terry *et al.*, Phys. Plasmas **3**, 1999 (1996).

[17] H. Biglari, P.H. Diamond, and P.W. Terry, Phys. Fluids B **2**, 1 (1990).

[18] T. Chiueh, P.W. Terry, P.H. Diamond, and J.E. Sedlak, Phys. Fluids **29**, 231 (1986).

[19] Ch.P. Ritz, H. Lin, T.L. Rhodes, and A.J. Wootton, Phys. Rev. Lett. **65**, 2543 (1990).

[20] R.J. Groebner, Phys. Fluids B **5**, 2343 (1993).

[21] F. Wagner *et al.*, Plasma Phys. Controlled Fusion **36**, A61 (1994).

[22] O. Sakai, Y. Yasaka, and R. Itatani, Phys. Rev. Lett. **70**, 4071 (1993).

[23] L.G. Askinazi *et al.*, Nucl. Fusion **32**, 271 (1992).

[24] R.J. Taylor *et al.*, Phys. Rev. Lett. **63**, 2365 (1989).

[25] T.D. Rempel *et al.*, Phys. Fluids B **4**, 2136 (1992).

[26] J.S. Sarff *et al.*, Phys. Rev. Lett. **72**, 3670 (1994).

[27] M.R. Stoneking *et al.*, Phys. Plasmas **4**, 1632 (1997).

[28] D. D. Schnck *et al.*, J. Comput. Phys. **70**, 57 (1986).

[29] G. Fiksel *et al.*, Plasma Sources Sci. Technol. **5**, 78 (1996).

2. BIASED PLASMA GUNS AS CURRENT SOURCES

Plasma sources are routinely used for many applications throughout science and industry. Although the idea of using a plasma source as an emitter of charged particles is not new [1,2,3,4,5], the use of a plasma source as a virtual electrode for biasing and current drive in a magnetic confinement device is [6]. Much effort has been made to characterize and understand the plasma gun source used for these studies with an eye toward optimizing it as a clean, reliable, intense current source. Indeed, these studies have demonstrated the advantages and disadvantages of this type of current injector and have established several important constraints on the successful use of these sources as electrodes.

In this chapter I describe in some detail the plasma gun construction and its operation both as a plasma source and a current source. In Section 2.1, I describe the relevant hardware and the source configuration. In Section 2.2, the character of the internal discharge is discussed. In Section 2.3, I describe the operation of the plasma gun as a current source and the properties of the injected current. In Section 2.4, I summarize and conclude with a list of advantages and disadvantages.

2.1 Source Configuration and Hardware

2.1.1 Source Configuration

The plasma gun sources used in this work evolved from earlier designs by researchers at the Institute of Nuclear Physics in Novosibirsk, Russia [7,8] and by G. Fiksel [9]. A schematic drawing of the plasma gun used for current injection in MST is shown in Figure 2.1. The discharge chamber (see Figure 2.2) is composed of a cathode and anode separated by a set of alternating conducting and insulating washers that define and stabilize the discharge (see Section 2.2). The anode is ring shaped so plasma is allowed to flow out

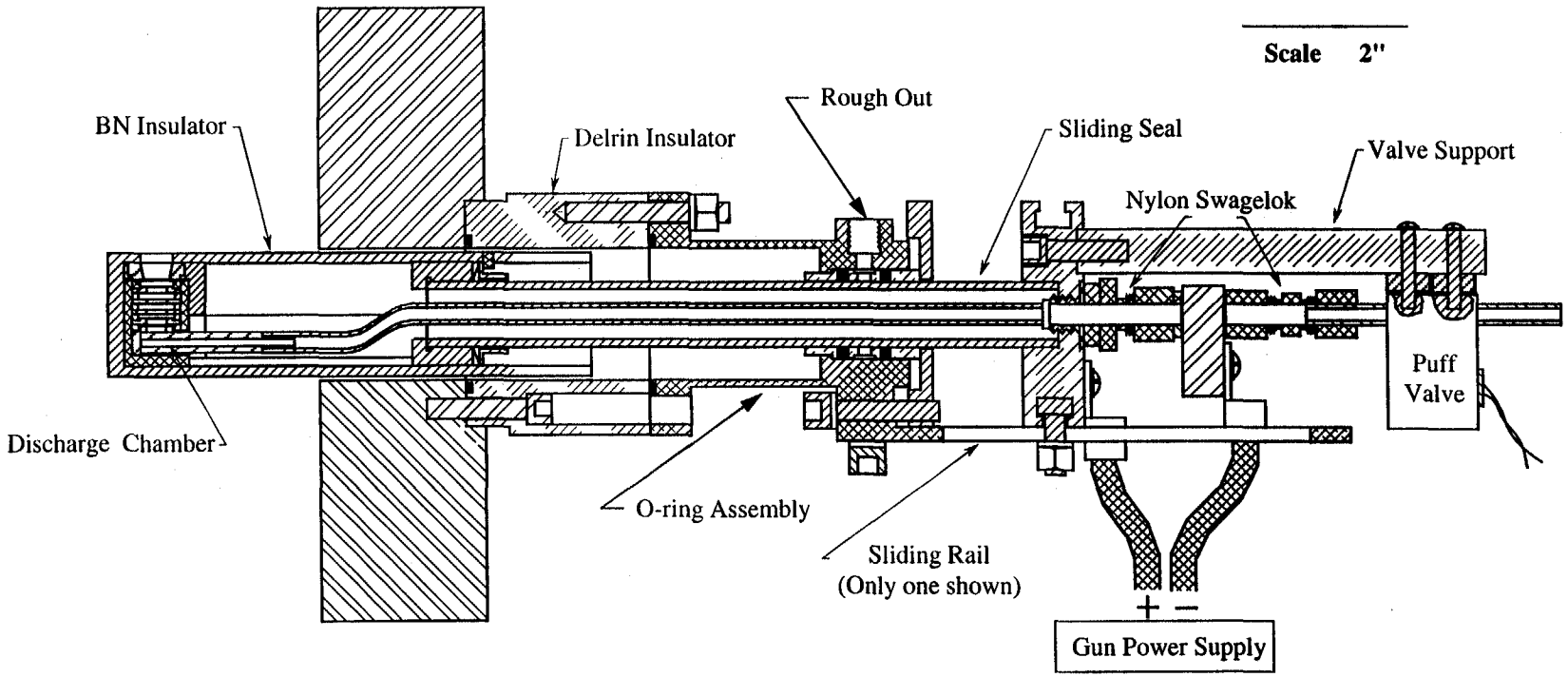

Figure 2.1. Schematic of MST style injector.

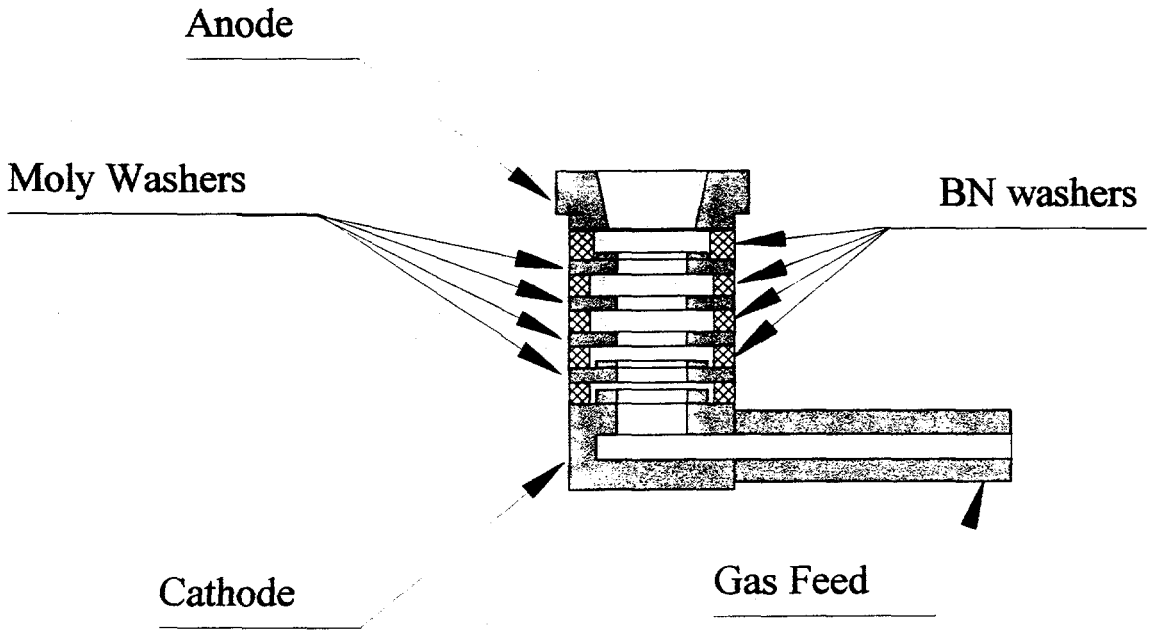

Figure 2.2. Magnified view of discharge chamber for plasma gun used in MST.

of the discharge chamber through the hole in the anode. The assembly of electrodes and washers, as well as all necessary gas and electrical connections, fit inside a cylindrical insulating shield with a hole that is aligned with the anode. It is through this opening that plasma and current are injected.

All plasma facing conductors are made of molybdenum and all plasma facing insulators are made from boron nitride. Molybdenum is chosen because it is relatively difficult to sputter, has a high melting point, has good thermal and electrical properties, and is readily machineable. Boron nitride is chosen for its excellent thermal properties and low-Z composition. Both materials are compatible with high vacuum plasma environments in which cleanliness and the ability to withstand large transient heat fluxes are crucial to performance. Electrical connections to the electrodes are accomplished with copper and the molybdenum electrodes are vacuum brazed to the copper leads for good electrical contact.

The latest version of the injector includes a vacuum interface with a double O-ring sliding seal, allowing the entire source to be easily inserted (up to r/a ~ 0.88) and rotated so that the discharge axis is aligned with the background magnetic field. Because of this compact and flexible arrangement, the injectors could easily fit through the many standard 1.5" diameter portholes that were already present in the MST vacuum vessel.

2.1.2 Puff Valve

The source is fueled with hydrogen gas through a hole in the cathode and the gas flow is controlled by a solenoid-type puff valve equipped with a small needle to restrict flow (see Figure 2.3). The valve, manufactured by Precision Dynamics, has a relatively fast time response. With a suitable choice of aperture, a gas flow waveform as shown in Figure 2.4 can be achieved. In order to minimize the perturbation to MST, it was desirable to puff as little gas as possible. For a given flow and discharge length, this means a "square" waveform in time is optimal.

To achieve a square gas pulse, several steps were taken. The first of these was to select a valve with fast time response. Measurements of valve performance indicate that the Precision Dynamics valve equipped with a stiff spring, can have an open-close time of as little as 5 ms. Secondly, the path for gas flow to the discharge chamber was chosen so that the valve was the dominant factor in determining the width of the gas pulse in time. All conductances for components before and after the needle are large compared with the needle and there is virtually no volume between the needle and the valve orifice. Upon opening the valve, gas flows through the system at a rate determined by the diameter and length of the needle as well as the gas pressure in the feed line. After leaving the needle, this fuel reaches the discharge chamber with relatively little resistance although with some delay (caused by the effective inductance of the long copper tube). Upon closing the valve, whatever gas remains in the volume between the valve orifice and needle flows out at a constantly slower

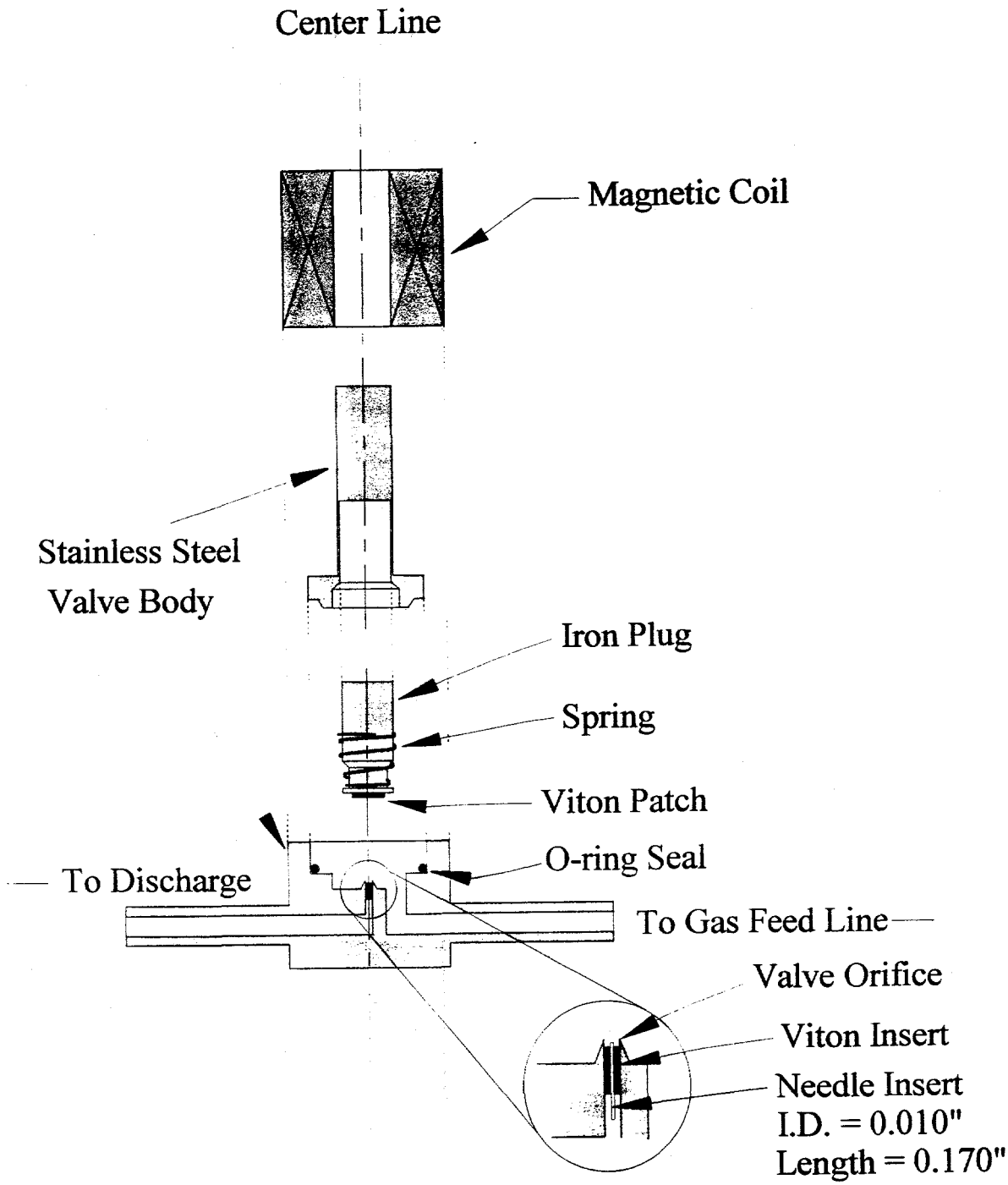

Figure 2.3. Schematic of gas puff valve used for fueling plasma gun discharges. The valve is manufactured by Precision Dynamics, Inc. of New Britain, CT.

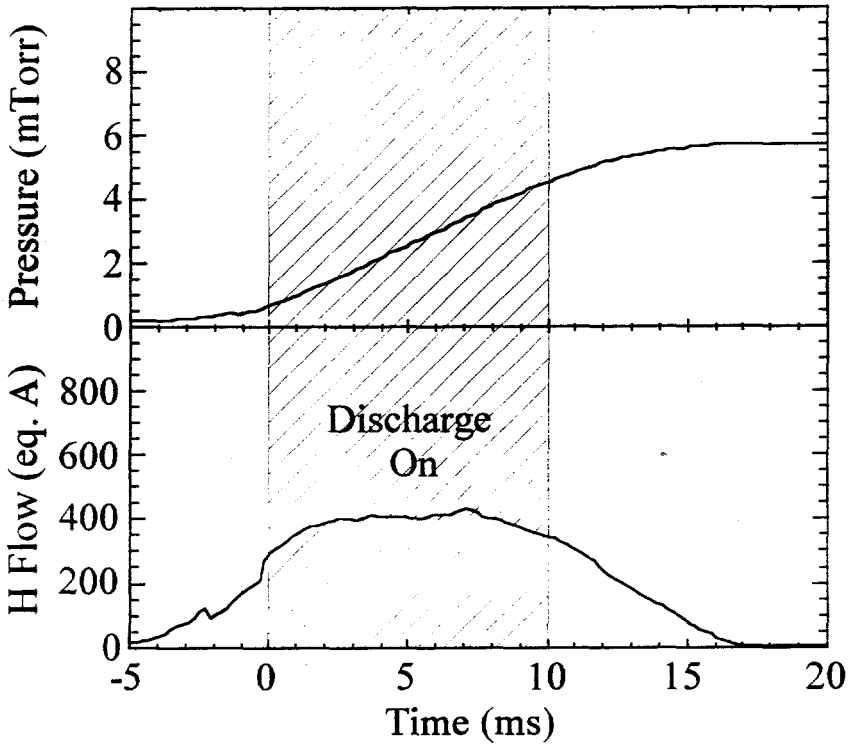

Figure 2.4. Measured waveforms for Fast Ion Gauge pressure in the test stand and the corresponding hydrogen flow. The time during which the plasma gun discharge would be active is indicated.

rate due to the constantly decreasing pressure in this volume. If the needle is placed further downstream, this volume becomes large and results in a long tail on the flow waveform. To minimize the tail contribution to the total gas released, the needle is placed as close as possible to the valve orifice.

Figure 2.4 shows the optimized waveform of flow through the valve and needle combination. Figure 2.5 shows the dependence of the flow rate on feed line pressure. The range of allowed flow rates encompasses the necessary flow rate for a discharge current of 1 kA (see Section 2.2) using feed line pressures in a comfortable operating range. A single gun operated at the optimum level of fueling releases enough gas to raise the pressure in the MST vessel to about 6×10^{-5} Torr. When a large set of injectors are employed (16 have been

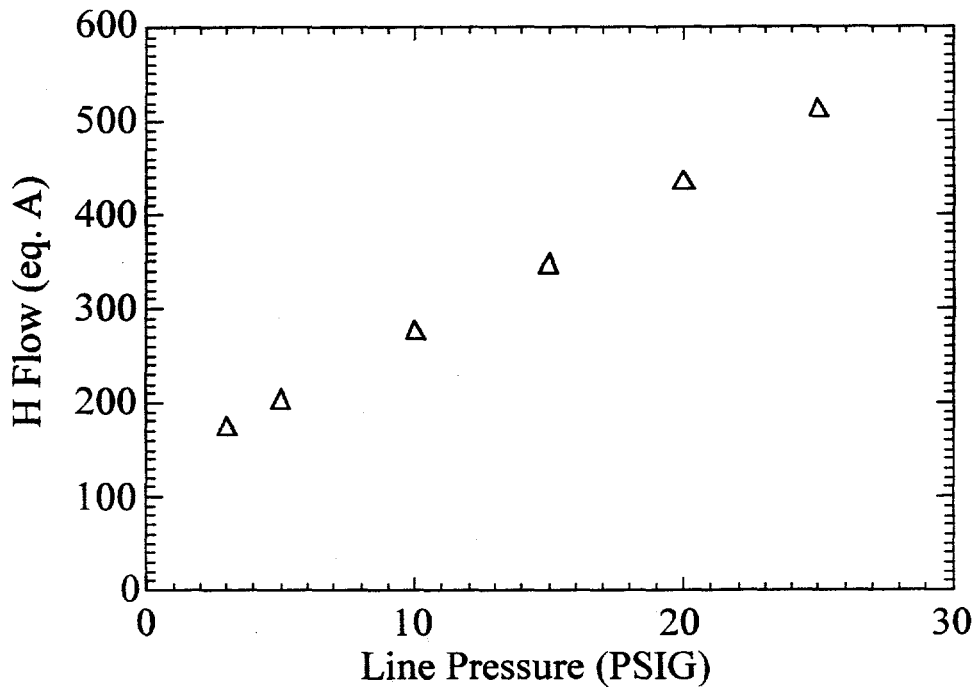

Figure 2.5. Dependence of flow rate through puff valve on feed line pressure.

implemented to date), this fueling becomes a dominant part of the fuel required to sustain the main MST discharge and sets a lower limit on what densities are achievable.

2.1.3 Power Supplies

Two power supplies are used for each injector -- a discharge supply and a biasing supply (see Figure 2.6). A four stage pulse forming network (PFN) is used for powering the internal discharge of the gun. A series resistor is used to facilitate breakdown and regulate the current once breakdown is achieved. The PFN is initially charged to between 500 V and 1 kV. Upon triggering, this entire voltage is presented to the gun electrodes since no current is flowing through the series resistor initially. Once the discharge starts and current begins to flow in the circuit, the series resistor is the dominant impedance (0.25 Ω compared with the characteristic discharge impedance ~ 0.1 Ω) and maintains the current at an acceptable level

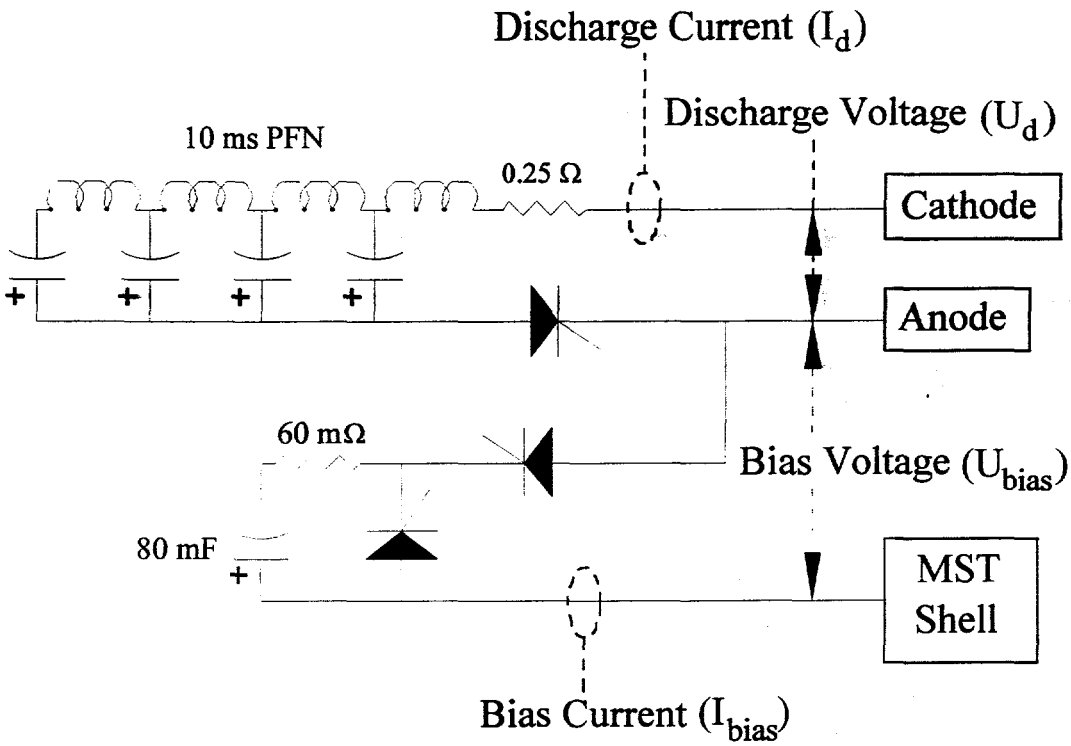

Figure 2.6. Schematic of power supplies used for a typical injector showing relevant components. One circuit of this type is used for each injector.

(~ 1 kA). The four stages result in a "square" current waveform of about 10 ms duration (see Figure 2.12b).

For current injection, a simple capacitor bank is used to bias the anode of the gun negatively. Although the effective impedance of the bias circuit depends on many factors, it is typically about 0.5 Ω. This gives an RC time constant for the bias circuit of about 40 ms which is significantly longer than the gun pulse length; thus the bias voltage does not drop much during the gun pulse. Since most of the initial charge in the bias bank is still present as the gun discharge ends, a dumping resistor/SCR combination is used to remove the voltage from the anode and prevent undesirable emission of current after the gun discharge is extinguished (see Section 2.3).

The sequence for a successful current injection event is as follows. Upon receipt of a trigger, the puff valve is pulsed and gas begins to flow into the discharge chamber. Once the flow rate has stabilized through the discharge chamber, voltage is applied between the gun electrodes, resulting in breakdown. The PFN power supply then regulates the discharge current and the bias supply drives electron current out of the gun. After 10 ms, the discharge extinguishes, the bias voltage is removed from the anode, and any remaining charge in the bias power supply is dumped through the external resistor. As will be demonstrated in the following sections, a plasma gun operated in this manner can provide intense, reliable current in a steady and relatively clean fashion.

2.1.4 Test Stand Configuration

Measurements of plasma parameters and optimization of the injector were accomplished almost entirely on a test stand that was equipped with magnetic coils, pumps, and diagnostics as shown in Figure 2.7. The two magnetic coils shown could be operated in steady-state with water cooling and each yielded a field on axis of about 2 Gauss/Amp. The power supply used could provide up to 450 A resulting in a field of about 1 kGauss. The coils were positioned to provide an approximately uniform field at the injector locations; the approximate resulting field lines are shown in Figure 2.8 It is important to note that the shape of the magnetic field lines causes the plasma and current injected by the gun to be spread out significantly at the location where plasma flow and current profiles were measured. As a result, the actual spatial distribution of plasma or current leaving the source is much narrower than measured. This effect is demonstrated in Figures 2.13 and 2.20.

Gas pressure in the vessel was measured with a fast ion gauge that was absolutely calibrated for hydrogen against a barometer. Since the fluid conductance of the vacuum vessel was quite large compared with that of the plasma source and the pumping rate was

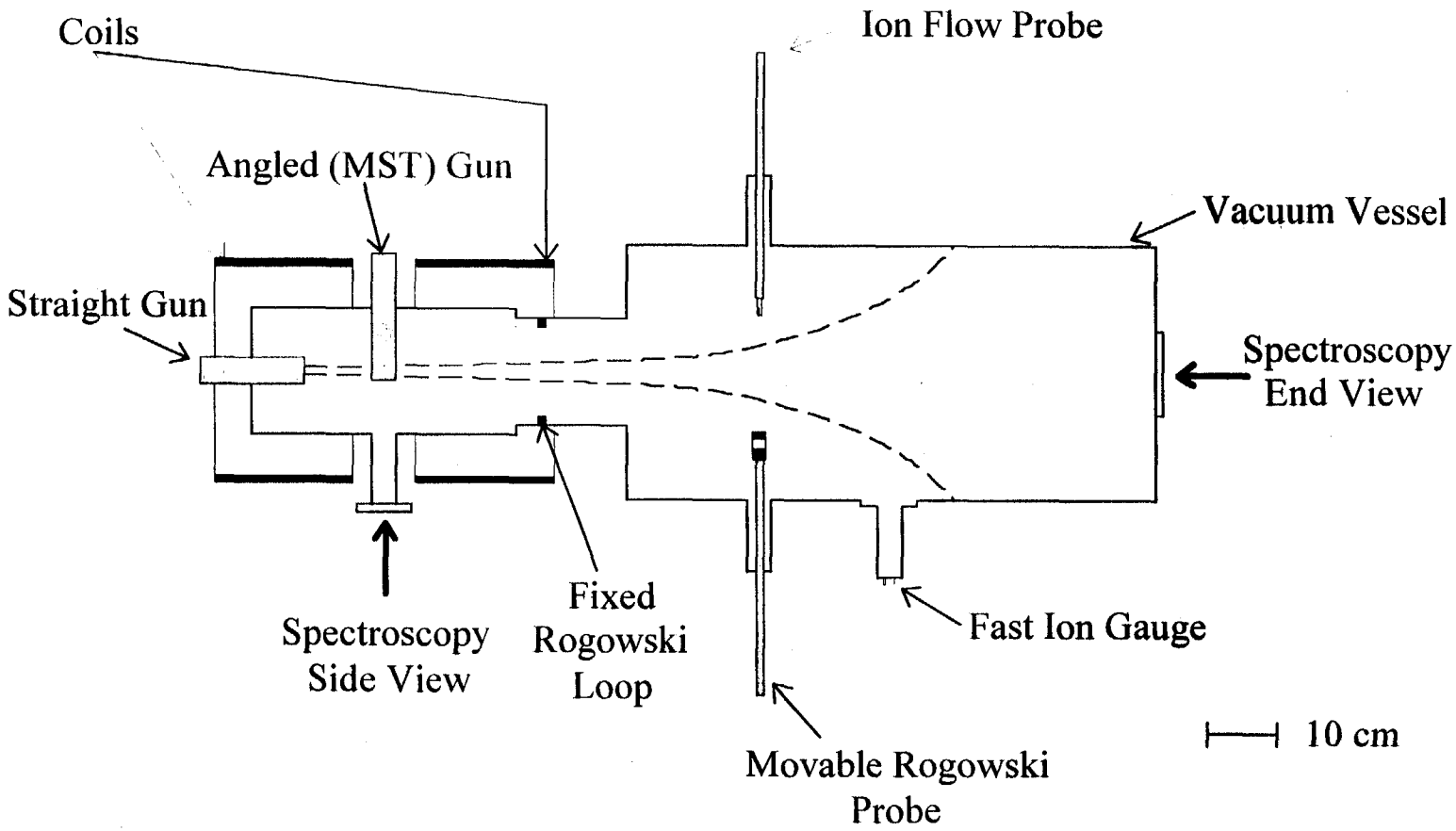

Figure 2.7. Test stand layout showing relevant diagnostics.

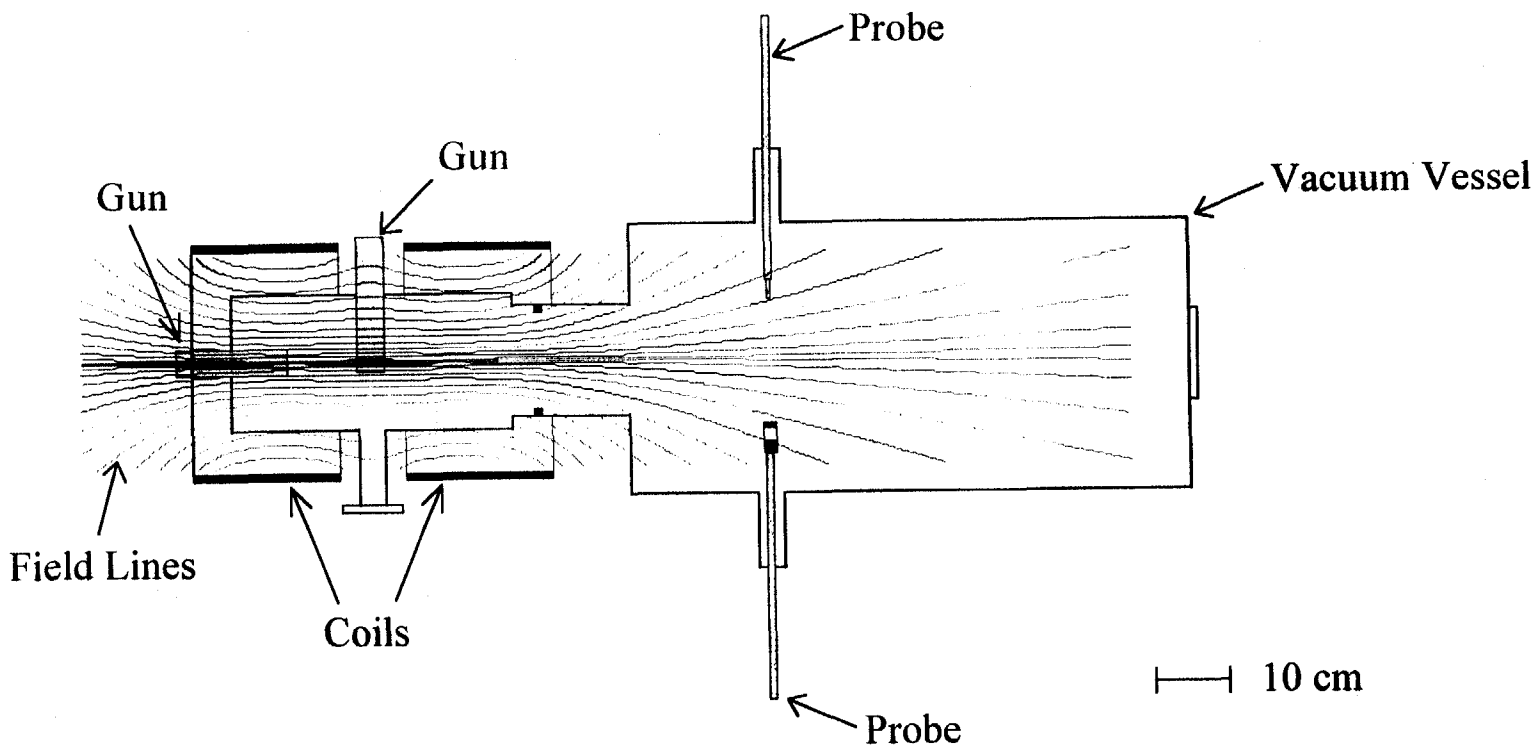

Figure 2.8. Test stand layout with magnetic field lines overlaid.

relatively slow, the time derivative of the measured pressure could be used to estimate the gas flow rate through the source. The flow rate in equivalent Amperes is given by

$$I_{gas} = 2e\left(\frac{V_{vessel}}{kT}\right)\frac{dP_{vessel}}{dt}, \tag{2.1}$$

where P_{vessel} is the measured pressure, V_{vessel} is the volume of the vessel, T is the temperature of the gas (assumed to be at room temperature), k is Boltzmann's constant, e is the electron charge, and the 2 accounts for the diatomic nature of hydrogen (each molecule yields 2 ions). In more conventional units, 10 equivalent Amperes of hydrogen atoms is the same as 1 Torr-l/s.

Plasma flux was obtained with a small movable collector biased to collect ions. A voltage of about -25 V with respect to ground was usually adequate to collect ion saturation current. The probe was designed to collect current from one direction only (facing the plasma source) through a 1.4 mm diameter circular aperture. The ion saturation current as measured by this probe indicated how much plasma was produced by the source and was a sensitive measure of its stability as well.

Impurity line radiation in the ultraviolet and visible portions of the spectrum were measured with several optical diagnostics. A monochromator/photomultiplier combination was used to measure time dependent emission at a single wavelength. For spectral surveys, a spectrometer equipped with a CCD camera on the exit plane was used [10]. By comparing light collected from two different views (see Figure 2.7) one could determine the relative abundance of impurities in the gun and in the plasma stream leaving the gun.

In addition to the source shown in Figure 2.1, many of the studies on the test stand were accomplished with the source shown in Figure 2.9. This source permitted easy modification allowing different anodes, cathodes, and washers to be combined to form internal discharges with a range of dimensions and aspect ratios. The inner diameter of the

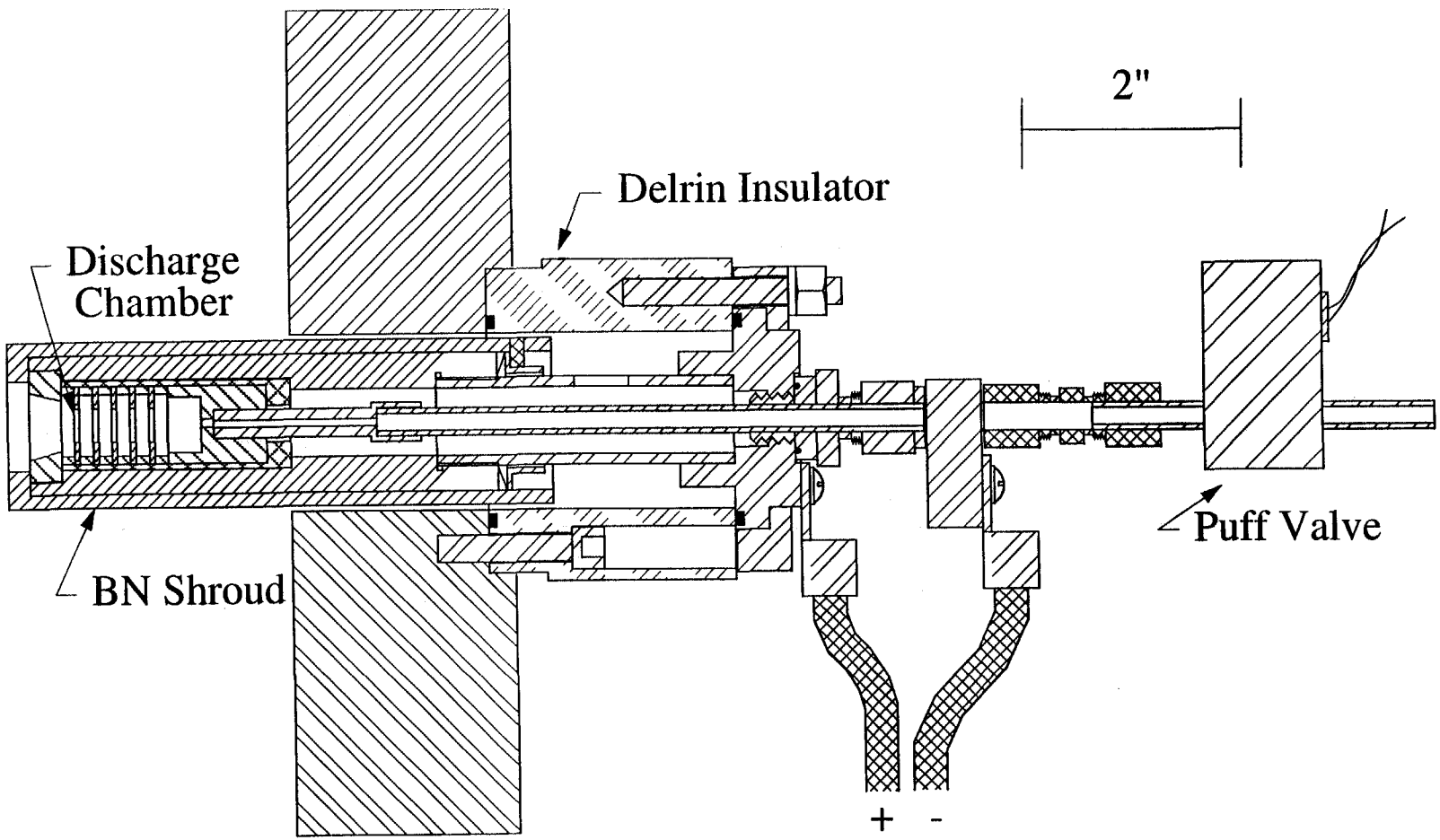

Figure 2.9 Schematic of "straight" gun configuration.

floating washers determines the discharge diameter. This could be varied from 2.5 mm to 10 mm. The distance between cathode and anode determines the discharge length. This could be varied from 10 mm to 25 mm. When the "angled" configuration (chosen for MST) was used, it was situated midway between the two magnetic coils (see Figure 2.7) and oriented so that the axis of the discharge chamber was aligned with the magnetic field. When the "straight" configuration shown in Figure 2.9 was used, the source was mounted on the end of the test stand, again with the discharge chamber and magnetic field aligned. Data from both gun configurations will be presented with reference made to the particular source used when relevant. The exact plasma parameters and performance do change somewhat as the discharge geometry is varied. Despite this variation, there exist certain thresholds, optima, and qualitative features which are common to all geometries.

2.2 The Internal Discharge

I will refer to the discharge sustained between the plasma gun cathode and anode as the "internal discharge". (This is to be contrasted with the external discharge which exists throughout the MST vessel.) It is clear from the parameters in Table 2.1 that the electrons in the discharge are well magnetized ($\rho_e << D$, $\nu_e << f_{ce}$) and fairly collisional ($\lambda_{mfp,e} \sim L$). The ions are only weakly magnetized ($\rho_i \sim D$, $\nu_i \sim f_{ci}$) but are also fairly collisional ($\lambda_{mfp,i} \sim L$). The resulting situation is one of approximate thermal equilibrium between the ions and electrons but about an order of magnitude difference between ion and neutral temperature. In similar plasmas for which the diameter is much smaller than the length, a long plasma approximation can be made and the effects of the electrodes are negligible for most of the discharge. This is not the case in the discharge used here and electrode effects are likely to play an important role in the discharge. In all, we have a short, somewhat collisional, partially magnetized plasma with at least two relevant dimensions to consider.

Parameter	Value	Parameter	Value
Discharge Diameter, D	0.6 cm	Pulse Length	10 ms
Discharge Length, L	1.7 cm	Electron Mean Free Path, $\lambda_{mfp,e}$	0.7 cm
Plasma Density, n_e	10^{14} cm^{-3}	Ion Mean Free Path, $\lambda_{mfp,i}$	0.4 cm
Electron Temperature, T_e	15 eV	Electron Collision Frequency, ν_e	75×10^6/s
Ion Temperature, T_i	10 eV	Ion Collision Frequency, ν_i	1×10^6/s
Neutral Temperature, T_n	1 eV	Electron Gyroradius, ρ_e	0.01 cm
Gas Pressure, P	1 Torr	Ion Gyroradius, ρ_i	0.3 cm
Discharge Current, I_d	1 kA	Electron Gyrofrequency, f_{ce}	3 GHz
Discharge Voltage, U_d	100 V	Ion Gyrofrequency, f_{ci}	1 MHz

Table 2.1. Typical values for relevant parameters within the internal discharge. Parameters inside the internal discharge were either extrapolated from probe measurements outside or inferred from spectral broadening of neutral hydrogen and impurity lines due to Doppler and Stark broadening. A magnetic field strength of 1 kGauss is assumed.

Because of the difficulty of modeling such a situation at a fundamental level, we have studied the source from an empirical perspective. In this section, I will describe the results of these studies, focusing primarily on the fueling requirements of the discharge and impurity generation. The identification of a minimum necessary fueling rate at a given discharge current was one of the main results of this work. In Section 2.3, it is shown that the discharge current determines the amount of bias current which can be extracted from the source so this fueling requirement can be viewed as the minimum amount of gas fueling needed for a desired level of injected current. The other main result of these studies was to show that most of the impurities generated in the gun do not escape into the plasma flowing out of the gun and hence the gun is a clean plasma source.

2.2.1 General Features

The internal discharge may be characterized as a medium pressure hydrogen arc discharge operated in a magnetic field. It has the parameters shown in Table 2.1. Reference [11] gives a classification of electric discharges according to the current and voltage drop between the electrodes. The plasma gun operates with a current of about 1 kA and a voltage drop of 50-100 V putting it squarely in the arc regime. Reference [11] also suggests a division of arc discharges into three categories: low pressure, high pressure, and transitional (or medium pressure). At high discharge pressures (> 100 Torr), there is an equilibration of all plasma and neutral species temperatures because of the high collisionality. At low pressures (< 1 Torr), collisions between electrons and ions are much less frequent and one sees substantial (orders of magnitude) difference between electron and ion temperatures. In our source, the pressure is about 1 Torr; the electron, ion and neutral temperatures are close but not exactly the same. For this reason the discharge may be described as a medium pressure arc.

Arc discharges have been studied for many years and implemented in many configurations. One interesting characteristic of arc discharges is that the current densities extracted from the cathode (~ 1 kA/cm^2 in our case) are much larger than that expected from thermionic or field emission alone. Instead, it has been observed that tiny spots form on the cathode within which very violent phenomena (melting, vaporization, explosive ejection of material, etc.) take place. It is through one or more of these spots that the discharge current is supplied [12]. Because of these phenomena, it is normally the cathode region where most impurities are introduced. Measurements were made of impurity line emission from the plasma inside and outside the gun in order to determine if these impurities escaped through the gun nozzle (see below); it appears that to a large extent they do not. Instead they are

likely trapped near the cathode by the combined efforts of a strong electric field and the dense plasma column.

Although the electron current density to the anode is comparable to that leaving the cathode, it is far easier to collect electrons on a metal surface than to emit them; hence the impurity generation that occurs at the cathode is much less likely to occur at the anode. The anode hole is larger than the discharge diameter and when a magnetic field is applied, this makes it more difficult for electrons to be collected. This may help to increase the plasma production of the source (source density is observed to be higher with a magnetic field) but at the same time, a significant potential difference develops which increases the average energy of particles collected on the anode. For this reason, the anode tends to be heated more strongly than the other components and is the first component to melt if the discharge power is too high. Simulations of heat transport indicate that for a 10 ms pulse at 1 kA, the MST-style source is close to, but slightly below the threshold for melting. In practice, melting is usually not significant unless the magnetic field and discharge chamber are not well aligned -- in which case the heat flux has strong asymmetry.

One distinguishing feature of these plasma guns is the set of floating metal washers between the cathode and anode. The role of the floating washers is not completely understood, but it is empirically known that they are crucial for stability. There are several conceivable ways in which the washers might stabilize the discharge. Since they are conductors, they can help to short out any azimuthal asymmetries in plasma potential and deter instabilities with azimuthal variation. In addition, if the plasma column distorts in such a way as to come in contact with a washer, then that part of the discharge will be cooled, plasma resistivity will increase and the current will be concentrated more on axis. In this sense the washers provide stability and also shape the plasma column.

The axial potential distribution was measured (see Figure 2.10) by assuming the potentials on the gun electrodes and washers were a reasonable indicator of relative

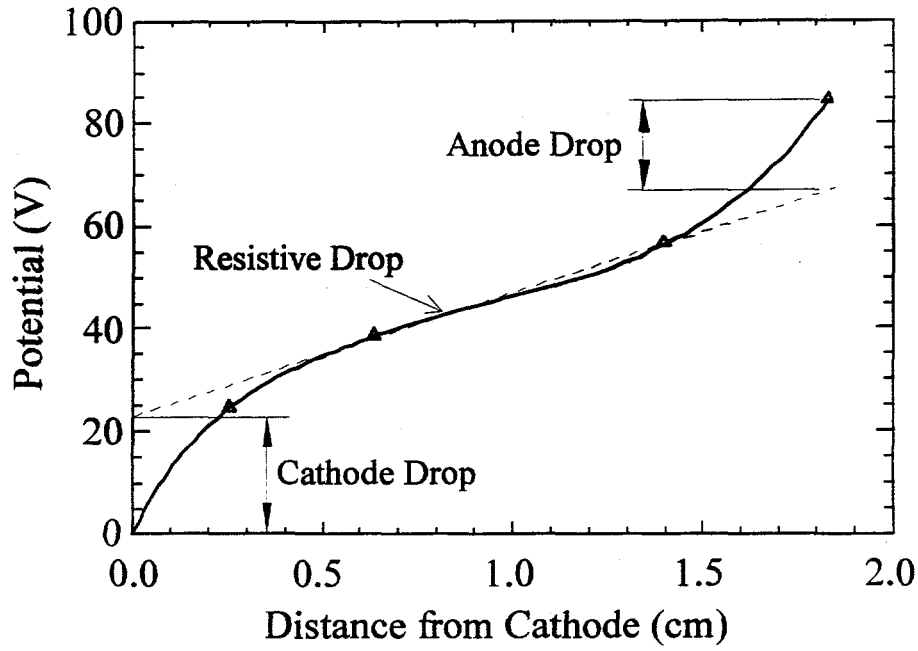

Figure 2.10. Measured potential of gun electrodes and washers demonstrating the three regions of the arc -- near cathode, plasma column, and near anode. Triangles show measured data.

potentials in the plasma. The shape of the curve is that of a classic electric discharge with three different regions. The near cathode region is dominated by interactions with the cathode and has a voltage drop characteristic of the cathode material (Mo). The plasma column occupies the middle portion of the discharge and here the potential drops in good agreement with an electric field that is balanced by resistive drag, i.e.. $E = \eta J$ with η determined by the classical Spitzer form. The near anode region is identified by another potential step that arises mostly due to the magnetic isolation of the anode as discussed above. If the magnetic field is turned off, the discharge voltage drops by about 10 V indicating that the anode is more easily reached by the current-carrying electrons.

2.2.2 Measurements of Plasma Production

To extract intense current from a plasma electrode, it is natural to expect that the source must produce an intense plasma. Studies of plasma production were done both to characterize the plasma created in the source and to define the boundaries of the operational space. As mentioned above, plasma production was quantified by measuring plasma flow out of the source with a small collector biased to collect ions. For purposes of investigating the internal discharge, most data were taken using a short pulse length power supply to allow more rapid cycling and more variation in discharge current. There appears to be no significant differences in plasma quantities between the 2.5 ms discharge and the 10 ms discharge as demonstrated in Figure 2.11.

Measurements of plasma flow demonstrate that the plasma produced by these sources is indeed intense. Figure 2.12 shows the profile of plasma flow along a radial cord through the axis of the test stand. Using the flux plot shown in Figure 2.8 and assuming that plasma flows out along magnetic field lines, one can estimate the distribution of plasma leaving the source as shown in Figure 2.12. The data suggest that plasma exits the source in an intense flow with an extent determined roughly by the discharge diameter. The plasma flow at the gun nozzle is roughly consistent with the thermal flux from a plasma with density ~ 10^{14} cm^{-3} and temperature ~ 10 eV. Langmuir probe and spectroscopic measurements (not shown) indicate similar values for these parameters and support the idea that the plasma guns used in this work generate a hearty plasma.

To arrive at the total amount of plasma produced by the source, the profile of ion flow was taken (see Figure 2.12) and integrated (assuming cylindrical symmetry) to obtain a total ion current. Figure 2.11 demonstrates that the plasma flow waveform looks very much like the discharge current waveform. The approximate proportionality of total ion current to discharge current is also evident as the discharge current is varied for any particular discharge geometry as shown in Figure 2.13. One striking feature of the data in Figure 2.13, however,

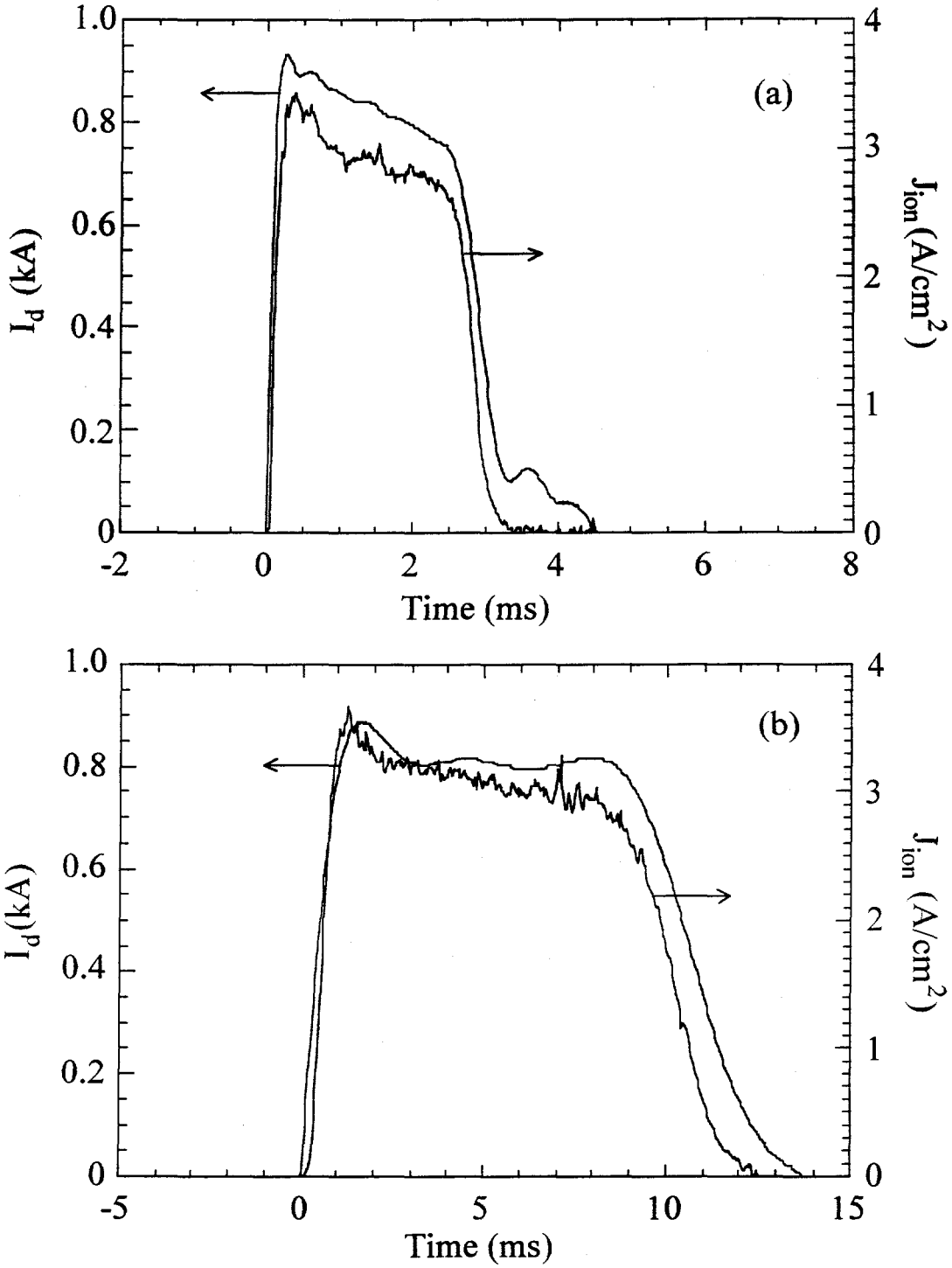

Figure 2.11. Waveforms for discharge current and plasma flow using a 3 ms power supply (a), and a 10 ms power supply (b).

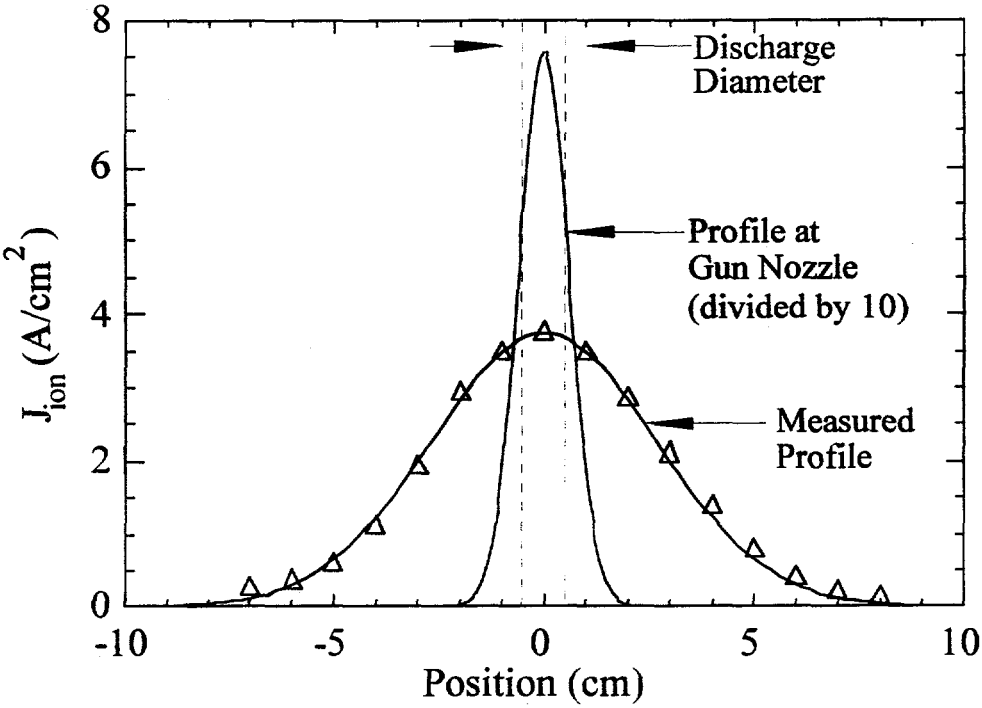

Figure 2.12. Measured plasma flow profile 60 cm away from a gun with a discharge diameter of 1.0 cm. An inferred profile at the gun nozzle is shown based on the magnetic field lines depicted in Figure 2.8.

is the saturation and eventual decrease of plasma production as the discharge current is raised while holding gas fueling constant. This behavior is a common attribute of all discharge geometries and is indicative of a minimum fueling requirement.

As the discharge current is increased for a given hydrogen flow rate, plasma production increases linearly until a critical point is reached. At this point, the discharge voltage increases and the amount of plasma flowing out of the gun saturates and becomes inconsistent (see Figure 2.14). The quality of the plasma in this "undergassed" state is generally worse -- exhibiting large fluctuations and higher levels of both low Z and Mo impurity radiation. It appears that for a given discharge current, a minimum hydrogen flow

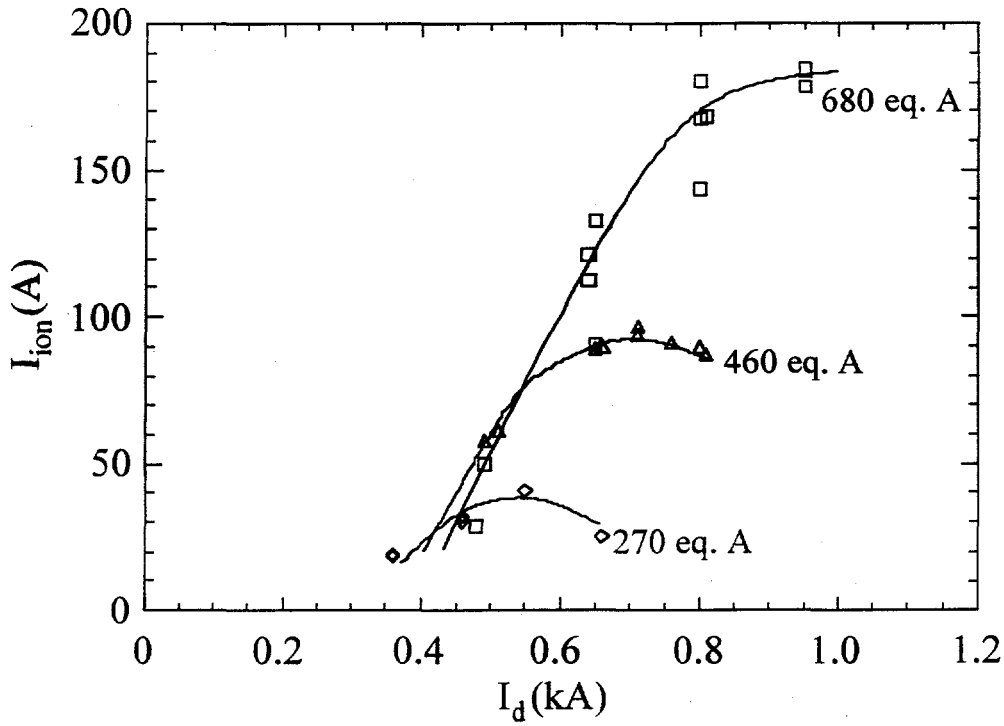

Figure 2.13. Total ion current is shown versus discharge current for three different hydrogen fueling rates. Data were obtained using the straight configuration with diameter 0.6 cm and length 1.8 cm.

rate is required for good operation. If not enough fuel is provided by gas puffing, solid components inside the discharge chamber are vaporized. The discharge then becomes more resistive and unstable.

An empirical study was done to determine how this minimum fueling rate depends on discharge current and chamber geometry. Figure 2.15 demonstrates the dependence of the minimum required gas flow rate on discharge current for several geometries including the one chosen for the MST injector. The general trend is that a higher fueling rate is needed for a higher discharge current and that for a given fueling rate, a larger diameter source can

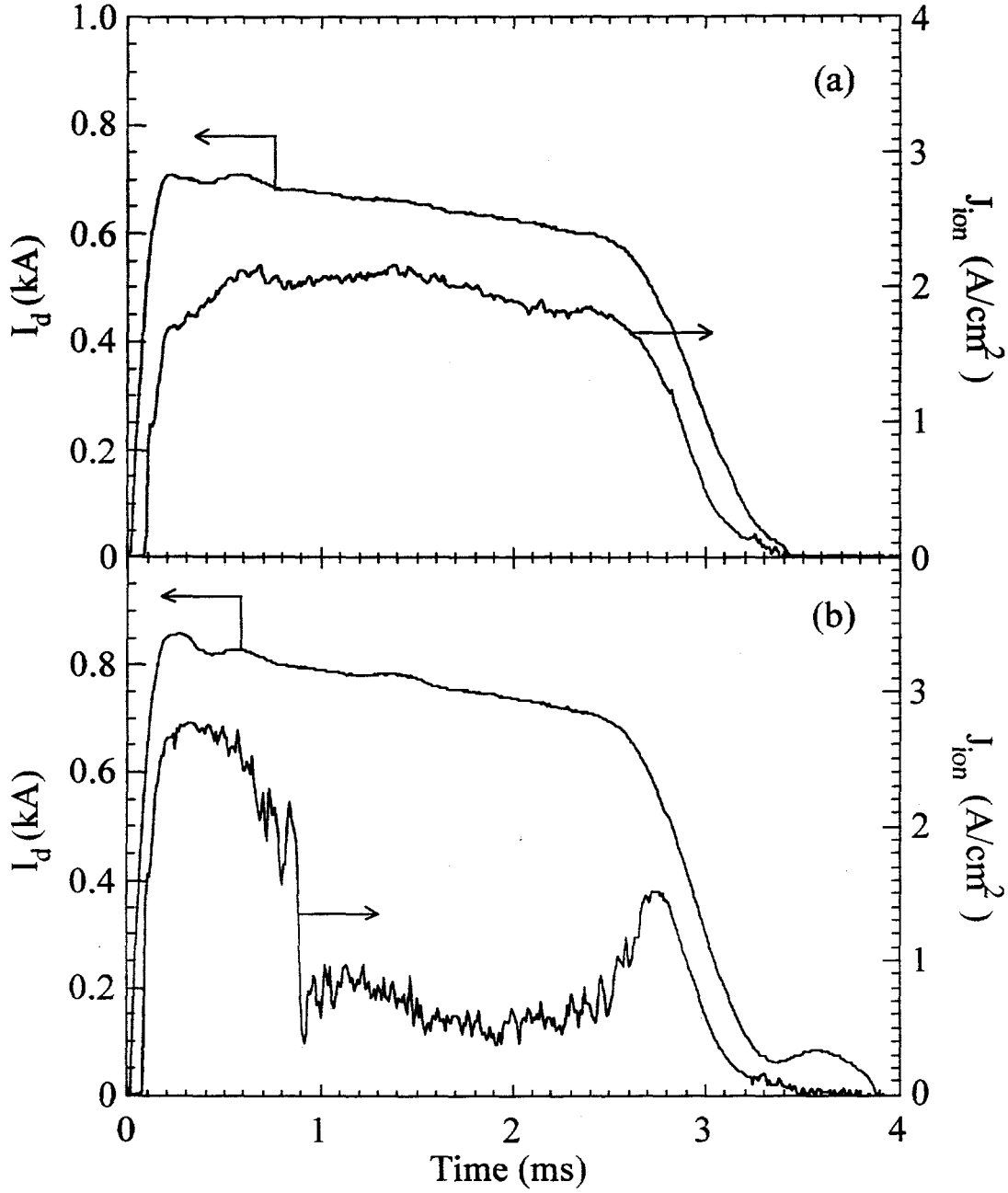

Figure 2.14. Plasma flow and discharge current for an optimally fueled (a), and an undergassed discharge (b). In both cases the fueling rate is ~ 650 equivalent Amperes.

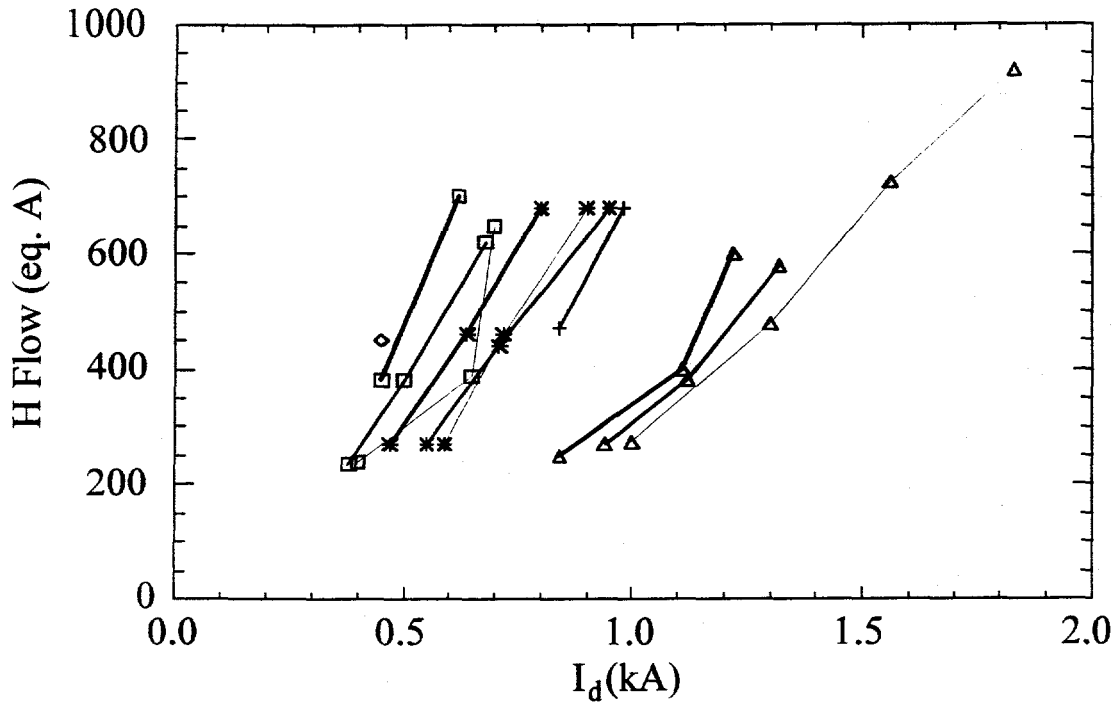

Figure 2.15. Dependence of minimum hydrogen fueling rate on discharge current for different discharge geometries. Different symbols represent various discharge diameters (◇ ↔ 0.25 cm, □ ↔ 0.4 cm, ✳ ↔ 0.6 cm, △ ↔ 1.0 cm) and line thickness represents discharge length (thin ↔ 1.0 cm, med ↔ 1.8 cm, thick ↔ 2.5 cm). The MST gun configuration (diameter of 0.6 cm, length of 1.7 cm) is represented by the + symbol.

provide a larger current. Both of these dependencies suggest that the required fueling rate is determined to a large extent by the discharge current density.

For purposes of injecting current in MST, it is desirable to have a large current and a low fueling rate. From the above studies alone, one would conclude that a larger diameter source is better and that it should be operated near the critical discharge current. For reasons to be discussed below, a large diameter is not necessarily best. In practice, the MST injector geometry is a good compromise.

2.2.3 Spectroscopic Measurements

Light emitted from the internal discharge and from the plasma flowing out of the source was collected and analyzed. This gave some indication of which impurities were produced in the source and to what extent they were present in the plasma leaving the gun [13]. All data presented in this section were obtained from the straight gun configuration using a spectrometer equipped with a CCD camera on the exit plane. With a 150 groove/mm holographic grating, the instrument had a bandpass of 110 nm with $\Delta\lambda \sim 0.3$ nm resolution. Such a scheme allowed for rapid acquisition of the full near-ultraviolet and visible spectrum while retaining enough resolution that spectral lines could be distinguished clearly.

Two views of the test stand/source system were used in this analysis. The "end" view (see Figure 2.7) permitted collection of emission from the internal discharge, the plasma leaving the source, and any light generated on or near the gun electrodes. Although this viewing geometry encompasses virtually every region of the test stand from which light would be emitted, the amount of light emitted from the internal discharge and electrodes far outweighs that from any other region. The "side" view permitted light collection only from the plasma leaving the source. Care was taken to look close enough to the source that plasma density and temperature were sufficient to give good excitation but far enough from the source that the internal discharge and electrodes were excluded from view.

Figure 2.16 shows a typical spectrum from 200 nm to 500 nm using the end view. The spectrum shown is a concatenation of spectra from three similar shots, each at a different spectrometer dial setting. Many lines are present in this view, due mostly to the presence of molybdenum which has a large number of lines in this region. Several strong lines are labeled in the figure and clearly indicate the presence of hydrogen, boron, carbon, nitrogen, and molybdenum in the internal discharge.

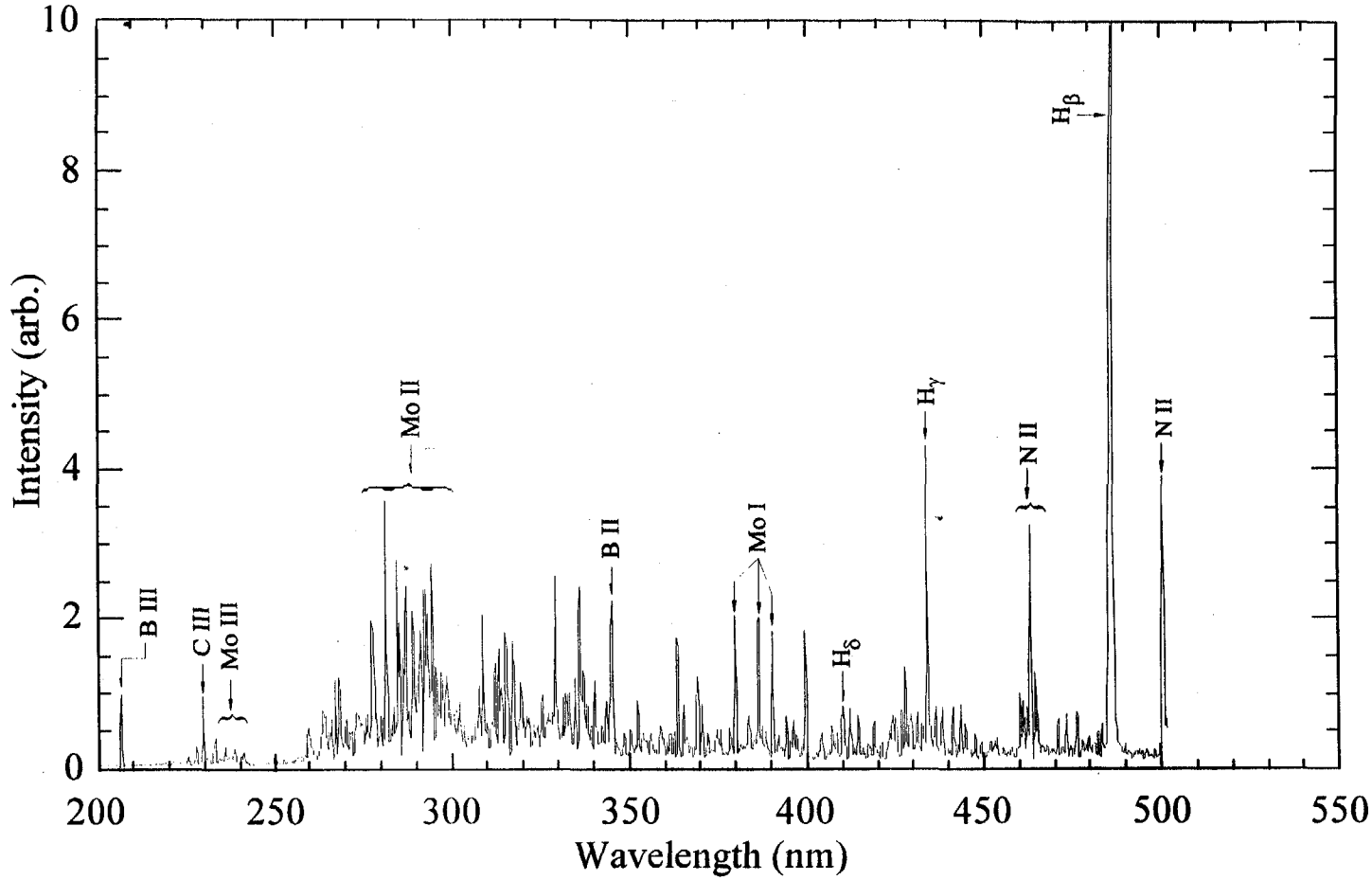

Figure 2.16. Spectral survey of a gun discharge showing several relevant lines. Data were taken from the end view on the test stand using the straight configuration.

The brightest lines are, not surprisingly, due to hydrogen which is undoubtedly the most abundant of all species present. Boron, presumably arising from the BN components of the gun, is present in the B^{+1} and B^{+2} states. Carbon is present in the C^{+1} and C^{+2} states and probably is due to surface impurities on gun and test stand components. Nitrogen, arising from atmospheric residue and BN, is present in the N^{+1} and N^{+2} states. Emission from carbon and nitrogen are not clearly tied to impurities produced in the gun since these elements are also present in the background vacuum vessel. Higher charge states of these elements do not appear to be present at significant levels, perhaps because the electron temperature is only 15 eV and the confinement time of the ions is quite short ($r_{discharge}/v_{thermal} \sim 1$ μs for boron).

By far, the majority of lines present are due to molybdenum in the Mo^{+0}, Mo^{+1}, Mo^{+2}, and Mo^{+3} states. (Mo IV lines were observed at shorter wavelengths than shown in Figure 2.16.) As discussed earlier, it is expected that most of the metal impurities are produced at the cathode because of the violent action of the cathode spots. The end view encompasses the cathode region so the strong presence of molybdenum in the spectrum is not too surprising. Since the release of molybdenum into MST would be highly undesirable, it is important to have some idea of the extent to which the molybdenum present in the internal discharge escapes through the gun nozzle. For this one must compare the side and end views.

When comparing line emission in various cases, it is important to understand what determines line intensity and hence, what changes in line intensity do or do not imply. Assuming that emission is dominated by collisional excitation of the ion or atom by electrons followed by spontaneous decay, the intensity per unit volume of a given line in steady state is given by [14]

$$I_{nm} = 5.1 \times 10^{-25} \frac{f_{nm} g_0 N_e N_0}{g_m T_e^{0.5}} \left(\frac{\Delta E_{nm}}{\Delta E_{n0}} \right)^3 e^{-\frac{\Delta E_{n0}}{T_e}} \frac{watt}{cm^3} \tag{2.2}$$

where n (m) is the initial (final) state, 0 stands for ground state, f is the oscillator strength, g is the statistical weight, N_e is the electron density, N_0 is the ground state density, T_e is the electron temperature, and ΔE_{nm} is the energy difference between states n and m. To get the intensity measured by the detector, an integral over the volume viewed by the detector must be performed. It is also important to note that the density of the emitting species, N_0, at any location depends on a balance between ionization from (and recombination to) lower charge states, recombination from (and ionization to) higher charge states, and transport processes -- all of which are in turn dependent on the full range of plasma parameters.

With this in mind, a qualitative measure of how much molybdenum leaves the gun can be obtained by comparing the ratio of intensities from the side and end views for different lines. One would expect that the side view should have a lower intensity than the end view for all lines due to a decreased collection volume. Indeed, hydrogen, boron, carbon, and nitrogen line intensities all drop by about an order of magnitude when changing from end to side views (see Figure 2.17). However, molybdenum line intensities drop by about two orders of magnitude indicating that most molybdenum is localized somewhere within the end view but outside of the side view. The only reasonable place for this localized molybdenum source is inside the gun discharge. It thus appears that most of the molybdenum produced in the gun discharge does not escape through the gun nozzle.

There are probably two main mechanisms that prevent molybdenum from escaping. Most molybdenum is produced at the cathode and is rapidly ionized because of the high plasma density. The positive metal ions are then attracted back to the negatively charged cathode where they are redeposited. Molybdenum neutrals, or ions with enough energy, can escape the cathode sheath but these rapidly encounter a dense hydrogen plasma that prevents them from leaving the gun and enhances the probability that they will be lost to the gun chamber walls before escaping through the nozzle. It is probably this combined electrostatic and dense plasma trapping that keeps most of the molybdenum in the gun.

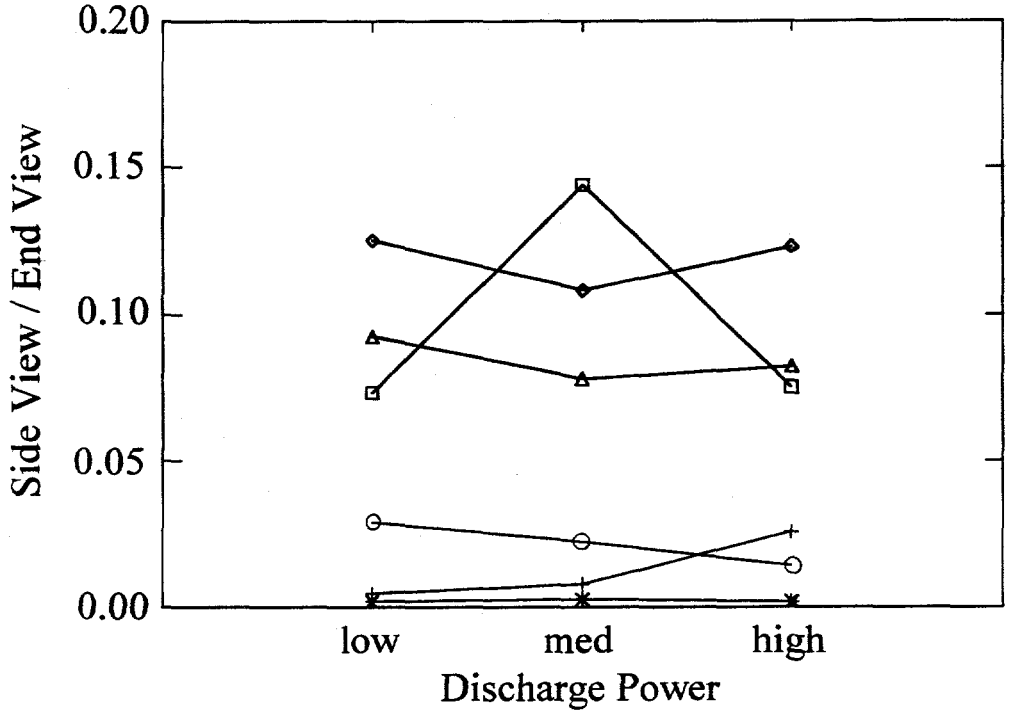

Figure 2.17. Ratio of intensities obtained from side and end views on test stand for several lines as a function of discharge power. The different symbols represent H_β (◇), H_γ (△), N II (□), Mo I (+), Mo II (✱), and Mo III (○) emission.

It is important to note that these measurements give only a qualitative measure of impurity production. To quantitatively determine how much molybdenum escapes from the gun would require a detailed transport calculation and measurements of the plasma parameters throughout the viewing volume. For current injection purposes, the impurity production is only relevant to the extent that it has an effect on the main MST discharge. Even with 16 injectors operating in MST, no molybdenum radiation has been observed except in cases where the main discharge ends during the gun discharge. (In such cases the magnetic field changes direction rapidly and is no longer aligned with the gun discharge axis.)

Incidentally, it is likely that longer discharge chambers have fewer impurities leaving the source since there is more dense plasma between cathode and nozzle. Also for a given diameter, a longer discharge chamber decreases the solid angle through which impurities leaving the cathode can escape. The best choice for discharge chamber aspect ratio from a cleanliness viewpoint would thus be thin and long. One will recall from the previous section that a wide and short aspect ratio gave the most plasma production for a given fueling rate. The MST injector is a good compromise between the desire for good plasma production and the desire for clean operation.

2.3 Plasma Guns as Current Sources

In choosing an electrode for current drive and biasing, one has several options. Cold metal electrodes readily draw electron current but do not emit electrons in large quantities unless arc spots can be induced on the metal surface. If a high enough negative voltage is applied, ion bombardment may produce secondary electrons but the current that can be driven will never be more than a few times the ion saturation current without arc spots forming. Once arc spots do form, they can produce substantial quantities of metal impurities which are not desirable in fusion relevant plasmas. Some materials (e.g., LaB_6 or thorated tungsten) readily emit electrons when heated strongly; they are capable of supplying currents much in excess of ion saturation current. Most of these materials, however, are either too fragile for use in high temperature plasmas or produce impurities along with the electrons. Depending on how the electrodes are introduced to the plasma, there may also be problems with directionality and uniformity of the emitted current, and fundamental limitations due to space charge effects.

One way to get around many of these problems is to use a plasma source as an electron emitter. Large currents can be extracted from a plasma with low voltages due to the

high electron mobility. The higher the source density and temperature, the higher the current which can be extracted. If the plasma from the source is allowed to flow out along the same path as the extracted current, space charge effects become irrelevant since any space charge due to the extracted electrons is constantly neutralized by a background of ions. The upper limit on how much current can be drawn out of the source is set in principle by how fast charge can be supplied to the source plasma itself. In the case of the arc discharges used in the present work, the maximum rate at which charge can be sourced is the discharge current. The maximum emission from the plasma source then corresponds to the case in which all charge introduced to the arc from the cathode is emitted and no electron current is returned at the anode.

The plasma electrode has two main attributes that make it attractive as a current source. First, large current densities (~1 kA) can be generated with relatively small voltages (~100 V). Secondly, production of high Z impurities can be substantially lower than for material electrodes, provided the source itself produces a clean plasma. In the previous section, it was shown that the plasma guns used in this work are clean, intense plasma sources. When a bias voltage is applied, the guns also become clean, intense current sources.

In Figure 2.18, the I-V curve for a biased plasma gun is shown. One can see the emitted current start to saturate when it reaches the discharge current. This is as expected from the discussion above. For bias voltages above this point, the character of the curve changes and it is apparent that a new source of current has been activated. The new source is the anode of the gun which begins to emit current once all available current from the discharge has been emitted. Operation in this region of the curve results in severe anode wear, higher impurity levels, and non-uniform, often erratic emission profiles. These features are undesirable. Hence, the optimal operating point for current extraction is with the bias current at or just below the discharge current.

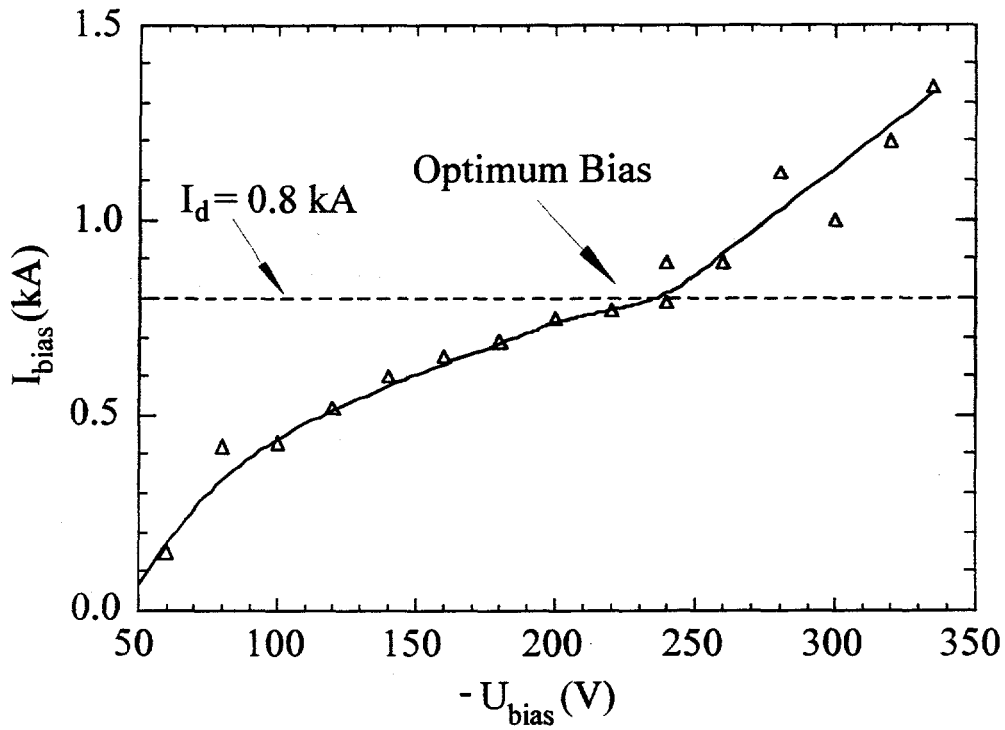

Figure 2.18. I-V curve for the biased MST style gun on the test stand. Triangles denote measured data and the dashed line indicates discharge current magnitude.

The profile of the emitted current, measured with a movable Rogowski probe on the test stand, is shown in Figure 2.19. Using the magnetic flux plot shown in Figure 2.8, and assuming that the electron current is well attached to the magnetic field, one can infer the distribution of current near the source nozzle. As was the case with the plasma flow, one sees that the current is emitted in an intense stream with a width dictated approximately by the hole in the BN shroud surrounding the gun. The peak current density for the case shown in Figure 2.19 is estimated to be about 130 A/cm^2 near the gun nozzle.

As the extracted bias current approaches the discharge current, the anode indeed plays less and less of a role in the internal discharge. This can be clearly seen in Figure 2.20 which shows the discharge voltage as a function of bias current. These data were taken with

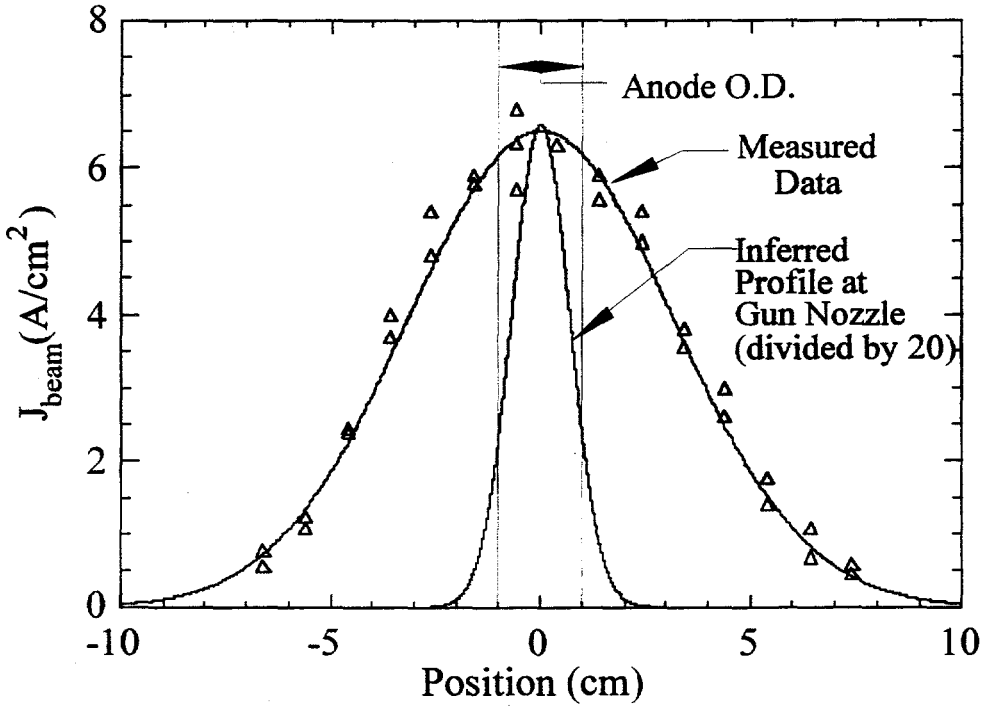

Figure 2.19. Emitted current profile measured 60 cm away from a gun on the test stand. An inferred emission profile at the gun nozzle is shown based on the magnetic field shown in Figure 2.8. The discharge diameter of the gun was 0.4 cm and the diameter of the opening in the BN shroud was 2 cm as shown.

a gun for which the anode inner diameter was substantially larger than the discharge diameter so that the part of the discharge voltage arising from magnetic isolation of the anode was enhanced. One can see from the figure that as the bias current increases, the discharge voltage drops slowly until the bias current matches the discharge current. At this point, the discharge voltage drops substantially (by about 15 V) demonstrating that the anode is no longer an important part of the discharge circuit.

If the bias dumping SCR is not used (see Figure 2.6), then the voltage still remains on the anode after the internal discharge has extinguished. Plasma exists in the vicinity of the

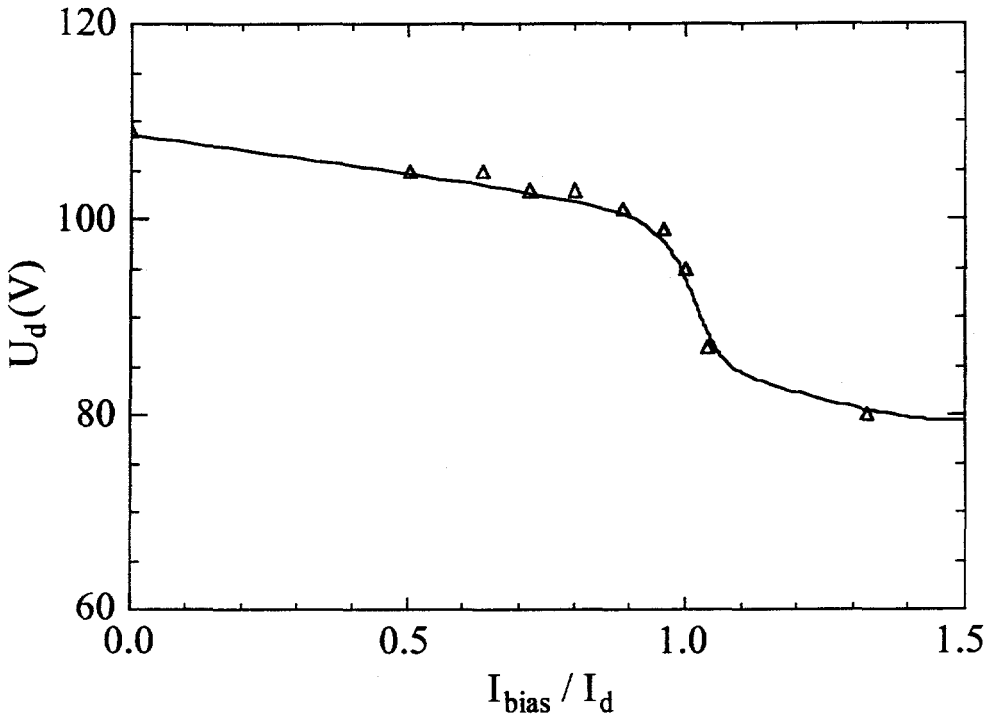

Figure 2.20. Discharge voltage versus bias current normalized to the discharge current.

gun for some time after the discharge current has dropped off and often at high bias voltages, an after-arc will occur as shown in Figure 2.21a. When this occurs, current is drawn directly from the metal anode of the gun, not from the plasma. Coincident with this arcing is a large burst of metal impurities as shown in Figure 2.21b. Such an event demonstrates rather dramatically the advantages to be gained by drawing current from a plasma rather than from a material surface. When the bias dumping SCR is used, the bias voltage is removed from the anode after the discharge is over and after-arcing is eliminated.

A continuation of the impurity studies presented above for the internal discharge was performed for biased discharges. Figure 2.22 shows a summary of the relative impurity levels leaving the gun nozzle for various non-biased and biased discharges. Again, the ratio of the

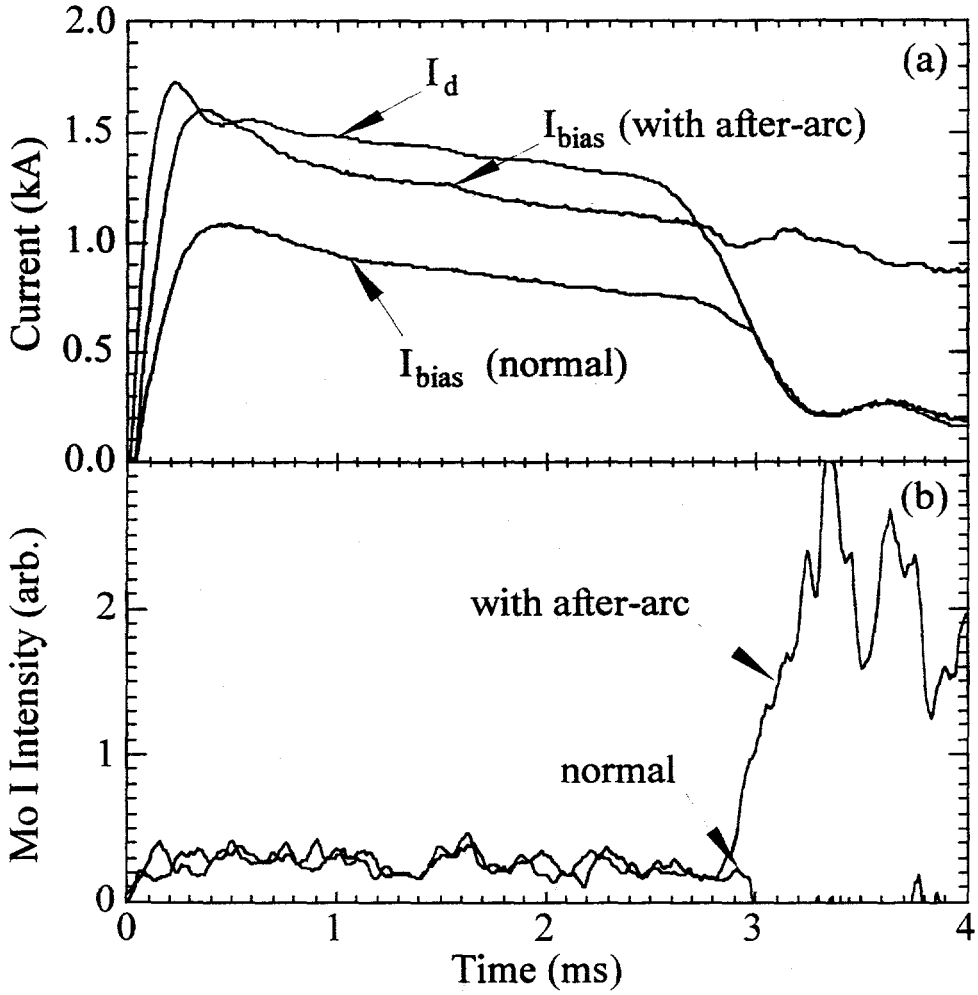

Figure 2.21. Bias current (a) and Mo I intensity obtained from the end view (b) are shown for a normally biased and after-arcing discharge. The discharge current is shown in (a) for reference.

side and end view intensities obtained with the CCD equipped spectrometer is shown for various species. As was the case for the internal discharge, most of the molybdenum remains in the internal discharge -- presumably near the cathode -- in the normally biased cases. In the case of an after-arc, however, the relative intensities of the molybdenum lines approach those of the hydrogen and other impurity lines, which indicates that a significant amount of the molybdenum generated escapes from the gun. In all, it appears that biasing does not

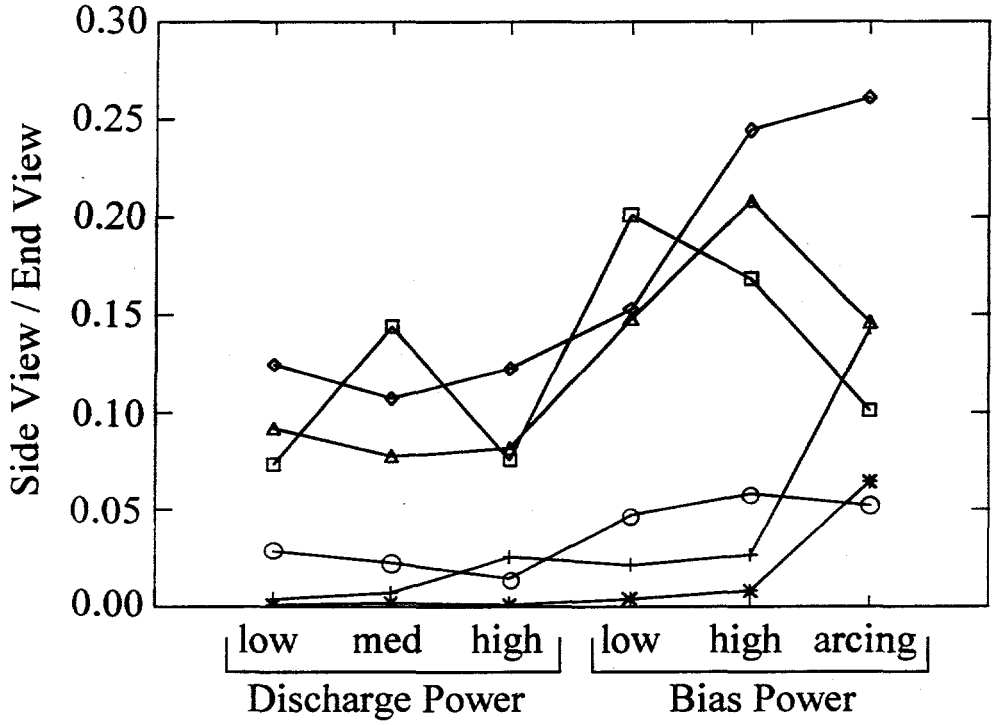

Figure 2.22. Ratio of intensities obtained from side and end views on the test stand for several lines and discharge types. The different symbols represent H_β (◇), H_γ (△), N II (□), Mo I (+), Mo II (✱), and Mo III (○) emission.

change the impurity production significantly unless current is drawn directly from the metal anode.

2.4 Summary

The internal discharge can be classified as a medium pressure arc discharge in hydrogen. For a given discharge current and chamber geometry there exists a minimum hydrogen fueling rate for good operation of the source. If this fueling requirement is not satisfied, the discharge becomes erratic and metal impurities become a problem. If the fueling

requirement is satisfied, then the source produces a dense, localized plasma and metal impurities are trapped within the source for the most part.

Upon biasing the anode, electron current can be extracted from the source along with plasma. The current emitted is very intense and highly directional making the source a good candidate for current drive applications. The maximum current that can be extracted with low impurity generation is about equal to the discharge current. Attempts to extract more than the discharge current result in arcing from the metal anode of the gun and severe impurity generation. When operated at or below the maximum bias point, the source is relatively clean and reliable.

Biased plasma guns operated within these guidelines hold several advantages over traditional emissive electrodes. High currents can be driven with low bias voltages and the current extraction is very reliable without the intermittent emission sometimes present with material electrodes. The emitted current is also very intense but at the same time relatively clean. And in the presence of a magnetic field, the emission is highly directional and not filamentary.

The main disadvantage of using plasma guns as electrodes is that they require substantial hydrogen fueling. This puts a lower limit on what densities can be achieved in the main MST discharge when guns are in use. In reality, of course, material electrodes fuel the discharge as well through the impurities that are generated. One can thus argue that both material and plasma electrodes perturb the discharge with extra fueling. In the case of the guns, however, this fueling is known, reliable, and composed primarily of warm hydrogen plasma.

References

[1] G.I. Dimov *et al.*, Sov. Phys. Tech. Phys. **13**, 754 (1968).

[2] S. Humphries *et al.*, J. Appl. Phys. **57**, 709 (1985).

[3] M.W. McGeoch, J. Appl. Phys. **71**, 1163 (1992).

[4] V.I. Gushenets and P.M. Shchanin, Tech. Phys. **38**, 1048 (1993).

[5] M. Hamagaki, T. Hara, T. Ohgo, and Y. Sadamoto, Rev. Sci. Instrum. **66**, 3469 (1995).

[6] G. Fiksel *et al.*, Plasma Sources Sci. Technol. **5**, 78 (1996).

[7] G.I. Dimov and G.V. Roslyakov, Sov. Pribori. Tech. Exp. **1**, 29 (1974).

[8] Yu.I. Belchenko *et al.*, Rev. Sci. Instrum. **61**, 378 (1990).

[9] G. Fiksel, Ph.D. thesis, University of Wisconsin - Madison (1991).

[10] D.J. Den Hartog and D.J. Holly, Rev. Sci. Instrum. **68**, 1036 (1997).

[11] Max F. Hoyaux, *Arc Physics*, Springer-Verlag, New York (1968).

[12] G.A. Lyubimov and V.I. Rakhovskii, Sov. Phys. Usp. **21**, 693 (1978).

[13] D. J. Den Hartog, D. J. Craig, G. Fiksel, and J. S. Sarff, Plasma Sources Sci. Technology **6**, 492 (1997).

[14] J.D. Huba. *NRL Plasma Formulary*, report NRL/PU/6790--94-265 (1994).

3. ELECTROSTATIC CURRENT INJECTION AND BIASING IN MST

In this chapter, the process of electrostatic current injection and biasing in the MST device will be described. In the previous chapter, the character of the internal discharge and the concept of current drive from a plasma source were presented in a simple cylindrical geometry where magnetic field lines connect the source to a grounded conductor. When injecting current along the magnetic field in the edge of a toroidal device, there are several additional factors to consider. One significant difference from the test stand geometry is that magnetic field lines no longer directly connect the source to ground. Instead the current is driven both along and across magnetic field lines. This changes the effective impedance of the system and can bring about plasma biasing. Another key difference from the situation of the previous chapter is in the trajectory of the injected current. In MST, the field lines are helical and have significant shear resulting in rather sophisticated current patterns.

In this chapter, the nature of these differences will be explored. In Section 3.1, a description of diagnostics used during injection experiments will be given. In Section 3.2, the character of current injection in a closed field line system will be discussed. In Section 3.3, an overview of the distribution of driven currents in MST will be presented. Finally, in Section 3.4, the results will be summarized and implications for the success of this scheme in achieving the desired current profile modifications will be discussed.

3.1 MST Diagnostics

Data from virtually every diagnostic tool available on MST was collected at some point during this work. However, only the most important measurements will be discussed in this thesis. The diagnostic tools used to acquire these data will be described in this section.

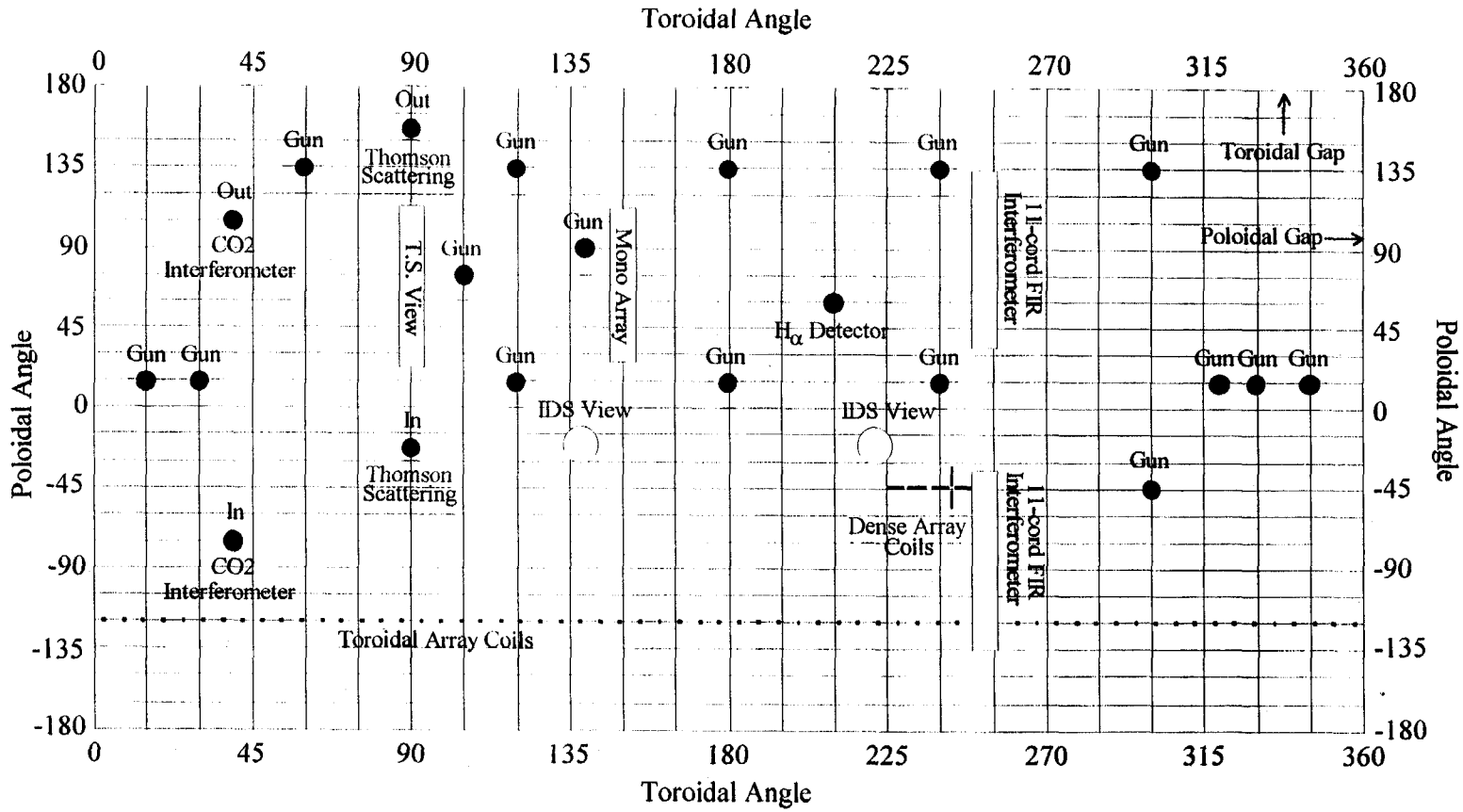

Figure 3.1. MST port diagram showing the 16 gun configuration and diagnostics.

Many of the commonly used techniques will not be described in detail and the reader is referred to reference [1] for a good review of diagnostic principles.

A map of the toroidal surface of MST (see reference [2] for a description of MST itself) is shown in Figure 3.1 along with the position of most of the diagnostics I will be describing. Insertable probes were used at many locations and when the position is relevant, it will be specified in terms of toroidal and poloidal angles. The convention for the toroidal angle is to define 0° T to correspond with the poloidal gap and for the toroidal angle to increase as one moves counter-clockwise around the torus as viewed from above. The convention for the poloidal angle is the define 0° P to correspond with the largest major radius point and for the poloidal angle to increase as one moves upward and inward from that point. The locations of the plasma guns in the 16 injector configuration are also shown in Figure 3.1.

3.1.1 Interferometer Measurements

Plasma density was measured with two interferometer systems. The CO_2 interferometer provided a central chord for general line-averaged density measurements on a daily basis. When profiles were required, an 11-chord FIR interferometer was used. This system provided for vertical line-averaged measurements from 32 cm inboard of the geometric axis to 43 cm outboard. Edge chords from this system proved to be extremely unreliable with more than a few injectors operating simultaneously so profile data with current injection is limited. The reason for this is not completely understood but probably is a combination of refraction from large edge density gradients and scattering by edge density fluctuations that increase when current is injected (see Chapter 4).

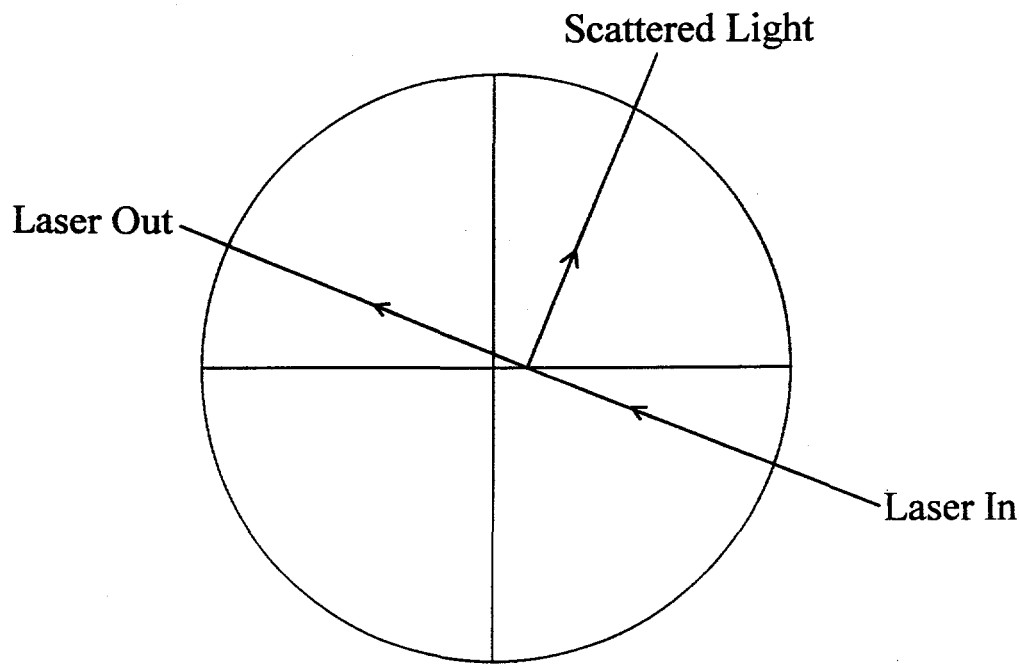

Figure 3.2. Schematic diagram of Thomson Scattering trajectories.

3.1.2 Thomson Scattering Measurements

Electron temperature was measured by Thomson scattering. A pulsed laser was fired through the plasma on a central chord and light which was scattered from the plasma axis (6 cm outboard from the geometric axis) was viewed perpendicular to the beam as shown in Figure 3.2. The scattered light was dispersed with a grating and the energy distribution was measured in five channels. Because of low signal levels, it was necessary to take many shots and ensemble the results to obtain reliable temperature information. For this reason, electron temperature measurements were only made in a few interesting cases.

3.1.3 Hydrogen Radiation Measurements

H_α radiation was measured with a single detector along a central chord to quantify the particle source rate due to neutral hydrogen ionization. In Chapter 4 it will be shown that

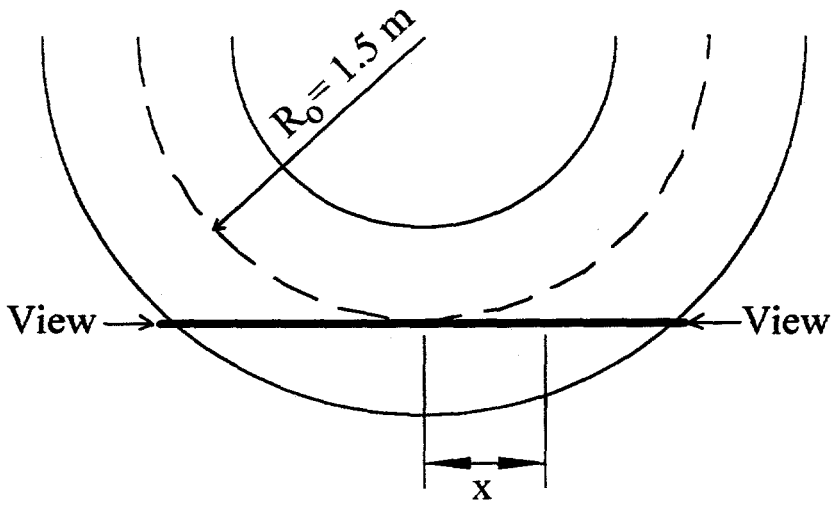

Figure 3.3. Top view of MST showing IDS viewing geometry.

there are often strong toroidal asymmetries in the H_α radiation connected with large m = 0 magnetic modes. If these modes are rotating, then the single chord measurement is a reasonable indicator of global levels once the data is averaged over time. However, if the modes lock, then the measurements from this detector yield only the local fueling rate and must be used with care. It will be shown that these modes always rotate when guns are injecting current, but are usually locked when guns are not biased.

3.1.4 Impurity Ion Flow Measurements

Impurity ion flow was measured with a fast Doppler spectrometer (referred to as Ion Dynamics Spectrometer or IDS) [3]. This device collected light from two opposing views along a chord tangent to the geometric axis but displaced vertically downward 13 cm. By fitting the collected light to a Gaussian shape, a "line-averaged" flow was determined. The measured signal is given by

$$I(\lambda) = \int I(x) e^{-\frac{[(\lambda - \lambda_o(x)]^2}{[\Gamma(x)]^2}} dx \tag{3.1}$$

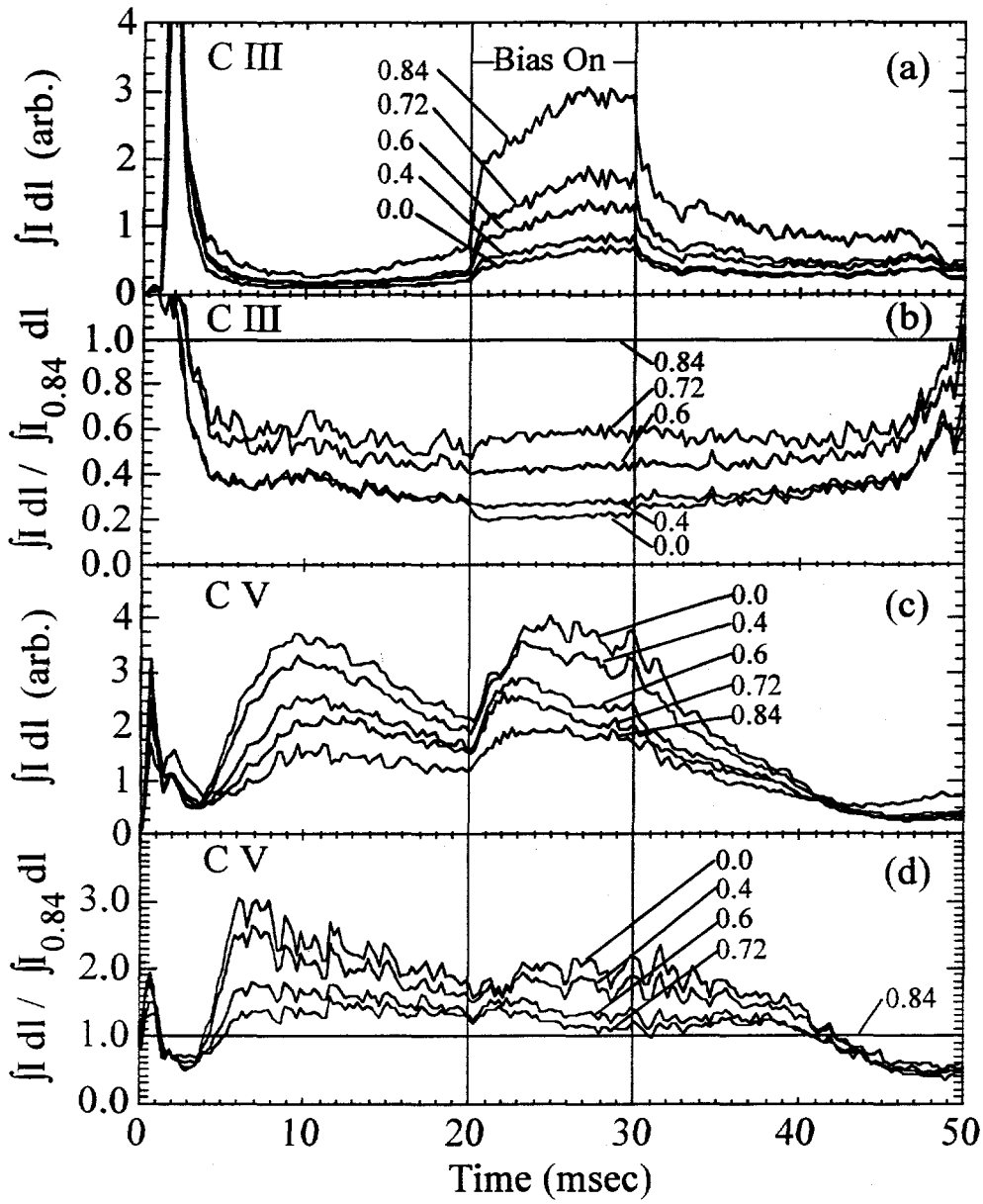

Figure 3.4. Line integrated impurity emission data are shown for five chords of the Impurity Monochromator Array (IMA) for C III (a and b) and C V (c and d). Labels indicate the minimum r/a sampled along the chord and both absolute data (a and c) and data normalized to the r/a = 0.84 chord (b and d) are shown.

where $I(\lambda)$ is the measured intensity as a function of wavelength, $I(x)$ is the intensity of light collected by the detector from position x (see Figure 3.3), $\lambda_0(x)$ is the peak wavelength of the emitted light coming from position x which has been Doppler shifted due to the component of flow in the direction of viewing, $\Gamma(x)$ is the width of the line due to thermal broadening, and the integral is performed over the entire line of sight. The emission profile must be known to interpret the data from this diagnostic correctly.

The two emission lines used were CIII @ 229.6 nm and CV @ 227.0 nm. The emission profiles were measured with a 5-chord array of monochromators (denoted "Mono Array" in Figure 3.1). Figure 3.4 shows the time dependence of the five chordal measurements for CIII and CV. The data shown are ensembles over many shots with 8 injectors operating. The first feature to note from this figure is that the CIII emission profile is quite hollow while the CV profile is not. Because central chords cover a larger path length, one would expect that for a roughly constant radial emission profile, central line-integrated signals would be larger than edge line-integrated signals. This is the case for CV but not for CIII. Despite the much reduced path length of the r/a=0.84 chord, the CIII intensity is much stronger for this chord than for all others indicating a strongly edge-peaked emission profile. Indeed, an inversion of the data (see Figure 3.5a) shows that CIII emission is dominated by the edge while CV emission is roughly constant throughout the plasma cross-section. (Note that the CIII profile is probably quite a bit narrower and more edge-localized than shown in Figure 3.5a because measurements could not be made all the way to the plasma boundary.)

The second feature to note is that although the overall emission increases a great deal when the injectors are operating, the relative emission between channels (or emission profile) does not change very much. This is shown most clearly in Figures 3.4b and 3.4d where each line-integrated measurement has been divided by the chordal measurement at r/a = 0.84. Thus, changes in the measured impurity flow with gun operation indicate true changes in

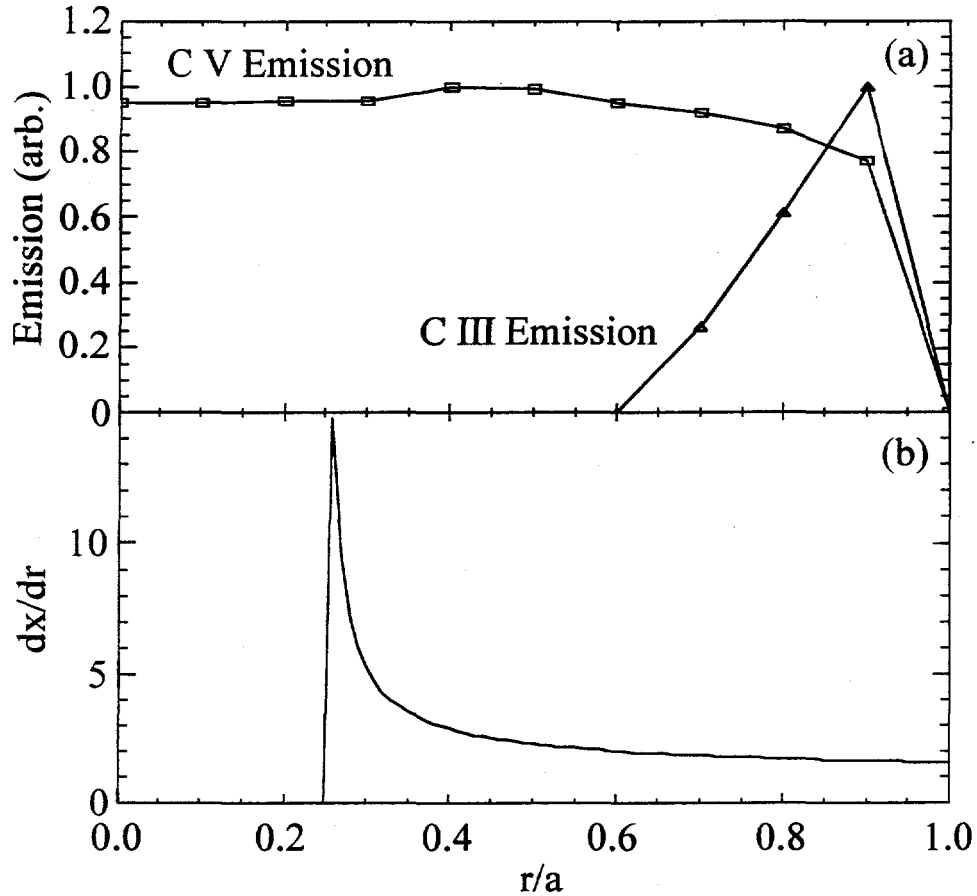

Figure 3.5. Inverted emission profiles are shown for C III and C V in (a) and the weighting of different radial positions due to spectrometer viewing geometry is shown in (b).

plasma flow and not simply a change in the position of the measurements. The overall increase in impurity radiation will be discussed in Chapter 4.

The emission profiles are measured as a function of radius but the integral above is performed over the line of sight of the spectrometer. One can convert the integral to one over radius using dx = (dx/dr) dr. For this geometry, dx/dr is a function of radius and this function is shown in Figure 3.5b. It is strongly peaked in the core and roughly flat over the

outer half of the plasma. Hence, for broad emission profiles, the dx/dr term determines the weighting of the different plasma regions and the spectrometer measurement will be indicative of the core plasma. For edge localized emission profiles, it is the emission profile that determines the weighting and the spectrometer measurement will indicate edge plasma quantities. By viewing both CV and CIII emission, one obtains an indication of core and edge impurity flow.

3.1.5 Magnetic Fluctuation Measurements

Magnetic fluctuations were measured with a large set of coils mounted on the plasma side of the conducting shell. Two sets were routinely used. A toroidal array of 64 evenly spaced triplets (B_θ, B_ϕ, B_r) was used (32 coils regularly) to identify long wavelength , low frequency, global modes. These signals were integrated prior to digitization and a spatial Fourier decomposition was performed so that

$$B(\phi, t) = \sum_{n=0}^{n_{max}} B_n(t) \cos(n\phi - \delta_n(t)) , \qquad (3.2)$$

where $B(\phi,t)$ is the measured magnetic field as a function of toroidal angle and time, and B_n and δ_n are the amplitude and phase of the mode with toroidal mode number n. A localized cluster of closely spaced coils (referred to as the Dense Array) was also used (2 B_θ and 2 B_ϕ coils regularly). These signals were amplified but not integrated prior to digitization and were used to measure short wavelength, high frequency, edge modes. A frequency-based analysis was typically applied to data from these coils.

Several methods were developed in the course of this work to analyze toroidal array data in a way that allows locked modes and m = 0 modes to be measured. There are two main difficulties in obtaining mode characteristics from the toroidal array. First, the coil areas and alignments are not known precisely. Typical mode amplitudes in MST are ~ 1% of the equilibrium field which means that coil areas must be known to better than 1%. Imperfect

alignments cause coils designed to measure B_ϕ to measure $B_\phi + kB_\theta$ instead where $k \leq 6\%$. Without correcting for these effects, the analysis of stationary or low frequency plasma modes is not reliable. Second, there may be time-dependant but stationary structures like field errors which interfere with plasma modes to produce a hybrid signal. If modes are locked, there is no way to decouple these unless the nature of the stationary structure is known and the relative coil calibration is very good.

To correct for some of these effects, the following procedure has been adopted. First, an absolute calibration of the B_ϕ coils is accomplished in vacuum B_ϕ shots (or the vacuum field that exists prior to each RFP discharge) using the measured $B_\phi(r=a)$ (which is really a measure of toroidal field coil current) and assuming that $B_\phi \sim 1/R$ where R is the major radius. The B_ϕ pickup in the B_θ coils is arrived at in the same way. The B_θ pickup in the B_ϕ coils is obtained by considering $F = 0$ shots for which the core modes ($n = 6,7,8,...$) are rotating. The reversal parameter F is defined by the ratio of B_ϕ at the wall to the cross-section averaged B_ϕ. Since $B_\phi(r=a) = 0$ in $F = 0$ shots (no current is allowed to flow in the toroidal field circuit), any residual signal that remains after averaging each coil over many mode rotation periods is dominated by the B_θ pickup. (The contribution from locked $m = 0$ modes is small in this case since the $q = 0$ surface is at the wall. Some coils, particularly those close to the poloidal gap, can have a contribution from field errors as well.) The ratio of this residual signal to the average of all B_θ coil measurements is then used to correct for the B_θ pickup in subsequent shots. Finally, a relative calibration of the B_θ coils is obtained by ensembling the ratio of each coil to the average of all B_θ coils for many shots in which all modes are rotating (including the $m = 0$ modes). This procedure removes most of the non-plasma part of the signal and was used for all toroidal array analysis. The contribution to the signal from field errors is not fully removed by this method and limits the ultimate reliability of mode amplitudes to about 0.2%-0.5%.

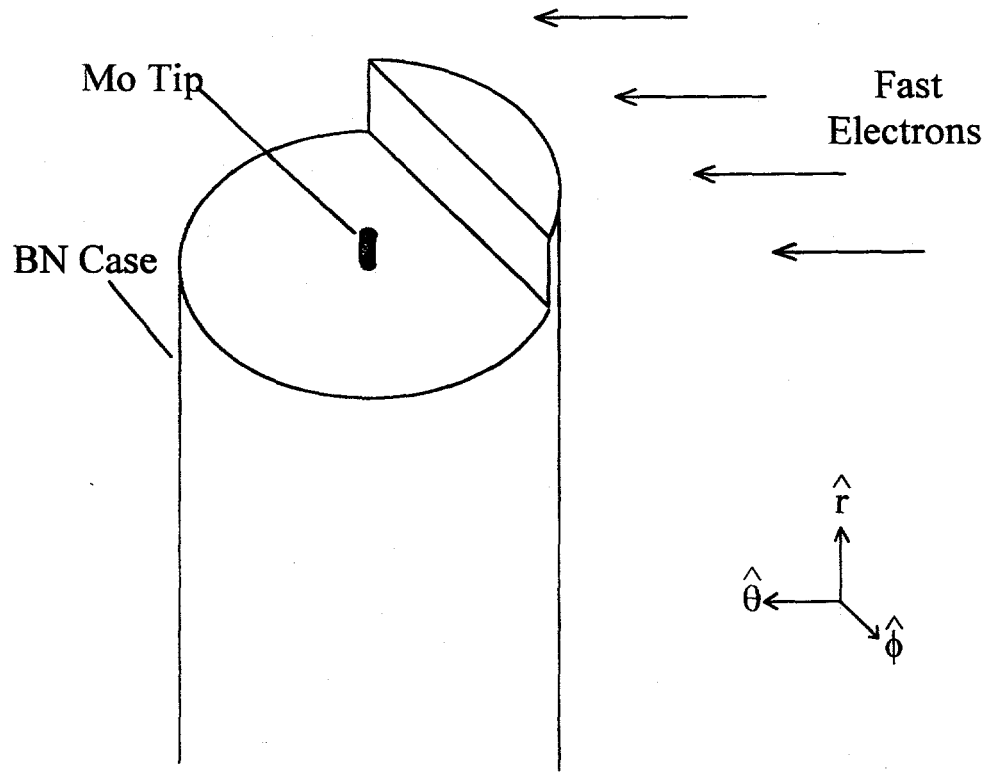

Figure 3.6. Schematic of single tipped swept Langmuir probe.

3.1.6 Langmuir Probe Measurements

Two different Langmuir probes were used to obtain plasma and floating potentials as well as the ion saturation current. A single-tipped Langmuir probe (shown schematically in Figure 3.6) was used as a swept probe [4] to measure the plasma potential. A sinusoidal voltage was applied to the probe with a frequency of 250kHz along with a dc offset roughly equal to the floating potential. Current and voltage were both digitized at 50 MHz for about 1.5 ms and a series of I-V curves were reconstructed from the data. The plasma potential was obtained from the measured I-V characteristic in the normal fashion by determining where electron saturation current starts to be drawn.

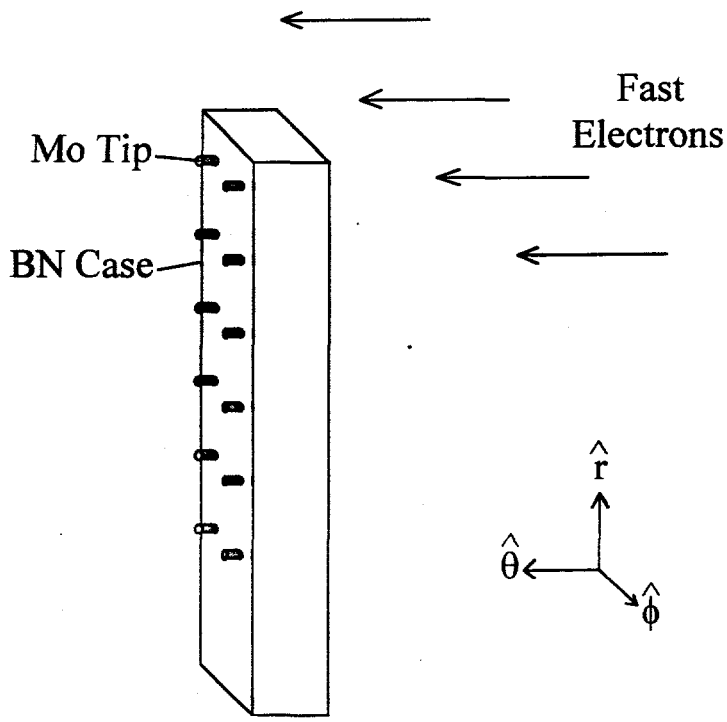

Figure 3.7. Schematic of "rake" Langmuir probe.

A second "rake" Langmuir probe (shown in Figure 3.7) was used to obtain radial profiles of the floating potential and floating potential fluctuations and to measure the ion saturation current at a single radial location. When measuring the ion saturation current, two tips at the same radius were biased relative to one another and used in a double probe configuration. One will note that both probes are constructed so that they do not sample fast electrons that stream along the magnetic field lines in the edge of MST [5]. Neglecting these electrons does alter the measurements somewhat but small metal tips do not survive long when exposed to the fast electrons. The quantities measured with these probes are thus characteristic of the bulk, slow electrons.

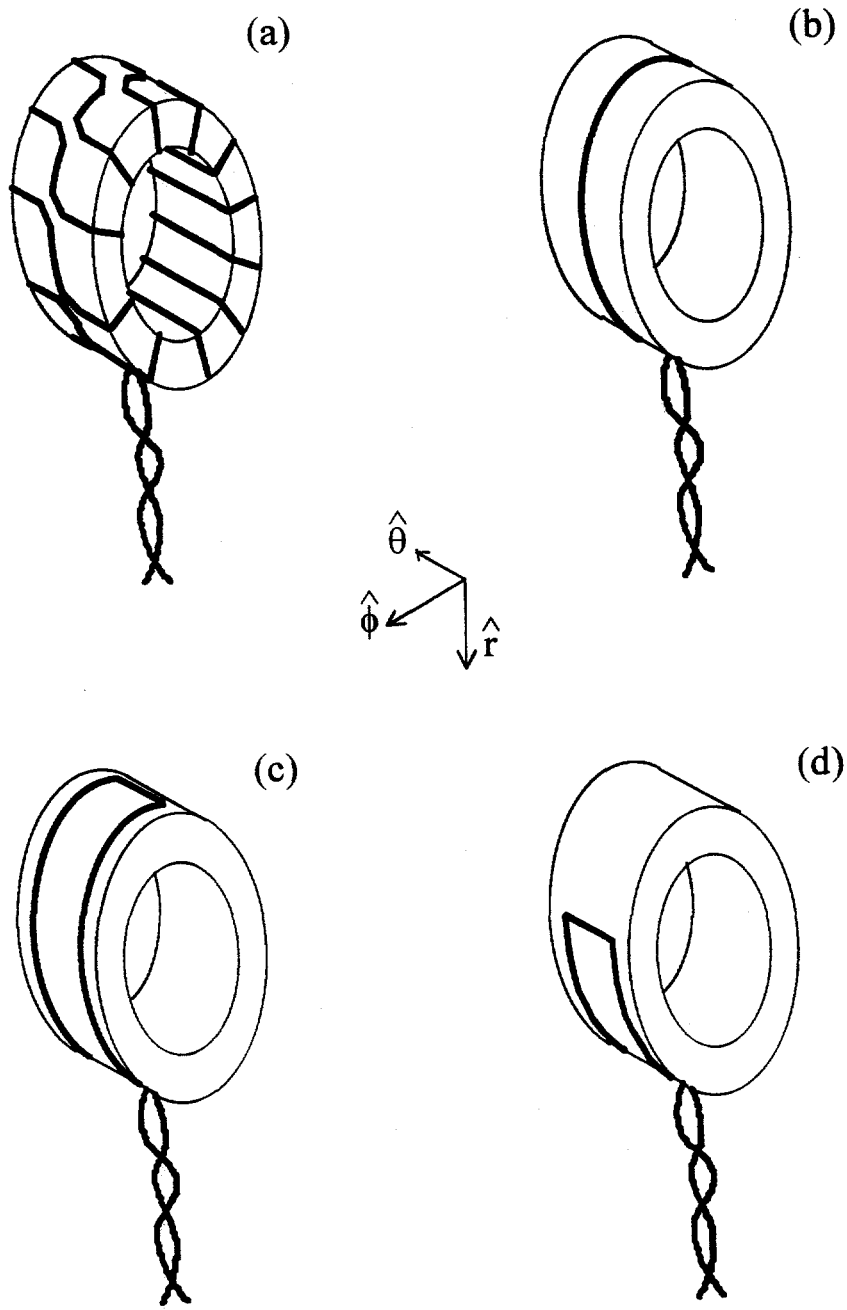

Figure 3.8. Schematic diagram of the four coils in the Rogowski probe. The probe is composed of a Rogowski coil (a), as well as poloidal (b), toroidal (c), and radial (d) magnetic field coils.

3.1.7 Rogowski Probe Measurements

Measurements of edge current densities were done with small insertable Rogowski probes. The most recent version of the probe combines 4 different coils on the same coil form for measuring one component of the current density J and all three components of the magnetic field B. The arrangement of the coils is shown in Figure 3.8. The Rogowski coil is composed of nearly 100 turns around the coil form and a single back winding. (Only 11 turns are illustrated in Figure 3.8 and the back winding is not shown.) The coil form is covered with an electrostatic shield (silver paint) and encased in a boron nitride shell (not shown) which has a hole of radius 0.91 cm through which current is allowed to pass. The center point of this hole was used to label the probe position. The current density is obtained by dividing the total measured current by the area of this hole and hence represents an average over a circle of radius 0.91 cm centered at the probe position.

The coil form has an outer diameter of 3.0 cm and a thickness of about 1 cm. Hence the poloidal magnetic field measurement is an average over a circle with 3 cm diameter centered at the probe insertion. The toroidal field coil is three dimensional but yields roughly a linear average of the toroidal field along a 3 cm long line segment whose midpoint corresponds to the probe insertion, provided the field does not have strong toroidal asymmetries. The radial field measurement is a three-dimensional average over a 1.5 cm extent in the radial direction and a 3.0 cm extent in the toroidal direction.

The magnetic coils are useful for measuring magnetic field profiles but are also necessary to correct for imperfections in the Rogowski coil. The signal from the Rogowski coil is dominated by pickup from the poloidal magnetic field and to a lesser extent from the toroidal magnetic field. It must be corrected for these pickups before any meaningful current measurement can be obtained. Calibration is done in the MST vacuum toroidal field with the probe deeply inserted (10 cm from the wall). By adding suitable fractions of the magnetic coil signals to the Rogowski signal, the measured "current" in vacuum shots can be made

zero for all probe orientations. The adjustment is not perfect since the magnetic coils do not average over exactly the same points where imperfections in the Rogowski exist. If magnetic fields vary substantially within the volume of the probe, the corrections can be incomplete and false currents of < 5 A/cm^2 will be measured. This problem seems most noticeable near and within portholes where magnetic fields do exhibit strong gradients. At insertions beyond about 3 cm, the effects are minimal and current measurements are good to within about 1 A/cm^2.

3.2 Current Injection in a Closed Field Line System

3.2.1 Overview

As mentioned at the start of this chapter, current injection from plasma guns in MST is significantly different from that in the test stand. While the presence of an external discharge does exert some influence over the source operation (e.g., breakdown of the internal discharge is easier with many free electrons already present), the dominant difference is due to the closed magnetic field lines on which current is injected in MST.

The difference between current injection in the test stand and in MST is illustrated in Figures 3.9 and 3.10. In the test stand, magnetic field lines link the source directly to a conducting boundary. When a bias voltage is applied, current flows out of the gun along the field and is collected where the field line penetrates the grounded vacuum vessel. The electric potential distribution along the field line probably looks something like that shown schematically in Figure 3.9b. The potential at the vessel is zero and the potential at the gun is that applied by the bias circuit, U_{bias}. A sheath forms at the vessel wall which limits the collected current to I_{bias}, there is a resistive drop in the cool plasma between the gun and the sheath, and there is a transition region near the gun which may be composed of several space charge layers. The transition region (shown in cross-hatch in Figure 3.9b) forms to keep the

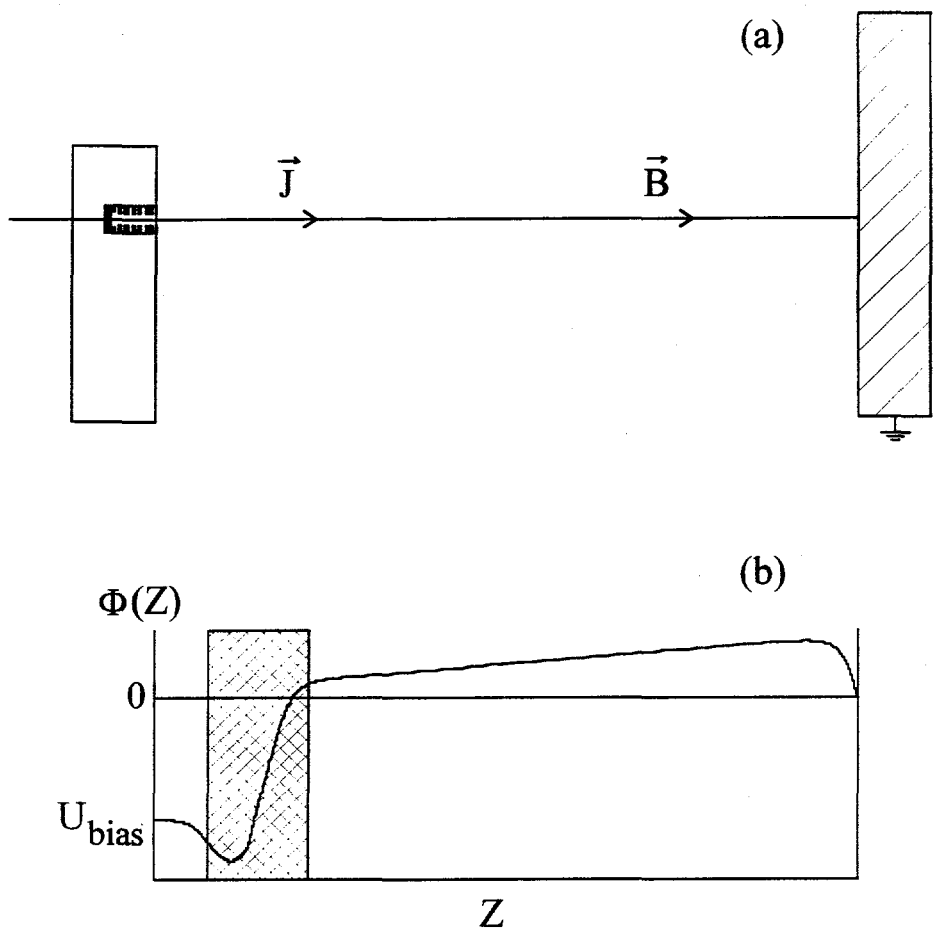

Figure 3.9. (a) Schematic diagram of current injection in the test stand geometry and (b) the potential distribution along the field line.

injected current below the electron thermal current (~ 1-3 kA) but enough to match I_{bias}. The injected current is determined by the gun plasma properties and the applied potential, U_{bias}.

In the MST geometry (Figure 3.10a) the injection is split into two parts. In the first part, electrons (and background plasma) leave the gun through a similar transition region and flow out along the magnetic field. Simultaneously, current is driven across the magnetic field between the flux surface on which current is injected and the wall. The currents driven along

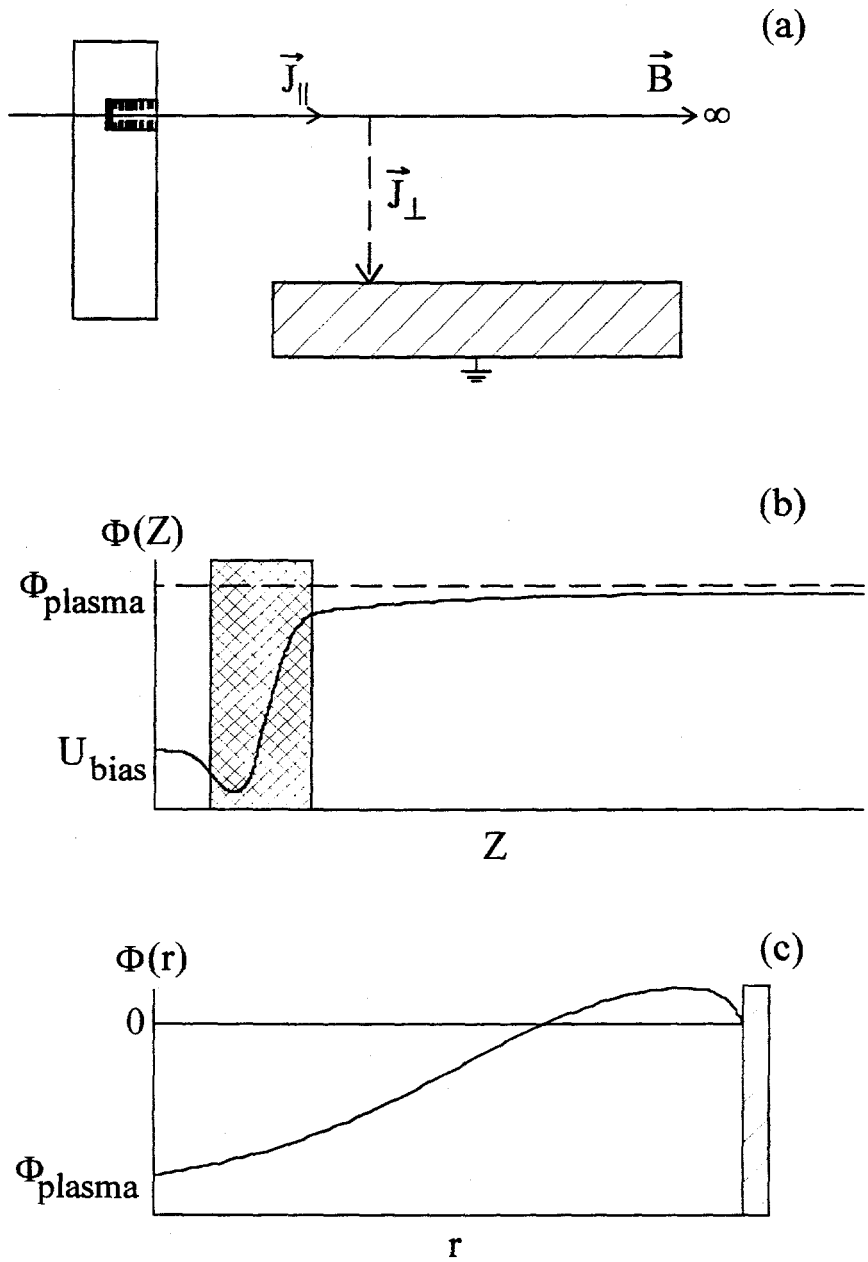

Figure 3.10. (a) Schematic diagram of injection in the MST geometry, (b) the potential distribution along the magnetic field, and (c) the potential distribution across the magnetic field.

the magnetic field and those driven across the field need not be (and probably are not) carried by the same electrons. The potential distribution along the magnetic field (Figure 3.10b) probably looks quite similar to that in the test stand except that there is no sheath voltage drop and the resistive drop is probably smaller due to lower collisionality. Far away from the gun, the potential assumes the value Φ_{plasma} which is the global plasma potential on the injector flux surface. The potential distribution across the magnetic field should look something like what is shown in Figure 3.10c. Current does not naturally flow across magnetic field lines and hence a radial electric field must arise to drive electrons out of the plasma. This electric field combined with that in the sheath at the wall determines what the potential Φ_{plasma} will be. Hence, Φ_{plasma} assumes a value that self-consistently allows I_{bias} to be injected from the gun and I_{bias} to flow across the magnetic field to the wall.

In the following sections, the consequences of these differences will be examined. It will be shown that forcing the injected current to return across magnetic field lines causes the plasma to become biased and causes the amount of current which is injected at a given voltage to depend on edge plasma parameters.

3.2.2 Plasma Biasing

It is clear from the above description that the effective impedance of the bias circuit will be sensitive to the edge plasma properties. In general, one expects the current driven at a particular U_{bias} to be lower in MST than in the test stand because in MST a portion of the bias voltage is taken up in accomplishing transport across the magnetic field. This trend is illustrated by comparing the I-V curve shown in Figure 3.11 with that shown in Figure 2.18. In the test stand, a bias voltage of -240 V can drive 800 A while in MST the same voltage drives only 600 A. To drive a current of 800 A, a voltage of ~ -340 V would be needed in MST; hence, it can be inferred that about -100 V is necessary to drive the current across the magnetic field to the wall.

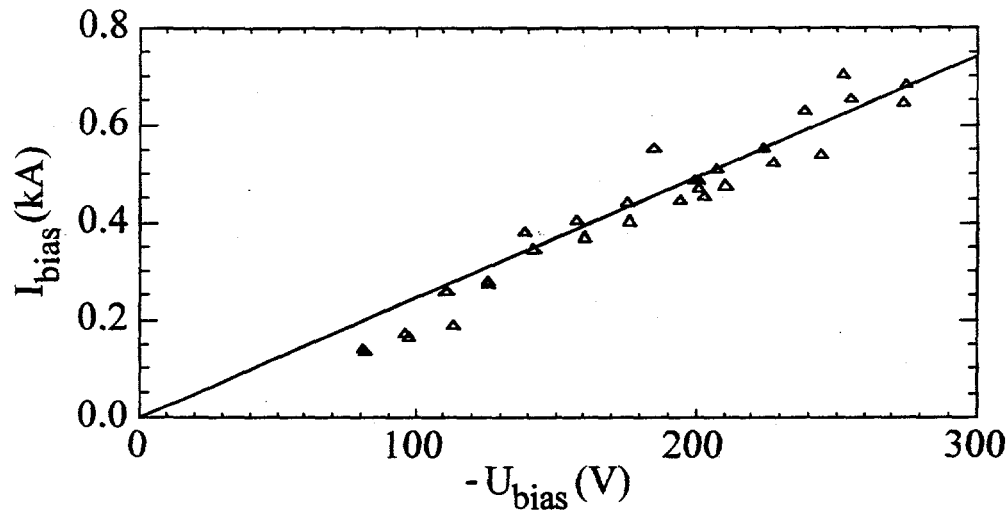

Figure 3.11. Typical I-V curve for a single gun operating in MST.

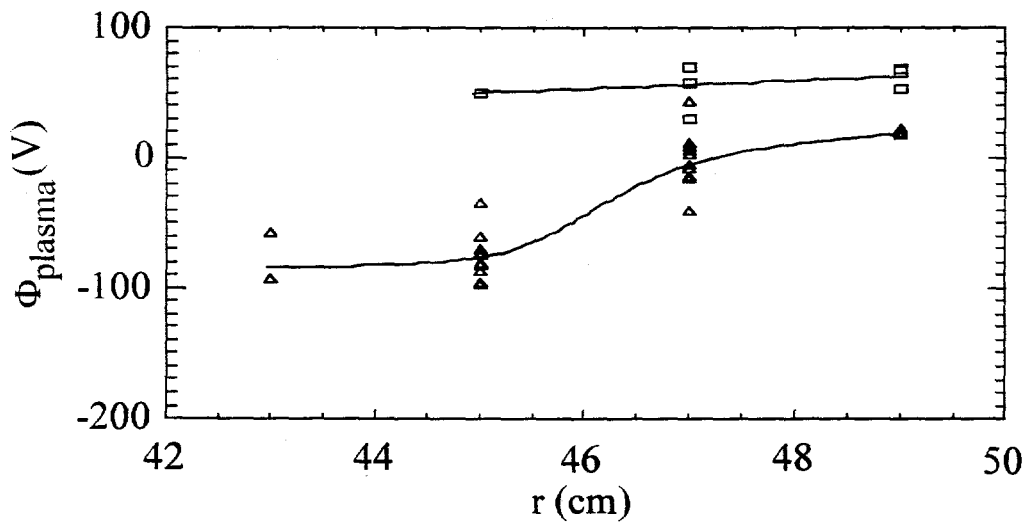

Figure 3.12. Radial profiles of plasma potential measured with the swept Langmuir probe are shown for discharges with 6 injectors biased (triangles) and not biased (squares).

Measurements of plasma potential confirm that this picture is roughly correct. Figure 3.12 shows edge plasma potential profiles measured with a swept Langmuir probe for discharges with bias voltage applied and for similar discharges without bias voltage. Six injectors were used in these shots and all were biased to about -280 V resulting in a total injected current of 3.3 kA. The injectors were located (after correcting for flux surface shifts as discussed in Section 3.3) at 7 cm. The probe was positioned so that the nearest injector was 90° away toroidally. Although the plasma parameters were not identical to those in which the I-V curve of Figure 3.11 was taken, the data do indicate that a potential drop of about -100 V develops to drive current across the magnetic field. The potential profile is also similar to what was indicated in Figure 3.10c.

The electric field that arises in these discharges allows the bias current to flow but it also can have an impact of the behavior of the MST plasma. Since this strong radial electric field (~ 2 kV/m) exists in the presence of a poloidal magnetic field (~ 0.1 T), one expects strong E×B flows to develop in the edge with a speed of about 20 km/s. Indeed such flows are observed (see Chapter 4), and may play a role in affecting transport and plasma dynamics. Hence the plasma guns, originally developed to drive field-aligned currents, also function as plasma biasing electrodes.

3.2.3 Dependence of Bias Circuit Impedance on Plasma and Gun Parameters.

The effective impedance of the bias circuit is the sum of that associated with current drive along the magnetic field and that associated with current drive across the field. The part linked with current drive along the field is virtually identical to the impedance measured in the test stand configuration. The part linked with current drive across the field is sensitive to edge plasma parameters and the specific geometry. In practice the impedance due to the

cross-field process is similar in magnitude to that due to the field-aligned process. Hence the total circuit impedance in MST is roughly twice as large as in the test stand configuration.

Although the details of the cross-field transport process are complex, some insight can be gained by considering a simple model for the bias circuit impedance. From the field-aligned part of the problem and the test stand data, we expect the total bias circuit current to be given by

$$I_{bias} = N \cdot k \cdot (\Phi_{plasma} - U_{bias}) \tag{3.3}$$

where N is the number of injectors in operation and k is an empirical constant (~ 3.3 Amperes/Volt). (Note that U_{bias} is more negative than Φ_{plasma} so I_{bias} is positive.) Now considering the cross-field part, we expect that the total bias current should be given by

$$I_{bias} = \sigma_r \cdot E_r \cdot A \tag{3.4}$$

where σ_r is the radial conductivity, E_r is the radial electric field, and A is the area through which the current is driven. I will ignore profile effects and consider that $E_r = -\Phi_{plasma} / x$ where x is the insertion depth of the injectors.

Equating the two expressions, one finds a relation between the plasma potential and the bias potential that can be used to eliminate Φ_{plasma}. Then we can write the current as

$$I_{bias} = N \cdot k \cdot \left(1 - \frac{1}{1 + \frac{\sigma_r A}{N k x}} \right) \cdot |U_{bias}| \tag{3.5}$$

Next we assume that the radial electrical conductivity is determined by a process which can be modeled as diffusive so that

$$\sigma_r = \frac{n e^2 D}{T} \tag{3.6}$$

where n is the electron density, e is the electron charge, T is the electron temperature, and D is the effective perpendicular diffusion coefficient from processes that are not inherently ambipolar (e.g., collisions, magnetic fluctuations, etc.). Substituting 3.6 in 3.5 yields the expected relationship between bias current and bias voltage based on this simple model.

We note first that if the cross-field transport were not an issue (e.g., if σ_r becomes infinite) then the injected current predicted from this expression is just as we would expect in the test stand configuration. With finite conductivity, however, the current is reduced by an amount which depends on the relative impedance of the cross-field and field-aligned processes. Using $n = 5\times10^{12}cm^{-3}$, $T = 50$ eV, $D = 10\ m^2/s$, $A = 30\ m^2$, $k = 3.3$ Amp/Volt, and $x = 5$ cm, one obtains about 10 kA with 16 injectors biased to -300 V. This is not too far from the observed current although the exact values of these parameters are not well known. Although the quantitative predictions of this model do not exactly reproduce all experimental results, the trends as parameters are varied seem to agree qualitatively with experiment.

The next aspect of Equations 3.5 and 3.6 to note is that the injected current at a given bias voltage should increase as density is increased. This is due to the direct dependence of the radial conductivity on the number of charge carriers. Figure 3.13 shows the measured dependence of the total injected current on the line-averaged density for two different bias voltages. (In this plot, bias voltage labels refer to capacitor bank voltage which is larger than the actual voltage applied to the gun anode by 10-30% -- see Figure 2.6) The density was varied by changing the MST fueling. As anticipated, more current is driven at higher densities. The linear dependence is predicted by the model in regimes where the perpendicular part of the impedance is much larger than the parallel part. The relevant parameter is really the edge density but the density profile probably did not vary too much during this scan so line-averaged and edge densities are roughly proportional.

Equation 3.5 also predicts that at a given bias voltage, deeper insertion results in less injected current. In the model, this results from a decreased electric field for a given bias voltage. This prediction is also reproduced in the experiments and can be observed during a single shot by considering the current emitted from injectors at the same insertion depth but at different poloidal angles. Since the flux surfaces are shifted outward, guns at outboard

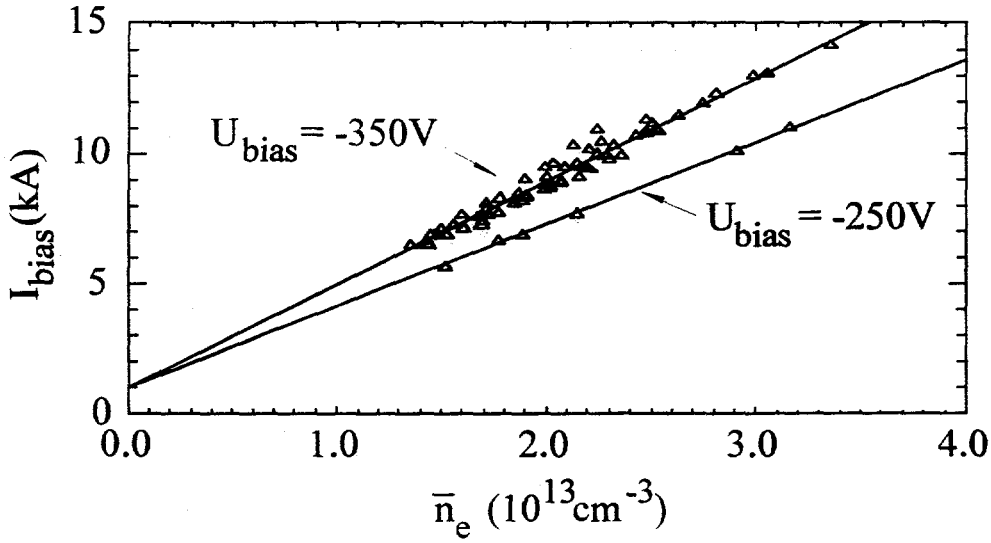

Figure 3.13. Total injected current from 16 guns is shown versus central line-averaged density for bias set points of -250 V and - 350 V.

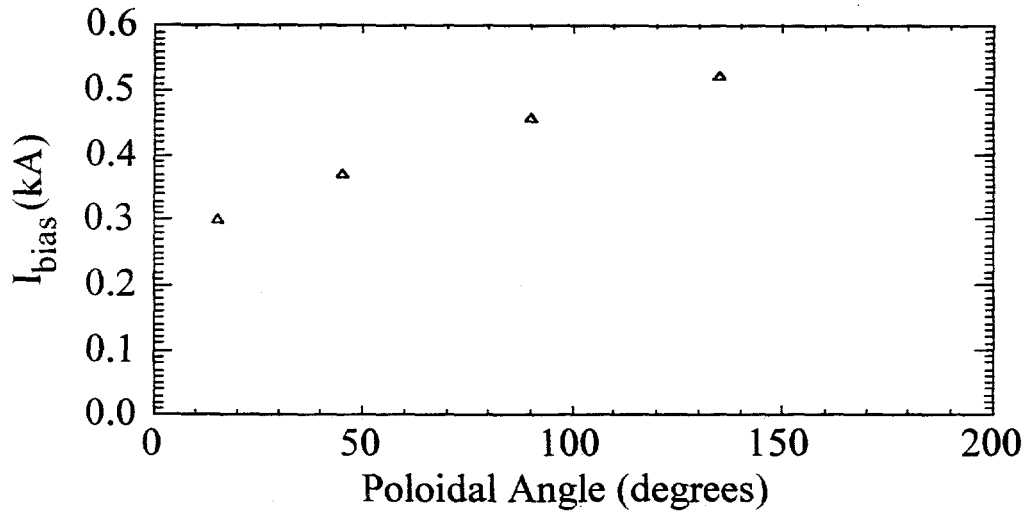

Figure 3.14. Injected current versus poloidal angle is shown for 4 different guns all inserted 5.7 cm from the wall.

angles are effectively deeper in the plasma than those at inboard angles. Figure 3.14 shows that the injected current subsequently varies with poloidal location.

Another important facet of this model is the connection between injected current and plasma confinement. One expects that injected current should increase if confinement decreases. Figure 3.15 shows the total injected current from 16 guns versus time along with the reversal parameter and the central line-averaged density. Vertical lines indicate sawtooth crashes during which confinement temporarily degrades while the magnetic equilibrium relaxes to a lower energy state. That confinement degrades at sawteeth can be seen somewhat in the density trace which is increasing with time away from sawteeth but exhibits a flatter or sometimes negative slope at sawtooth events. Coincident with the decreases in confinement (increases in D) are momentary increases in the injected current as expected from the discussion above.

The dependence of injected current on confinement is not particularly good from the standpoint of transport reduction by current profile control. The difficulty is that if edge current drive becomes large enough to significantly improve confinement, it is possible that this will result in a decrease in injected current. Hence the electrostatic scheme as implemented is self limiting to some extent. Of course, it is also possible that the mechanism that provides for the edge radial conductivity could remain unaffected or get stronger even though the core particle and energy transport are reduced. This would be the case, for example, if core transport is due to core-resonant tearing modes and edge radial conductivity is due to edge-resonant tearing modes.

The final trend to note from Equation 3.5 is the dependence of injected current on the number of injectors. For few injectors, the current scales linearly with injector number. As the number of sources increases, however, the plasma potential increases to accommodate a greater cross-field current. Eventually, the potential approaches the bias voltage and a limit is reached where additional injectors do not add additional current. Figure 3.16 shows the

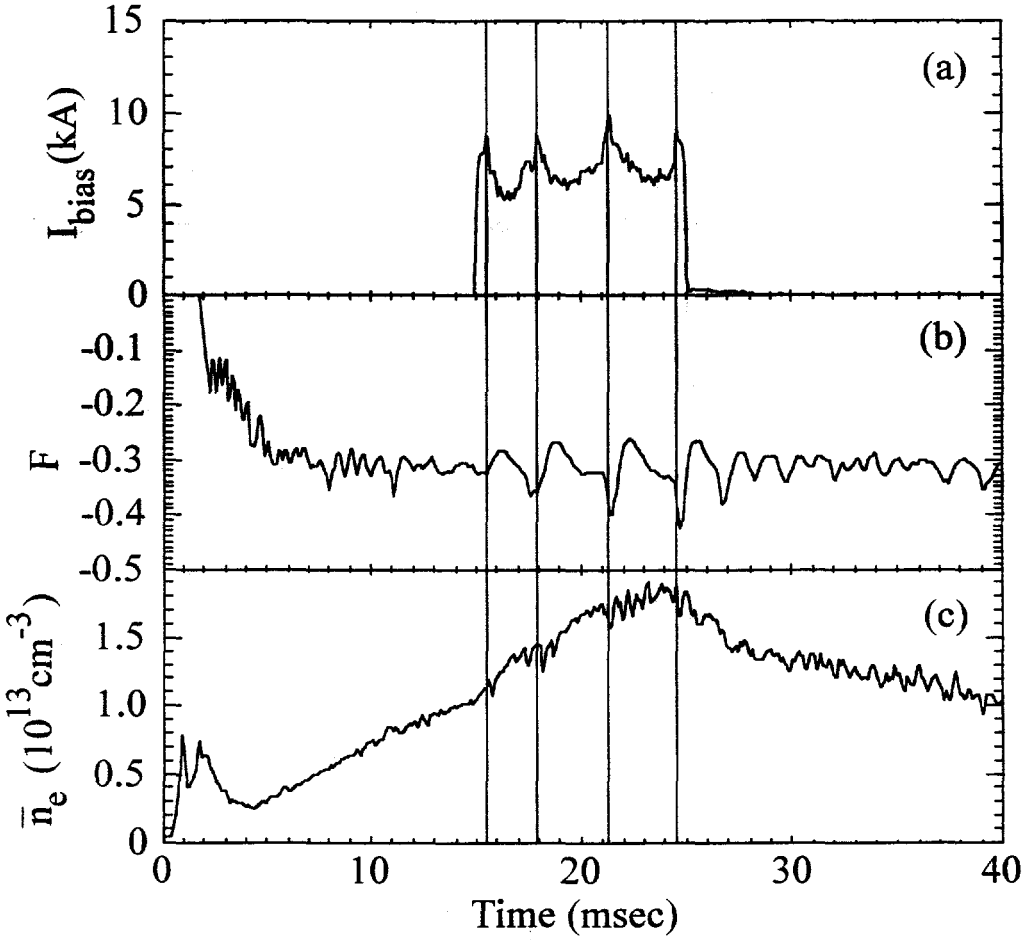

Figure 3.15. (a) Total injected current from 16 guns, (b) the reversal parameter, and (c) the central line-averaged density versus time for a single shot.

injected current per gun versus bias voltage as the number of injectors used was increased from 1 to 13. Although it appears that the saturation point is not reached with 16 injectors, there is an increase in the circuit impedance per gun as expected.

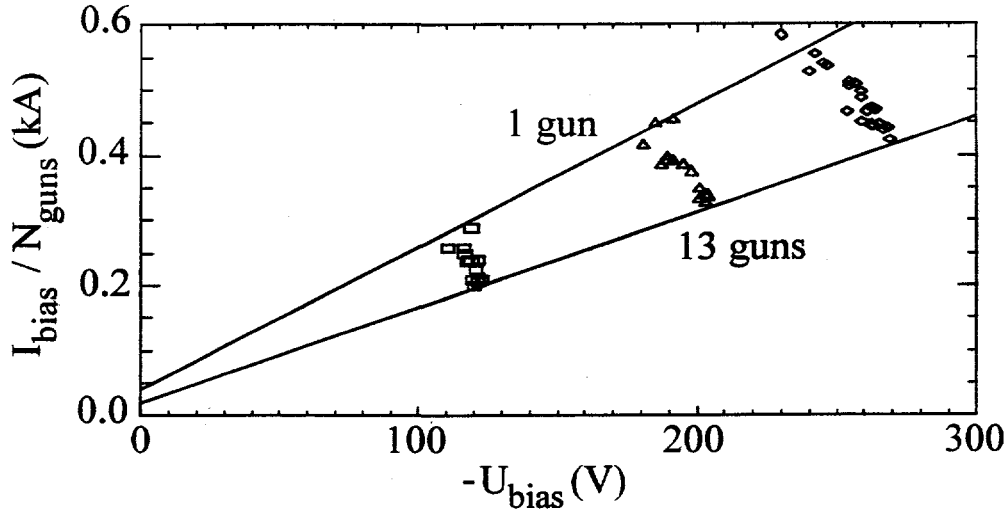

Figure 3.16. Injected current per gun is shown versus bias voltage as the number of injectors in use was increased from 1 to 13.

3.3 Distribution of Injected Currents in MST

Simulations of transport reduction with edge current drive in the RFP suggest that the effectiveness of such schemes depends to some extent on how the current is distributed [6]. Both the radial profile and the overall symmetry of the current driven are important. In this section I will discuss how the currents injected by the plasma guns are distributed spatially in MST. To accurately specify the trajectories of the injected currents requires detailed knowledge of the magnetic field profiles and toroidal effects must be included. In Section 3.3.1 I will describe the results of magnetic equilibrium measurements in the edge of MST and will present a simple model for describing edge magnetic field lines. In Section 3.3.2 measurements of edge currents with an insertable Rogowski probe will be presented and compared with what is expected from field line mapping. Finally, in Section 3.3.3 the results of simple cylindrical equilibrium modeling of current injection discharges will be described.

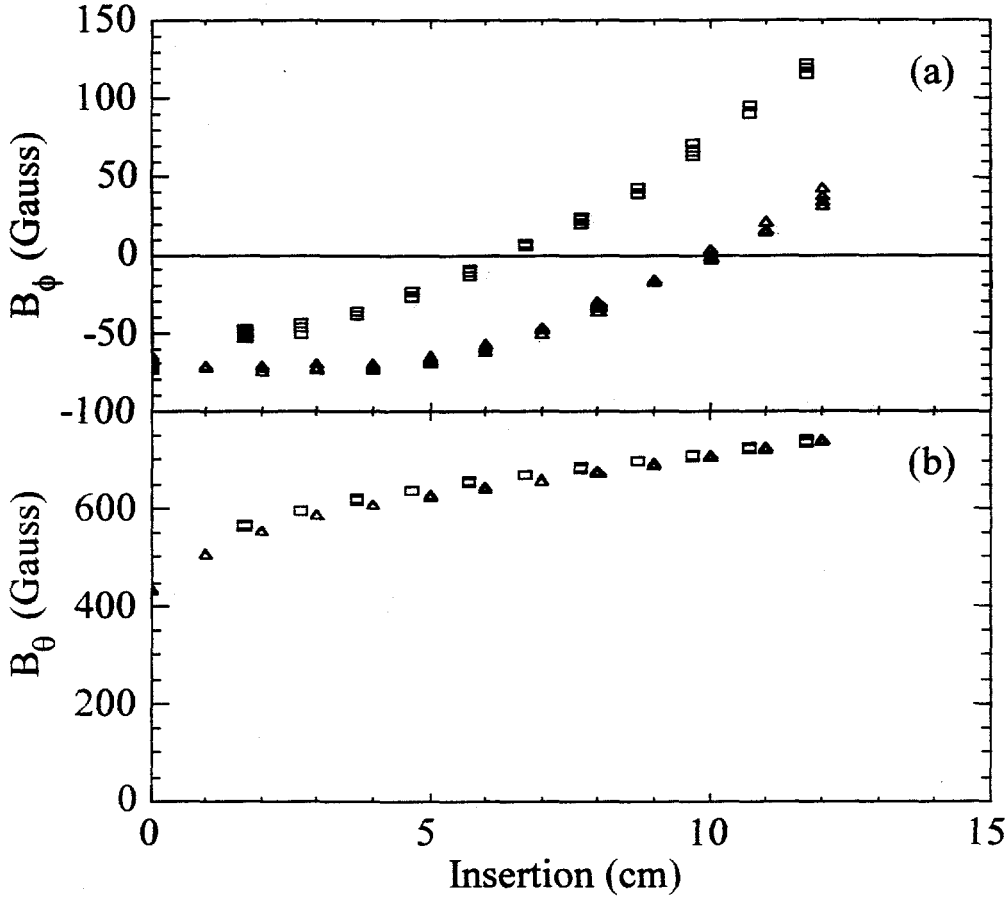

Figure 3.17. Edge toroidal (a) and poloidal (b) magnetic field profiles are shown for both the magnetic pickup coils of a Rogowski probe at 105° P (triangles) and a different magnetic probe at 37° P (squares).

3.3.1 Edge Magnetic Equilibrium Measurements

Magnetic field profiles have not as yet been measured in MST throughout the entire plasma cross-section because diagnostics capable of measuring core magnetic fields have not been implemented. Edge measurements of magnetic fields are fairly routine in low current plasmas ($I_p \sim 200$ kA) but a description of the toroidal effects needs to be obtained in order to accurately predict the path of magnetic field lines on which current is injected. For this

purpose, many measurements of magnetic field profiles were made and a summary of the results is given in this section.

Figure 3.17 shows radial profiles of toroidal and poloidal magnetic fields for a set of typical low current discharges ($I_p \sim 150$ kA) with F = -0.2 and line-averaged density about 5×10^{12} cm^{-3}. Profiles were taken simultaneously with the 3 magnetic pickup coils in the Rogowski probe (see Figure 3.8) mounted on a port at 105° P and with another magnetic probe at 37° P. One notices that while the poloidal magnetic field measurements are quite similar, the toroidal magnetic field profiles are different. The differences are due to two toroidal effects. First, flux surfaces are not concentric with the vacuum vessel (except at r = a) but are instead shifted outward from the geometric axis of the machine (see Figure 3.18). This means that when two probes at different poloidal angles are inserted the same distance from the wall, the probe which is most outboard will be effectively deeper in the plasma than the other.

The second effect is that bending the cylindrical plasma into a torus breaks the symmetry in the poloidal direction; hence the components of the magnetic field can no longer be expected to be symmetric. The asymmetries in the poloidal field are typically small (< 10%), as demonstrated in Figure 3.17b. The asymmetry in the toroidal field is not small unless the aspect ratio (R_o / a) is very large. If one assumes that currents flow mainly within flux surfaces (a good assumption) and that the magnetic fields and currents are toroidally symmetric (a good assumption if mode amplitudes are small and guns are not in use) then it is easy to show that the toroidal magnetic field must vary as 1/R on any given flux surface where R is the major radius. Of course, in going from one flux surface to another, this need not hold.

The easiest flux surface to identify is the reversal surface for which $B_\phi = 0$. The position of the $B_\phi = 0$ point at different poloidal angles can be used to calculate the outward shift of the reversal surface assuming that the flux surfaces have a circular cross-section

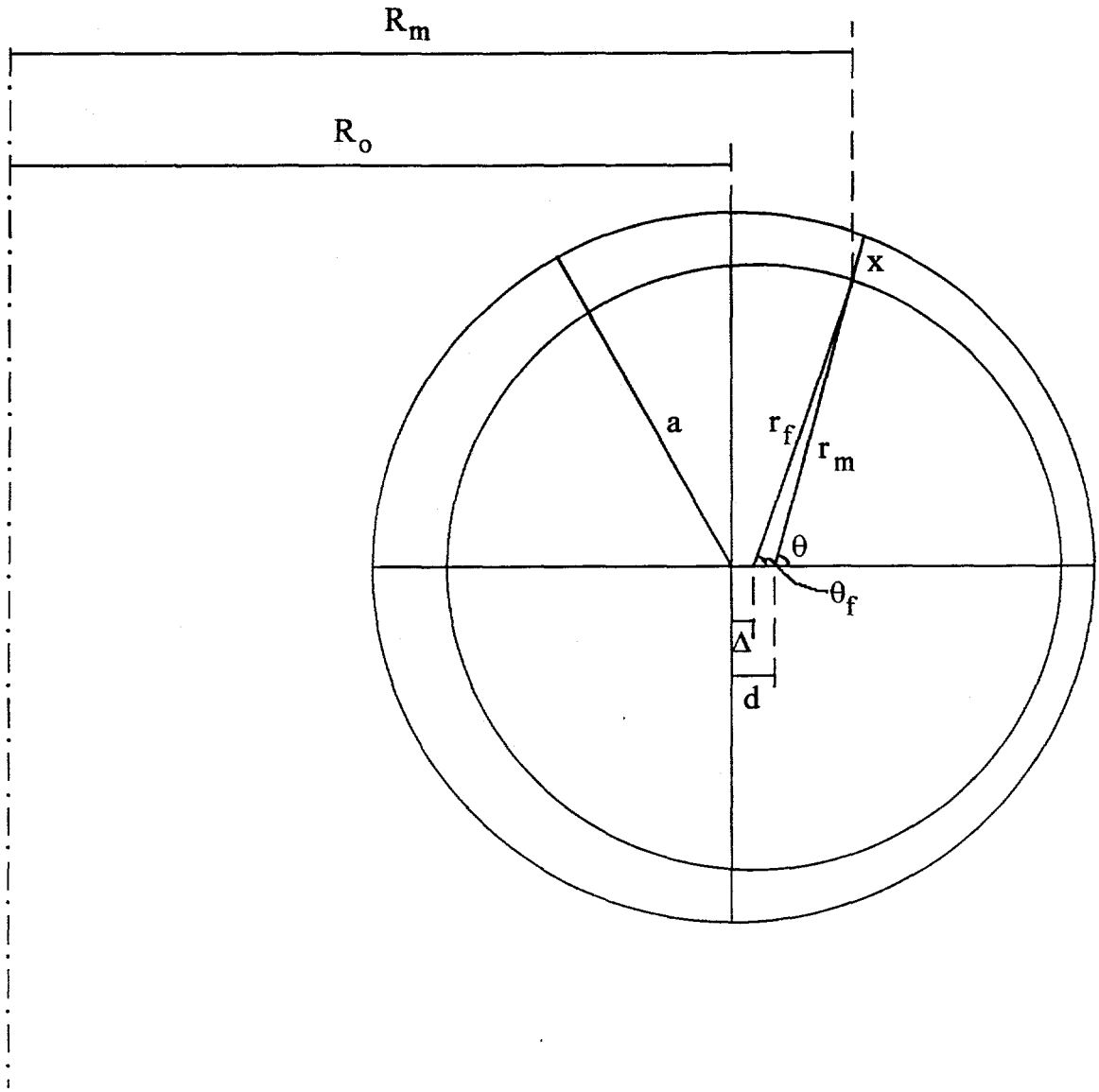

Figure 3.18. Schematic drawing of flux surface and MST geometry.

(probably a good assumption for MST). From Figure 3.17a we see that the reversal surface is at an insertion of about 10.0 cm at 105° P and at 6.3 cm at 37° P. This implies that the reversal surface in these discharges has an outward shift of about 3.9 cm and a radius of 42.7 cm. (One must be careful in this analysis to note that most ports are drilled toward an axis

shifted 6 cm outward from the geometric axis. This is the case for the 105° port but not for the 37° port.) This shift compares favorably with initial results from toroidal equilibrium reconstructions [7].

Another requirement of any equilibrium is that the shift of the flux surface whose radius is 52.0 cm (r = a) be 0 cm so that field lines do not penetrate the conducting shell. If we assume that the shift of flux surfaces changes linearly with radius between these two points, we arrive at an expression for the shift, valid in the edge only:

$$\Delta(r_f) = \gamma\,(a - r_f), \tag{3.7}$$

where γ is the slope of the line and r_f is the radius of the flux surface. A fit to the data of Figure 3.17 gives $\gamma = 0.42$. An examination of similar data in other configurations (different currents, densities, and reversal parameters) indicates that γ can vary from about 0.35 to 0.45 with the higher values typical of shallow reversal (F close to zero). This may imply either that the relationship in Equation 3.7 is not quite correct or that it changes slightly with plasma configuration. Certainly the relationship is not linear all the way to $r_f = 0$ and probably the deviation from a straight line is significant for radii less than $r_f / a \sim 0.8$.

Once a value for γ has been specified, it is straightforward to calculate the flux surface radius corresponding to any insertion at any poloidal angle. Hence the first toroidal effect can be accounted for. For purposes of field line trajectories, the most important variable to know is the pitch of the field line at every position. This is given by

$$\zeta \equiv \frac{d\phi}{d\theta} = \frac{r_f B_\phi}{R B_\theta} \tag{3.8}$$

with all quantities evaluated at the same point in space and the derivative is performed following a magnetic field line. (Technically, the θ in this expression is in a coordinate system with origin at the flux surface axis but the correction to the measured B_θ for this effect is small and will be ignored. In a cylindrical geometry, ζ is equal to the safety factor, q.) Profiles of ζ obtained from both probes are shown versus r_f in Figure 3.19a using $\gamma = 0.42$ to

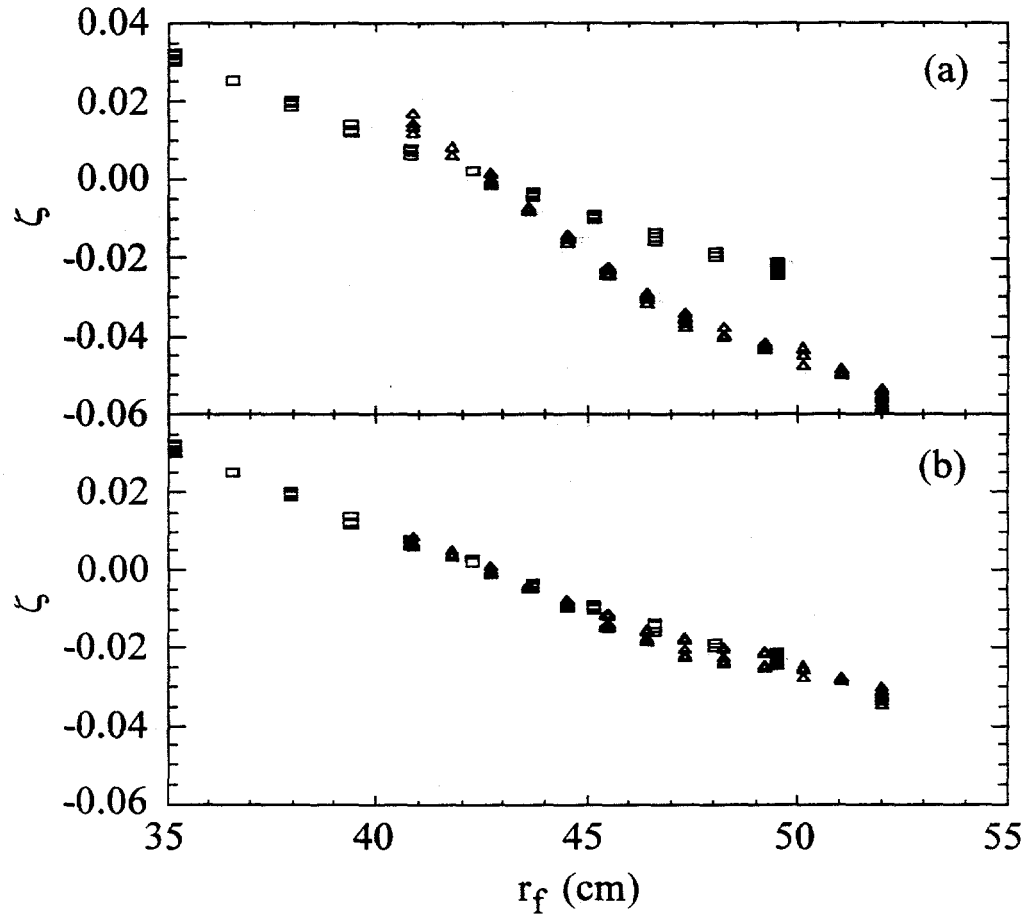

Figure 3.19. (a) Measured profiles of the field line pitch parameter, $\zeta = d\phi/d\theta$ calculated from the data in Figure 3.17 are shown versus flux surface radius. (b) The same profiles are shown with the data from 105° P (triangles) adjusted to represent data at 37° P (squares) using a $1/R^2$ dependence.

compute the flux surface radii. Now the $\zeta = 0$ points (or $B_\phi = 0$ points) are aligned because the flux surface shifts have been taken into account. The profiles are not identical because the second toroidal effect has not been compensated for.

From Equation 3.8 and the discussion above, it is clear that $\zeta \sim 1 / R^2$ on any given flux surface provided that the poloidal field does not vary too much on a flux surface. In

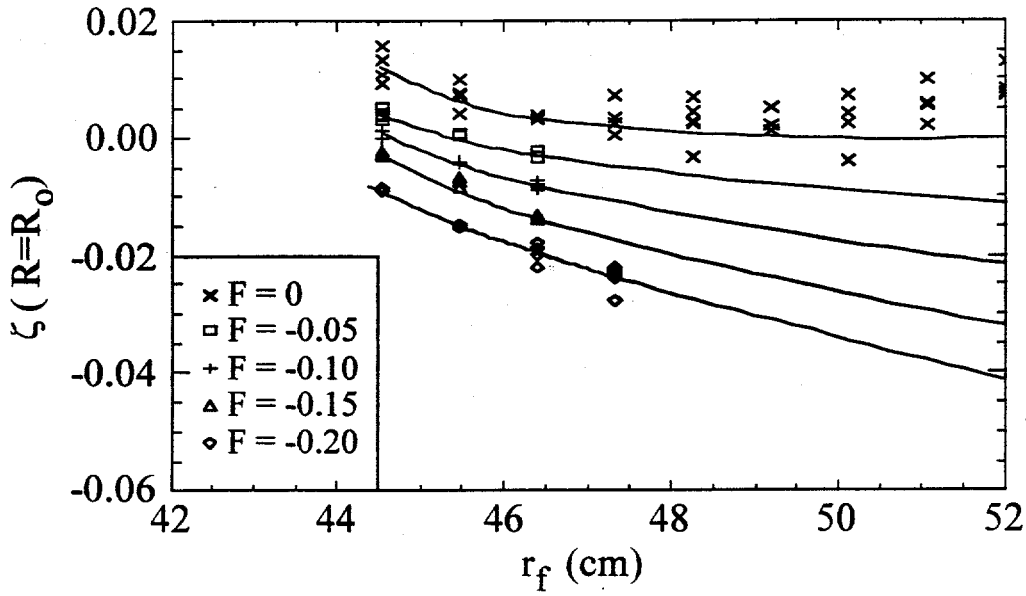

Figure 3.20. Measured ζ profiles for several reversal parameters are shown versus flux surface radius. Data have been adjusted to represent the value at $R = R_0$.

Figure 3.19b, the data taken at 105° P have been modified to reflect what would be measured at 37° P assuming that $\zeta \sim 1 / R^2$. The adjusted data agree well with the actual profile measured with the probe at 37° P. Hence it appears that the variations in poloidal field can probably be neglected to first order.

In the next section, what is desired is to predict the trajectories of all edge field lines in the vicinity of a Rogowski probe using only the magnetic field measured with the same probe at a single radius and poloidal angle. Since the field line mapping depends on the entire ζ profile, what is needed in addition to the above relations is an expression for how the profile depends on plasma configuration. The most significant variation is expected to be linked to changes in the reversal parameter. Figure 3.20 shows the measured ζ profiles for several reversal parameters corrected for flux surface shift using $\gamma = 0.4$ and adjusted to represent the ζ at $R = R_0$. Lines have been drawn to connect the measured profiles with the

expected value at the wall obtained from F/Θ where $\Theta \equiv B_\theta(r=a) / \langle B_\phi \rangle$ is the pinch parameter and $B_\theta(r=a) = (\mu_o I_p / 2\pi a)$. What one observes is that the radial derivative of ζ in the region of interest ($r_f \sim 46$ cm) varies only slightly with F.

An appropriate model for edge field line trajectories can now be formulated. In the subsequent simulations of Rogowski probe measurements, I will assume the flux surfaces are circular with a shift given by Equation 3.8 with $\gamma \sim 0.4$. The field line pitch parameter, ζ, will be assumed to vary on a flux surface as $1 / R^2$ and the radial profile will be taken as linear near the point where measurements are made. The slope in the ζ profile will be treated as a restricted parameter. With these assumptions and the measured magnetic fields at a particular point, the field lines near that point can be followed around the torus.

3.3.2 Measurements of Injected Current from Plasma Guns

There are two important aspects of the current driven by the plasma guns that must be measured to estimate how effective the current should be in controlling magnetic fluctuations. The first is the characteristic length for current dissipation along a field line and the second is the characteristic length for current diffusion perpendicular to field lines. The first length is important because it determines the number of poloidal transits the current will make and hence the multiplication factor to convert from bias circuit current to total driven poloidal current. The second length plays a role in determining the radial profile of the current that is injected.

Although the measurements presented in this section shed light on these two quantities, neither one has been successfully determined. For reasons that will be apparent, the measurement requires precise knowledge of field line trajectories during gun operation and precise mapping of very small scale current structures without interference. The Rogowski probe is limited to measuring currents with ~ 1-2 cm resolution. It appears that

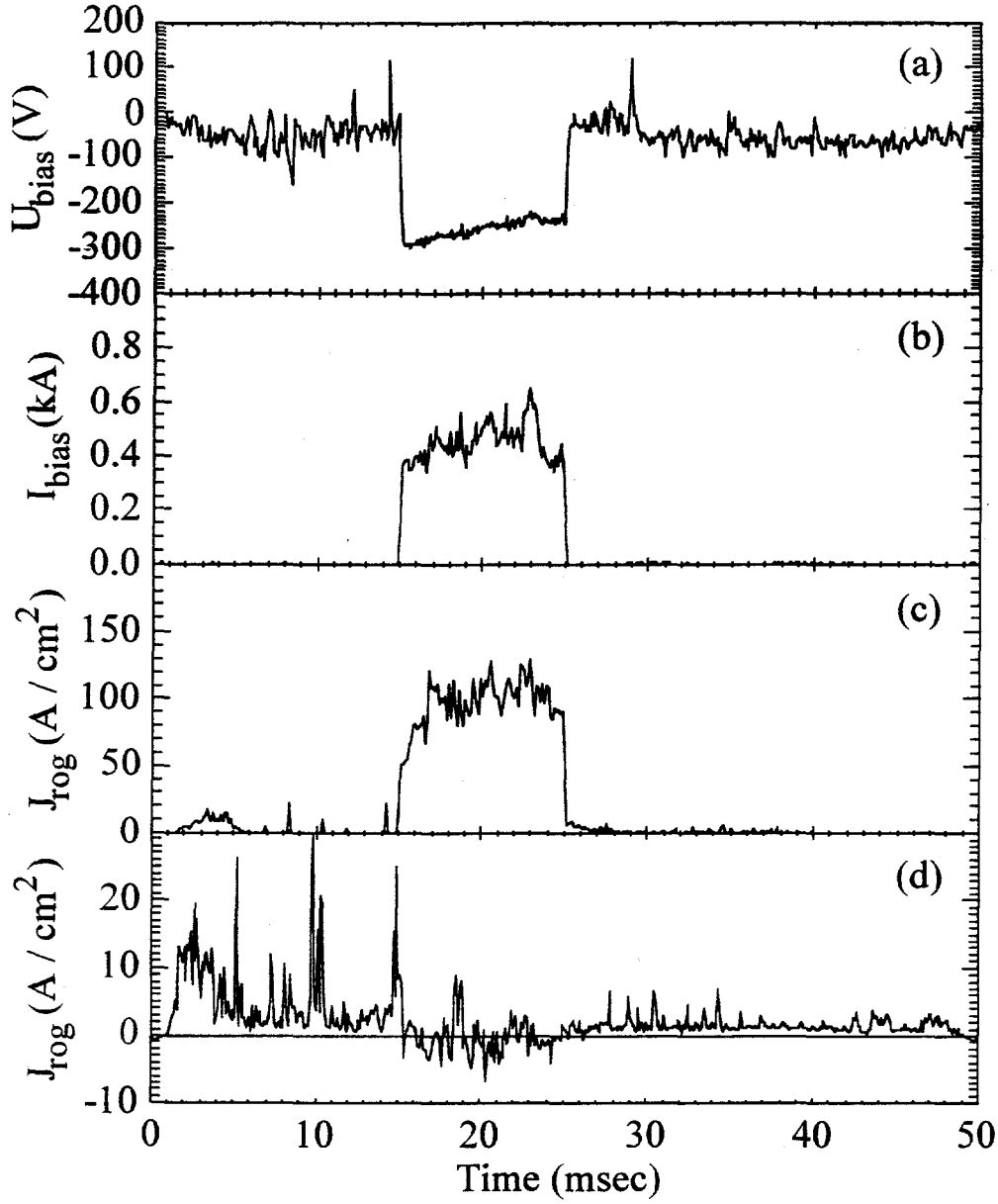

Figure 3.21. Bias voltage (a) and bias current (b) are shown versus time for a typical injector operating in MST. Also shown are the current density measured 25 cm downstream (c) and the current density 25 cm upstream (d) of the gun.

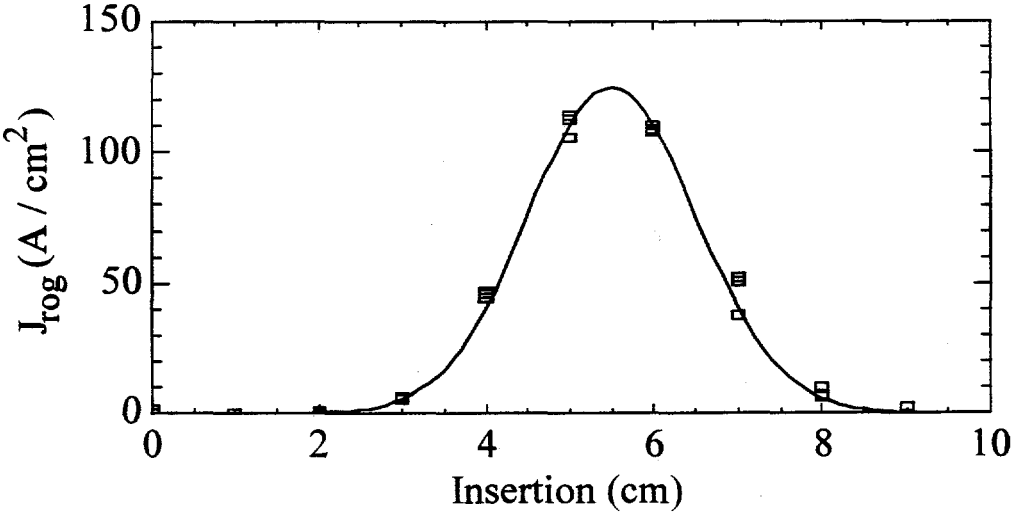

Figure 3.22. The measured current density profile 25 cm downstream of a gun is shown with the background current subtracted.

this is too coarse a scale to determine the exact value of the two length scales mentioned above.

Still, much can be learned from these measurements. Figure 3.21 shows the bias voltage and current from a single gun in a typical MST discharge. Also shown are two current density measurements by a Rogowski probe situated on the field line going through the center of the gun discharge. The data of Figure 3.21c were taken with the probe 25 cm downstream of the gun position and those in Figure 3.21d were taken 25 cm upstream of the gun position. As in the test stand, one observes that the injected current is highly directional. (Note the different scales in c and d.) Figure 3.22 shows the measured radial profile 25 cm after the current has left the gun as well as a Gaussian fit with a radial HWHM of about 1 cm and a peak current density of ~ 125 A/cm^2. The integrated profile (2 dimensional Gaussian) gives a total current very close to the measured bias current of 500 A.

Measurements of the injected current further downstream can only be interpreted by mapping the injected current along the magnetic field lines to the Rogowski position and then integrating over the Rogowski coil area. Before presenting these measurements, I will demonstrate the behavior of the field lines and motivate the need for precise field line mapping. The contour plot in Figure 3.23 depicts the initial current density distribution leaving the gun which is assumed to be symmetric about the gun discharge axis. Using a simple cylindrical model (see Section 3.3.3) for an F = -0.2 plasma, the contours in Figure 3.23 were mapped along field lines for one complete poloidal turn. The resulting distribution is shown in Figure 3.24.

Since the magnetic configuration has strong shear, field lines at different radii move different toroidal distances after one poloidal turn and the current distribution becomes elongated in the toroidal direction. The total area as well as the current density on any given field line do not change but the toroidal extent and location do change with poloidal angle. Figure 3.25 shows the resulting current patterns from the initial through the 10th poloidal turn for a case with F = -0.35. One will note that after 10 turns, the current extends over 100° toroidally (a length of about 260 cm!) and the radial extent at a given toroidal position is very small. Certainly the Rogowski probe which integrates over a circle 2 cm in diameter will have a difficult time measuring any current after many poloidal transits even if there is no diffusion or dissipation. It is expected, however, that the probe should be able to see current after a few poloidal turns.

Another difficulty in the Rogowski measurements that is apparent from Figure 3.25 is that the different turns begin to stack up after several poloidal transits so that a finite-sized Rogowski probe will actually measure several turns at once. This complication is particularly severe if the safety factor at the injector depth is close to zero because in that case the distribution does not travel very far toroidally with each poloidal turn and hence the stacking is compounded. It is thus important when measuring the injected current far from the gun to

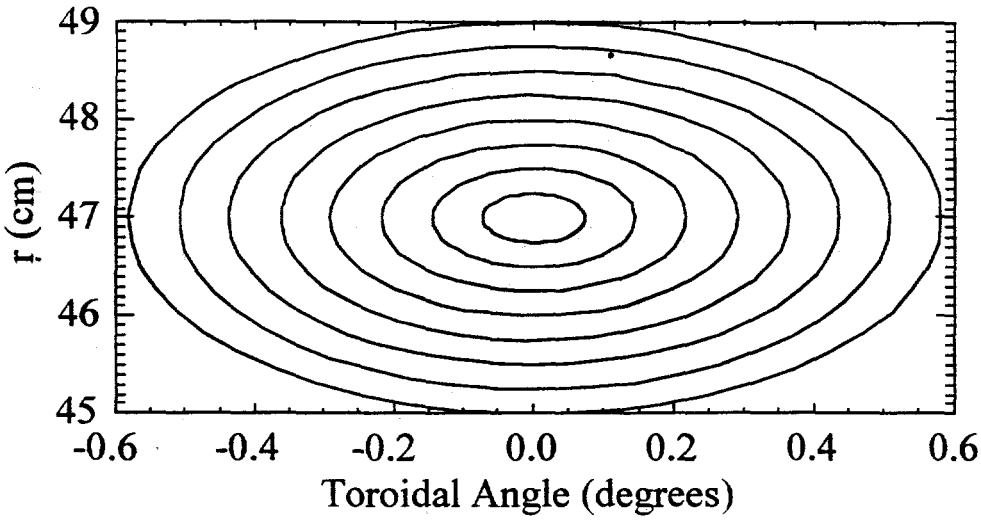

Figure 3.23. A hypothetical initial injected current distribution is shown as a contour plot.

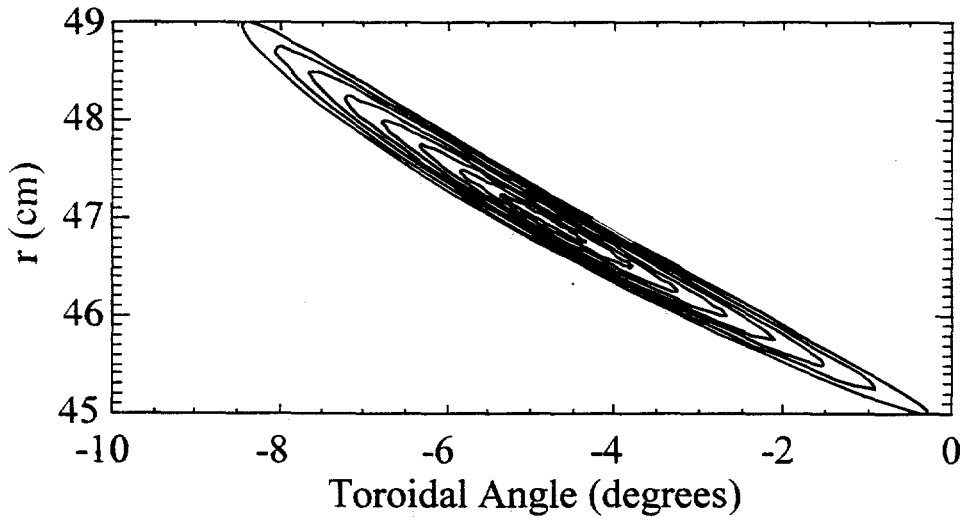

Figure 3.24. The injected current of Figure 3.23 is shown after completing one poloidal transit.

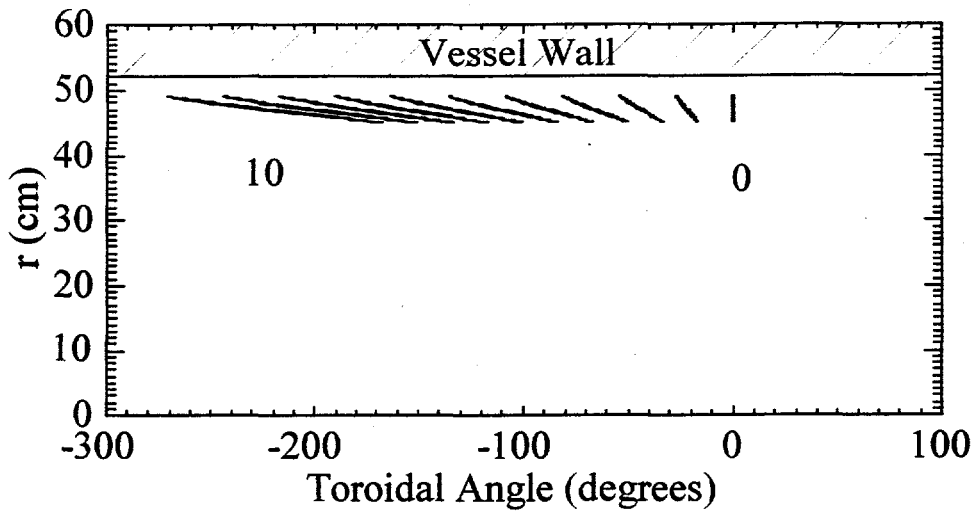

Figure 3.25. A hypothetical current distribution from one injector at 0° T is shown in a deeply reversed equilibrium after completing 0,1, ...,10 poloidal transits.

choose both the position of the Rogowski probe and the magnetic configuration carefully. In addition, because the Rogowski integrates over a substantial area, the magnetic field line trajectories need to be well known in order to determine what current one is looking at in any given measurement.

With this in mind, we turn our attention to the data of Figure 3.26 which show the measured current profile at 105° P produced by a gun at 15° P but at the same toroidal angle. The reversal parameter in this discharge was F ~ -0.05 and even after a displacement of only 70 cm the sheared magnetic field has already moved much of the injected current away from this toroidal location. To interpret these results, the magnetic fields measured by the magnetic pickup coils in the Rogowski probe were used along with the model described in Section 3.3.1 to simulate what the Rogowski would measure if the current from the gun simply traveled along the field lines. Each point within the 0.91 cm radius circle through which the probe measures current was mapped back along the field lines to the injector

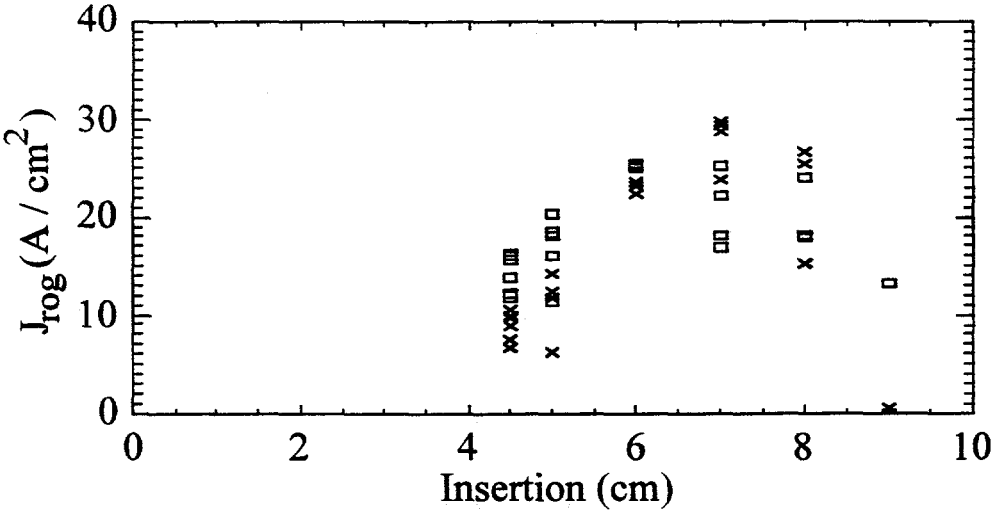

Figure 3.26. The measured current density profile (squares) is shown from a Rogowski probe located 90° P downstream of a gun. The background current has been removed. Also shown is simulated data (x) based on the field line trajectory model of Section 3.3.1.

location. The current density at that point was determined assuming that the initial current distribution was Gaussian in the toroidal and radial directions. The data could only be fit well by assuming an initial current distribution with a HWHM of 2 cm. The simulated data are shown in Figure 3.26 by the + symbols. If the field line model is accurate, this suggests that there may be a broadening of the current distribution as one travels along the magnetic field lines since the data of Figure 3.22 imply a narrower initial current distribution. It appears, however, that the center of the distribution does not drift very far in this distance nor does the total integrated current decrease.

To measure the injected currents after one or more poloidal transits, two Rogowski probes were used along with one gun. The probes were placed at 320° T, 75° P and 300° T, 75°P and the gun in use was at 330°T, 15°P (see Figure 3.1). To measure the current after

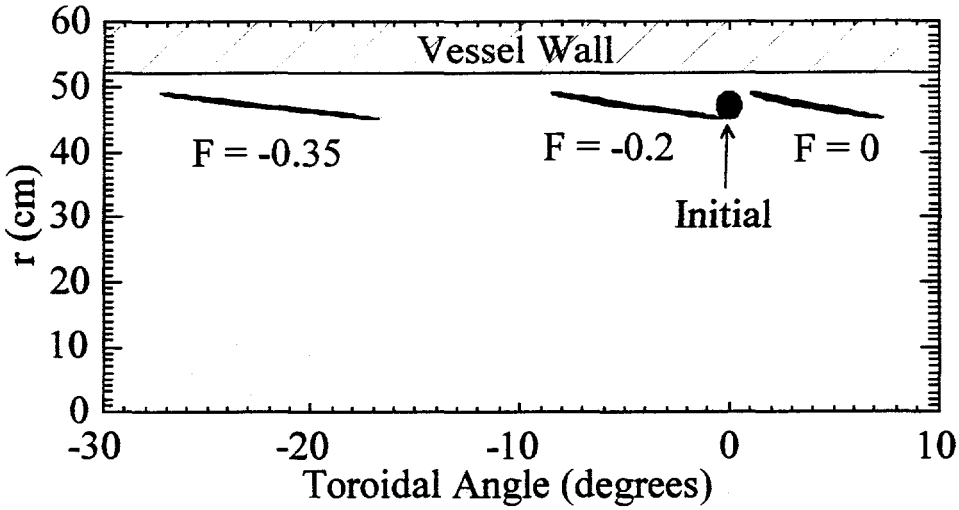

Figure 3.27. The effect of varying F on the one poloidal turn current distribution is shown.

various numbers of poloidal turns the reversal parameter was scanned to sweep the field lines back and forth across the Rogowski probes. Figure 3.27 illustrates the effect of changing F on the one turn current distribution. As the reversal parameter was varied, different portions of the currents shown in Figure 3.25 were sampled by the probes. The field line model described in the previous section was again applied and a comparison between measured and simulated data was performed.

Figure 3.28a shows the simulated Rogowski current for the probe at 320° T as a function of the B_ϕ/B_θ ratio measured by the probe. The individual contributions from current going through the Rogowski after 1 to 5 poloidal turns is shown as well as the sum of these. One can see the effect of the finite Rogowski coil size and current stacking as the various turns are mixed together. Figure 3.28b shows the measured change in current density as a function of the same ratio for both discharges with the gun biased and in similar discharges without gun bias. The data shown are calculated by subtracting the measured current before the time of injection from that during injection (or in the no-bias cases, the time when

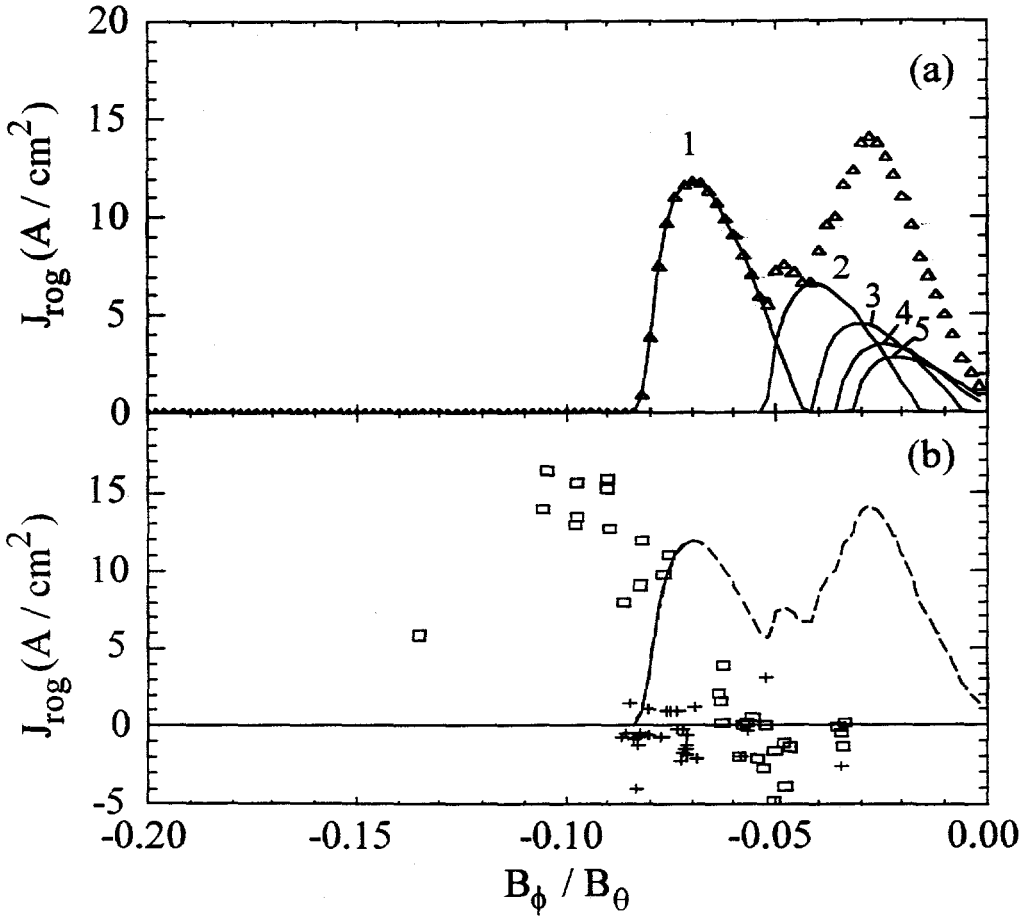

Figure 3.28. (a) Simulated Rogowski probe measurements of the 1 to 5 turn currents as well as the sum (triangles) of the 1 to 5 turn currents are shown versus the measured magnetic field ratio for the Rogowski probe located at 320° T. (b) Also shown are the measured data with (squares) and without (+) bias applied to the injectors along with the simulated sum of the 1 to 5 turn currents (solid line). The dashed line indicates simulated current which is blocked by an inactive gun.

injection normally occurs). Unfortunately, additional guns were inserted (but not active) at 320° T, 15° P and 300° T, 15° P during this run. For low B_ϕ/B_θ ratios, the Rogowski probes were in the "shadows" of these guns and hence current could not be measured. The

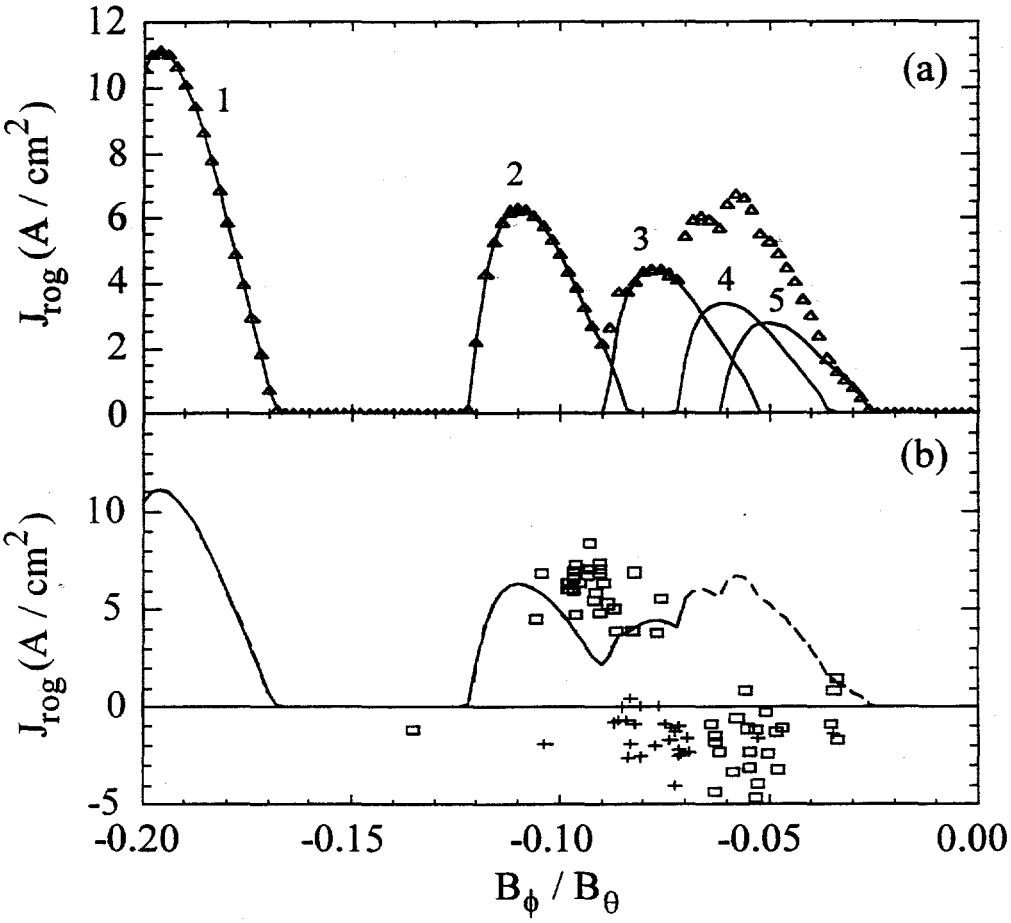

Figure 3.29. The same information shown in Figure 3.28 is shown for the Rogowski probe at 300° T.

simulated sum of the 1 to 5 turns from Figure 3.28a is overlaid in Figure 3.28b; the dashed part of the line indicates approximately the portion which is not expected to be measured due to shadowing.

The first thing to note is that a substantial current density is measured after at least one poloidal transit. Exactly which currents are being measured by the probe is not clear because the simulated data do not agree completely with the measured data. However,

whatever current is being measured is definitely associated with field lines that have gone around poloidally at least once. The amplitude of the measured current density agrees fairly well with what is predicted using a 1 cm HWHM initial distribution. However, current is consistently measured at B_ϕ/B_θ ratios for which the field line mapping predicts no field lines are linking the probe and the injector.

Figure 3.29 shows data from the Rogowski probe at 300° T for which the agreement is better but still not perfect. This probe definitely measures current which has made at least two poloidal transits but it is not clear if current from more than two turns is measured or not. Again the probe does not measure current at low $|B_\phi/B_\theta|$ due to shadowing. This incidentally illustrates a key issue for experiments with many injectors. Injectors should not be placed too close together or they will screen out a significant fraction of the injected currents. This is particularly a problem for guns located at the same toroidal angle in shallow reversal cases. Figure 3.27 shows that when injecting current ~ 5 cm from the edge, either F = 0 or deep (very negative) F should be used to ensure that currents are not blocked by nearby guns.

The data in Figures 3.28 and 3.29 demonstrate that injected current persists after at least two poloidal transits. A similar experiment was done without any extra guns inserted to look for current after more than two poloidal turns. Figure 3.30 shows data from a different run with a Rogowski probe at 300° T, 90° P and a gun operating at 320° T, 15° P. This data affirms that the small measured currents at low $|B_\phi/B_\theta|$ in Figures 3.28 and 3.29 were due to shielding by the inoperative guns and also suggests that a significant portion of the injected current remains after more than three poloidal transits. The mismatch between measured and simulated current amplitudes in Figure 3.30 is probably due to a combination of errors in the field line mapping (which are compounded with each poloidal turn) and errors in measurement of probe and/or injector insertion measurements.

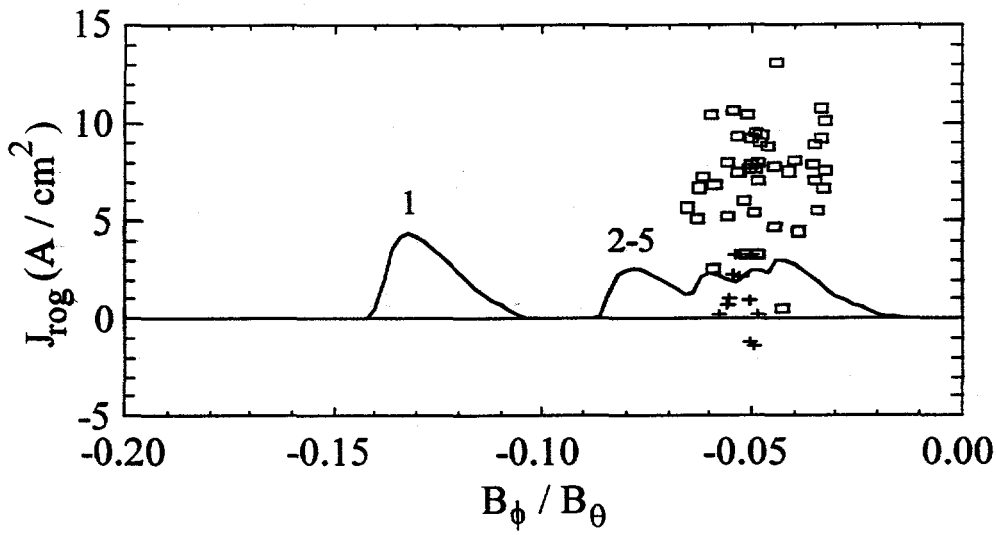

Figure 3.30. Measured Rogowski data at 300° T, 90° P are shown for both discharges with (squares) and without (+) a nearby gun biased. Simulated data (solid line) from current traveling 1 to 5 poloidal turns is also shown.

The fact that current is measured in Figure 3.28 at $|B_\phi/B_\theta|$ values larger than those that the model predicts should give current is more difficult to explain. The two best possibilities are that the field line model used to project the gun currents along the magnetic field is incorrect or that the injected current is diffusing somewhat toroidally and/or radially. The most important variable in the field line mapping is the field line pitch parameter, ζ. The two sets of independently-calibrated pickup coils in the Rogowski probes give virtually identical $|B_\phi/B_\theta|$ measurements so the measurements of ζ at the probe positions are probably correct, although, as discussed above, the measurements do average over a significant spatial extent. Another possibility is that the assumptions that $\zeta \sim 1/R^2$ on a flux surface and that the surfaces are circular may not be correct. Asymmetries in the poloidal magnetic field may also be important and there are deformations of the flux surfaces due to the magnetic fields produced by the injected current.

Figure 3.31 shows the measured perturbations of the toroidal and radial magnetic fields produced by the current shown in Figure 3.22. For current flowing along a magnetic field line, a magnetic field is produced azimuthally around that field line. This implies that at radii outside and inside that of the injected current, the toroidal field would be made more negative and more positive respectively. At toroidal angles that are less than (greater than) that corresponding to the field line on which current is injected, a positive (negative) radial field should be produced. For a current of 500 A, the field a distance 1 cm away would be about 100 Gauss. The field measured in Figure 3.31 is somewhat less than this but the dependence on radius is as expected.

These fields tend to twist the injected current helically around the center of injection and cause a toroidally and poloidally asymmetric variation of the field lines. The actual trajectory of the current is along a self-consistent set of field lines produced both by the MST discharge and the injected current pattern. These injection-induced fields will be strongest near the gun where the current density is largest and get weaker as the current is spread out by the magnetic shear and dissipated. How these fields change the simulated Rogowski current is difficult to estimate.

It is also possible that there is some diffusion of the current toroidally and/or radially. The fact that the magnitudes of measured and simulated current match fairly well suggests that the diffusion is not too large. However, the measurements of Figure 3.26 indicate that the current distribution probably does broaden somewhat during the first poloidal turn. The data in Figure 3.28 and 3.39 were obtained with Rogowski probes on flux surfaces that were slightly outside of the one on which the initial current distribution was centered. Hence, including some radial diffusion would tend to increase the simulated signal and move the solid lines of Figure 3.28 and 3.29 to the left. (Flux surfaces inside of the probe position have both more current density and lower B_ϕ/B_θ). It is difficult to determine which of these effects is

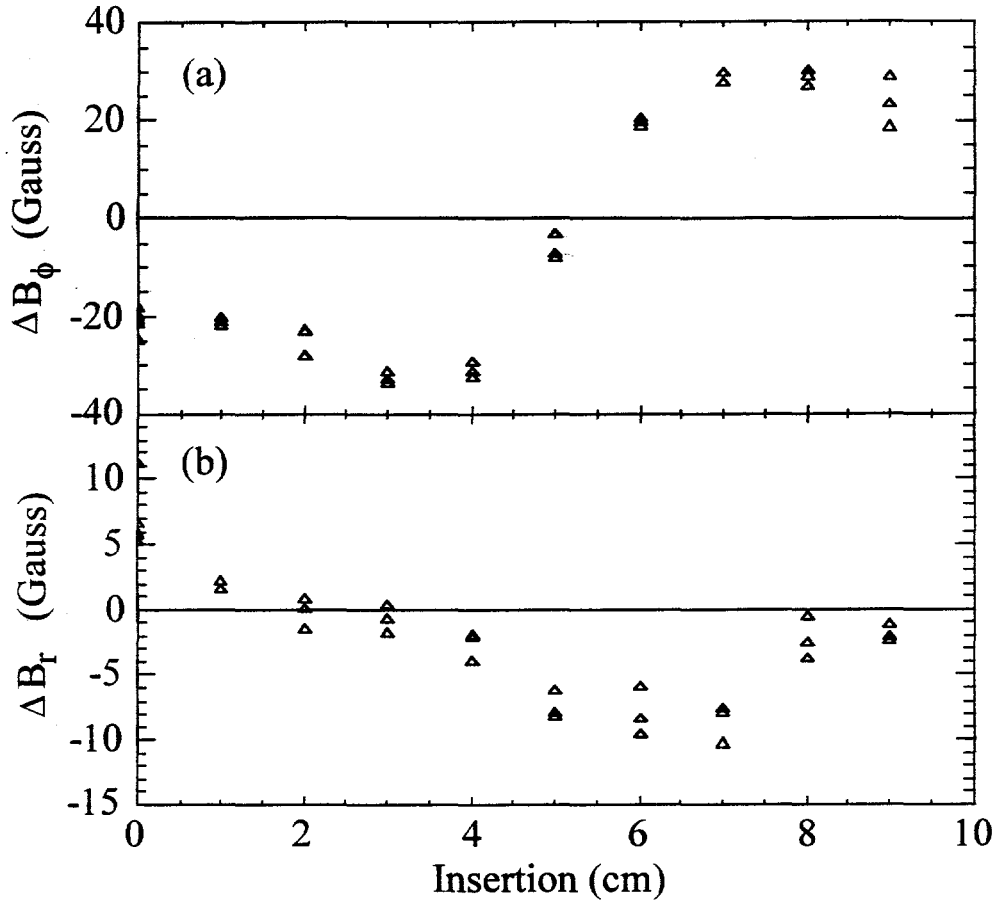

Figure 3.31. The change in the toroidal (a) and radial (b) magnetic fields measured with a Rogowski probe near the injected current are shown versus insertion. These data result from comparing the fields during injection to those immediately before.

important without measurements of magnetic fields and current densities with much higher spatial resolution.

In all, it appears from the combined measurements that the injected current stays attached to the field line for at least 2 to 3 poloidal turns and maybe more. There is some evidence for radial broadening of the current channel during the first poloidal turn, but no evidence for diffusion of the entire distribution into or out of the machine during the first few

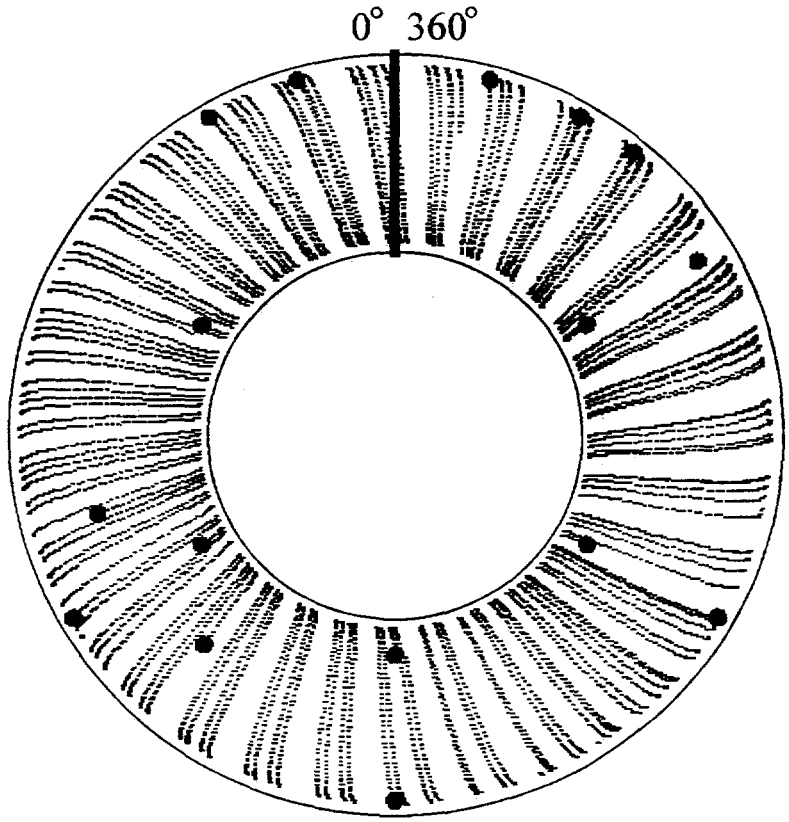

Figure 3.32. A top view of MST is shown with a hypothetical current mapping from 16 injectors superimposed. Filled circles represent injector locations and dotted lines indicate the projection of injected current trajectories onto the horizontal midplane.

poloidal turns. We can put a theoretical upper bound on the dissipation length by considering the effect of collisions between the injected electrons and background ions. The classical momentum damping length is sensitive to the electron energy ($\lambda_m \sim v^4$); for 200 eV electrons in the MST edge it is about equal to 13 poloidal turns. The actual dissipation length is probably somewhere between this and the 2 to 3 turns that have been measured. To arrive at

an exact value, however, the currents need to be measured on much smaller spatial scales than the Rogowski probe can accomplish.

Figure 3.32 shows a hypothetical mapping of the currents from 16 guns (shown as circles) on a particular flux surface as seen from above the torus. A constant field line pitch was assumed with a value corresponding to F ~ -0.3 and the currents were assumed to complete 10 poloidal transits. The actual 3-D distribution of currents is really represented by a combination of this diagram and that shown in Figure 3.25 (and is impossible to plot in any legible format!). One sees that with 16 injectors, the distribution approximates a toroidally symmetric current drive scheme.

3.3.3 Cylindrical Equilibrium Modeling of MST Discharges with Current Injection

One goal of this research is to use edge current drive to modify the current profile in an attempt to control magnetic fluctuations. Although no capability yet exists to measure full current profiles throughout the MST discharge, an indication of the profile changes during injection can be obtained by using magnetohydrodynamic (MHD) equilibrium models. It is easy to show from the ideal MHD equations that

$$\vec{J} = \frac{\lambda \vec{B}}{\mu_o} + \frac{\vec{B} \times \vec{\nabla} P}{B^2} \tag{3.9}$$

where

$$\lambda \equiv \mu_o \frac{\vec{J} \cdot \vec{B}}{B^2} \tag{3.10}$$

is a normalized measure of the parallel current density.

Several models for λ have been developed for the RFP in cylindrical geometry [8,9,10]. For analyzing MST discharges with guns injecting current, I will use a common model [11] in which the parallel current profile is described by $\lambda = \lambda_o (1 - (r/a)^{\alpha})$ and the pressure profile is taken to be parabolic with $\beta = 10\%$. (Changes in the pressure profile do

not change the conclusions of the analysis presented here.) The two parameters λ_0 and α can be mapped into the two experimentally observed parameters F and Θ and hence time dependent profiles of the equilibrium can be easily determined. The details of the current profile (particularly in the edge) cannot be reproduced with this model, but the average behavior of the entire profile will be captured.

The parameter α determines the shape of the parallel current profile. Profiles with large α are flat in the core and steep in the extreme edge. Figure 3.33 shows the four parameters F, Θ, α, and λ_0 for a discharge with 16 guns injecting current in the sense to add to the background current density in the edge. If the plasma had no response to the current drive, the α would increase during current drive because on average the current profile would be flatter with guns injecting current. Figure 3.33 shows that the plasma does respond to the current drive, however, and develops large, extended sawtooth oscillations during strong current injection. The resulting equilibrium has, on average, a steeper current profile when the average is done over time and radius. This is at first glance a perplexing result since the additional current is certainly in the sense to make the profile flatter.

There are two comments to make in regard to these results. First, although the profile is on average steeper, in some regions of the plasma (namely the edge) the gradients are not as steep when α is reduced. This may have implications for how modes in different regions of the plasma are affected by the current drive. For example, low α may be bad for core mode stability but good for edge mode stability. The second thing to consider is that the RFP system is complex. The current profile is self-consistently determined by applied and fluctuation-driven fields and at the same time the saturated fluctuation amplitudes are determined by the current profile, the resistivity profile, and the rate of energy transfer between different modes [12]. The addition of parallel current in the edge alters this balance and it is not inconceivable that the current profile may get more peaked as a result.

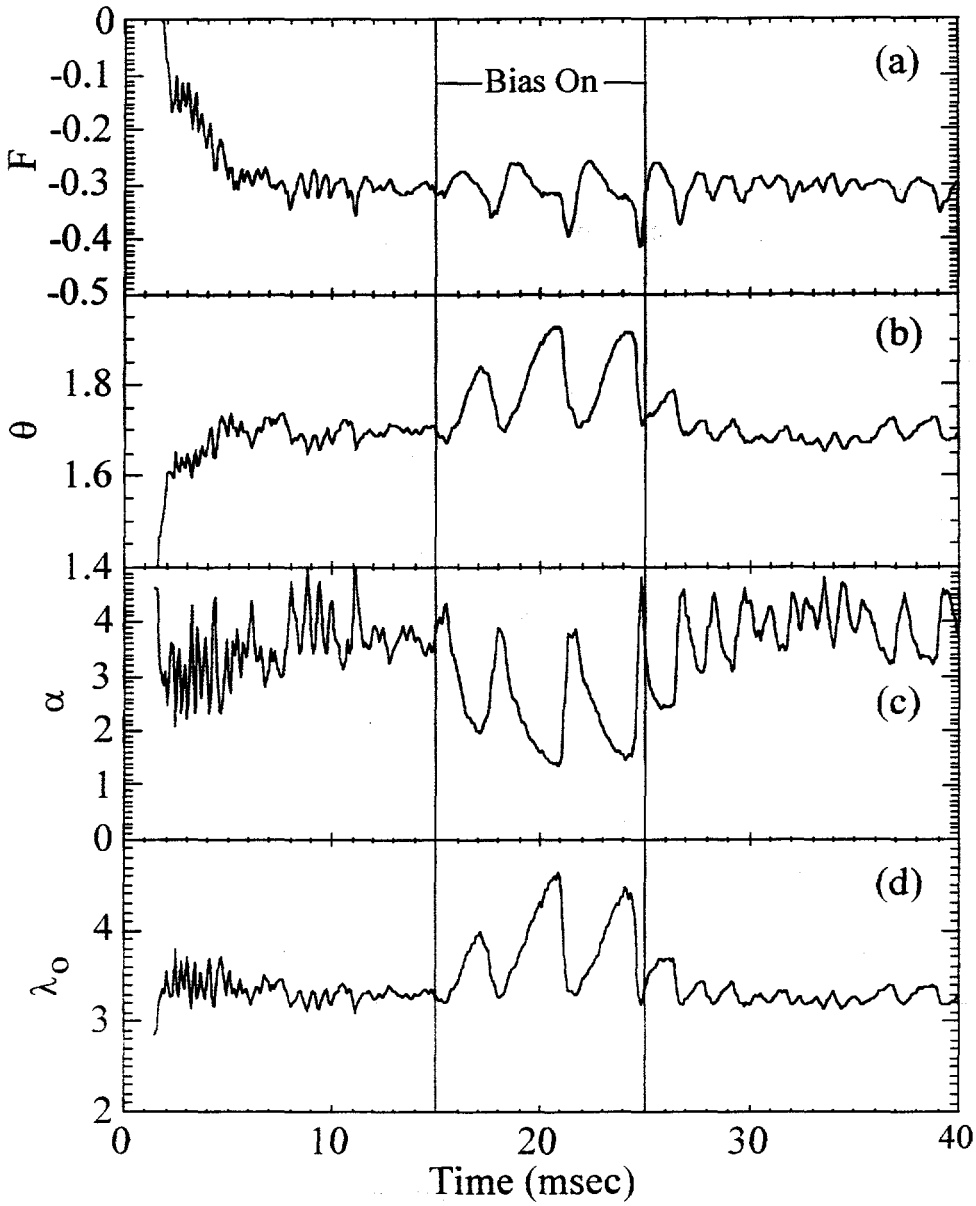

Figure 3.33. The measured F (a) and Θ (b) are shown versus time for a discharge with 16 injectors operating. Also shown are the α (c) and λ_o (d) parameters that best fit the data.

It is interesting that in the Pulsed Poloidal Current Drive (PPCD) experiments, a similar "peaking" of the current profile is observed [13], yet the total magnetic fluctuation amplitude drops substantially. The key issue for confinement improvement is whether or not the magnetic fluctuations decrease with current drive. In Chapter 4 it will be shown that total magnetic fluctuation amplitudes also decrease when auxiliary current is driven in the edge with electrostatic injection.

3.4 Summary

In this chapter, we have seen that current drive with plasma guns is significantly different in MST than in the test stand configuration because the injected current must be driven both along and across magnetic field lines. This results in a higher effective bias circuit impedance so that less current is injected at a given bias voltage. The degree to which the impedance changes depends on the edge plasma parameters and on the specific geometry (i.e., number of guns used, depth of insertion, etc.) as one might expect from simple models of radial conductivity. Although the cross-field current drive makes field-aligned current drive more difficult, it can be used to bias the plasma and offers another degree of control in the edge.

Measurements of injected current distributions in MST suggest that the injected current is highly directional and propagates along magnetic field lines for at least 3 poloidal turns. This means that the total poloidal current driven by 16 guns which each inject about 600 A is at least 30 kA and possibly much more. A theoretical upper bound of about 100 kA is obtained by assuming the injected current is damped by classical collisions alone. The injected current distribution has an initial HWHM of about 1 cm and appears to broaden to some extent within the first poloidal turn. It does not appear, however, that the current distribution as a whole moves to larger or smaller radii during the first few poloidal turns.

Equilibrium modeling of MST discharges shows that with 16 guns injecting current in the sense to add to the background parallel current in the edge, the parallel current profile becomes on average more peaked. This result is similar to what is observed in inductive current drive experiments.

References

[1] I.H. Hutchinson, *Principles of Plasma Diagnostics*, Cambridge University Press, New York (1987).

[2] R.N. Dexter *et al.*, Fusion Technol. **19**, 131 (1991).

[3] D.J. Den Hartog and R.J. Fonck, Rev. Sci. Instrum. **65**, 3238 (1994).

[4] R. Balbin *et al.*, Rev. Sci. Instrum. **63**, 4605 (1992).

[5] M.R. Stoneking, Ph.D. thesis, University of Wisconsin - Madison (1994).

[6] C.R. Sovinec, Ph.D. thesis, University of Wisconsin - Madison (1995).

[7] J.K. Anderson, private communication.

[8] J.B. Taylor, Phys. Rev. Lett. **33**, 1139 (1974).

[9] J.C. Sprott, Phys. Fluids **31**, 2266 (1988).

[10] W. Shen and J.C. Sprott, Phys. Fluids B **3**, 1225 (1991).

[11] V. Antoni, D. Merlin, S. Ortolani, and R. Paccagnella, Nucl. Fusion **26**, 1711 (1986).

[12] P. Nordlund and S. Mazur, Phys. Plasmas **1**, 4032 (1994).

[13] M.R. Stoneking *et al.*, Phys. Plasmas **4**, 1632 (1997).

4. RESULTS OF FLUCTUATION AND TRANSPORT CONTROL EXPERIMENTS

In the two preceding chapters, the machinery and process of electrostatic current injection in MST have been reviewed. In this chapter, the results of experiments designed to control fluctuations and transport using the plasma guns are presented. One will recall from Chapter 1 that there are two main goals in these experiments. The first is to test whether steady edge current drive along the magnetic field is successful in controlling magnetic fluctuations and the transport connected with them. The second is to test whether or not plasma biasing in the RFP can have an impact on electrostatic fluctuations and the associated particle losses in the edge.

In Section 4.1, an overview of the results will be given and the techniques used to isolate different physics effects described. In Section 4.2, the effect of directional current drive on magnetic fluctuations and confinement is presented. In Section 4.3, the consequences of plasma biasing are discussed. In Section 4.4, changes in confinement due to the presence of the injectors in the plasma are presented. Finally, in Section 4.5, the results are summarized and the implications for understanding and improving confinement are considered.

4.1 Overview and Methods

4.1.1 Overview of Results

Measurements of magnetic fluctuation induced transport in MST [1,2] have shown that magnetic fluctuations in the frequency range corresponding to the core resonant tearing modes account for energy and particle transport inside the reversal surface but not outside r/a ~ 0.85. Consequently one expects that flattening the parallel current profile to stabilize the core modes may result in greater particle and energy confinement. In addition, measurements

of electrostatic-fluctuation induced transport have shown that electrostatic turbulence contributes to particle transport in the edge but not to energy transport [3]. Hence, it is possible that plasma biasing could increase particle confinement by generating sheared flows which mitigate edge particle losses.

The first main result of this chapter is that the understanding of confinement summarized above is generally correct but not complete. The core modes are not the only magnetic fluctuations that must be controlled. It will become apparent in Sections 4.2 and 4.4 that the m = 0 modes resonant at the reversal surface also play an important role in global confinement. This conclusion is supported by two observations. The first and most convincing observation is that energy and particle confinement respond to current drive with the guns even though the core magnetic mode amplitudes do not. Instead, it is the m = 0 mode amplitudes that increase or decrease when current is injected with or against the background edge current. The second observation is that the loop voltage in normal MST discharges increases monotonically as F decreases even though the electron temperature and core magnetic mode amplitudes do not strongly depend on the degree of reversal. The m = 0 modes, however, increase linearly as F is reduced and hence the behavior of the loop voltage could be explained if both the m = 0 modes and the core modes contribute to the anomalous part of the loop voltage.

These results are not necessarily at odds with previous magnetic fluctuation induced transport measurements in MST. Such measurements likely missed any transport due to the m = 0 modes because, as shown in Section 4.3, these modes are usually locked in unbiased discharges. Hence, the fluctuations cannot be distinguished from the equilibrium unless a large spatial array of probes is employed. Even if these modes do rotate, the wavelengths are very large (10 m for n = 1) and the low frequency (1-2 kHz) oscillations could easily be confused with sawtooth oscillations.

The second main result of the experiments described in this chapter is that electrostatic current injection is effective in controlling the m = 0 modes. This result is particularly important because of the finding that these modes play a role in global confinement. The MHD simulations discussed in Chapter 1 suggested that the m = 0 modes would be sensitive to edge current drive and these experiments show that this is indeed the case. Mode amplitudes can be reduced by adding parallel current outside the reversal surface or increased by driving current against the background current. This behavior is consistent with the general notion that adding current in the sense to flatten the parallel current profile reduces mode amplitudes while adding current in the opposite direction increases mode amplitudes.

The third main result of this work is that edge plasma biasing generates strong flows with shear and may cause an increase in particle confinement with no change in energy confinement. That particle confinement increases is supported by an observed increase in stored particle content with biasing despite no increase in the hydrogen ionization rate. Present diagnostics are not sufficient to quantify the contribution of impurities to the particle source rate; hence, the particle confinement time is not known for certain. However, unless the impurities contribute ~ 50% of the global electrons, the increases in density cannot be explained without an increase in particle confinement. As expected, magnetic fluctuations are not reduced by plasma biasing and energy confinement does not improve.

4.1.2 Distinguishing Between Multiple Causes and Effects

There are at least four significant ways in which the plasma guns can affect the main MST discharge: as fuel sources, limiters, field-aligned current sources, and plasma biasing electrodes. The first manner in which guns influence the external discharge is fueling. As was mentioned earlier, each gun requires a certain level of hydrogen fueling and this fuel eventually makes its way into the external discharge. Before and after the internal discharges

operate, this fuel enters as neutral gas at room temperature. During operation of the internal discharges, virtually all of the fueling comes in the form of a warm, high density hydrogen plasma. With 16 injectors operating at 1 kA, the total fueling by guns is adequate for supplying the entire MST discharge (aside from a small amount of puffed fuel for startup) and frequently leads to "overgassing" if the MST vessel wall is not well conditioned.

One effect of this fueling is to virtually eliminate the possibility of low density experiments. Low density operation may be possible with extensive wall conditioning, boronization, and repeated "no-gun" shots between shots with injectors functioning, but steady-state low density operation appears to be impossible. Since the average and spread of allowable densities increases as plasma current increases, a greater fraction of operational space is available to gun experiments at higher plasma currents. However, at high currents erosion of the sources becomes severe. This results in a deterioration of the main discharge and a shortening of the injector lifetime. Thus, most experiments were done at $I_p \leq 250$ kA.

The second means through which guns influence the main discharge is in their role as limiters. If enough injectors were inserted to completely restrict all currents in the edge, one would expect the plasma with guns inserted to be very different from that with them retracted. Although all edge current is not blocked by the 16 injectors, some is. This has a significant effect on the MST discharge. As injectors are inserted, the loop voltage and magnetic fluctuations increase, and confinement decreases. It is important to understand this effect if any net gains in confinement are to be realized using plasma guns.

When the guns inject current, there are two additional ways in which the discharge may be affected. First, since each source produces a magnetic field-aligned current, the edge portion of the parallel current profile can be altered. The present design allows for rotation of the injectors so current can be made to flow either with (co-injection) or against (counter-injection) the background current. Secondly, whenever current is injected along the magnetic field, it is also driven across the magnetic field to the wall. Since the radial

conductivity is finite, a subsequent voltage drop appears and the plasma becomes biased. This phenomenon was discussed in the Chapter 3 in some detail. It is important to understand that in every current-drive experiment in this chapter, there is also plasma biasing. The role of current drive can be diminished by orienting equal numbers of injectors in opposite directions (opposing injection). However, the role of biasing cannot be diminished without using one (or several) return electrodes capable of removing the same amount of electron current the guns inject.

All four of these influences act simultaneously and it is important to devise sets of experiments that can identify the separate effects. To this end, five standard types of shots are used and compared. First, shots are taken with guns fully retracted as a measure of normal MST behavior. Second, discharges are obtained with guns inserted but not active (no fuel or voltage is supplied). A comparison of these first two types allows the limiter effects to be determined. Third, shots are taken with guns inserted and internal discharges operating but no bias voltage applied. This type of shot will be denoted "no-bias" or "bias off" throughout and adds the fueling influence to the limiter effect. Finally, discharges are obtained with bias applied to the injectors and current injected parallel (co-injection) and antiparallel (counter-injection) to the background current density. Differences between co- and counter-injection indicate the influence of current drive. Changes from the no-bias case that are common to both co- and counter-injection indicate the influence of plasma biasing.

4.2 The Effect of Current Profile Control on Fluctuations and Confinement

In this section, the results of experimental studies of current profile modification with up to 16 injectors will be described. As discussed above, the influence of directional current drive is deduced by contrasting co- and counter-injection shots. We are specifically interested in answering three questions. First, do overall magnetic fluctuations decrease with

co-injection and increase with counter-injection as expected? Second, how are each of the three classes of modes -- core, m = 0, and high frequency -- affected by current drive? Third, do particle and energy confinement change with varying magnetic fluctuation amplitude? Except where noted, data were obtained in MST discharges with $I_p \sim 200$-250 kA and reversal parameter $F \sim -0.2$.

4.2.1 Behavior of Magnetic Fluctuations with Electrostatic Current Drive

The impetus behind these experiments has been our understanding that magnetic fluctuations are the primary cause of anomalous transport in the RFP. As described in Chapter 1, I will divide the magnetic fluctuations into three groups: core modes, m = 0 modes, and high frequency edge modes. All three groups are affected to some extent by electrostatic current drive but it appears that the m = 0 modes are the most sensitive.

The behavior of the core modes is well represented by the (m,n) = (1,6) mode which is the largest core mode in MST. This mode is resonant near $r/a \sim 0.2$ but has a very large radial correlation length. Hence, it can be measured anywhere in the plasma, including at the plasma surface. Near the wall, the (1,6) mode appears in both the poloidal and toroidal components of the magnetic field and $B_{\phi,(1,6)}$ is about twice as large as $B_{\theta,(1,6)}$. Poloidal mode numbers cannot, however, be distinguished with the toroidal array. Hence each measured n is a mix of all m numbers. All n = 6 data shown here are derived from the B_θ coils of the toroidal array because the fraction of $B_{\theta,n=6}$ due to poloidal mode numbers other than 1 (e.g., from the n = 6, m = 0 mode) should be very small.

The behavior of the m = 0 modes is well represented by the n = 1 mode which is the largest m = 0 mode. This mode is resonant at the reversal surface ($r/a \sim 0.85$) and although the correlation length has not been measured, it is large enough that the mode is easily monitored at the wall. All n = 1 data shown are derived from the B_ϕ coils of the toroidal

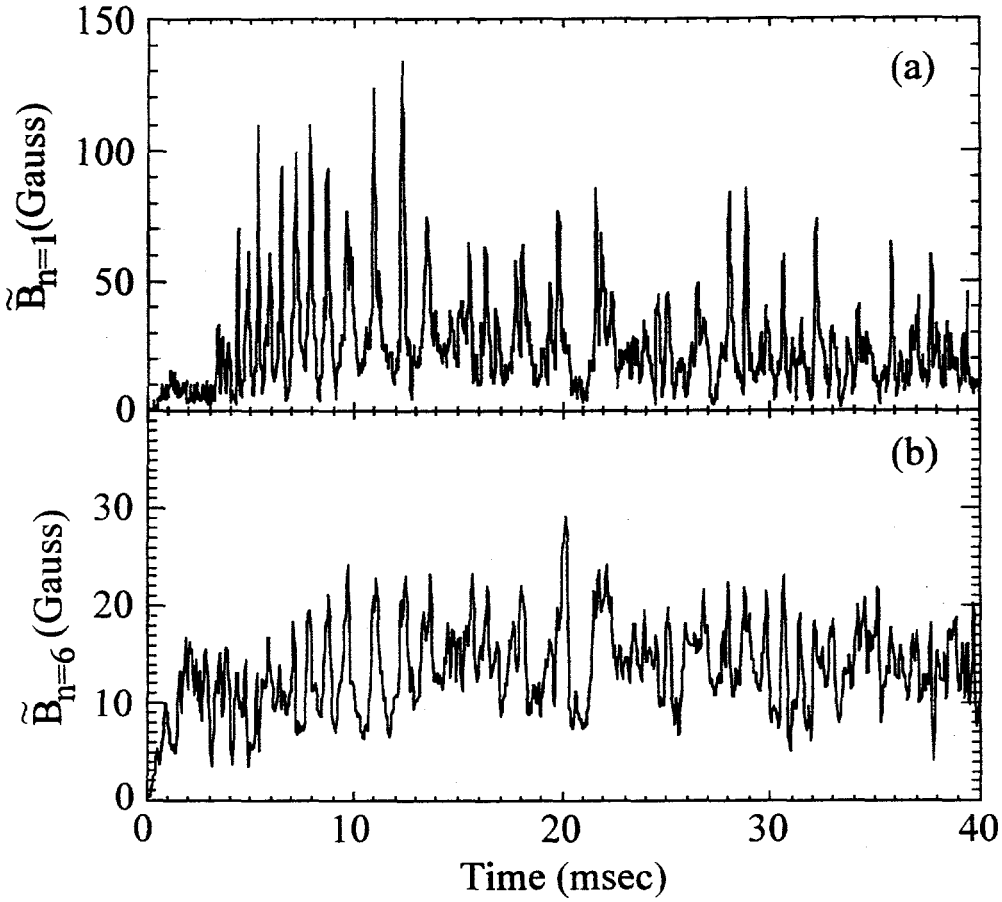

Figure 4.1. Measured n = 1 (a) and n = 6 (b) magnetic fluctuation amplitudes are shown versus time for a standard no-bias shot. The n = 1 amplitude is obtained from the B_ϕ coils of the toroidal array; the n = 6 amplitude is obtained from the B_θ coils of the toroidal array. The n = 6 amplitude has been multiplied by $\sqrt{5}$ to represent the total amplitude from all components of B.

array. Since the B_θ perturbation associated with any m = 0 mode is small, the $B_{\phi,\, n=1}$ will be considered equal to the total amplitude.

Figures 4.1 - 4.3 show the time dependence of the n = 6 and n = 1 amplitudes for representative no-bias, co-injection, and counter-injection shots. The injectors are situated

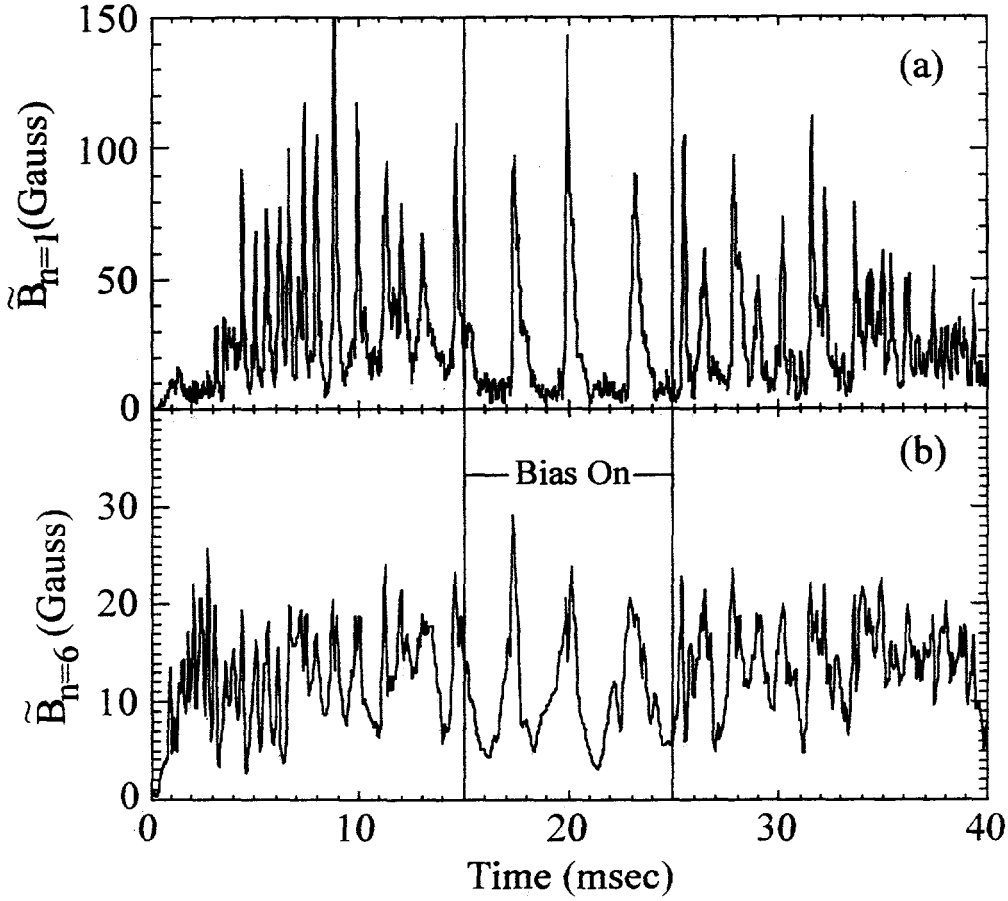

Figure 4.2. Measured n = 1 (a) and n = 6 (b) magnetic fluctuation amplitudes are shown versus time for a standard co-injection shot.

about 2-5 cm outside the reversal surface in these discharges. Hence, co-injection should tend to flatten the parallel current gradient and tend to reduce both the n = 1 and the n = 6 mode amplitudes. One notes that indeed the time-averaged n = 1 amplitude is substantially lower with co-injection than with counter-injection. The time-averaged n = 6 amplitude, however, is not very different in the two cases, although the time dependence is different.

The bursts in both amplitudes are due to sawteeth which, in the RFP, are a cyclical relaxation phenomenon [4]. The current profile steepens, due to resistive diffusion and the

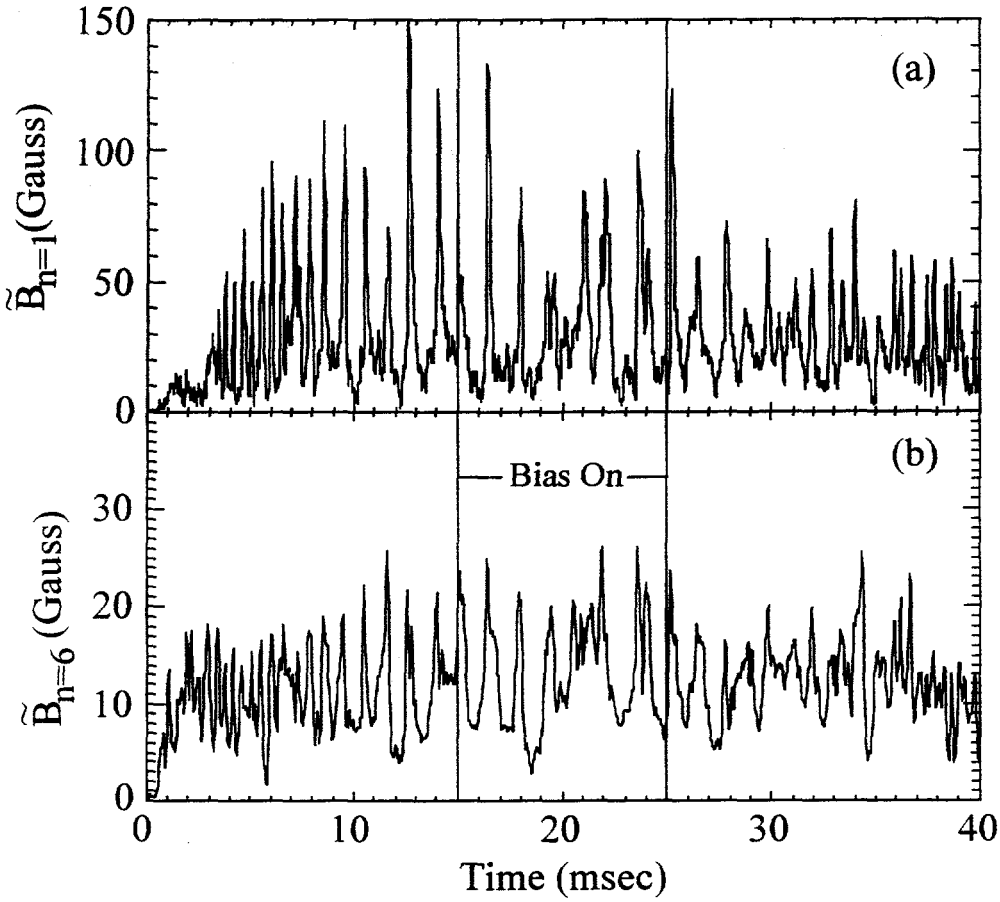

Figure 4.3. Measured n = 1 (a) and n = 6 (b) magnetic fluctuation amplitudes are shown versus time for a standard counter-injection shot.

strong applied parallel electric field on axis, until core modes are driven unstable and amplitudes grow. Nonlinear coupling transfers some of the power to modes at the edge. The combination of core and edge modes then rapidly reconfigure the magnetic field, driving parallel current in the edge and suppressing it in the core. Once the profiles have been relaxed, the mode amplitudes decay and the process begins again. It is not understood exactly why the sawtooth period is different in co- and counter-injection discharges but

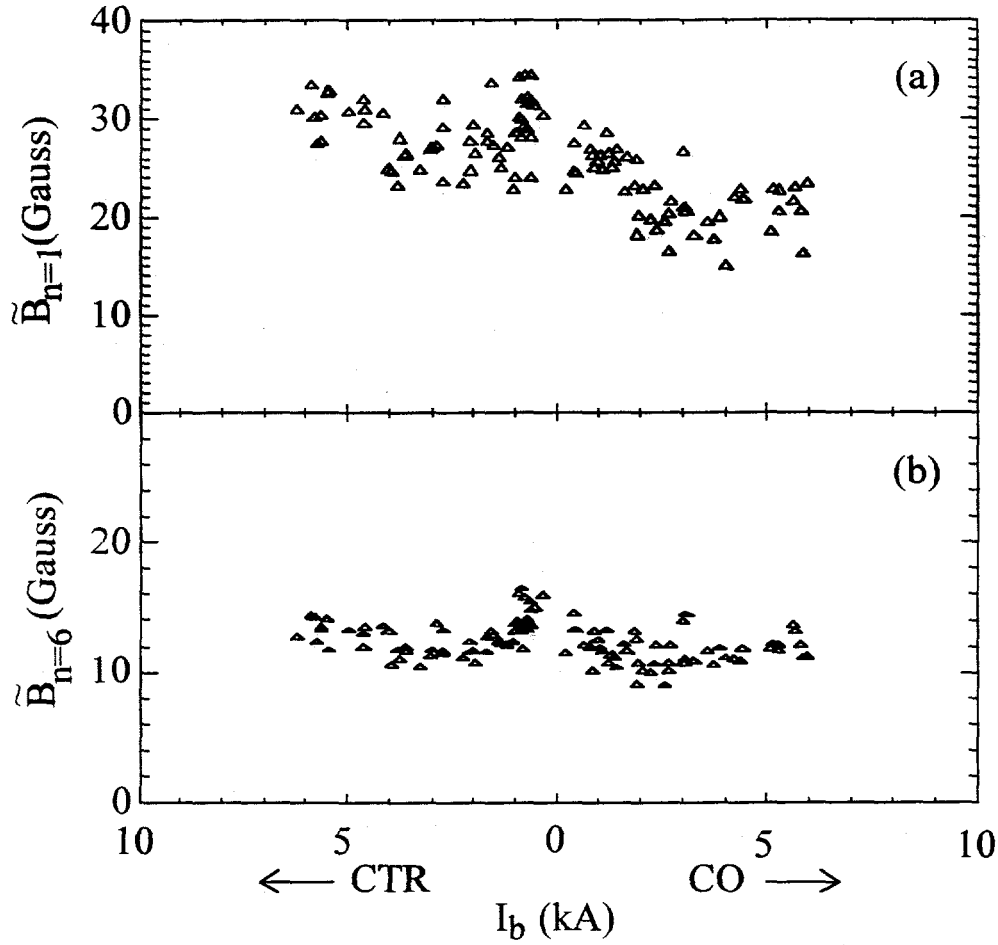

Figure 4.4. Scatter plots of time-averaged n = 1 (a) and n = 6 (b) magnetic fluctuation amplitudes are shown versus total injected current.

evidently the presence of additional parallel current in the edge can postpone the rapid growth and/or nonlinear transfer that result in a sawtooth event.

Figure 4.4 summarizes the dependence of the time-averaged n = 6 and n = 1 amplitudes on the direction and magnitude of injected current. Each point represents a different shot. The signals are averaged during an 8 ms long period in the middle of the 10 ms current injection period. Different currents were obtained by varying both the number of

injectors that were biased and the bias voltage. The number of internal discharges in operation was held constant during this scan so that the fueling is similar for all discharges shown.

It appears that directional current drive can modify the n = 1 amplitude for injected currents above 2-3 kA. (Recall from Chapter 3 that the actual poloidal current driven is larger than this because the current from each source makes several poloidal transits.) The time-averaged n = 6 amplitude is not strongly affected by electrostatic current drive for currents up to at least 7 kA. It is not too surprising that the core modes are not as sensitive as the m = 0 modes. The driven current is well away from the core resonant surfaces and the amount of current is probably below what is necessary to significantly affect these modes. Still, that the m = 0 modes can be controlled with current drive is a significant result. In addition, when all mode amplitudes are combined, the total power in magnetic fluctuations decreases when current is driven in the sense to flatten the parallel current profile.

The reason for the decrease in the m = 0 amplitudes is not entirely clear. As discussed in Chapter 1, the saturated amplitude of any mode is determined by a balance between the energy transfer rate into and out of that mode. MHD simulations [5] predict that the m = 0 modes are not normally linearly unstable but can be made unstable by current drive inside of the reversal surface. In the simulations the amplitudes are normally sustained by nonlinear transfer of energy from the core modes which are coupled to each other through the m = 0 modes. It is not clear if the m = 0 modes are linearly stable or not in MST experiments. If they are linearly unstable, then the injected current would tend to flatten the parallel current profile outside the reversal surface and reduce the linear drive for the modes, resulting in a reduced amplitude. If they are sustained nonlinearly, the injected current can still extract energy from the m = 0 modes quasilinearly through the mean fluctuation induced electric field which is produced by each individual m = 0 mode. Once energy is removed and

the mode amplitude decreases, the nonlinear transfer from core modes would also diminish and the mode would saturate at a lower level.

To complete the discussion of magnetic fluctuations, let us examine to what degree the edge high frequency modes are affected by current drive. The Dense Array coils (see Section 3.1) are typically used to measure these modes and since the amplitudes are small, the time derivative of B is measured rather than B itself. This has the benefit of amplifying the high frequency modes but the disadvantage that the modes must be rotating to be observed. For this analysis, two toroidally separated B_ϕ coils were used (4 cm apart) and the data were Fourier analyzed in time. Specifically, shots were broken into 0.5 ms intervals, the average and trend of the signal in each interval were removed, a Hanning window was applied, and a Fast Fourier Transform was then accomplished to transform to the frequency domain. Equivalent intervals and shots were ensemble averaged together to obtain autopower spectra (after removing the extra factor of ω) and coherence spectra for no-bias, co- and counter-injection discharges.

Figure 4.5a shows the resulting power spectra for no-bias and co-injection ensembles. Although the details of the low and medium frequency portions of the spectra differ (probably as a result of differences in mode rotation) the most obvious difference is a distinct peak that appears in the co-injection case around 120 kHz. An increase in coherence is also observed at the same frequencies as shown in Figure 4.5b. It would appear from these data that either high frequency (short wavelength) modes are excited with current drive or that these modes always existed but were stationary prior to biasing the edge. The FIR density fluctuation spectrum often exhibits similar peaks in this frequency range (see Figure 4.22).

Figure 4.6 shows the power spectrum for co- and counter-injection discharges. These two cases can be more easily compared than the bias and no-bias pair since the mode rotation is similar for both directions of current injection and hence mode frequencies are similar. One observes a generally lower fluctuation level for co- than for counter-injection except at the

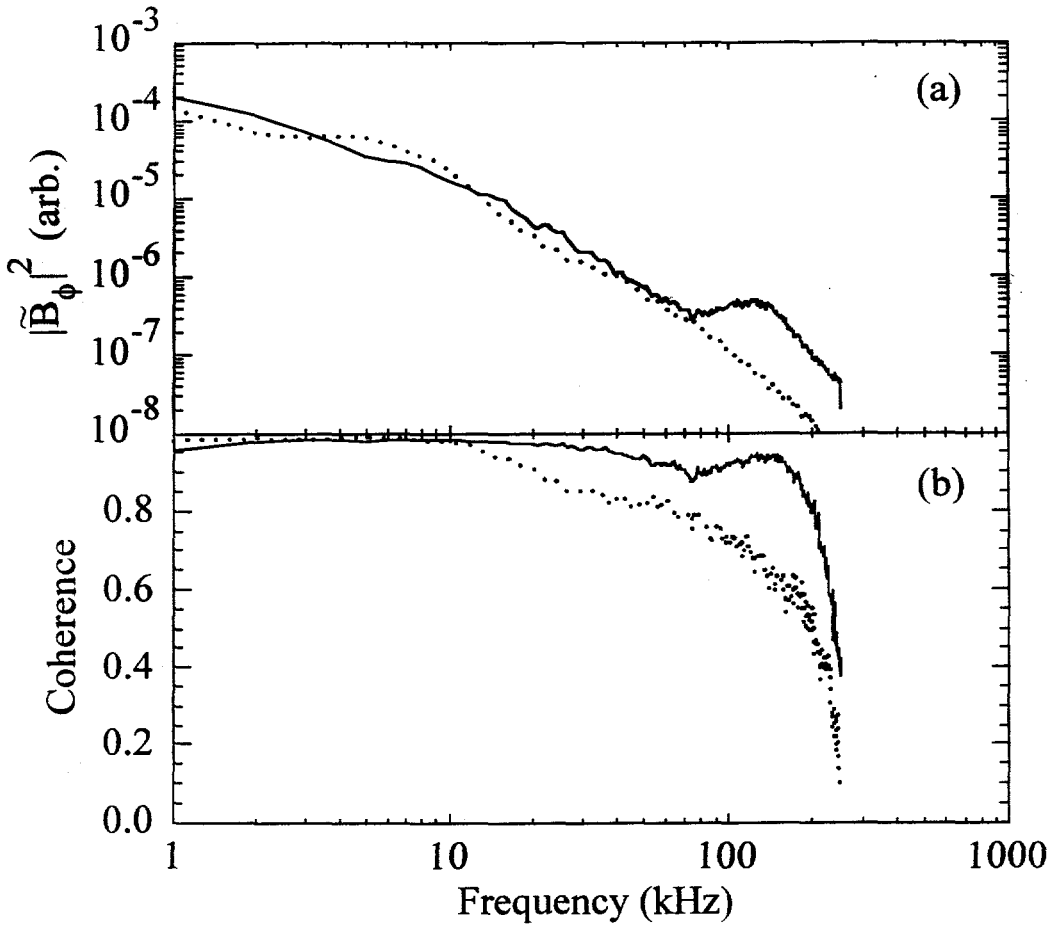

Figure 4.5. Autopower spectra and coherence spectra are shown for B_ϕ fluctuations for co-injection (solid) and no-bias (dotted) discharges. Each curve represents an ensemble average over many shots.

frequencies near 120 kHz. A peak appears at these frequencies in both the co- and counter-injection cases but is much more pronounced with co-injection. Furthermore, the response is opposite to that of the m = 0 modes described above. The amplitude increases when injected current adds to the background current density.

An interesting characteristic is the dependence of the peak frequency on the reversal parameter, F. This dependence is illustrated in Figure 4.7 which shows an ensemble-averaged

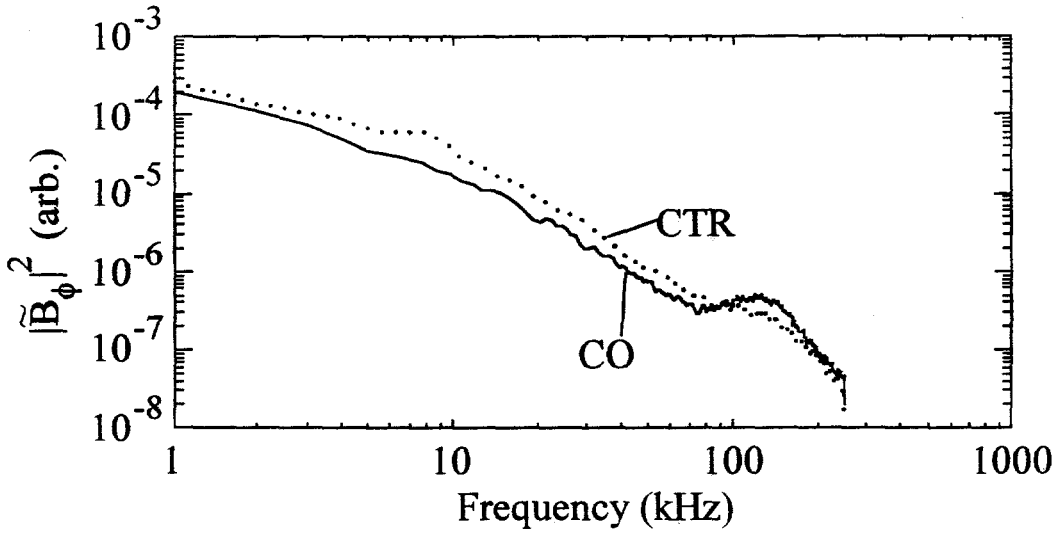

Figure 4.6. Autopower spectra are shown for B_ϕ fluctuations in co-injection (solid) and counter-injection (dotted) discharges. Each curve represents an ensemble average over many shots.

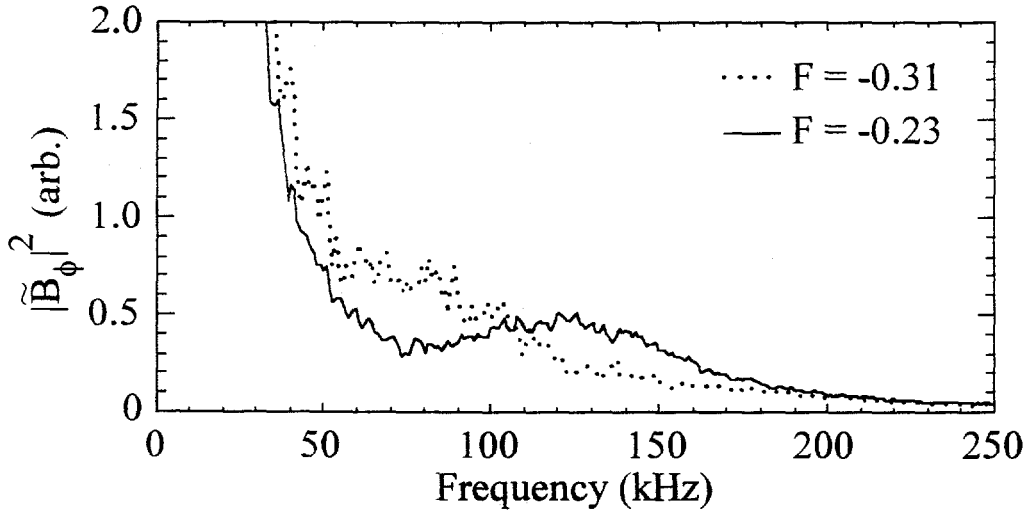

Figure 4.7. Autopower spectra of B_ϕ fluctuations are shown for co-injection discharges with F = -0.31 (dotted) and F = -0.23 (solid).

power spectrum for discharges with F = -0.31 and F = -0.23. One observes the peak frequency to decrease as reversal is made deeper, as the safety factor at the wall becomes more negative. This suggests that these modes are connected with a fixed radius that corresponds to different resonant surfaces as the q profile is varied. This possible relationship will be explored in the next few paragraphs.

Unfortunately, knowing the frequency alone does not allow us to determine which modes these are. If we assume, however, that they are resonant m = 1 modes and that the frequency is given by $f = n\,v / 2\pi R$ where n is the toroidal mode number, v is the toroidal phase velocity, and R = 1.87 m is the major radius of the coil set, then we can make some comments about what and where these modes are. Two point measurements of mode phase velocity are very scattered but seem to suggest that the toroidal phase velocity of these modes is around 40 km/s. Hence, the toroidal mode number corresponding to a frequency of 120 kHz (F = -0.23 case) is about 35. The toroidal mode number associated with a frequency of 80 kHz (F = -0.31 case) is about 25.

Figure 4.8 shows a plot of -1/q versus radius for both the F = -0.31 and F = -0.23 cases. The q profile was determined using an equilibrium model (see Section 3.3.3) with the time-averaged F and Θ as input parameters. For m = 1 perturbations, $|n| = |1/q|$ so this plot can be considered a plot of resonant toroidal mode number versus radius. One observes that the modes corresponding to the high frequency peak appear to be modes located near the outer edge of the region where current is injected. For these modes, co-injection actually tends to steepen the current profile gradient whereas counter-injection tends to reduce or reverse it. Hence, these may be locally-resonant tearing modes that are sensitive to current gradients in the usual way. It is also possible that these modes are sensitive to pressure or density gradients that increase in all current drive discharges but are greater for co-injection than for counter-injection. The contribution of these modes to transport is probably small since even with current drive, the amplitudes are quite low. They may, however, play a role

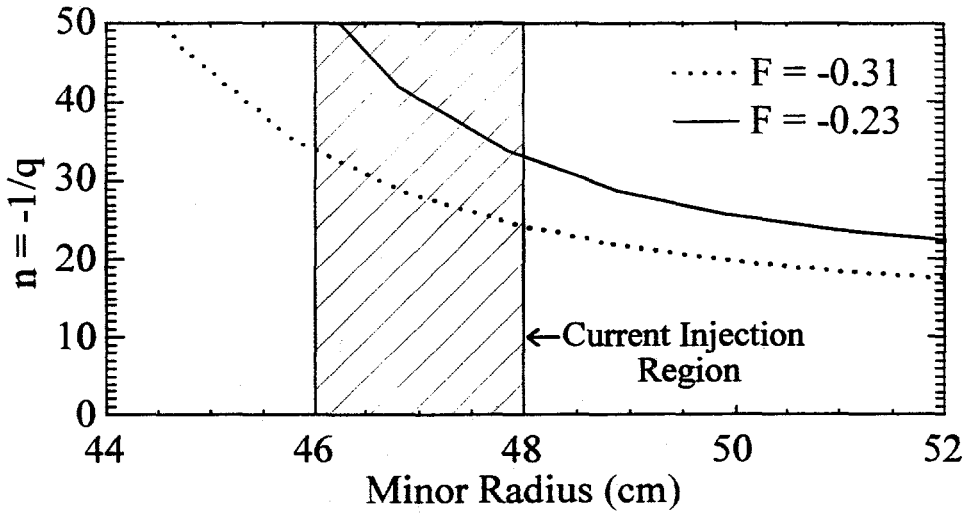

Figure 4.8. Edge profiles of -1/q are shown for F = -0.31 (dotted) and F = -0.23 (solid) discharges. Profiles were calculated using the model described in Section 3.3.3 to reconstruct the magnetic equilibrium from edge magnetic field measurements.

in transporting the injected current back to the wall but further studies need to be done to determine if this is the case.

In all, then, we find that magnetic fluctuations do decrease with co-injection and increase with counter-injection. The core mode amplitudes are not affected in a time-averaged sense although the sawtooth period does change with co-injection. The time-averaged m = 0 amplitudes are affected and account for the overall changes in magnetic fluctuation power with current drive. High frequency modes resonant near the injected current appear to be driven in both co- and counter-injection cases, consistent with strong current and/or pressure gradients near the injection radius. It was expected based on earlier transport measurements that confinement would improve if the core mode amplitudes were

reduced. Since it is the m = 0 modes which are instead reduced with added edge current, it is not clear *a priori* what changes in confinement to expect.

4.2.2 Changes in Particle Confinement Due to Electrostatic Current Drive

Mass continuity requires that for each species in the plasma

$$\frac{dN}{dT} = G - L \tag{4.1}$$

where N is the total (volume integrated) number of particles of that species, and G and L are the total particle source and loss rate for that species, respectively. In the case of electrons, G is determined by ionization of hydrogen and impurities (and plasma sourcing by the injectors), and L is determined by recombination and transport across the plasma boundary to the wall. Recombination is generally a weak effect compared to direct wall losses and will be neglected. It is common to write the loss term as $L = N / \tau_p$ where τ_p is the particle confinement time. This supposes that if all particle sources were turned off, the number of particles in the device would exponentially decay with some characteristic time τ_p. Of course, in practice this may or may not adequately describe the transport processes and τ_p will be a time dependent quantity. For typical MST plasmas, τ_p is of order 1 ms.

To determine whether or not particle confinement changes with current drive, one must measure both the total number of particles and the particle source rate and solve Equation 4.1 for τ_p. Figure 4.9 shows the central line-averaged density as a function of time (measured with the CO_2 interferometer) for typical co-injection and counter-injection discharges. (For comparison, similar no-bias discharges are also shown, although the discussion of these discharges is left to Section 4.3.) One observes that the density is highest in the co-injection case. The FIR interferometer measurements suggest that the density profiles are very similar in co- and counter-injection discharges. Hence the difference in line-averaged density represents a real difference in the stored particle content, N.

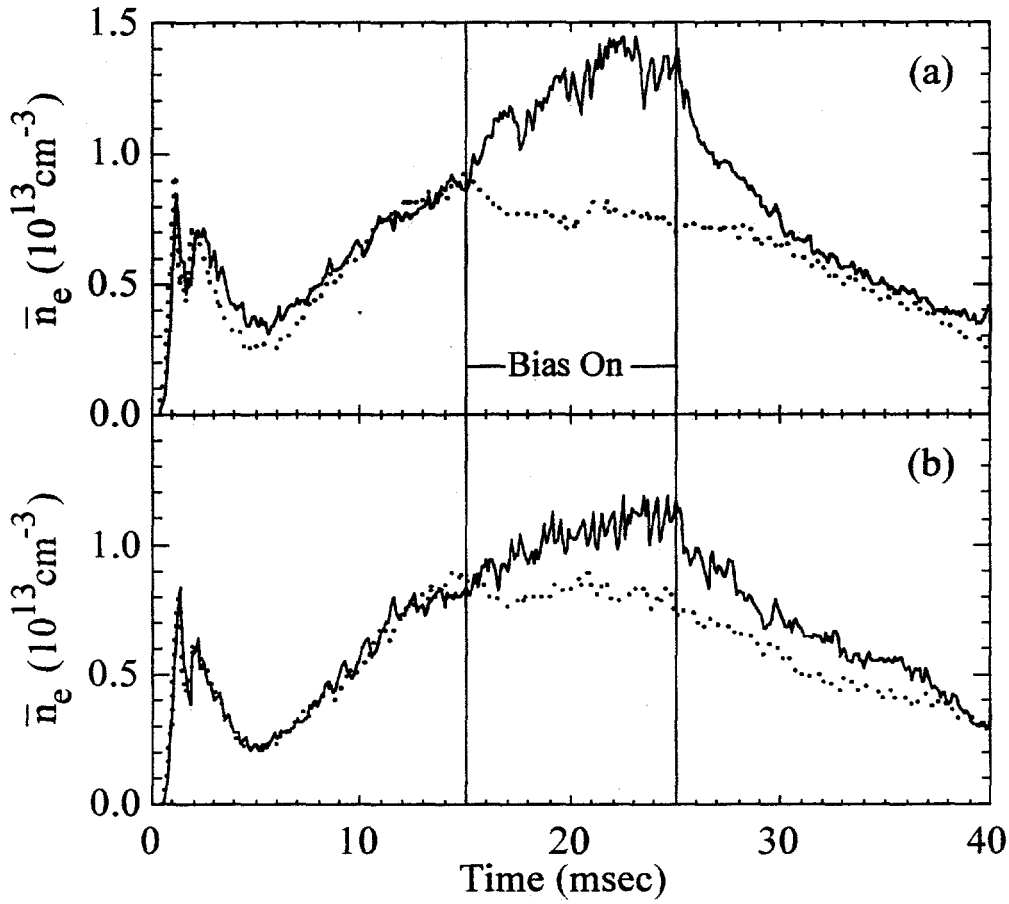

Figure 4.9. Line-averaged density obtained from the CO_2 interferometer is shown versus time for biased (solid) and no-bias (dotted) discharges. Data for both co-injection (a) and counter-injection (b) are shown.

Measuring the particle source rate is in general quite difficult. Particles are generated by ionization of both the main fuel neutrals and impurities, and from the plasma flowing out of the guns. The fueling from guns is identical in co- and counter-injection discharges. Ionization is generally dominated by electron impact ionization and hence is proportional to both electron density and the number of atoms present. (In this discussion, atom will mean any entity with bound electrons.) Line radiation is typically dominated by electron collisional

excitation so it is also proportional to electron density and the number of atoms present. Hence, line radiation can be used to infer ionization rates. It should be noted that changes in radiation reflect changes in ionization only to the extent that the ratio of the ionization and excitation cross-sections remains constant. This requirement is usually well satisfied if the electron temperature does not change too much or is well above the ionization energy. For many impurity states the ionization energy can be close to or above the electron temperature so the ratio of ionization rate to excitation rate may be sensitive to plasma parameters.

To do the ionization measurement correctly, radiation should be collected from every part of the plasma and for every species that could be ionized. This is not possible to do in practice. Instead, radiation from a few species is usually measured at one location and assumptions are made regarding the symmetry of the radiation. For these studies, a central line-averaged H_α measurement was used to estimate the ionization of hydrogen. Several spectroscopic tools were used to get a general indication of the impurity radiation. The H_α detector was absolutely calibrated and a calculation was done to convert photons to the rate of electron/proton production. The impurity measurements were not absolutely calibrated and a calculation of the number of ionizations per photon has not been done. Consequently, measurements of impurity radiation are not as useful as the H_α measurement.

As was stated earlier, to determine particle source rates from these measurements, an assumption must be made about how well the single measurement approximates a global average. Usually, it is assumed that either the radiation is toroidally symmetric or that any asymmetries rotate such that ensemble averaging the radiation measurements over time or over many shots gives a good indication of global levels. It will be shown in Section 4.3 that although there are asymmetries connected with the n = 1 magnetic mode, these rotate reliably in biased shots. Thus, the radiation measurements approximate global averages when averaged over time during current drive. (Note that there may be additional asymmetries tied

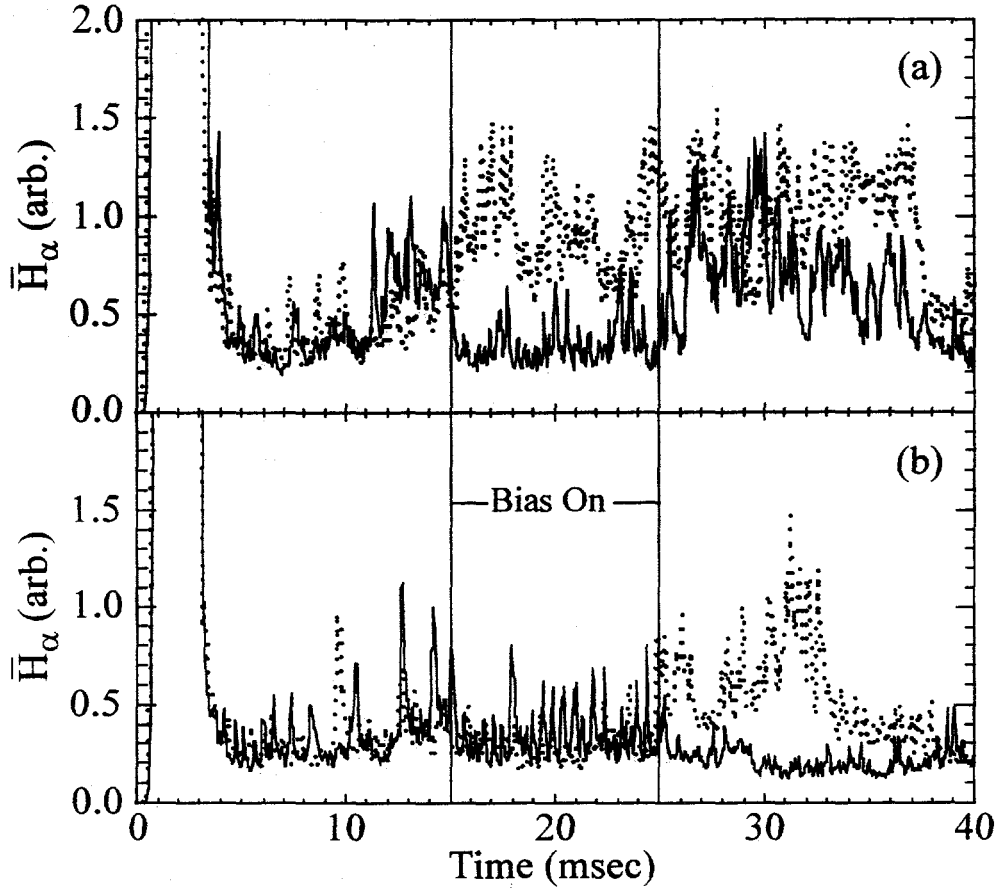

Figure 4.10. Central line-averaged Ha radiation is shown versus time for biased (solid) and comparable no-bias (dotted) shots. Both co-injection (a) and counter-injection (b) discharges are shown.

to field errors, limiters, etc. which exist in all discharges. These cannot be accounted for with present diagnostics and will be neglected here.)

Figure 4.10 shows the measured H_α radiation for co- and counter-injection as well as comparison discharges with no-bias. (The shots shown in Figure 4.10 are the same as those in Figure 4.9 and Figures 4.1-4.3.) The time-averaged hydrogen ionization rate appears to be very similar for both directions of current drive. Since the plasma density is also contributed

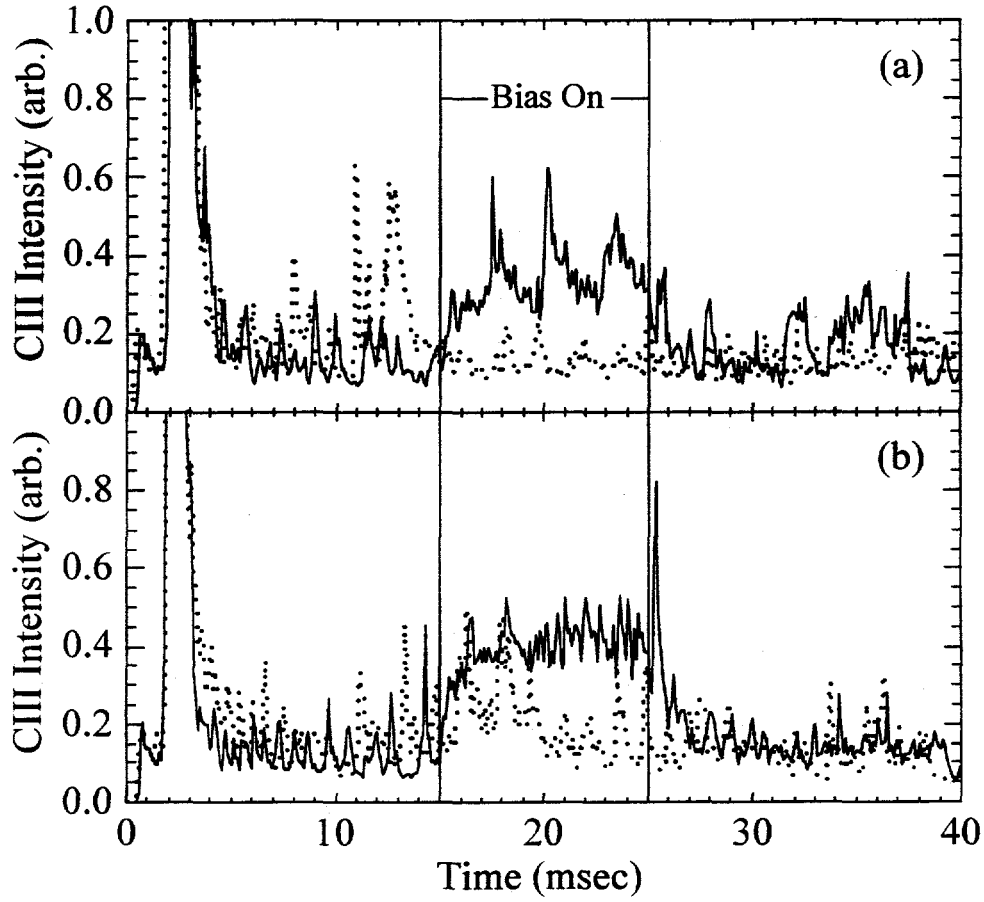

Figure 4.11. Central line-averaged C III emission is shown in biased (solid) and no-bias (dotted) discharges. Both co-injection (a) and counter-injection (b) cases are shown.

to by impurities, we must also check for differences in impurity radiation. Figure 4.11 shows the time behavior of the C III line radiation in the same shots. Again no significant time-averaged differences exist between the co- and counter-injection shots. Other impurity lines behave in a similar fashion.

Figure 4.12 gives a summary of the dependence of the various terms in the particle balance on the direction and magnitude of edge current drive. One will note that the density increase (see Figure 4.12a) with co-injection is greater than that for counter-injection when

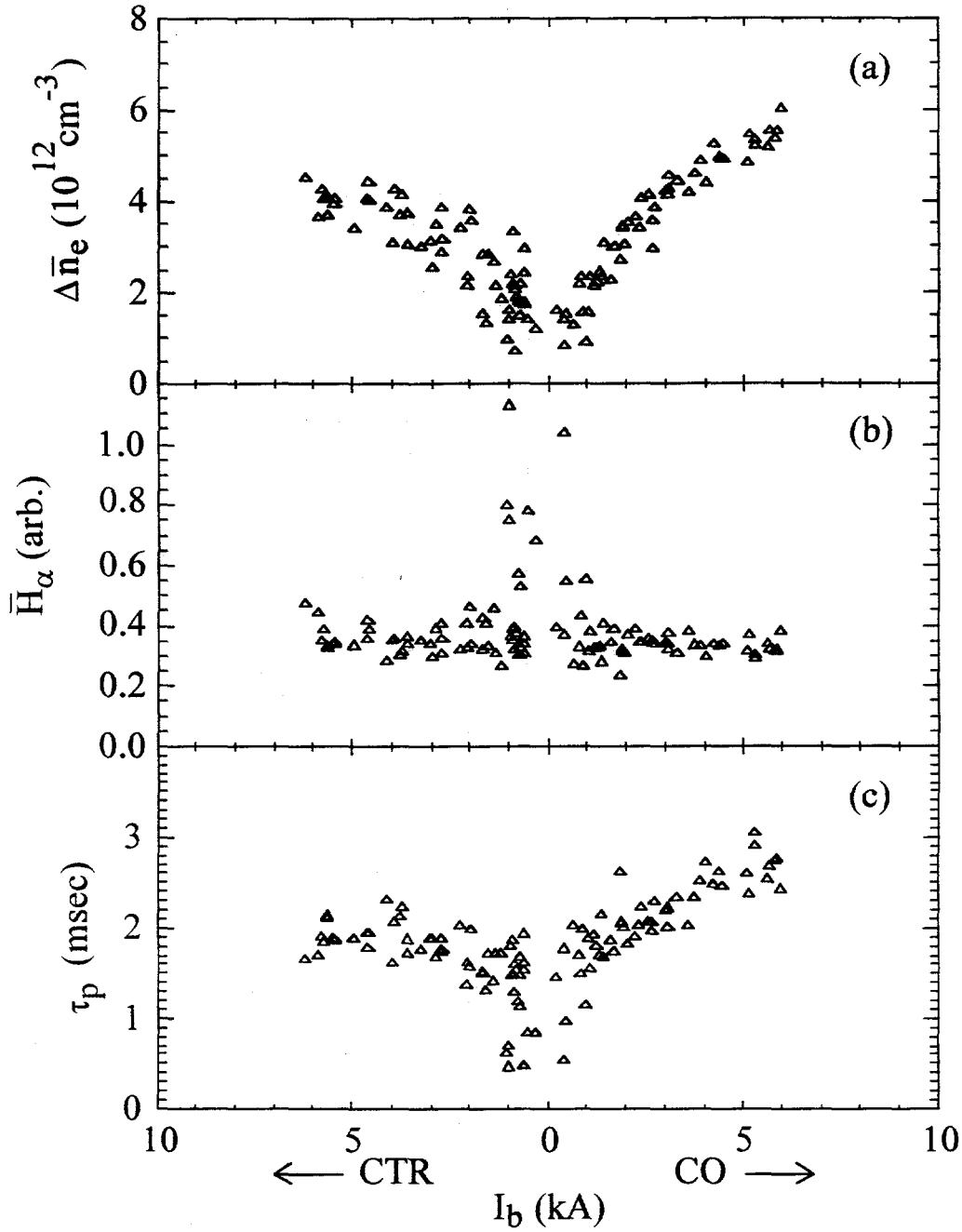

Figure 4.12. Scatter plots of the change in central line-averaged density (a), central line-averaged H_α emission (b), and estimated particle confinement time (c) are shown versus total injected current.

the injected current is greater than 2-3 kA. The fueling rate, represented in Figure 4.12b by the central line-averaged H_α radiation, is not significantly different for co- and counter-injection. Hence the particle confinement time (calculated in Figure 4.12c assuming that hydrogen ionization dominates the source term) is greater for co- than for counter-injection.

It is interesting that the discrepancy is only apparent for injected currents above about 2-3 kA which is the same amount of current required to change the m = 0 mode amplitudes. One concludes then that the m = 0 mode amplitude is anti-correlated with the global particle confinement time and may play a role in particle transport (at least in discharges with injectors inserted).

4.2.3 Changes in Energy Confinement Due to Electrostatic Current Drive

The conservation of energy implies that

$$\frac{dU_{th}}{dt} + \frac{dU_m}{dt} = P_{in} - P_{out} \tag{4.2}$$

where $U_{th} = \int 3/2\ nT\ dV$ is the stored thermal energy in the plasma, $U_m = \int B^2/2\mu_o\ dV$ is the stored magnetic energy, and P_{in} (P_{out}) is the power flowing into (out of) the plasma volume at the boundary. Here, P_{in} is given by the Poynting flux into the plasma which is easily determined from the voltages across the poloidal and toroidal gaps, the toroidal plasma current, and the poloidal current in the conducting shell. P_{out} is determined by all mechanisms of energy loss including radiation, conductive and convective transport, charge exchange, etc. As was done for particle confinement, it is common to define an energy confinement time, τ_E, such that $P_{out} = U_{th} / \tau_E$. This presumes that if all power sources were turned off and the confining magnetic fields did not change, then the stored thermal energy

would decay exponentially with a characteristic time τ_E. In general, τ_E will be a time dependent quantity. It has a typical value in MST of about 1 ms.

Equation 4.2 is often rewritten as

$$\frac{dU_{th}}{dt} = P_{ohmic} - P_{out} \tag{4.3}$$

where $P_{ohmic} = P_{in} - dU_m/dt$ is the source term for the stored thermal energy in the plasma. The loop voltage is defined by $V_{loop} = P_{ohmic} / I_p$ where I_p is the toroidal plasma current. In the following discussion, V_{loop} will be used to indicate the behavior of the energy source term. The Polynomial Function Model [6] has been used to compute the change in stored magnetic energy based on external measurements of magnetic fields. Other available models do not yield very different results in these experiments.

The first term to be considered in the energy balance relation is the stored thermal energy. In Section 4.2.2 it was shown that the number of stored particles is greater for co- than for counter-injection. The central electron temperature has been measured by Thomson scattering and indications are that the electron temperature does not change very much with co-injection but drops significantly with counter-injection (see Table 4.1). No measurements of proton temperature have been possible in these discharges and dominant impurity ion temperatures do not change substantially with current drive. I will assume, as is usually the case in normal MST discharges, that the ion temperature is half the electron temperature.

The combined density and temperature measurements indicate that the stored thermal energy increases with co-injection and decreases with counter-injection. These changes are quantified in Table 4.1 by computing the plasma beta (ratio of plasma pressure on axis to magnetic field pressure at the wall), which is about twice as large for co-injection as for counter-injection. Hence, the stored thermal energy is greater when current is added to flatten the parallel current profile.

	T_e (r=0) (eV)	$\bar{n}_e$ ($10^{19} m^{-3}$)	β (%)	P_{ohmic} (MW)	P_{inj} (MW)	τ_E (ms) (P_{inj} = IV)	τ_E (ms) (P_{inj} = 0)
No Bias	187	1.0	6.8	6.84	0.0	0.80	0.80
CO	181	1.5	9.2	5.61	2.2	1.06	1.47
CTR	91	1.4	4.5	7.23	2.2	0.40	0.52

Table 4.1. A summary of the power balance parameters in no-bias, co-injection, and counter-injection discharges is shown. Each value represents an average of many shots.

The other important term in determining energy confinement is the energy source rate. Figure 4.13 shows the derived loop voltage as a function of time for the standard set of co- and counter-injection discharges and for comparable no-bias discharges. (These discharges are the same as those shown in Figures 4.1-4.3, and 4.9-4.11.) It is clear from Figure 4.13 that the time-averaged loop voltage decreases with co-injection and is the same or increases slightly with counter-injection. Figure 4.14 shows the dependence of V_{loop} on the direction and magnitude of the injected current. The behavior of the energy source term closely follows the behavior of the m = 0 modes, as discussed in Section 4.2.1. This is an important point. It implies that the m = 0 modes are an integral part of the anomalous resistance in the RFP along with the core modes.

Before determining an energy confinement time, it is necessary to acknowledge that the current injection system does some heating of the main discharge and this should be included in energy confinement calculations. It is not clear how much power the system injects. It certainly is more than zero and less than $I_{bias}V_{bias}$ because some of the bias voltage is taken up in sheaths at the gun and the wall which do not result in plasma heating.

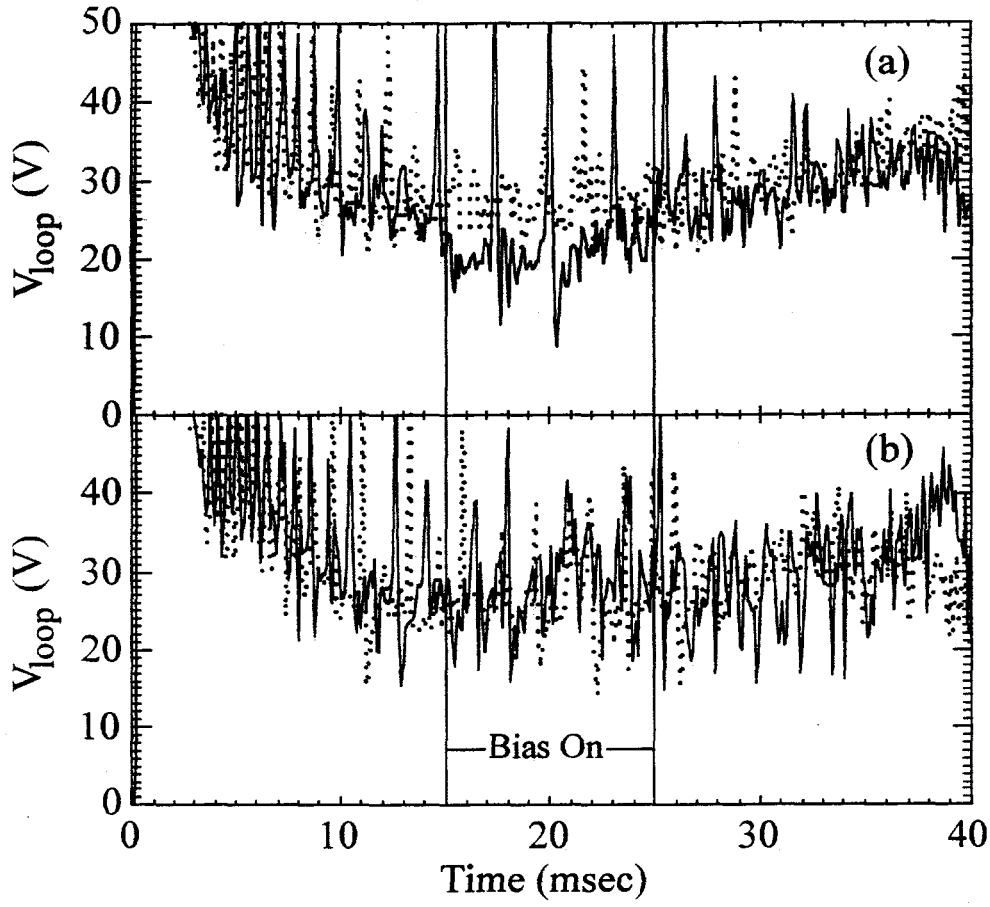

Figure 4.13. Loop voltage is plotted versus time for representative biased (solid) and no-bias (dotted) discharges. Both co-injection (a) and counter-injection (b) shots are shown.

To illustrate the effect of the gun injected power, two calculations will be done. The first will not include any power injected by the guns and the second will include the full $I_{bias}V_{bias}$.

Table 4.1 summarizes the changes in the energy confinement time with current injection. Energy confinement increases by 30-80% with co-injection and decreases by 30-50% with counter-injection. We conclude that the m = 0 modes are anti-correlated with global energy confinement. It thus appears that these modes play a role in both particle and

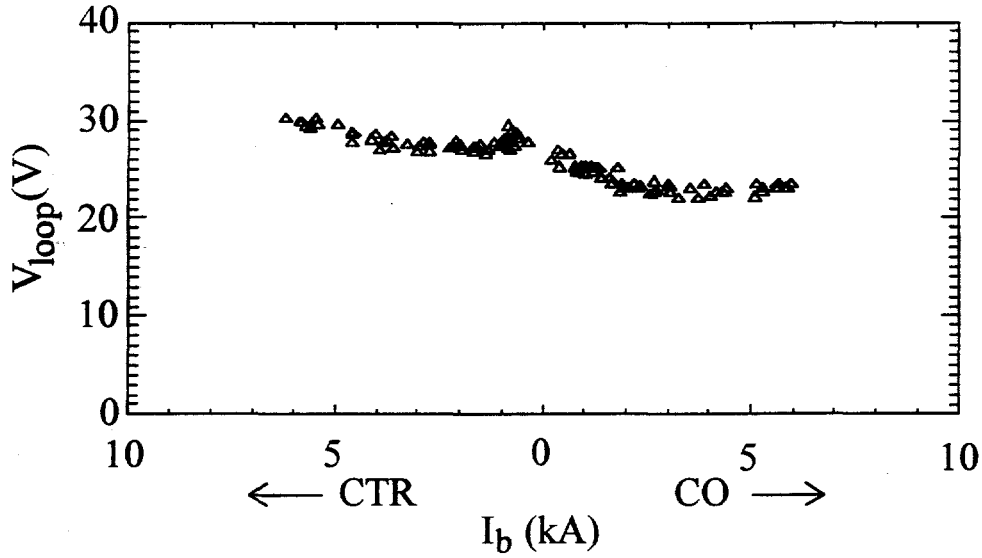

Figure 4.14. A scatter plot of loop voltage versus total injected current is shown. Each point represents a different shot.

energy confinement in MST. We further conclude that edge current drive is an effective means of controlling these modes and any transport they may cause.

Unfortunately, although confinement increases with co-injection, there is a degradation which occurs when the guns are inserted into the plasma in the first place. This point will be taken up in detail in Section 4.4. The result of the combined effects is that confinement is not very different with co-injection from what it is with guns completely removed from the plasma.

4.3 The Effect of Plasma Biasing on Fluctuations and Confinement

The previous section explored the effects of directional current drive by considering the differences between co- and counter-injection shots. In this section, the influence of plasma biasing will be examined by focusing on changes from the no-bias case that are

common to both co- and counter-injection discharges. Four questions will be addressed in regard to plasma biasing. First, are flows generated by edge biasing and do the flow profiles exhibit shear? Second, how do electrostatic fluctuations respond to the driven flows? Third, does particle confinement improve with biasing and is this improvement limited to the edge where electrostatic fluctuation induced transport is large? Fourth, do magnetic fluctuations and energy transport remain the same in biased discharges as expected? In answering these questions, data presented in the last section will be revisited and new data presented where necessary.

4.3.1 Flows in Biased Discharges

It is likely that any improvements due to plasma biasing will be related to the strong edge flows that are produced. Whenever the guns are biased, current injected by the guns is forced to return across magnetic field lines to the vessel wall. The resulting J×B force exerts a torque on the plasma and spins up a strong toroidal flow (from a radial J and mostly poloidal B). The velocity in the edge of the plasma will be determined by a balance between the J×B torque and drag forces related to viscosity, field errors, coupling to the plasma core, etc. The velocity in the core will be determined by a balance between viscous or other coupling with the edge plasma and similar drag forces. There are flows that exist naturally in MST (due to ambipolar electric fields, pressure gradients, etc.) and one expects that they will add to the effects of biasing in a linear way to give some net flow profile.

Figure 4.15 shows the time dependence of C^{+2} and C^{+4} ion flow for representative shots with co-injection and no-bias. Figure 4.16 shows the same signals for the counter-injection case. These data are obtained from the IDS diagnostic and one will recall from Section 3.1 that the C^{+2} and C^{+4} ion velocities are representative of the edge and core plasma flow velocities, respectively. Upon biasing, toroidal flows of 20-30 km/s are observed in the edge where previously little rotation existed. These flows are consistent in magnitude

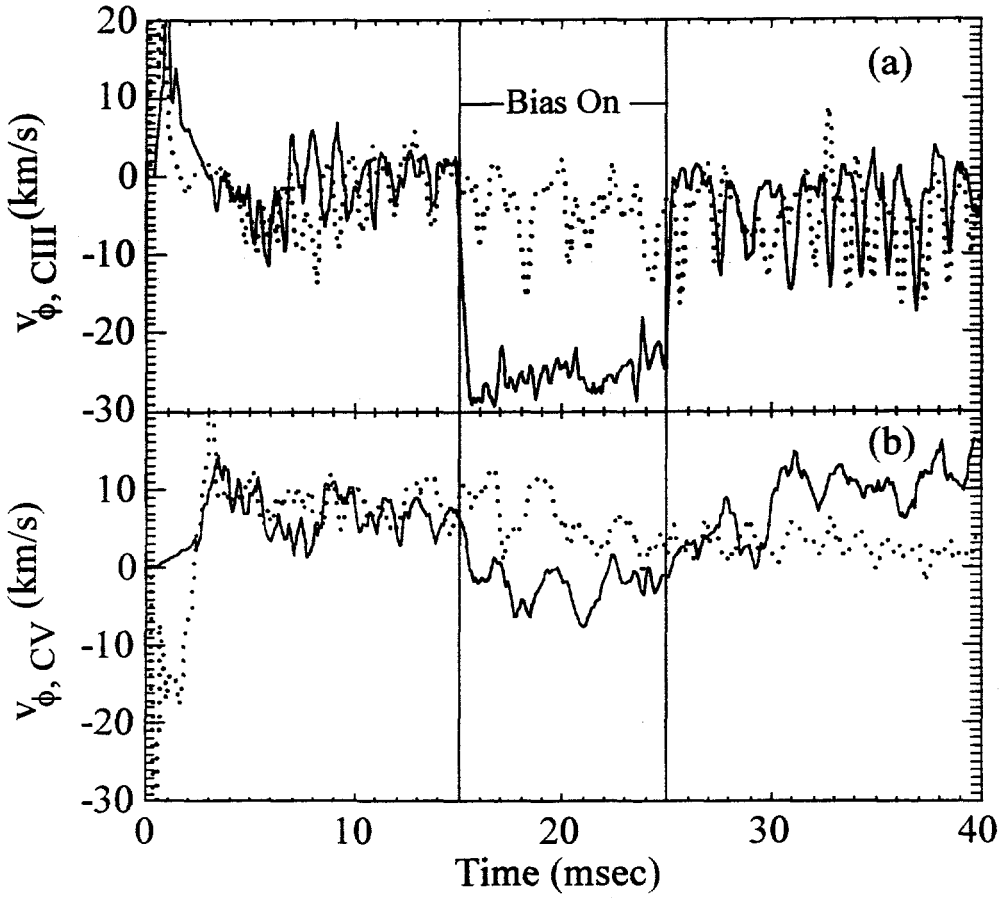

Figure 4.15. Toroidal ion flow measurements obtained from Doppler shifted C III (a) and C V (b) emission are shown for counter-injection (solid) and no-bias (dotted) discharges. Positive velocity corresponds to motion towards lower toroidal angles. The C III data have been multiplied by 1/cos(42°) to convert from velocity along the line of sight to toroidal velocity.

and direction with E×B velocities constructed from Langmuir probe measurements of the radial electric field (see Figure 3.12) and the known poloidal magnetic field at the edge.

The response of the edge to biasing is fast and large because the torque is applied directly to this region of the plasma. The change in the core flow is not as large or rapid,

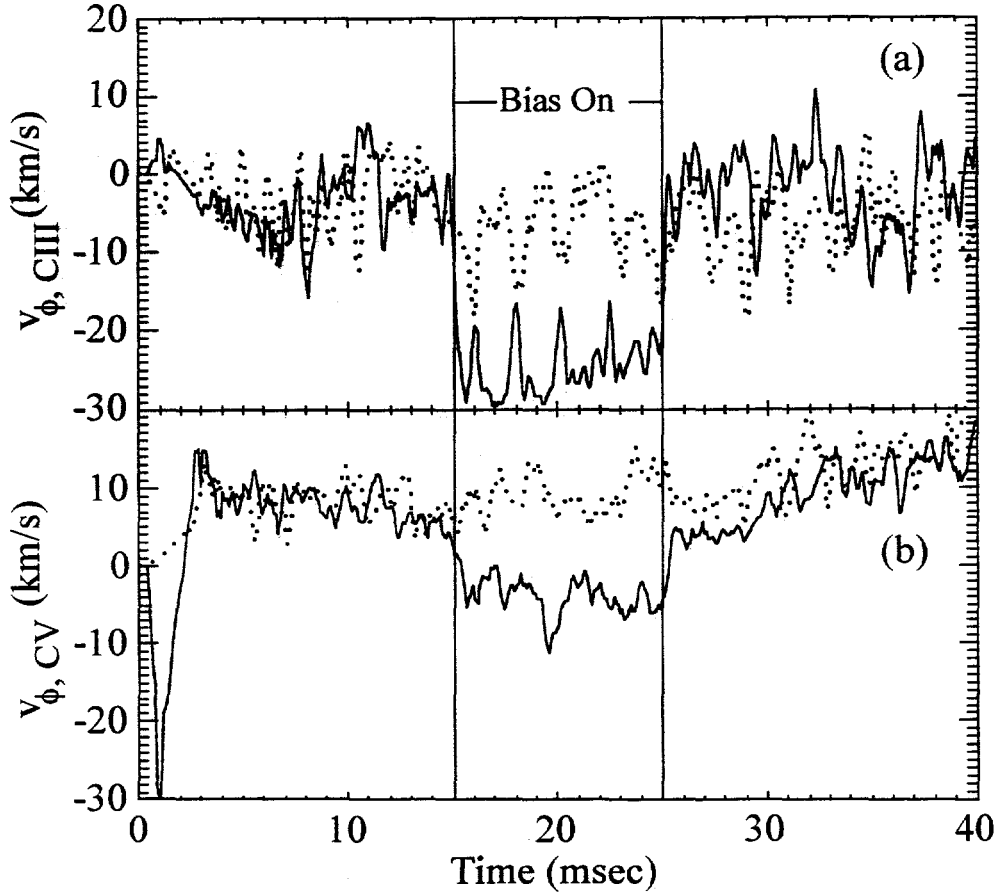

Figure 4.16. Toroidal ion flow obtained from Doppler shifted C III (a) and C V (b) emission is shown for counter-injection (solid) and no-bias (dotted) discharges.

presumably because the flow changes only through coupling with the edge plasma. Depending on plasma conditions, the behavior of the core flow with biasing can vary but the direction of the change is always as indicated by Figures 4.15 and 4.16.

Coincident with changes in the plasma flow are changes in the toroidal phase velocity of the various magnetic modes. The phase velocity is obtained from $v_{\phi,n} = (R_o/n)\, d\delta_n/dt$ where R_o = 1.5 m is the major radius, n is the toroidal mode number, and δ_n is the phase obtained from the toroidal array as described in Section 3.1. Typical behavior is

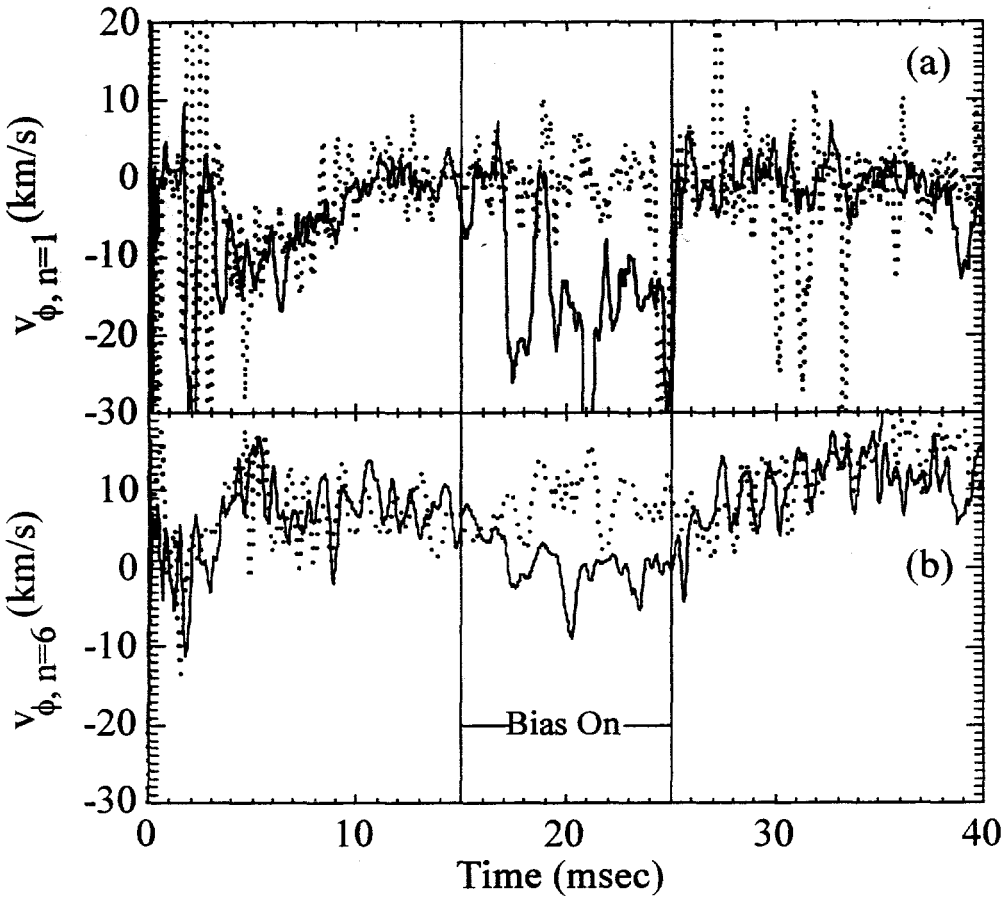

Figure 4.17. Toroidal phase velocity of the n = 1 (a) and n = 6 (b) magnetic modes are shown versus time for co-injection (solid) and no-bias (dotted) discharges. Positive velocity corresponds to motion towards lower toroidal angles.

demonstrated in Figures 4.17 and 4.18 for co- and counter-injection respectively. The n = 6 (m = 1) mode is resonant in the core of the plasma and hence exhibits features similar to C^{+4}. The n = 1 (m = 0) mode is resonant at the reversal surface and thus behaves much like C^{+2}. It is particularly significant that the n = 1 mode rotates with bias because it is usually locked (stationary) in other MST discharges.

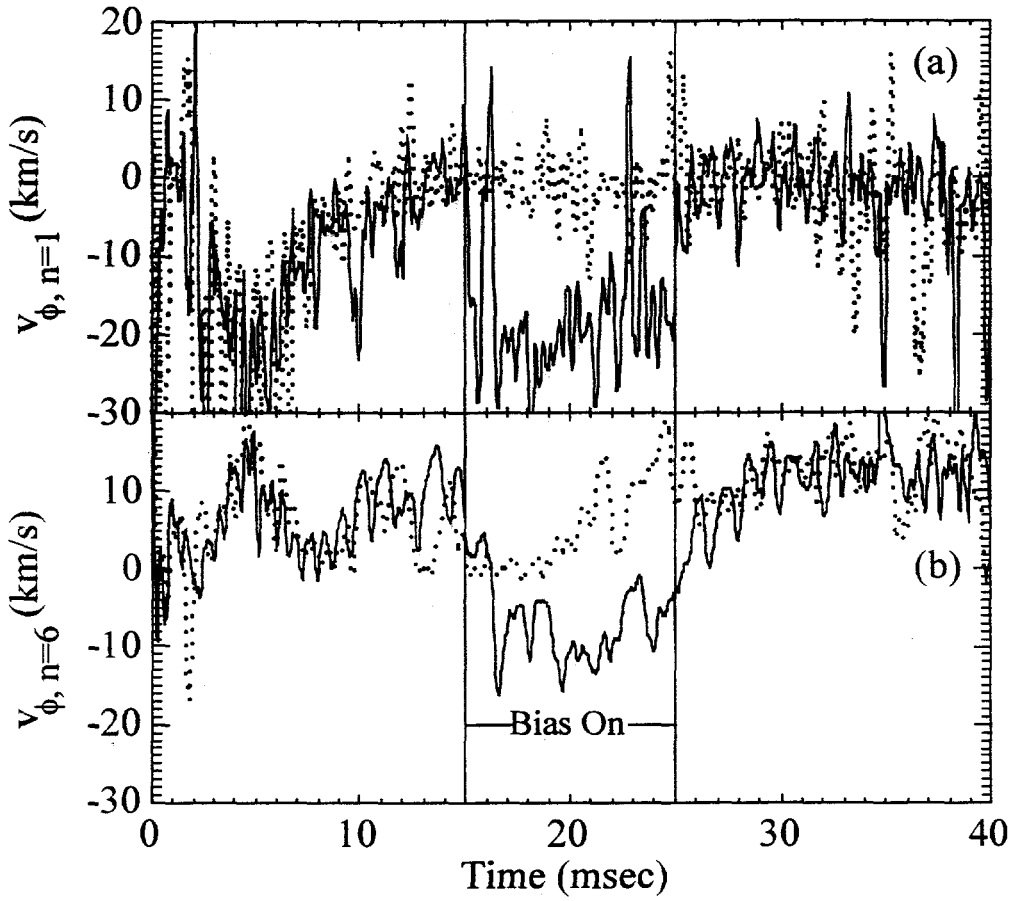

Figure 4.18. Toroidal phase velocity of the n = 1 (a) and n = 6 (b) magnetic modes are shown versus time for counter-injection (solid) and no-bias (dotted) discharges.

The dependence of $v_{\phi,n=6}$, $v_{\phi,n=1}$, and $v_{\phi,CIII}$ on the amount of current injected is shown in Figure 4.19. (Note that the scales are different for the core and edge velocities.) Both the n = 1 and C^{+2} velocity vary linearly with current (as expected if drag forces are roughly proportional to v) and appear to be the same for co- and counter-injection. The dependence of the n = 6 velocity on current is not quite as linear and frequently there are extended ranges of bias current for which the mode locks. This phenomenon occurs for both co- and counter-injection (although for the scan shown in Figure 4.19a, only

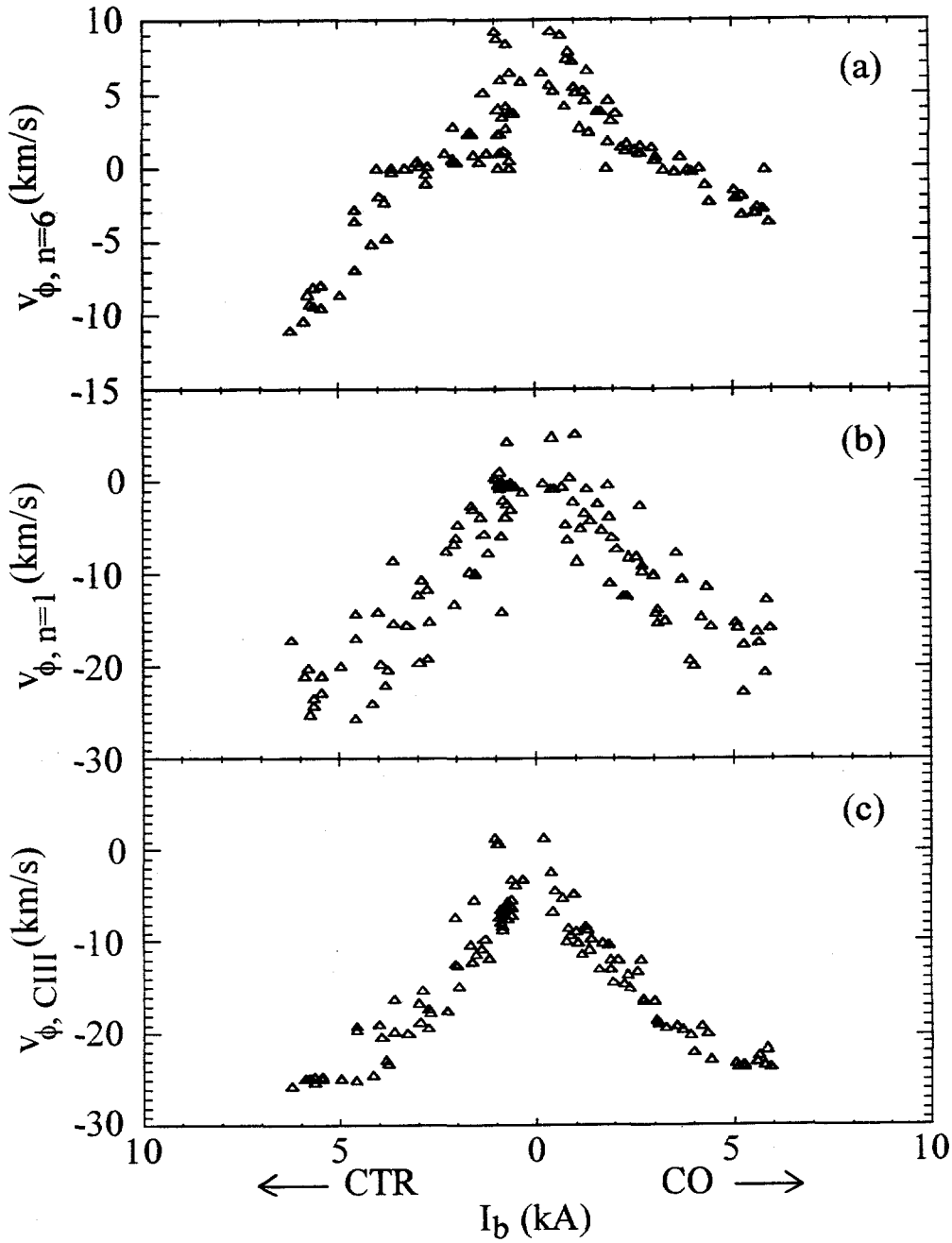

Figure 4.19. Scatter plots of n = 6 (a) and n = 1 (b) toroidal phase velocities and toroidal ion velocities from C III emission (c) are shown versus total injected current.

counter-injection exhibits this feature) and is frequent but not reliable. Presumably, the variation arises because the biasing influences the core only indirectly and the coupling mechanism(s) may change with plasma conditions. One consistent feature, however, is that strong negative n = 6 rotation is easier to achieve with counter- than with co-injection. This feature is evident in Figure 4.19a despite the locking region that is present on the counter-injection side. This suggests a stronger coupling of edge and core with counter-injection and hence a lower momentum "confinement time." As was shown earlier, magnetic fluctuation amplitudes tend to be higher in counter-injection cases and hence this stronger coupling may be evidence for anomalous viscosity or mode-mode coupling.

In other magnetic configurations, it is the shear in the flow that is responsible for confinement improvement. High resolution measurements of the flow profile, particularly in the edge, are not available. However, some insight can be obtained from the C III and C V measurements. From Figures 4.15 and 4.16 we note that the difference between core and edge flow is larger with bias than without. This implies a greater degree of shear somewhere between the core and edge when bias is applied. Assuming the flow velocity is zero at the wall, shear also exists somewhere between the radius of strongest C III emission and the wall.

In most models of transport reduction by sheared flows, it is actually the component of flow due to E×B drifts that is important [7]. The toroidal flow derived from C V emission includes contributions from diamagnetic and other flows as well as a contribution from flows along the magnetic field. The toroidal flow derived from C III, however, is mostly due to E×B drifts since the emission profile is very narrow and hence diamagnetic flows due to positive and negative pressure gradients tend to cancel in doing the chordal average shown in Figure 3.3. The radial electric field profile shown in Figure 3.12 was taken with only 6 injectors operating (such measurements with more injectors have proven to be extremely difficult). From this data one would conclude that shear in the E×B velocity exists in the

vicinity of the injection radius and hence electrostatic-fluctuation-induced transport may be reduced in the edge.

In summary, plasma biasing results in strong edge flows and flow profiles that do exhibit shear. Hence, there exists the possibility that electrostatic fluctuations could be modified by biasing in a way which reduces edge particle losses. It is worth noting that although flows with and without bias may be quite dissimilar, the differences between co- and counter-injection discharges are not significant enough to explain the changes in confinement discussed in Section 4.2.

4.3.2 Changes in Electrostatic Fluctuations Due to Plasma Biasing

In other magnetic configurations, the particle confinement increases with plasma biasing because the transport due to electrostatic fluctuations is reduced by the flows which are generated. As discussed in Chapter 1, electrostatic-fluctuation-induced particle flux is determined by a correlated product, $\Gamma = \langle n_1 v_{r1} \rangle$, with v_{r1} given by the radial component of the fluctuating E×B drift which in the RFP edge is given by $v_{r1} = - E_{\phi 1} / B_{\theta 0} = i\, k_\phi\, \Phi_1 / B_{\theta 0}$. The flux can thus be obtained by measuring density and potential fluctuations, the wavelengths of the modes, the degree of coherence between n and Φ, and the phase relationship. It is difficult to measure all of these quantities simultaneously in normal discharges and even more so in strongly biased discharges. In this section we consider two of the components -- namely the amplitude of density and potential fluctuations.

The data will show that floating potential fluctuations decrease during biasing throughout the edge but that density fluctuations obtained from FIR interferometer data increase. At least part of the increase in density fluctuations is connected with the rotation of magnetic modes that are locked without bias and the advection of a steeper edge density gradient by these and other magnetic modes. Such density fluctuations do not contribute to electrostatic-fluctuation-induced losses.

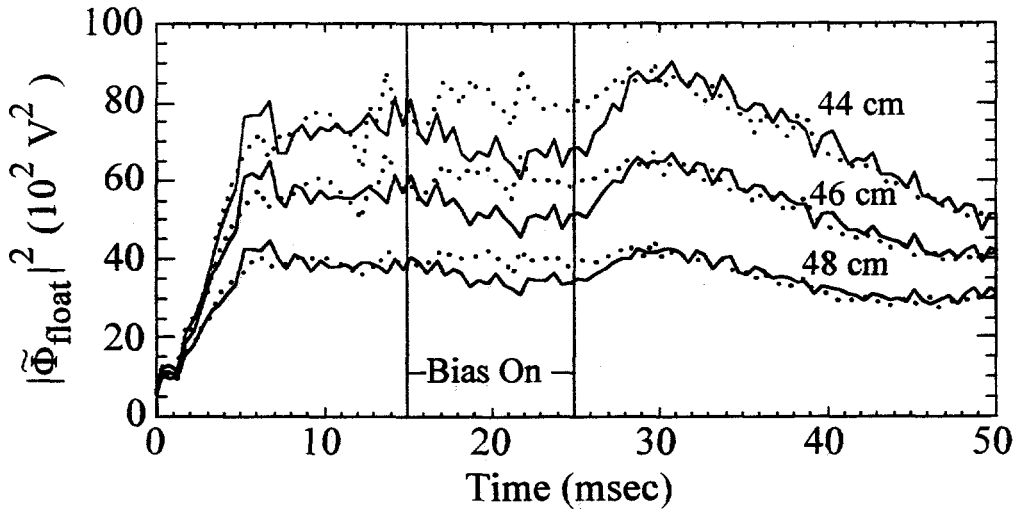

Figure 4.20. Total rms floating potential fluctuation power is plotted versus time for three different radial locations in biased (solid) and no-bias (dotted) shots. Each curve represents an ensemble average over many shots with 4 injectors operating.

Figure 4.20 shows the time dependence of the rms floating potential fluctuation power in discharges with and without biasing for three different edge locations. This data was obtained with the rake probe (described in Section 3.1) and has been ensemble averaged over many shots. Only 4 injectors were used in these shots yet a decrease in the floating potential fluctuations is seen throughout the edge. A frequency analysis reveals that the reduction is broadband.

Figure 4.21 shows the rms line-averaged density fluctuation power in both a central and an edge FIR interferometer chord for strongly biased shots and comparable no-bias shots. There is a marked increase in density fluctuations in both the central and edge chord during biasing. One will note that the fluctuations in both cases are stronger in the edge where the density gradient is steepest. This may be evidence for pressure-gradient-driven fluctuations or it may be that a portion of the line-averaged density fluctuations are due to advection of

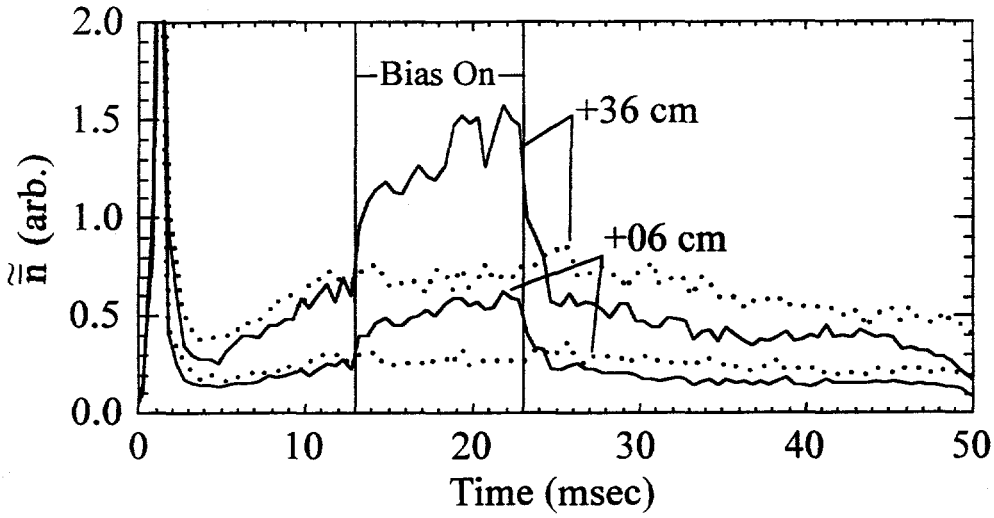

Figure 4.21. Measured rms line-averaged density fluctuations are shown for two FIR interferometer chords in strongly biased (solid) and no-bias (dotted) discharges. Each curve represents an ensemble average over many shots. Labels indicate how far each vertical chord is displaced outward from the geometric axis.

the density gradient by magnetic fluctuations. The first type of fluctuations can drive electrostatic particle transport but the second type do not.

Figure 4.22 shows that the increase in density fluctuations is broadband. The density fluctuations shown here were analyzed in a fashion similar to the magnetic fluctuations shown in Figure 4.5-4.7. The biased ensemble consisted of strong counter-injection shots. It is interesting that a peak in the density fluctuation spectrum appears near 100 kHz which is similar in many ways to that in the magnetic fluctuation spectrum shown in Figure 4.6. This again suggests that a portion of the density fluctuation power is connected with magnetic modes and does not contribute to electrostatic-fluctuation-induced transport.

The (m,n) = (1,0) mode provides one clear example of density fluctuations connected with magnetic modes. With the plasma rotating toroidally at 10-20 km/s, the frequency of a

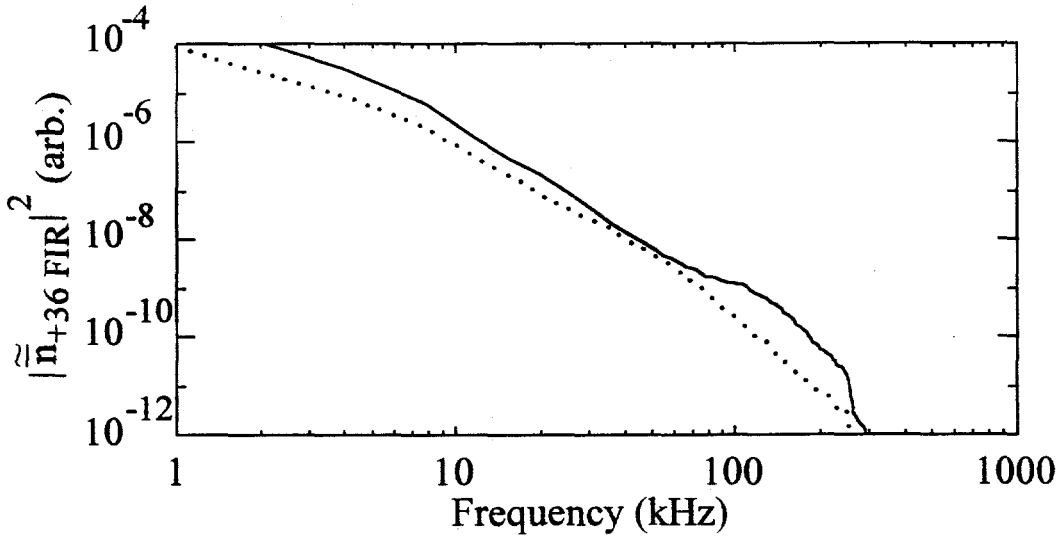

Figure 4.22. Measured autopower spectra of line-averaged density fluctuations in the +36 cm FIR interferometer chord are shown in strongly biased (solid) and no-bias (dotted) discharges. Each curve represents an ensemble average over many shots and time intervals.

mode with n = 1 will be 1-2 kHz. Figure 4.23 shows four different line-averaged density measurements from a strong counter-injection shot with large n = 1 amplitude. Indeed density oscillations are observed at this frequency. The oscillations in the FIR chords are nearly out of phase with the CO_2 measurement and we recall from Figure 3.1 that the FIR and CO_2 measurements are toroidally displaced by 150° so that oscillations due to an n = 1 structure should be roughly out of phase. The FIR data also show that the inboard, central, and outboard chords all oscillate in phase. Hence the structure is consistent with an m = 0 mode. The oscillation is large (~ 50 %) for the edge chords and small (~ 20 %) for the central chord, indicating that the perturbation is edge localized.

Figure 4.24 shows inverted density profiles obtained from 10 FIR chords (positions indicated by solid vertical lines) from the shot shown in Figure 4.23 at 17.7 ms and 18.0 ms.

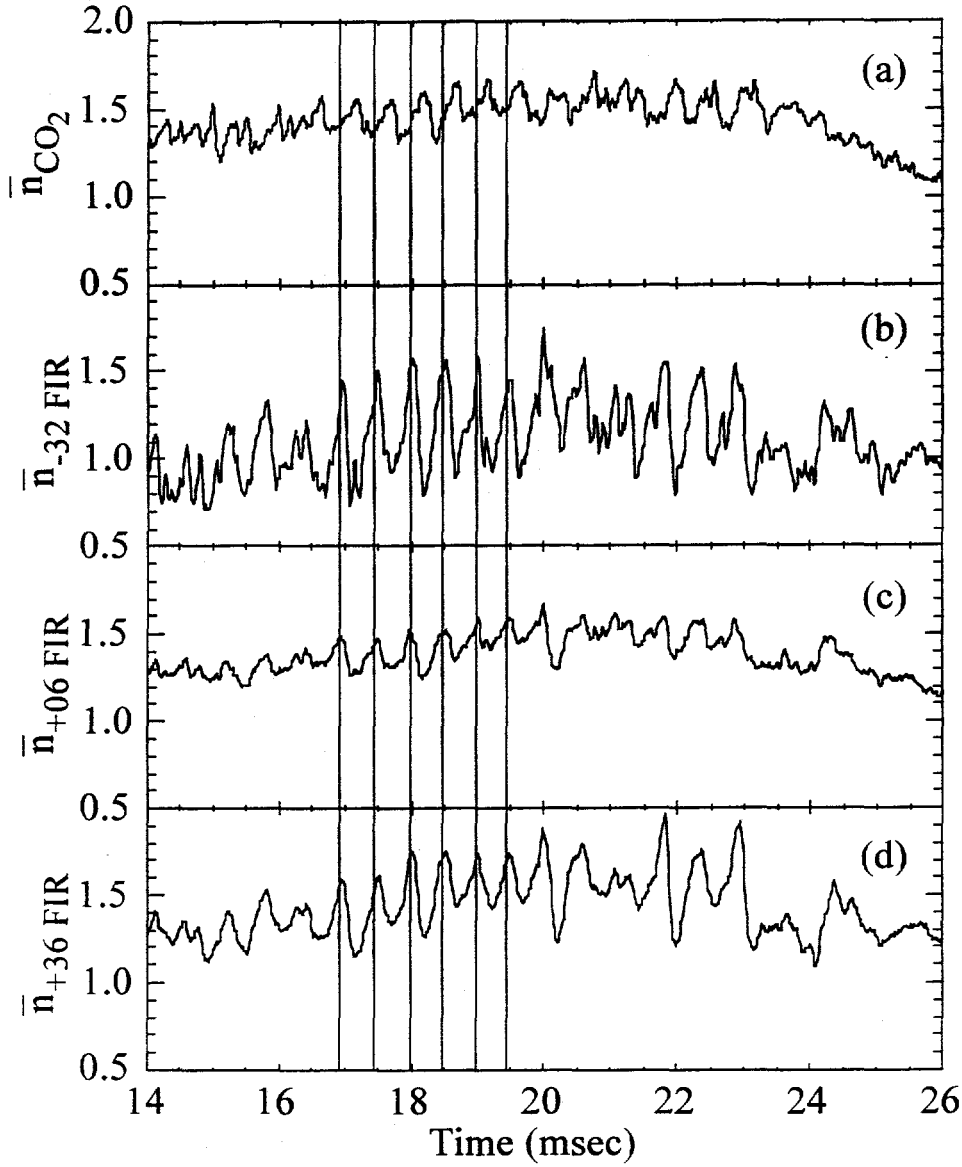

Figure 4.23. Line-averaged density is plotted versus time for the single central CO_2 interferometer chord (a) and for 3 chords of the FIR interferometer (b-d) during a counter-injection shot with 16 injectors in operation. Vertical lines indicate times for which the n = 1, m = 0 density perturbation is large at the FIR location. All vertical scales are in units of 10^{13} cm^{-3}.

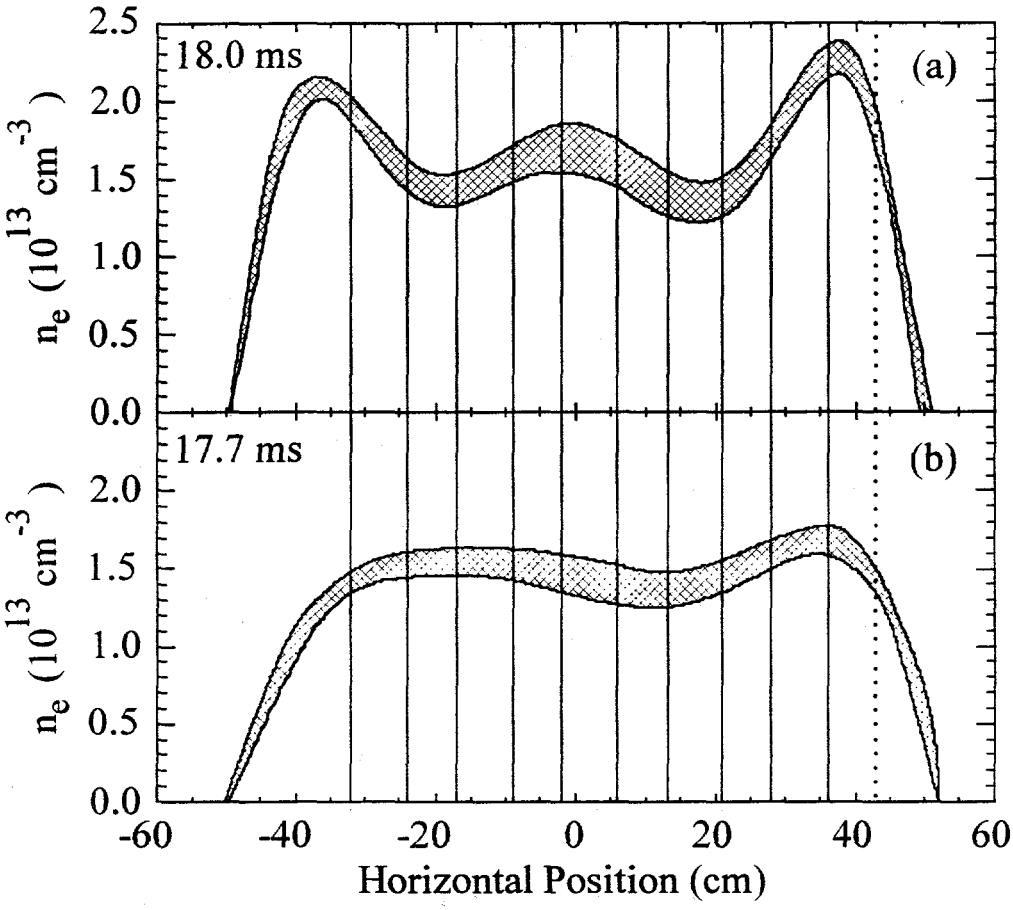

Figure 4.24. Inverted density profiles from 10 FIR chords are shown during the high (a) and low (b) phases of the n = 1 oscillation. The shading indicates an estimate of the error in the inversion. Solid vertical lines indicate the positions of chords used in the inversion and the dotted line indicates the location of the +43 chord which could not be used in the inversion.

These times correspond to the low and high density phase of the n = 1 oscillation respectively. The inversion confirms that the density perturbation resides close to the reversal surface (q = 0 at r ~ 40-45 cm) and is quite large. Since this mode is normally

locked in no-bias discharges, there will be an increase in observed density fluctuation power due simply to the rotation of the mode with biasing.

In all, we conclude that biasing does have an effect on potential and density fluctuations. Floating potential fluctuations decrease throughout the edge and density fluctuations increase although at least part of the density fluctuation increase comes from the excitation and/or rotation of edge magnetic modes. A portion of the measured density fluctuations may also be due to advection of the edge density gradient that becomes steeper with biasing (see Figure 4.29). Hence, a portion of the density fluctuation increase with bias is also due to this effect. Better simultaneous measurements of fluctuation amplitudes and wavelengths as well as the coherence and phase between n and Φ are needed to ascertain the impact of plasma biasing on the transport due to electrostatic turbulence.

4.3.3 Changes in Particle Confinement Due to Plasma Biasing

One hallmark of biased H modes in other configurations is a marked increase in the particle confinement time [8]. In this section, we examine to what degree this feature is present during biased discharges in the RFP. The number of stored particles definitely increases with biasing and the H_α emission is unchanged with bias after necessary corrections for toroidal asymmetries are taken into account. With these factors known, the change in particle confinement time with biasing hinges on the significance of impurity fueling which is not well known. Simple estimates of the contribution of impurities to the electron source term will be presented below. It will be shown that although these are significant and do increase with biasing, they are probably not enough to explain the 50% increases observed in the stored particle content. In addition, we observe a steeper density gradient in the edge with biasing which is difficult to explain without a decrease in edge particle transport.

Figure 4.9 shows the central line-averaged density in biased and non-biased discharges and it is apparent that the density increases significantly during biasing. Figure

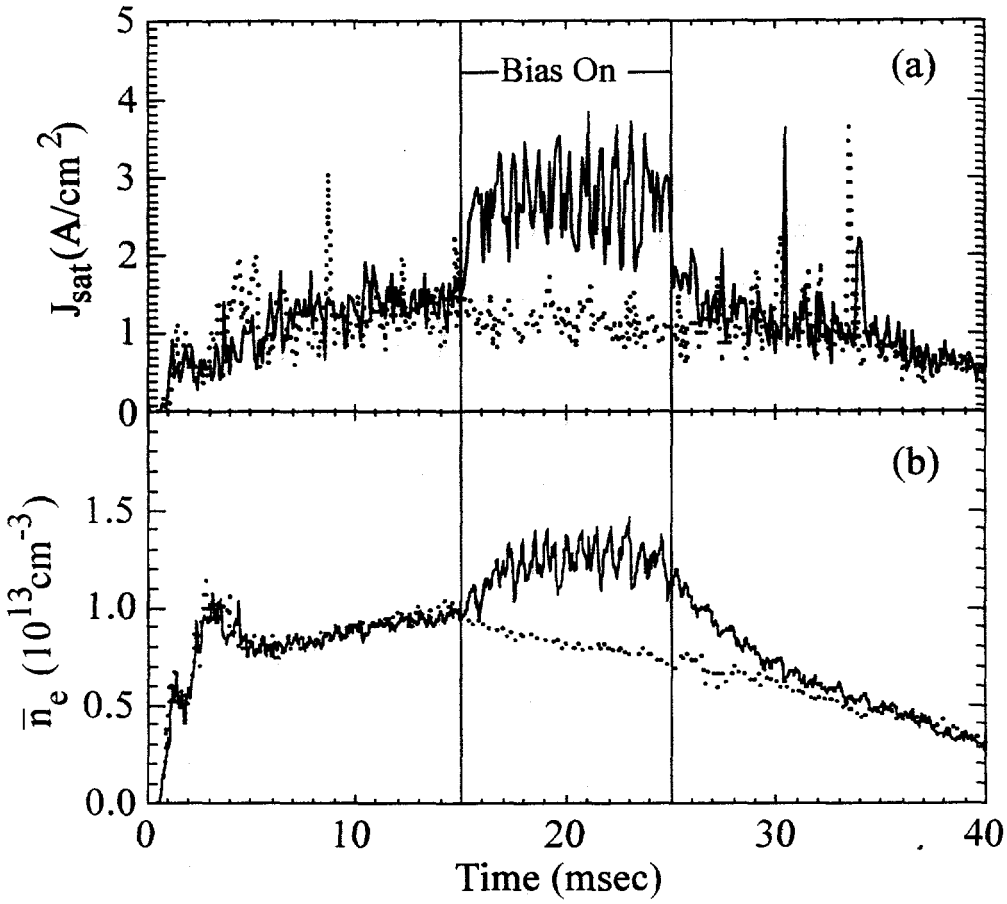

Figure 4.25. Ion saturation current measured at 45 cm (a) and central line-averaged density (b) are shown for a co-injection discharge (solid) and a comparable no-bias shot (dotted).

4.25 demonstrates that this increase is global by showing the ion saturation current (measured with a double probe at r = 45 cm) along with the central line-averaged density obtained from the CO_2 interferometer for a co-injection shot with 8 injectors and a comparable no-bias shot. The ion saturation current is proportional to ion density and to the speed at which ions enter the probe sheath ($v \sim T_e^{0.5}$). Unless the edge temperature increases by a factor of 4 with biasing (extremely unlikely), the doubling of the ion saturation current represents a density

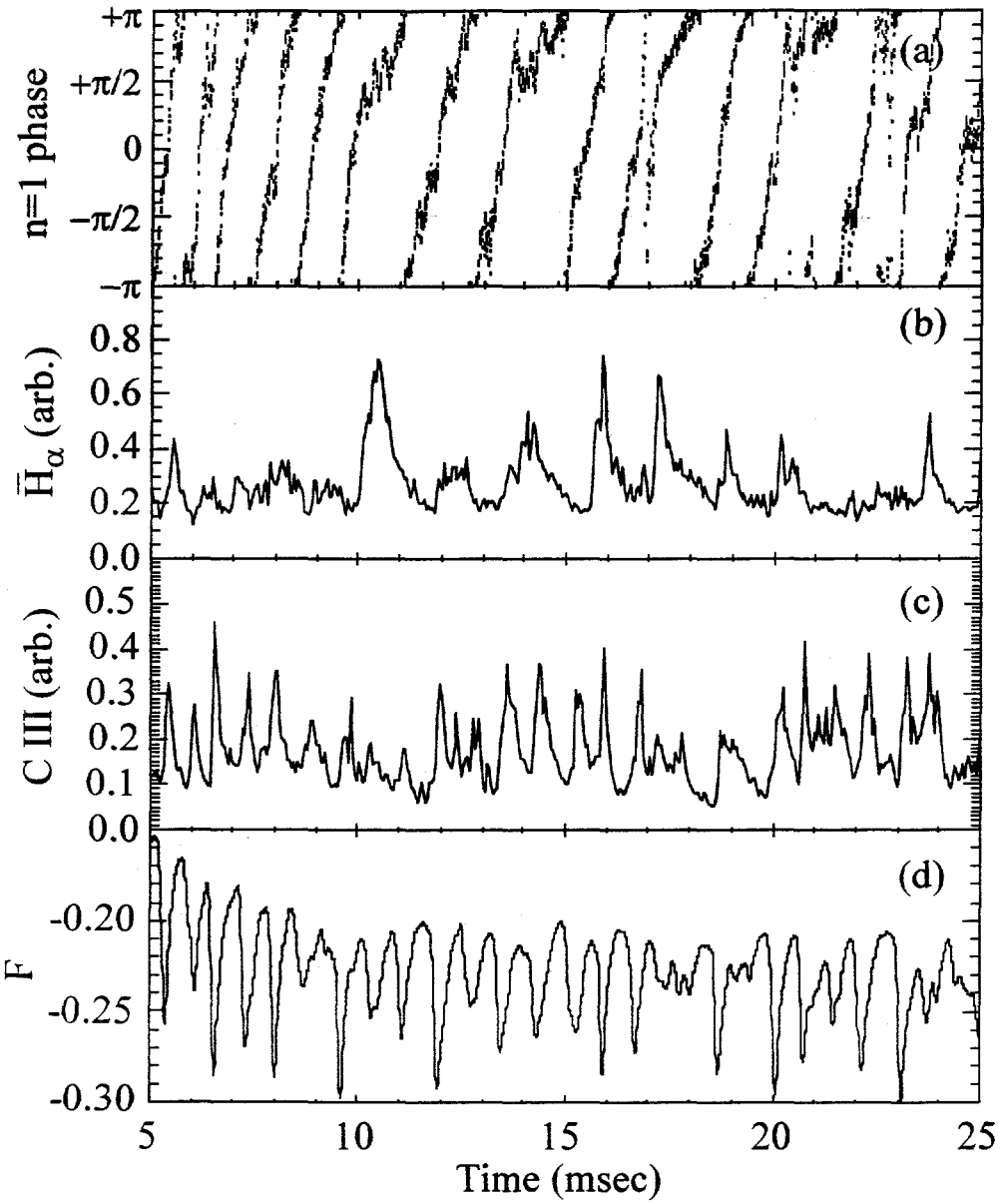

Figure 4.26. (a) The phase of the n = 1 B_ϕ perturbation, (b) central line-averaged H_α radiation, (c) central line-averaged C III radiation, and (d) reversal parameter are shown for a shot with guns inserted but not operating.

increase in the edge. The central line-averaged density measurement is most sensitive to the core density. Hence, the combined measurements illustrate a global density increase and a larger stored particle content with bias.

Now let us consider the particle source rate with and without bias. As mentioned in Section 4.2.2, source rates are estimated using measurements of hydrogen and impurity line emission at one location. It is assumed either that asymmetries are small or that they rotate so that an ensemble average over time and over different shots gives a good indication of global levels. Unfortunately, it appears that both of these assumptions are incorrect in discharges with guns inserted but not biased. The H_α emission in MST has a strong toroidal asymmetry due to the n = 1 magnetic mode that rotates in biased discharges but is normally stationary in non-biased discharges.

Figure 4.26 shows the measured H_α and C III line radiation versus time for a shot with guns inserted but not operating (no fuel or voltage is supplied). Also shown are the reversal parameter, F, and the phase (δ_n) of the B_ϕ component of the n = 1 magnetic mode. The negative excursions in F indicate sawtooth events. It is expected and observed that many parameters, particularly in the edge, are perturbed strongly by sawtooth crashes. Indeed, bursts can be seen in the CIII radiation that are well correlated with these events. There are pronounced features in the H_α radiation, however, which are not associated with sawtooth crashes but instead are well correlated with the phase of the n = 1 mode. In fact, there is little change in H_α at sawtooth crashes by comparison.

These data suggest that there are strong toroidal asymmetries in the hydrogen emission connected with the n = 1 magnetic mode. Figure 4.27b demonstrates this asymmetry. A scatter plot is shown of H_α intensity versus n = 1 phase and a peak is observed at a phase of about $+\pi/2$. This means that the measured H_α is maximum when the B_r component of the n = 1 mode is maximum near the location of the H_α detector. (Since the H_α detector is situated at 210° T and the B_r component of the fluctuation is 90° out of

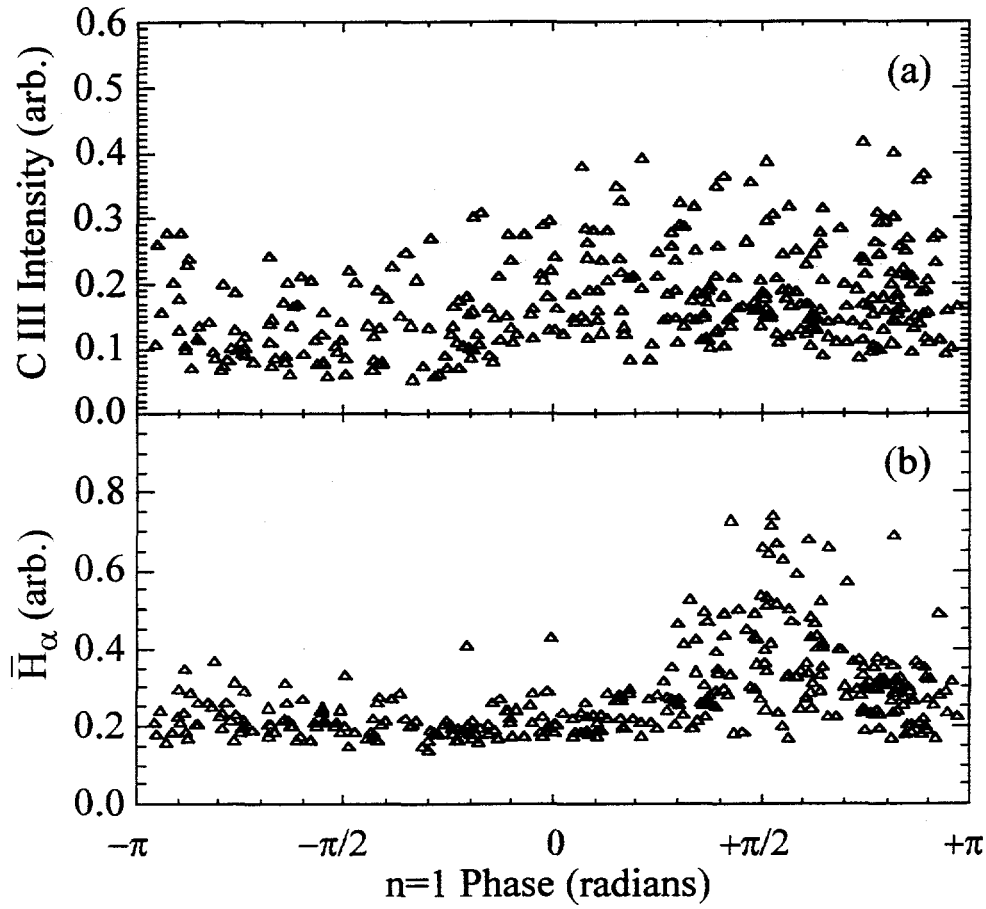

Figure 4.27. Scatter plots of C III radiation (a) and H_α radiation (b) are shown versus the phase of the n = 1 B_ϕ perturbation for the shot shown in Figure 4.26.

phase with the B_ϕ component, this means the H_α radiation is largest when the measured $\delta_{n=1}$ from the B_ϕ toroidal array coils is close to $+\pi/2$.) Asymmetries like this have been observed in other RFP devices [9] and have been attributed to localized particle losses connected with several phase-locked modes.

Figure 4.27a shows a similar plot for the CIII radiation. A slight asymmetry appears to exist in this case as well but the scatter from sawtooth events is large in comparison. Although for the particular shot shown in Figures 4.26 and 4.27 the n = 1 mode is rotating

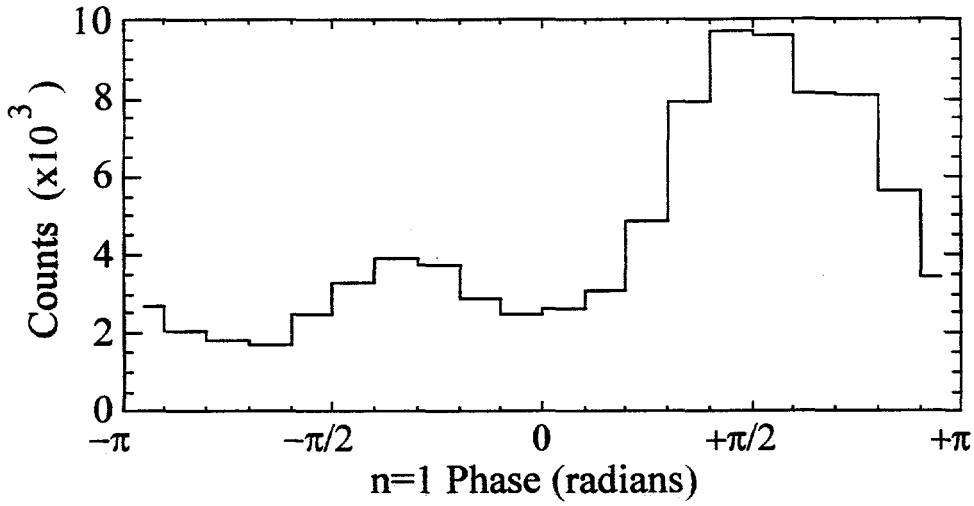

Figure 4.28. A histogram of measured n = 1 phase compiled from many no-bias shots is shown.

(i.e., $d\delta/dt \neq 0$) this is not generally the case for no-bias shots. Figure 4.28 shows a histogram compiled from several no-bias shots. It is clear that the n = 1 is up to five times more likely to be found in the $+\pi/2$ phase than in other phases. Since this phase corresponds to that for which the measured H_α is high, a random ensemble of no-bias shots will yield a value above the actual toroidal average. During biasing, however, the n = 1 rotates (see Figures 4.17 and 4.18) and has an equal probability of being in any particular phase. Hence, time-averaged measurements with bias represent toroidal averages while such measurements without bias do not.

We now turn our attention to Figure 4.10 which shows the measured H_α emission in a typical co- and counter-injection discharge as well as comparable no-bias discharges. One first notices that the measured radiation is very different in the two no-bias shots shown. This is because of the asymmetries which have just been described. In the no-bias shot of Figure 4.10a, the n = 1 mode was present in the $+\pi/2$ phase for most of the shot. Hence, the measured H_α emission is high. Conversely, in the no-bias shot of Figure 4.10b, the n = 1

phase was not near $+\pi/2$ until late in the shot and the measured H_α emission is low. When bias is applied, the full toroidal emission pattern rotates past the detector and bursts can be seen at 1-2 kHz in the H_α signal during biasing. A careful comparison of no-bias and biased cases shows that the fueling rate from hydrogen does not change significantly with biasing when these asymmetries are treated properly.

One will recall from Section 4.1.2 that all internal discharges are still active during the no-bias cases and hence the fueling influence of the guns is the same for biased and unbiased shots. Since we have just shown that the hydrogen source rate does not change significantly with biasing, the final ingredient in the particle confinement time calculation is the contribution of impurities to the particle source rate.

Figure 4.11 shows that impurity emission (indicated by C III line radiation) increases whenever guns are biased. This is not too surprising since we already know that electron density increases with bias and collisional excitation rates are proportional to electron density. Hence, even if the impurity density remained unchanged, one would expect the radiation to increase. In fact, if all of the increase in ion saturation current shown in Figure 4.25 is due to changes in density, one would expect line emission from edge charge states to roughly double during biasing, which is consistent with observations.

Regardless of whether or not the impurity concentration changes with biasing, the increase in line emission indicates that electron production due to ionization of impurities roughly doubles, provided the ratio of excitation and ionization cross sections does not change. The important question is what fraction of the electron source rate do impurities account for and hence what does an increase in impurity ionization mean in terms of the global electron particle balance? Present measurements of Z_{eff} and impurity composition are not sufficient to answer this question precisely, but estimates can be made.

For simplicity, let us assume that all impurity ions have charge $+eZ_{imp}$. We then use

$$Z_{eff} \equiv \frac{\sum_i n_i Z_i^2}{\sum_i n_i Z_i} \tag{4.4}$$

to solve for the ratio of the impurity and proton densities in terms of Z_{eff}. We find

$$\frac{n_{imp}}{n_p} = \frac{Z_{eff} - 1}{Z_{imp}(Z_{imp} - Z_{eff})} . \tag{4.5}$$

Now, if we invoke quasineutrality, we can arrive at a relation between electron and proton density given by

$$n_e = n_p \left(1 + \frac{Z_{eff} - 1}{Z_{imp} - Z_{eff}} \right) , \tag{4.6}$$

which shows that the amount of positive charge due to impurities is determined by a combination of Zeff and the "average" charge of impurities in the plasma.

In high density MST discharges it is reasonable to expect $Z_{eff} \sim 2$ and $Z_{imp} \sim 6$. This means that about 20% of the positive charge density comes from impurity ions and the rest is due to protons. If we assume that 20% of the electrons were generated by these impurities (the actual ionization/transport processes require more information and modeling), then we can expect a doubling of the impurity ionization to result in a 20% increase in electron density. Figure 4.9 shows that the electron density increases by about 50%. Thus although the impurities may be a significant particle source, it is unlikely that they account for the entire increase in electron density with biasing.

In summary, the total number of particles increases substantially with biasing despite no significant change in the source rate due to hydrogen. The particle confinement calculation then hinges on the contribution of impurities to the source term. Simple estimates suggest that impurities are a significant fuel source but are probably not enough to account for the observed increase in stored particles. Hence, particle confinement probably increases with plasma biasing but better impurity diagnostics are needed to know for sure.

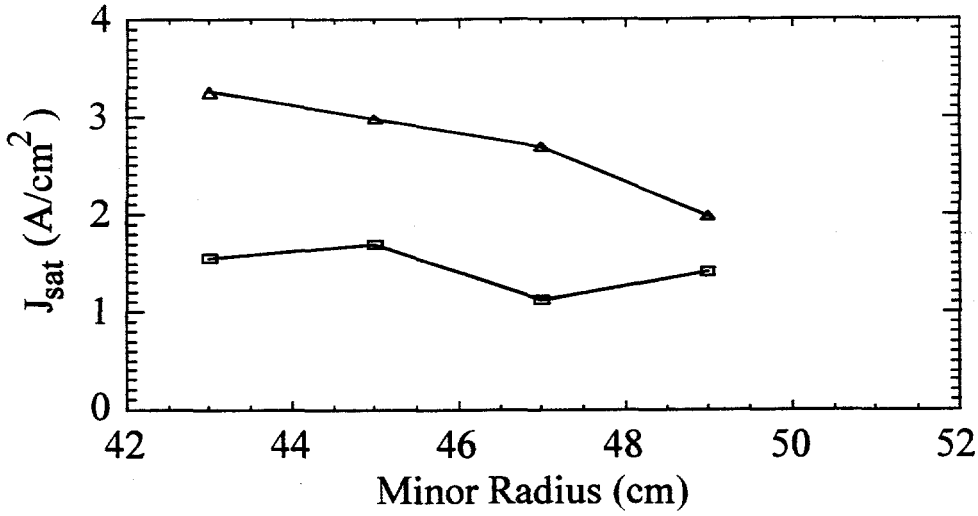

Figure 4.29. Edge radial profiles of ion saturation current are shown for an ensemble of co-injection (triangles) and no-bias (squares) shots with 8 injectors operating. Each point represents an average of several shots.

If particle confinement is improved with biasing, one expects that the enhancement will be limited to the edge where the strongest flow shears exist and where electrostatic fluctuations are known to play a role. The result of edge-localized transport reduction is a steeper edge density gradient. Figure 4.29 shows that indeed a steeper gradient does appear throughout the edge in the ion saturation current profile. This gradient does not prove that transport is reduced, but it does support the notion that plasma biasing results in improved particle confinement.

4.3.4 Magnetic Fluctuations and Energy Confinement in Biased Discharges

In Section 4.2 it was shown that directional current drive can reduce magnetic fluctuations and increase both particle and energy confinement. Plasma biasing and the generation of flow shear is not expected to have a similar impact on the dominant magnetic

fluctuations and hence energy confinement is not expected to change with biasing. Figure 4.4 and Table 4.1 show that this expectation is born out in these experiments. Both the m = 0 and the core modes are relatively insensitive to plasma biasing and the increase in energy confinement with co-injection is matched by a decrease of similar magnitude in counter-injection discharges. The high frequency modes resonant in the edge are excited by both directions of current drive but their amplitude is small and their impact on confinement negligible.

4.4 The Impact of Injector Insertion on Confinement

The previous sections have demonstrated that fluctuations can be modified using the plasma guns as tools to drive edge currents and bias the plasma. The ultimate success of any attempt to improve confinement using guns depends on the combination of these positive influences with the negative aspects of inserting materials into the plasma edge. The consequences of having injectors protruding into the plasma will be discussed in this section.

To illustrate the importance of these effects, consider the two co-injection discharges shown in Figure 4.32. All plasma parameters were similar for these two shots except the reversal parameter F. One will note that the density behavior is similar in the two cases but that the response of the loop voltage is quite different. The change in loop voltage with co-injection at deep F is one of the most striking effects observed with electrostatic current injection. Equally significant, however, is the lack of any reduction in V_{loop} for F=0 cases. Despite this very different behavior, the resulting loop voltage with current injection is the same in both discharges due to a much higher starting value in the deep F discharge.

The high starting value of the loop voltage is a consequence of the presence of the guns in the plasma. Figure 4.33 shows that the loop voltage increases almost linearly with

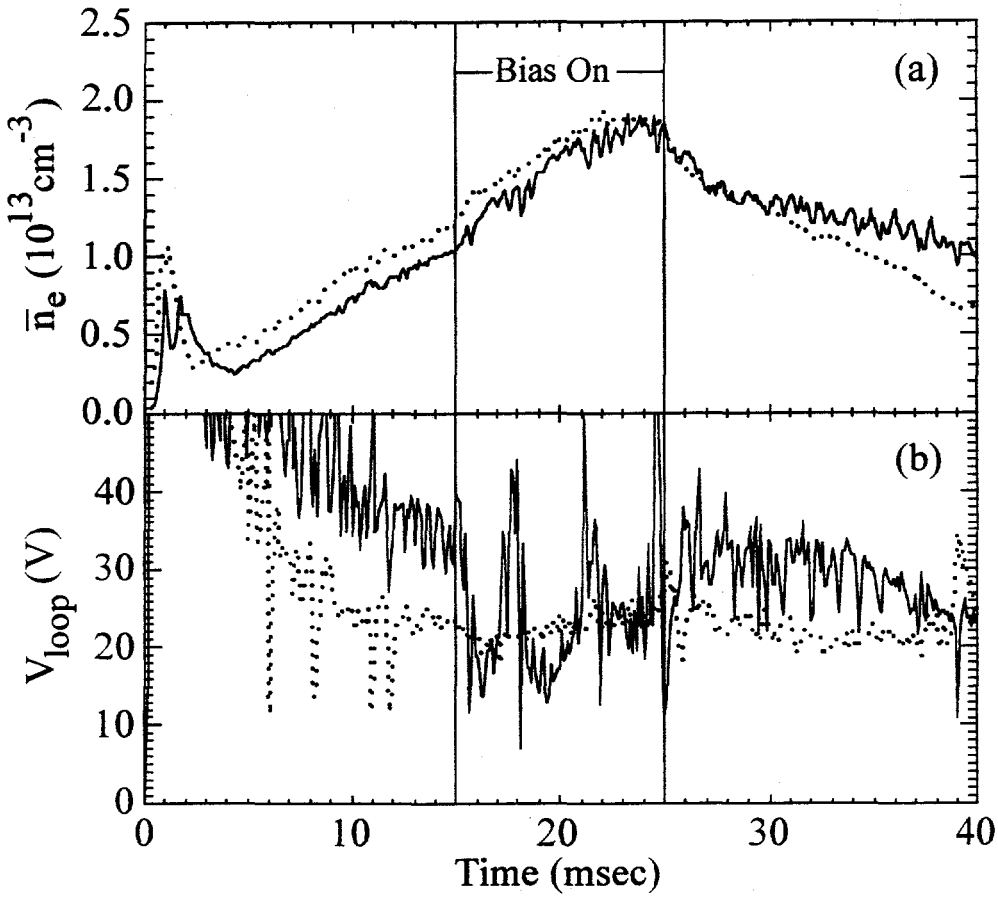

Figure 4.32. Central line-averaged density (a) and loop voltage (b) are shown for comparable co-injection shots at F = -0.31 (solid) and F = 0 (dotted).

the number of injectors inserted in the plasma. Figure 4.34 demonstrates that the degree to which the loop voltage is perturbed is not the same in all discharges. Individual symbols in this figure represent time averages of loop voltage and line-averaged density with 16 guns inserted in the plasma but without any fuel or voltages supplied. Lines indicate the same averages but in discharges with injectors fully retracted. The first thing to notice is that the perturbation to the loop voltage is greatest in low density discharges. The reason for this is not completely understood. However, it is likely connected with the fact that the electron

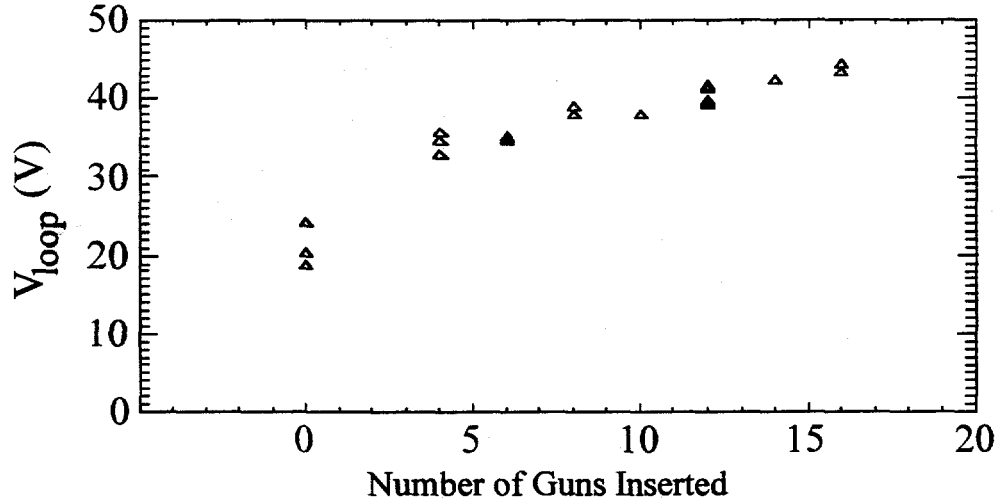

Figure 4.33. Loop voltage is plotted as a function of the number of guns inserted in the plasma. Data are a composite of different shots with density and reversal parameter held fixed.

energy distribution in the edge of many RFP devices has a fast tail population [10,11] and these "fast electrons" are a more important part of the distribution at low densities. The fast electrons are efficient at eroding material objects and hence the dependence of loop voltage on density may be due to an impurity effect. If energy transport coefficients depend on the average edge electron energy (as would be the case if the edge magnetic field is stochastic) then the density dependence may also represent a change in the energy transport rate as the electron energy distribution is varied.

The second observation to be made from Figure 4.34 is that the loop voltage perturbation is greater in more deeply reversed discharges. It is unlikely that this is an impurity effect and past measurements indicate that core electron temperatures are relatively insensitive to the degree of reversal [12]. It is interesting that the loop voltage has an F dependence in normal discharges as well. Thus, it is as if the normal dependencies become

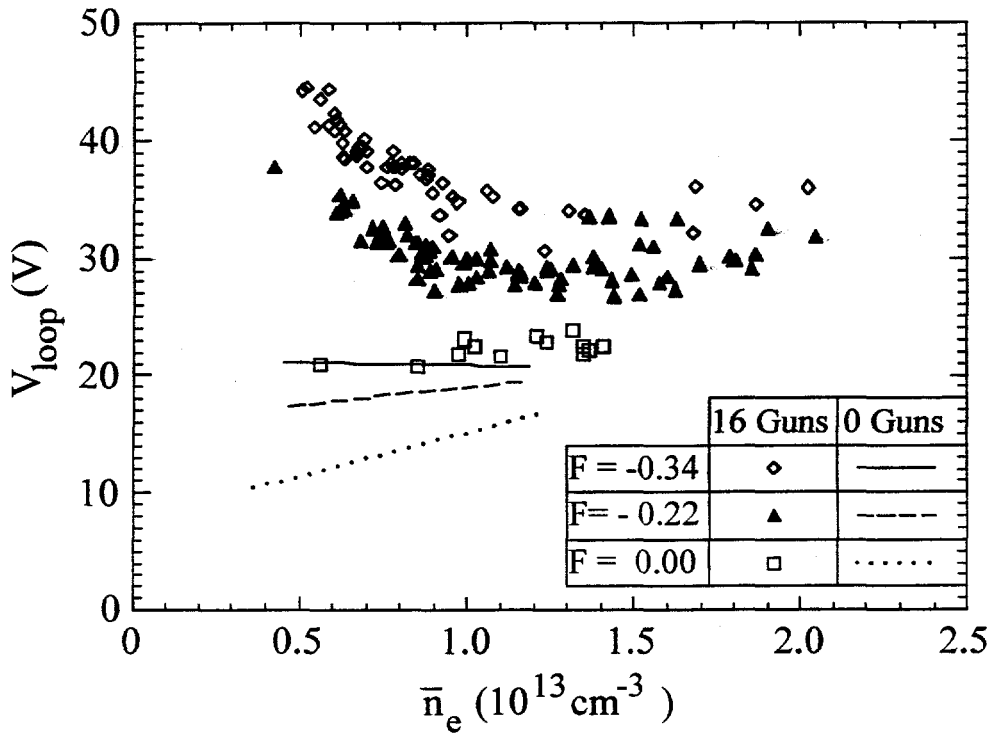

Figure 4.34. Loop voltage is plotted versus central line-averaged density for shots with 16 injectors inserted 5 cm in the plasma but not operating (individual symbols) and for shots with no injectors in the plasma (lines).

magnified when guns are inserted. These dependencies are most likely related to the anomalous part of the loop voltage [13].

Loop voltage anomalies are ascribed to magnetic fluctuations that influence the power balance in two key ways. First, magnetic fluctuations produce a dynamo electric field which acts against the applied toroidal electric field in the core. This means for a given toroidal current and magnetic equilibrium, the loop voltage will have to be higher if the magnetic fluctuation amplitude is higher. Second, magnetic fluctuations cause energy transport. In steady state, the ohmic input power must exactly balance this energy transport. Hence, for a

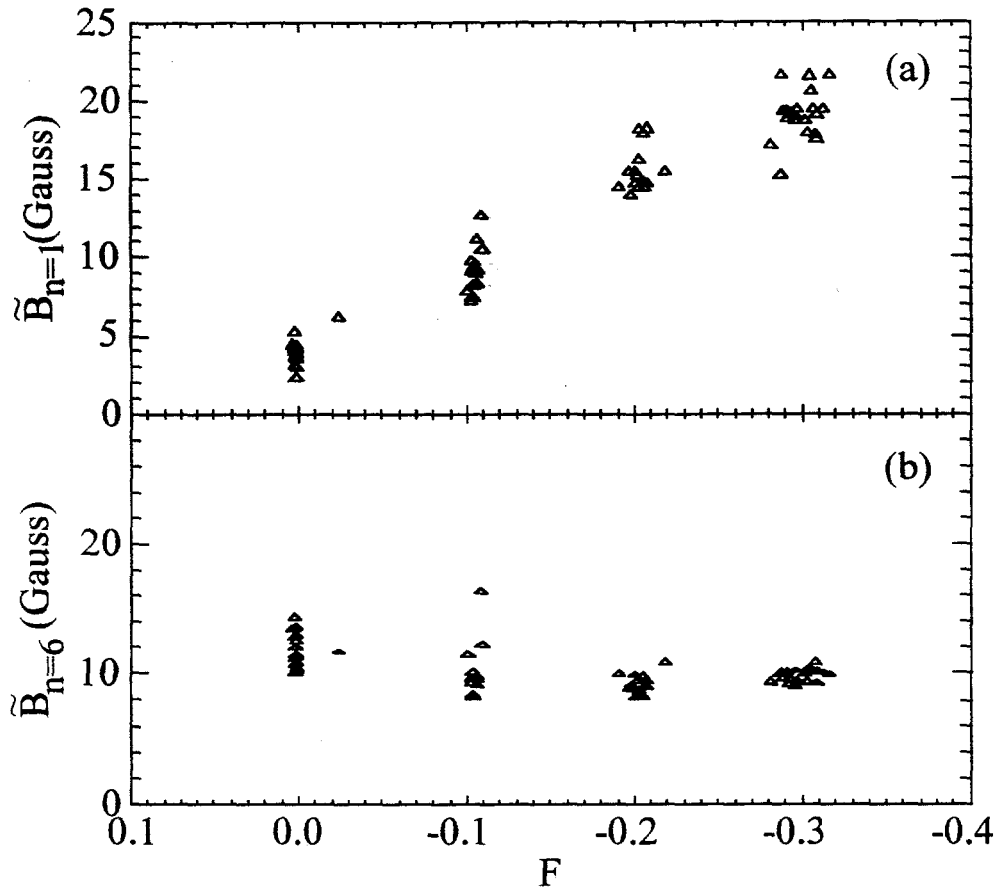

Figure 4.35. Measured n = 1 (a) and n = 6 (b) magnetic fluctuation amplitudes are plotted versus reversal parameter for shots with no injectors inserted in the plasma. The distribution of points at a given F represents the variation due to scanning density from 5×10^{12} cm^{-3} to 1.2×10^{13} cm^{-3}.

given plasma current and pressure, the loop voltage will be higher if the transport due to magnetic fluctuations is higher.

The dependence of loop voltage on F is probably due to the dependence of magnetic fluctuations on F. Figure 4.35 shows the dependence of the n = 1 and n = 6 mode amplitudes on F in normal discharges with no guns inserted. One notices that the core modes do not

strongly depend on the degree of reversal but that the modes resonant at the reversal surface depend almost linearly on F. If we suppose that the dependence of V_{loop} on F in normal discharges is due to the m = 0 modes, then it is not too surprising that the relationship between V_{loop} and F is magnified with guns because the mode amplitudes are observed to be magnified with guns. This can be seen by comparing Figures 4.35 and 4.25. Figure 4.25 shows that the n = 1 amplitude with guns inserted but not injecting current is about 28 Gauss whereas from Figure 4.35 we see that in normal F = -0.2 discharges, the level is about 16 Gauss. The n = 6 amplitude is also larger with guns inserted.

The obvious next question is what causes magnetic fluctuations to increase when guns are inserted? This rapidly becomes complicated. However, since the guns obstruct edge parallel currents, our understanding of the relationship between edge currents and mode amplitudes suggests that mode amplitudes will increase. The obstruction of current matters both because it changes the current profile and because it makes the dynamo drive less efficient, much like an increase in edge resistivity would. To maintain the magnetic configuration, mode amplitudes must increase. This effect has been observed in simulations when the edge resistivity is increased [5].

In summary, the insertion of the injectors causes significant degradation of confinement and is roughly proportional to the number of injectors that are inserted. The perturbation to the loop voltage depends on both density and the reversal parameter and is greatest in low density, deeply reversed discharges. The density dependence may be related to changes in the electron energy distribution but the dependence on reversal is most likely due to changes in magnetic fluctuations. Even in normal MST discharges, the loop voltage increases as reversal deepens, yet the core magnetic modes change very little with F. The m = 0 modes, however, increase linearly as F decreases. Thus the dependence of V_{loop} on reversal could be explained if the m = 0 modes are included in the power balance.

4.5 Summary

In this chapter, attempts to control fluctuations and transport with biased plasma guns have been reviewed. Two techniques were studied: edge parallel current drive and plasma biasing. Each technique has been used to study a different aspect of fluctuation induced transport in the RFP. Edge parallel current drive targets magnetic fluctuations and the particle and energy transport associated with them. Plasma biasing targets electrostatic fluctuations and the associated particle fluxes.

The most important result of these studies is that the core resonant magnetic modes are not the only magnetic modes that determine global confinement. The m = 0 modes resonant at the reversal surface also contribute. This conclusion is supported by two main pieces of evidence. First, particle and energy confinement have been shown to increase when current is driven that adds to the background current and decrease when injected current opposes the background current. The magnetic fluctuation amplitudes simultaneously decrease with co-injection and increase with counter-injection, but only because the m = 0 modes are modified by the current drive. The core modes are not reduced in a time-averaged sense. The second piece of evidence is the dependence of the loop voltage on F. This dependence is present in normal discharges but is amplified when injectors are inserted. The core mode amplitudes do not vary strongly with F but the m = 0 mode amplitudes increase linearly as reversal deepens. This suggests that the m = 0 modes are an important part of the global energy balance. The amplified dependence of V_{loop} on F with injectors inserted is consistent with the enhanced m = 0 amplitudes.

That the m = 0 modes play a role in global confinement should not be too surprising because these modes have amplitudes that are comparable to those of the core modes and sometimes larger at sawtooth crashes. Past measurements of fluctuation-induced-transport likely missed the contribution of these modes because in non-biased discharges they are

normally locked and cannot be distinguished from the equilibrium without spatially distributed arrays of probes. The dominant wavelengths are also very long (n = 1 is the largest mode) and hence even if the modes rotate, the low frequency oscillations can easily be mistaken for sawtooth oscillations. In fact, careful analysis shows that there are large asymmetries in H_α radiation, edge density, and many other quantities which are connected with these modes. Hence, they are important to consider in all edge measurements.

The second important result of this work is that electrostatic current drive outside the reversal surface is effective in changing m = 0 mode amplitudes. Although not exactly as anticipated, this result confirms that magnetic fluctuations in the RFP can be controlled with current profile modification. Furthermore, the fact that co-injection decreases mode amplitudes and counter-injection increases mode amplitudes confirms expectations regarding the sense of current profile modification necessary for confinement improvement. When additional parallel current is injected outside the targeted mode's resonant surface the mode amplitude is decreased.

The behavior of the core modes demonstrates that not just any current drive will do. The amplitude, position, and distribution of the driven current are probably important just as MHD simulations predict. It would appear that the necessary conditions for core mode reduction are not satisfied in the experiments discussed in this chapter. Certainly, the simulations predict that to significantly reduce core mode amplitudes, the injected current should be greater and/or deeper in the plasma. It appears necessary, however, that any current drive scheme address both the m = 1 and the m = 0 modes by driving current throughout the entire edge.

The final main result of these control experiments is that plasma biasing does not appear to improve energy confinement but may improve particle confinement. When the edge is biased, strong flows are driven and plasma potential measurements suggest a sheared E×B flow develops near the injector radius. As in other devices, such flows may have an

impact on electrostatic fluctuation-induced-transport and this is known to be important for edge particle transport in the RFP. Potential fluctuations are reduced with biasing, and a steeper gradient appears in the edge ion saturation current profile, consistent with expectations. However, density fluctuations measured with an interferometer increase with biasing although a portion of this increase is likely connected with magnetic modes. A detailed study of electrostatic fluctuations in these discharges is necessary to determine whether or not the flow patterns are affecting changes in the particle transport.

That particle confinement increases with bias is supported by an increase in the number of stored particles despite no significant change in hydrogen ionization. The contribution of impurities to the electron source term is not precisely known. However, simple estimates suggest that the increases in impurity ionization are probably not sufficient to explain the entire density increase. Definitive measurements of particle confinement await improvements in impurity diagnostics and particle balance modeling.

It is significant that although particle confinement may increase with biasing, energy confinement does not. In addition, magnetic fluctuation amplitudes do not respond to biasing (although the sawtooth cycle is sometimes affected). This observation adds to the evidence that magnetic fluctuations determine RFP energy confinement and hence gains in energy confinement only come about with reduction of magnetic fluctuations. It also shows that magnetic fluctuations are not directly reduced by edge flow shears of the type created in these experiments.

Net confinement gains with electrostatic current drive and biasing are limited due to the deleterious effects associated with the insertion of the injectors. The degree to which injector presence degrades confinement depends on the plasma parameters, particularly the density and degree of reversal. The enhanced losses associated with injector insertion are about the same as the gains that appear with co-injection. Hence a net improvement in confinement has not been realized in these experiments. However, the changes in confinement

that are observed when injectors are operated are encouraging and confirm many of the important aspects of fluctuation-induced-transport in the RFP.

References

[1] G. Fiksel, S.C. Prager, W. Shen, and M. Stoneking, Phys. Rev. Lett. **72**, 1028 (1994).

[2] M.R. Stoneking *et al.*, Phys. Rev. Lett. **73**, 549 (1994).

[3] T.D. Remple *et al.*, Phys. Rev. Lett. **67**, 1438 (1991).

[4] J.A. Beckstead, Ph.D. thesis, University of Wisconsin - Madison (1990).

[5] C.R. Sovinec, Ph.D. thesis, University of Wisconsin - Madison (1995).

[6] J.C. Sprott, Phys. Fluids **31**, 2266 (1988).

[7] H. Biglari, P.H. Diamond, and P.W. Terry, Phys. Fluids B **2**, 1 (1990).

[8] R.J. Taylor *et al.*, Phys. Rev. Lett. **63**, 2365 (1989).

[9] S. Mazur *et al.*, Nucl. Fusion **34**, 427 (1994).

[10] S. Ortolani, "The behaviour of fast electrons in reversed field pinches," in *Proceedings of the Int. Conf. on Plasma Physics*, Innsbruck, Austria (1992).

[11] M.R. Stoneking, Ph.D. thesis, University of Wisconsin - Madison (1994).

[12] M.R. Stoneking, S. Hokin, D.J. Den Hartog, and W. Shen, University of Wisconsin - Madison PLP 1089 (1991).

[13] K.F. Schoenberg, R.W. Moses, and R.L. Hagenson, Phys Fluids **27**, 1671 (1984).

5. SUMMARY AND DISCUSSION

5.1 Main Results and Implications

A novel approach to edge current drive has been realized and used to modify fluctuations and transport in the RFP. Miniature plasma sources are biased to inject electrons along and across edge field lines in order to affect changes in the parallel current profile, and accomplish plasma biasing. This type of injector has been developed to the point that clean, intense, directional currents can be extracted in a reliable fashion. Using the electrostatic current drive system as a tool for studying transport, many of the pre-existing notions regarding fluctuations and confinement in the RFP have been tested. Although the general picture of transport and how to reduce it appears to be correct, there are many details that emerge as a direct result of this work.

Let us first review the aspects of previous understanding that are supported by the experiments discussed in this thesis. It has long been held that magnetic fluctuations play an important role in determining RFP plasma confinement. These experiments support this general contention in several ways. First, total magnetic fluctuation levels have been varied using edge current drive; both the particle and energy confinement respond. Higher magnetic fluctuation levels are correlated with lower confinement and lower fluctuations are correlated with higher confinement. Second, energy confinement does not improve during plasma biasing and neither do magnetic fluctuation levels. Third, the insertion of the injectors results in a degradation of confinement and at the same time, higher magnetic fluctuations. Based on these results, it appears that the connection between magnetic fluctuations and confinement is solid.

Equally solid, it appears, is the idea that the magnetic fluctuations can be controlled by modifications to the parallel current profile. Amplitudes are decreased when current is

driven in the edge in the sense to flatten the overall current profile and increased when current is injected that makes the profile steeper. This adds to the results of MHD simulations and PPCD experiments to further strengthen the case for global current profile control in the RFP as a route to improved confinement.

The third aspect of RFP physics that has been tested to some extent in these experiments is the role of electrostatic fluctuations in edge particle transport. Although much more can be done, indications are that with plasma biasing, particle confinement improves and floating potential fluctuations are reduced. At the same time, steeper gradients form in the edge ion saturation current profile. These results are all consistent with the idea that electrostatic fluctuations contribute to edge particle transport.

Now let us move beyond these generally correct ideas to some of the new details that have been exposed in these studies. The first point is that the core magnetic modes are not the only modes that need to be controlled to achieve good confinement. The m = 0 modes are important as well. This is supported primarily by the observation that currents driven in these experiments affect m = 0 mode amplitudes in a time-averaged way but not core mode amplitudes; yet confinement responds to the current drive. That the modes at the reversal surface play a role in energy confinement is also attested to by the dependence of the loop voltage on the reversal parameter both in normal discharges and those with injectors inserted in the plasma. Core mode amplitudes do not change significantly with the degree of reversal but m = 0 amplitudes do.

This is an important point because it expands the group of magnetic modes believed to cause transport in MST. That the m = 0 modes contribute to edge transport does not necessarily conflict with earlier measurements of magnetic fluctuation induced transport [1] because these modes are usually stationary in the lab frame and spatial arrays of probes would be necessary to separate the fluctuations from the equilibrium. Such measurements may demonstrate that the m = 0 modes are responsible for part or all of the energy transport in the

edge and fill in a missing piece of the transport puzzle in MST. The fact that these modes participate in the global energy balance certainly suggests that any complete current drive scheme should control the current profile throughout the edge so as to reduce both the m = 0 and the core modes.

Another important point that was exposed in these studies is that control of the flow profile may be an important means for fluctuation control and confinement improvement in addition to current profile modification. That sheared flows have an impact on RFP confinement has been proposed already in the context of spontaneous enhanced confinement periods within PPCD discharges and normal deeply reversed discharges in MST [2]. In these experiments, several factors may simultaneously be at work but one of them appears to be a region of strongly sheared E×B flow in the edge which resembles H modes in other devices [3].

In this thesis, plasma biasing has been used to directly drive flows and particle confinement appears to improve as a result. This is the first time such an effect has been observed with biasing in the RFP [4]. It suggests that not only are sheared flows associated with improved confinement, but that shear may be added to the flow profile to bring about improved confinement. This aspect of control is important both for improving the reactor prospects of the RFP and for making it possible to systematically study the effects of flow shears on the magnetic and electrostatic turbulence and transport in the RFP edge.

5.2 Possible Extensions of This Work

There are many possible extensions to this work. In regard to plasma biasing, there is much that could be done to quantify the role of impurity fueling, expose the details of the potential profile, and accurately measure the density profile, particularly in the edge. Probably the most important (and most difficult) measurement yet to be made in biased

discharges is that of the fluctuation induced transport driven by electric field fluctuations. Biased discharges offer a reproducible way of studying the effect of flow shear on fluctuations. With some minor additions to the electrostatic injection system (for example electrodes which collect electrons), edge potential profiles could be customized and the fluctuation response tested.

The edge of the RFP offers a regime for testing the effects of sheared flow that differs somewhat from that in other magnetic configurations. Transport in other configurations is dominated by small scale instabilities on which sheared flows are expected to have an effect. The transport in the RFP, however, is dominated by large wavelength modes. Hence the effect of localized flow shear on large scale structures can be studied. This presents an opportunity for both theoretical and experimental progress since relatively little work has been done in this regime.

Because biased discharges also result in reliable rotation of the m=0 modes, the contribution of these modes to particle and energy transport may be more easily measured in these discharges. The measurement is not simple and probably still requires a limited spatial array of probes. Even with the modes rotating at 20 km/s, the large wavelengths result in frequencies of only 1-5 kHz which could be easily confused with sawtooth oscillations. The rotation of the m = 0 modes may also be beneficial in understanding the nonlinear coupling processes that occur between the m = 0 and m = 1 modes.

In regard to current drive, there are several important questions that remain unanswered. First, what is the mechanism by which the m = 0 modes are reduced with current injection? If the modes are linearly unstable, then current drive may stabilize them. If they are sustained by nonlinear coupling, then the driven current may extract energy quasilinearly, forcing the mode amplitude to saturate at a different level. In the MHD simulations described in Chapter 1, one run was done with extreme edge current drive ($r/a \sim 0.95$) and it was seen that m = 0 modes could be reduced somewhat through quasilinear

processes, but that core modes were not affected without a great deal of current being driven [5]. It would be interesting to utilize the flexibility of the plasma guns to test in more detail the simulations in order to learn more about the stability of the m = 0 modes and the coupling processes that move so much energy from the core to the edge in the RFP. The present current injection system appears to be well suited to address these issues.

For progress to be made in improving overall plasma confinement, the core modes need to be reduced. Without this, the m = 0 modes will always receive some energy through nonlinear coupling and the bulk of the plasma cross-section will continue to be dominated by a stochastic magnetic field. For the core modes to be reduced with electrostatic current drive, two hurdles must be overcome. First, it appears that the total injected current needs to be increased and/or moved deeper. In Chapter 3, it was shown that the injected current probably remains in the edge and the total effective current from 16 guns is about 8-10 kA times a number of poloidal turns greater than 3. If the multiplication factor is 10, then close to 100 kA are driven. This is close to the level of the PPCD experiments [6]. If the multiplier is 5 then only about 50 kA are driven. This is almost certainly not enough to significantly modify the core modes except possibly through indirect nonlinear processes. In either case, the current does not penetrate as in the PPCD experiments and hence either the injectors must be moved deeper, or the current must be greatly increased.

The easiest way to increase the current is to maximize the current injected by each of the injectors presently used. One obvious way to do this is to decrease the circuit impedance by shorting out the cross-field part of the circuit. This could be done with several grounded electrodes inserted to the injector depth but strategically located to interfere as little as possible with the field-aligned currents. By doing this, the plasma potential could be controlled independently of how much bias current is driven; hence the impedance could be restored to approximately that of the test stand system. It is estimated that the total poloidal current driven with the present system could be about doubled by doing this alone.

Another option for increasing the current drive capabilities is to add more injectors. There are several factors to consider in deciding whether more injectors will be useful or not. First, we note that based on the results presented in Chapter 3, the total current driven in the bias circuit would increase if more injectors were introduced. This, however, does not necessarily mean that the total poloidal current driven will increase with more injectors. If additional injectors block the current from existing injectors, then the currents may not simply add. If additional injectors are used, the magnetic configuration and injector locations would need to be carefully coordinated so that the driven current is maximized. Also, if the number of poloidal transits made decreases (due for example to the larger edge densities that will inevitably result from more injectors) then additional sources may actually decrease the total poloidal current driven.

Another factor to consider in deciding whether or not to add injectors is the effect of the additional fuel that the injectors will supply to the MST discharge. At the 16 gun level, this is already a dominant part of the required source and one wonders if more fuel would have a negative effect on machine performance. Hence, it appears that increasing the current driven by increasing the number of injectors should be done with caution, if at all.

The other hurdle that must be overcome if progress is to be made in reducing core mode amplitudes is the degradation that occurs with insertion of the injectors. This is a difficult problem to address. It is an inherent part of any electrostatic scheme since magnetic field lines must penetrate into electrodes for current to be driven. When this occurs, however, any pre-existing currents already flowing on these field lines are interrupted so the injection system must act to replace these first and drive additional current second. Also, particle and energy losses are enhanced because particles can flow directly along magnetic field lines to a material boundary.

In the case of the present injectors, current is very efficiently injected through a 1 cm diameter hole. However, this hole is situated near the end of a 7.5 cm long, 3.7 cm diameter

insulating cylinder, which with equal efficiency blocks all current on field lines that intercept it. It is possible to dream up all sorts of fixes for this problem (e.g., inserting coils in the guns to bend field lines around the BN shroud), but at this point they are all unproven ideas which need to be tested. If this problem can be solved, however, then the prospects for reducing magnetic fluctuations and improving RFP confinement with electrostatic current injection seem very promising.

References

[1] G. Fiksel, S.C. Prager, W. Shen, and M. Stoneking, Phys. Rev. Lett. **72**, 1028 (1994).

[2] B.E. Chapman, Ph.D. thesis, University of Wisconsin - Madison (1997).

[3] R.J. Groebner, Phys. Fluids B **5**, 2343 (1993).

[4] D. Craig *et al.*, Phys. Rev. Lett. **79**, 1865 (1997).

[5] C.R. Sovinec, private communication.

[6] J.S. Sarff, private communication.